Univariate parametric and nonparametric double generally weighted moving average control charts

by

Hossein Masoumi Karakani

Submitted in partial fulfilment of
the requirements for the degree

Philosphiae Doctor (Mathematical Statistics)

in the
Faculty of Natural & Agricultural Sciences
University of Pretoria
Pretoria

July 2020

UNIVERSITEIT VAN PRETORIA
UNIVERSITY OF PRETORIA
YUNIBESITHI YA PRETORIA

Declaration

I, Hossein Masoumi Karakani, declare that the PhD thesis entitled, Univariate parametric and nonparametric double generally weighted moving average control charts, which I hereby submit for the degree Doctor of Philosophy (Mathematical Statistics) at the University of Pretoria, is my own work and has not previously been submitted by me for a degree at this or any other tertiary institution.

Signature: *Hossein Masoumi Karakani* Date: 01/07/2020

Acknowledgements

First and foremost, praises to my creator, the Almighty God, the greatest of all, on whom ultimately, we depend for sustenance and guidance, for his showers of blessings throughout my PhD journey to complete the research successfully. The journey could never be accomplished without genuine and committed involvement from others. I would like to convey my salutations to all the people who supported me and cared about me throughout this academic tour.

- My sincere gratitude goes to my doctoral advisors, Dr. Schalk W. Human and Dr. Janet van Niekerk, for all the endless encouragement, infinite patience, and constructive ideas which have benefited me. They provided me with priceless guidance when I lost my direction in research. Their everlasting enthusiasms for high-quality research will continue to drive me to future achievements after the journey towards the PhD.

- To my beloved family, thank you for encouraging me in all my pursuits and inspiring me to follow my dreams and make them come true. I am extremely grateful to my parents for their love, caring, prayers, and sacrifices for preparing and educating me to become who I am today. They are the ultimate role models. I always knew that you believed in me and wanted the best for me. Special gratitude to my sister, Zeinab, for her infinite love and support.

- I express my gratitude to Prof. Andriette Bekker, the Head of the Department of Statistics, University of Pretoria, for her support during my Master and PhD studies. Her encouragement and sincere guidance have played an immense role in this endeavour.

- I would like to express my sincere gratitude and deep appreciation to my esteemed academic mentor and guide Prof. Mohammad Arashi, for his constant encouragement and valuable suggestions through my academic adventure at University of Pretoria.

- Sincere appreciation is also due to all staff members (both teaching and non-teaching) at the Department of Statistics for the quality of education and research they provided, which excessively improved my background in academics. Special gratitude to Ellen Mataboge and Gamu Malela for all their hard work and dedication at the Department of Statistics.

- To my friends scattered in different continents, thank you for your thoughts, well-wishes, emails, texts, phone calls, visits, and being there whenever I needed a friend. This includes, but not limited to the following friends: Buwang (Ngiyabonga ndoda enkulu), Iketle, Seitie and Brenda. Special gratitude to my “best” friends, Ali Moayedi Azarpour and Siavash Valizadeh

for their infinite kindness, friendship, and being there when others disappeared. By the time I am submitting this thesis, we are celebrating our 10th year friendship anniversary.

- To my relatives, Auntie Parvaneh, Auntie Marjan, Uncle Afshin, Uncle Abbas, Uncle Khosro, and other relatives and family friends, thank you for creating unforgettable memories during my regular visits to Iran. Special thanks to my cousin, Mahya, for her support during my Master and PhD endeavour.
- This research was supported in part by the National Research Foundation (NRF) under Grant Number 71199 and the postgraduate research bursary supported by the University of Pretoria. Any findings, opinions, and conclusions expressed in this thesis are those of the author and do not necessarily reflect the views of the parties.

This Thesis is dedicated to my parents and my sister, the hidden strength behind my every success and for their endless love, support and encouragement.

Abstract

Statistical process control (SPC) is a collection of scientific tools developed and engineered to diagnose unnecessary variation in the output of a production process and eliminate it or perhaps accommodate it by adjusting process settings. The task of quality control (QC) is of fundamental importance in manufacturing processes, when a change in the process causes misleading results, this alteration should be detected and corrected as soon as possible. Statistical QC charts originated in the late 1920's by Dr. W. A. Shewhart provide a powerful tool for monitoring production lines in manufacturing industries. They are also have been implemented in various disciplines, such as sequential monitoring of internet traffic flows, health care systems, and more. Shewhart-type charts are effective in detecting large shifts in the process but ineffective in detecting small to moderate shifts. This blind spot allows small shifts (smaller than one standard deviation) to continue undetected in the process, thereby incurring larger total costs for manufacturers.

This thesis addresses this issue by augmenting current time-weighted charts (charts that use all the information from the start of a process until the most recent sample/observation) with a Double Generally Weighted Moving Average (DGWMA) chart, leading to more effective process monitoring. The objective of this thesis is to provide the fundamentals and introduce the researcher/practitioner to the essentials of the univariate DGWMA chart from both parametric and nonparametric perspectives. Numerous concepts and characteristics of proposed DGWMA charts are discussed comprehensively. Theoretical expressions and detailed calculations have been provided to aid the interested reader to familiarize and study the topic more thoroughly. This thesis paints a bigger picture of the DGWMA chart in a sense that other time-weighted charts such as the Generally Weighted Moving Average (GWMA), Exponentially Weighted Moving Average (EWMA), Double Exponentially Weighted Moving Average (DEWMA) and Cumulative Sum (CUSUM) fall under this umbrella. Both real-life data and simulated examples have been embedded throughout the thesis. We make use of R and Mathematica software packages to calculate numerical results related to the run length distribution and its associated characteristics in this thesis.

We only consider control charts for monitoring the process location parameter. However, our conclusions and recommendations are extendable for the process dispersion parameter. In this thesis, we consider the DGWMA chart as the main chart and the EWMA, DEWMA, GWMA, and CUSUM charts as special cases. The thesis consists of the following chapters with a short description for each chapter as follows:

Chapter 1 provides a brief introduction to SPC concepts and gives a literature review in terms of background information for the research conducted in this thesis. The scope and objectives of the present research are highlighted in detail.

Chapter 2 provides an overview and a theoretical background on the design and implementation of the DGWMA chart derived from the SPC literature review. The properties of the DGWMA chart, including the plotting statistic, the structure for the weights, the control limits (exact/steady-state), etc. are considered in detail. The weighting structure of the DGWMA chart and its special case are discussed and pictured to emphasize the impact of weights in increasing the detection capability of time-weighted charts. Three approaches are described and investigated for calculating the run length distribution and its associated characteristics for the DGWMA chart and its special case the DEWMA chart; this includes: (i) exact approach; (ii) Markov chain approach; (iii) Monte Carlo simulation.

In **Chapter 3** we develop a one-sided generalized parametric chart (denoted by DGWMA-TBE) for monitoring the time between events (TBE) of nonconformities items originating from the high-yield processes when the underlying process distribution is gamma and the parameter of interest is known (Case K) and unknown (Case U). A Markov chain approach is implemented to derive the run length distribution and its associated characteristics for the DGWMA and DEWMA charts. An exact approach is also used to derive closed-form expressions for the run length distribution of the proposed chart. Performance analysis has been undertaken to execute a comparative study with several existing time-weighted charts. The proposed chart encompasses one-sided GWMA-TBE, EWMA-TBE, DEWMA-TBE and Shewhart-type charts as limiting or special cases. The CUSUM-TBE chart is also included in the performance comparison. The necessary design parameters are provided to aid the implementation of the proposed chart and finding the optimal design and near optima design that is useful for practitioners. Alternative discrete distributions are considered for the weights of the GWMA-TBE chart and a discussion is provided to address the connection between new weights originating from the suggested distributions and the chart's capability in detecting shifts. As a result, one can design an optimal GWMA-TBE chart by replacing weights from the discrete Weibull distribution without the implementation of the double exponential smoothing technique.

Chapter 4 focuses on developing a two-sided nonparametric (distribution-free) DGWMA control chart based on the exceedance (EX) statistic, denoted as DGWMA-EX, when the parameter of interest is unknown (Case U) and the underlying process distribution is continuous and symmetric. An exact approach and a Markov chain approach are considered to calculate the run length distribution and its associated characteristics for the proposed chart. A performance comparison has been undertaken to

execute analysis with other nonparametric time-weighted charts available in the SPC literature. The proposed chart encompasses two-sided

GWMA-EX, EWMA-EX, DEWMA-EX and Shewhart-type charts as limiting or special cases. The CUSUM-EX chart is also included in the performance comparison Also, the performance of the proposed DGWMA-EX chart has been evaluated under different symmetric and skewed distributions in comparison with its main counterparts, and the necessary results and recommendations are provided for practitioners to design an optimal chart.

Chapter 5 encloses this thesis with a summary of the research conducted and provides concluding remarks concerning future research opportunities.

Table of Contents

Acronyms & Symbols

ARL	Average run length	X_{ij}	j^{th} observation from the i^{th} random sample
ARL_0	In-control average run length	T_i	Sample statistic from the i^{th} sample
ARL_1	Out-of-control average run length	Z_t^1	The plotting statistic (single exponential smoothing)
ARL_0^*	Desired value of ARL_0	Z_t^2	The plotting statistic (double exponential smoothing)
IC	In-control	N	The run length random variable (Chapters 1, 2 & 3)
OOC	Out-of-control	K	The run length random variable (Chapter 4)
TBE	Time between events	v_i	Weight for the i^{th} statistic in GWMA chart
MDRL	Median of the run length	w_i	Weight for the i^{th} statistic in DGWMA chart
SDRL	Standard deviation of the run length	θ	Scale/location parameter
p.d.f.	Probability density function	θ_0	In-control scale/location parameter
p.m.f.	Probability mass function	θ_1	Out-of-control scale/location parameter
QC	Quality control	UCL_e	Exact upper control limit
SPC	Statistical Process Control	LCL_e	Exact lower control limit
EWMA	Exponentially Weighted Moving Average	UCL_s	Steady-state upper control limit
UWMA	Uniformly Weighted Moving Average	LCL_s	Steady-state lower control limit
DEWMA	Double Exponentially Weighted Moving Average	UCL	Upper control limit
GWMA	Generally Weighted Moving Average	LCL	Lower control limit
DGWMA	Double Generally Weighted Moving Average	CL	Centerline
CUSUM	Cumulative Sum	SPRT	Sequential Probability Ratio Test
GMA	Geometric Moving Average	L	Width of the control limits from the centerline
NP	nonparametric	F_θ	Underlying process distribution
EWMV	Exponentially Weighted Moving Variance	G_θ	Distribution of the sample statistic under consideration
EWMS	Exponentially Weighted Mean Square Error	H_θ	Distribution of the plotting statistic
EX	Exceedance	n	Sample size
WOS	Web of Science	μ	Expected value for the test statistic
EGWMA	Exponentially Generally Weighted Moving Average	σ	Standard deviation for the test statistic
$q_1, q_2, \alpha_1, \alpha_2$	Design parameters for the DGWMA chart (Case 1)	q, α	Design parameters for the DGWMA chart (Case 2)
q_1, α_1	Design parameters for the GWMA chart	$\lambda = 1 - q_1$	Design parameter for the EWMA chart
$\lambda_1 = 1 - q_1$, $\lambda_2 = 1 - q_2$	Design parameters for the DEWMA chart	h, k	Design parameters for the CUSUM chart

Research Outputs

We provide a list of research outputs related to this thesis. This list includes the details of the peer-reviewed article that was published, the local and international conferences, where the topics were presented and two seminars held at the Department of Statistics at the University of Pretoria.

Published article

(i) Masoumi Karakani, H., Human, S. W., and van Niekerk, J. (2019). A Double Generally Weighted Moving Average Exceedance Control Chart. *Quality and Reliability Engineering International*, 35(1): 224-245. https://doi.org/10.1002/qre.2393

International conference

(i) The 11th International Conference of the ERCIM WG on Computational and Methodological Statistics (CMStatistics 2018) in University of Pisa, Italy, where the results for the double generally weighted moving average control chart for time between events (Chapter 3) was presented.
http://www.cmstatistics.org/RegistrationsV2/CMStatistics2018/viewSubmission.php?in=1218&token=80ns4o0p1ro3538rq7ps862626n1sqqs

Local conference

(i) The annual conference of the South African Statistical Association (SASA) hosted by the Department of Statistics of the University of Free State in Bloemfontein (2017), where the results for the double generally weighted moving average control chart for time between events (Chapter 3) was presented.

Departmental seminar

(i) The weekly seminar hosted by the Department of Statistics of the University of Pretoria (2018), where the results for the double generally weighted moving average control chart for time between events (Chapter 3) were presented.

(ii) The weekly seminar hosted by the Department of Statistics of the University of Pretoria (2019), where the results for the double generally weighted moving average exceedance control chart (Chapter 4) were presented.

Addendum

This addendum is included for examination purposes as well. The purpose of creating an addendum is pointing out the similarities and dissimilarities between the following articles:

1. **Title**: A Double Generally Weighted Moving Average Chart for Time Between Events – Human, S. W., Masoumi Karakani, H., & van Niekerk, J.
    - ✓ Submitted: 13th February 2018 – rejected: 17th July 2018, Journal of Statistical Computation and Simulation
    - ✓ Submitted: 30th October 2018 – rejected: 25th November 2018, Journal of Quality Technology

2. **Title**: Monitoring of time between events with a double generally weighted moving average control chart – Alevizakos, V., Koukouvinos, C., & Lappa, A. (Received: 30th June 2018, revised: 4th October 2018, Accepted: 21st October 2018, Journal of Quality and Reliability Engineering International)

This addendum consists of the comparison between the Average Run Length (*ARL*) values, the tables, the graphs, etc. The purpose of this addendum is to point out to the examiners that I, Hossein Masoumi Karakani, has independently reached the same conclusions, where there are similarities.

Similarities

Article 1 Human, Masoumi Karakani, van Niekerk	Article 2 Alevizakos, Koukouvinos, Lappa
Page 4, line 48, "Although the shape parameter $k > 0$ can theoretically be any positive real number, in the development that follow it is assumed that k is a known/specified integer".	Page 3, lines 18 & 19, "The parameter k can be any positive real number, but here, it is assumed to be a positive integer".
Page 4, line 53, "If $k = 1$, the p.d.f. in (1) reduces to that of an exponential distribution with the scale parameter θ and the main interest is in monitoring the time until one failure".	Lines 21-23, "If we are interested in monitoring the time until only one failure, the Gamma (1, θ) distribution reduces to the exponential distribution with scale parameter θ".
Page 5, line 14, "The objective is to construct a control chart to monitor scale parameter θ for a sustained downward step shift, i.e., a decrease in the inter-arrival times, which would be indicative of deterioration in the process".	Page 3, line 26, "Our aim is to construct a control chart to monitor θ for a downward shift, ie, a decrease in the inter-arrival times which means that the process may have deteriorated".
Page 5, line 37, "The probability $P(M_1 > t)$ is considered as the weight for the starting value, denoted by Z_0^1, which is typically taken as the in-control (IC) expected value of the statistic under consideration, i.e., $Z_0^1 = E(X_i \mid IC) = k\theta_0$".	Page 3, column 2, above Equation (3), "… and the probability $P(N > t)$ is the weight of the starting value which is considered to be equal with the IC expected value of the statistic Z_t, i.e, $Z_0 = k\theta_0$".
Table 1, for $q = 0.9$, $\alpha = 0.9$, and $t = 10, 50, 100$, the values for weights are 0.0058, 0.0188, and 0.0191, respectively.	Table 1, for $q = 0.9$, $\alpha = 0.9$, and $t = 10, 50, 100$, the value for weights are 0.005825, 0.018773, and 0.019096.
Title for Section 3 is: "The design and implementation of DGWMA-TBE chart".	Title for Section 3 is: "The design of DGWMA-TBE chart".
Page 10, lines 16-20, "To reduce the number of false OOC signals, a sufficiently large in-control ARL (denoted as ARL_0) to avoid false alarms and sufficiently small OOC ARL (denoted as ARL_1) to detect shifts rapidly when the process is out-of-control is required".	Page 5, 1st column, 2nd paragraph in Section 3, "When a process is in an IC state, the control chart should signal a false alarm as slow as possible; that means one would like to have a large value of IC ARL (ARL_0). On the other hand, when a process is in an OOC state, the control chart should signal as soon

	as possible, i.e., one would like to have a small value of ARL (ARL_1)".
Page 14, lines 20-22, "In the next section, the "near optimal" design given the out-of-control (OOC) ARL values for different shift sizes will be considered".	Page 6, 1st column, the last paragraph in Section 3.2, "Following this section, we investigate the design of the DGWMA-TBE control chart that is near to its optimal design for different values of shifts".
Page 15, point iv., "As the value of k increases, the performance for both the DGWMA-TBE and GWMA-TBE charts improves. The improvement and increase in sensitivity of a control chart for higher values of k is due to the fact that larger value of k implies more observations/failures to be collected".	Page 6, 2nd column, point 2, "For specified values of the parameters, as the value of k increases, the performance of the DGWMA-TBE chart improves. A higher value of k entails collecting more observations before a decision can be made about the status of the process".
The L, ARL_0, ARL_1 and SDRL values for the DGWMA-TBE chart and same combinations of parameters are identical for both articles. For example, in Table 4, when k = 1, shift = 1, $q = 0.9$, and $\alpha = 0.9$, the values for L and ARL_0 are equal to 1.649 and 369.78, respectively. From Table 4, when k = 1, shift = 0.9, $q = 0.9$, and $\alpha = 0.9$, the SDRL and ARL_1 values are equal to 112.48 and 130.85, respectively.	The L, ARL_0, ARL_1 and SDRL values for the DGWMA-TBE chart and same combinations of parameters are identical for both articles. For example, in Table 3, when k = 1, shift = 0.9, $q = 0.9$, and $\alpha = 0.9$, the values for L and ARL_0 are equal to 1.671 and 370.08, respectively. From Table 3, the SDRL and ARL_1 values are equal to 115.33 and 128.08, respectively. Table 3, when k = 1, shift = 1, $q = 0.9$, and $\alpha = 0.9$,
From Table 5, when k = 2, shift = 0.925, $q = 0.9$, $\alpha = 1$, and L = 1.756, the values for SDRL and ARL_1 are equal to 119.01 and 134.61, respectively.	From Table 4, when k = 2, shift = 0.925, $q = 0.9$, $\alpha = 1$, and L = 1.772, the values for SDRL and ARL_1 are equal to 124.14 and 130.27, respectively.
From Table 4, when k = 1, shift = 0.5, $q = 0.9$, $\alpha = 0.8$, and L = 1.868, the value for ARL_1 is 17.25	From Table 4, when k = 1, shift = 0.5, $q = 0.9$, $\alpha = 0.8$, and L = 1.869, the value for ARL_1 is 14.94.
• The structure for both articles is similar. More specifically, the titles selected for different section are similar as well. This include the notation used for the gamma distribution, the GWMA control chart, the DGWMA control chart, the control limits, and the convergence for the weights.	

- Section 3.1 title for the 2nd article is selected the same as the 1st article, "The run-length distribution of the DGWMA-TBE chart".
- The number of simulations runs in both articles is selected as 10 000.
- Section 3.2 title for the 2nd article is selected the same as the 1st article, "The IC design of the DGWMA-TBE chart".
- Section 3.3 title for the 2nd article is selected the same as the 1st article, "The OOC design of the DGWMA-TBE chart".
- Section 4 title for the 2nd article is chosen the same as the 1st article, "Phase II DGWMA-TBE chart".
- Both articles concluded that the estimation of the unknown parameter from an IC Phase I sample affects the performance of the Phase II chart.

Dissimilarities

Article 1 **Human, Masoumi Karakani, van Niekerk**	**Article 2** **Alevizakos, Koukouvinos, Lappa**
The main objective is to investigate the capability of the DGWMA-TBE chart in **detecting small or tiny shifts**.	The main purpose is to study the ability of the DGWMA-TBE chart in **detecting moderate to large shifts**.
Construct and design a parametric DGWMA control chart for the gamma distribution. The robustness of the chart has been studied in a different paper published by same authors in the Journal of Quality and Reliability Engineering International for the DGWMA nonparametric chart. The link to the published article is: https://onlinelibrary.wiley.com/doi/full/10.1002/qre.2393	The robustness of the parametric DGWMA-TBE chart is considered when the TBE observations follow a Weibull or lognormal distributions.
A one-sided DGWMA-TBE chart with a **steady-state control limit** based on the gamma distribution is proposed for monitoring the TBE and detecting a deterioration in a process.	A one-sided DGWMA-TBE chart with a **time-varying control limit** is proposed for monitoring the TBE and detecting a deterioration in a process.
A brief discussion is included to answer the question, why the main focus is on constructing a one-sided chart and refer to scholarly works to support this idea. The reasons provided with	No justification is provided for the unbiasedness of the proposed DGWMA-TBE chart. One may raise the question that

respect to the biasness of the chart are supported by Chakraborty et al. (2017).	why a one-sided chart is considered, and the response is related to the biasness of a control chart in SPC.
The GWMA-TBE, EWMA-TBE, and Shewhart-TBE charts have been considered as "limiting cases" of the proposed DGWMA-TBE chart. The performance comparison is conducted between the DGWMA-TBE, GWMA-TBE, EWMA-TBE, and Shewhart-TBE charts. Further, the DEWMA-TBE is considered and discussed as the "special case" of the DGWMA-TBE chart.	The DEWMA-TBE chart is mentioned as the "special case" of the DGWMA-TBE chart, and the performance comparison is conducted only between the DGWMA-TBE, GWMA-TBE, and DEWMA-TBE charts. Note that, the EWMA-TBE and Shewhart-TBE charts are not included in the performance comparison, i.e., OOC performance. Hence, the conclusion made by authors that the DGWMA-TBE chart is efficient in detecting moderate and large shifts is questionable. The EWMA-TBE and Shewhart-TBE charts are more effective and superior to the DGWMA-TBE chart in detecting moderate and large shifts, respectively in the SPC literature.
The range for the parameters q_1 and q_2 are selected as (0,1) (see page 5, line 53). Sheu and Hsieh (2009) proposed the DGWMA chart for the first time in the SPC literature under the normal distribution and also defined the range for the aforementioned parameters as (0,1).	The range for the parameters q_1 and q_2 are selected as [0,1).
Authors concluded that the weights for the GWMA-TBE and DGWMA-TBE charts follow a two-parameter discrete Weibull distribution. The same type of distribution is mentioned in Chakraborty et al. (2017) for the GWMA-TBE chart. The distribution of the weights plays a major role in increasing the sensitivity of a chart in detecting shifts.	The distribution of the weights is not mentioned by the authors. A reader may raise a question that what is the effect of the distribution on the performance of the proposed DGWMA-TBE chart?
To check the convergence rate for the weights, the chart parameters are selected as $q = 0.5, 0.7, 0.9$ and $\alpha = 0.5, 0.9, 1.3$. Same set of values are used in Chakraborty et al. (2017).	To check the convergence rate for the weights, the chart parameters are selected as $q = 0.7, 0.8, 0.85, 0.9$ and $\alpha = 0.6, 0.8, 0.9, 1.1$.
A brief discussion is provided on two different cases of the DGWMA-TBE chart. The first case is referred to the DGWMA-TBE chart (Case 1) with four parameters, i.e., q_1, q_2, α_1, α_2, whereas the second case is referred to the DGWMA-TBE chart (Case 2) when two parameters are involved, i.e., $q_1 = q_2 = q$	Authors only focused on the case where two parameters are involved for the DGWMA-TBE chart, i.e., DGWMA-TBE (Case 2). The DEWMA-TBE chart where the parameters are set equal to each other is considered and no information is

and $\alpha_1 = \alpha_2 = \alpha$. The conclusion is that in some cases the DGWMA-TBE chart with four parameters outperforms the DGWMA-TBE chart with two parameters due to its flexibility gained by additional parameters. Further to this, two cases for the DEWMA-TBE chart as a "special case" of the DGWMA chart based on the equality and/or inequality of the chart parameters are discussed in detail. The charting statistic for the DEWMA-TBE chart is presented.	provided in terms of the DEWMA-TBE chart when the parameters are not equal.
The terms Case K (i.e., when the parameters are known) and Case U (i.e., when the parameters are unknown) have been used through the manuscript. These are common terminologies used frequently amongst SPC researchers.	Authors used case I and case II instead of Case K and Case U.
The exact approach has been considered and discussed in detail for the DGWMA-TBE chart in addition to the Markov chain and Monte Carlo simulation method to calculate the run length distribution of the chart. To the best of authors knowledge, the methods are investigated for the first time in the SPC literature for the DGWMA chart.	The Monte Carlo simulation is the only method used by the authors to calculate the run length distribution of the DGWMA-TBE chart.
The values for the parameters q (0.5, 0.6, 0.7, 0.8, 0.9, and 0.95) and α (0.5, 0.6, 0.7, 0.8, 0.9, 1.0, and 1.3) are chosen exactly the same as the ones from Chakraborty et al. (2017). This is done to conduct a fair and reliable performance comparison between the GWMA-TBE and the DGWMA-TBE charts.	Authors decided to exclude some of these values for the chart's parameters and select q as 0.7, 0.8, 0.85, and 0.9 and α as 0.6, 0.7, 0.8, 0.9, 1.0, and 1.1.
Results for the GWMA-TBE, EWMA-TBE, and Shewhart-TBE charts are compared with those obtained by Chakraborty et al. (2017) to ensure the validity of the algorithm developed in R and the reliability of results.	Results are not compared for the similar chart, i.e., the GWMA-TBE chart, proposed by the Chakraborty et al. (2017).
Other percentiles, i.e., 5^{th}, 25^{th}, 50^{th}, 75^{th}, and 95^{th}, as well as the ARL and the SDRL are calculated and included in the manuscript.	Results provided in terms of the run length distribution are only limited to the calculation of the ARL and the SDRL.
Authors concluded that the DGWMA-TBE chart is more sensitive than other charts, i.e., the GWMA-TBE and the EWMA-	Authors concluded that the GWMA-TBE chart is more sensitive than the proposed DGWMA-TBE chart in detecting tiny

TBE charts when tiny shifts occur in the process. The conclusion is accurate and reliable since Sheu and Hsieh (2009) mentioned that the DGWMA-TBE chart outperforms the GWMA-TBE chart in detecting tiny shifts in the process.	shifts in the process. Although one can select the parameters for the GWMA-TBE in a manner to outperform the DGWMA-TBE chart for tiny shifts. However, in general, the DGWMA-TBE chart frequently outperforms the GWMA-TBE chart in detecting tiny shifts.
Authors concluded that, the DGWMA-TBE chart outperforms the GWMA-TBE chart for tiny shifts and the GWMA-TBE chart outperforms the DGWMA-TBE chart for moderate to large shifts.	Authors concluded that the GWMA-TBE chart outperforms the DGWMA-TBE chart for tiny shifts and vice versa for moderate to large shifts. In order to make a correct and reliable decision, it's important to mention that in all of the articles published and available in the SPC literature where the performance between the GWMA and DGWMA charts is of interest, researchers concluded that the DGWMA charts are more effective and efficient in detecting tiny shifts in the process in comparison to the GWMA charts.

Chapter 1 Introduction

"Quality is everyone's responsibility."

W. Edwards Deming

1.1 Introduction

The task of quality control (QC) is of fundamental importance in any manufacturing process. When a change in the process causes misleading results, this alteration should be detected and corrected as soon as possible. Statistical process control (SPC) is a collection of scientific tools developed and engineered for detecting shifts in the output of a production process originating from special causes in the process at the earliest time, diagnose the cause and eliminate it or perhaps accommodate it by adjusting process settings. The relationship between "quality" and "variation" is summarized in Montgomery (2013) as: "Quality is inversely proportional to variability". This statement demonstrates the contribution of statistical methods to quality improvements

Dr. W. A. Shewhart introduced the most commonly used tool in SPC known as the control chart (i.e., Shewhart-type charts). Since then and over the past century, the development and application of control charts has gained enormous popularity in different disciplines such as health care systems, internet traffic flows and other which laid the foundation of SPC. The SPC literature has witnessed a rapid increase in research with new, innovative charts being developed and implemented by considering the following aspects: 1) underlying process distribution (when the distribution is known then parametric charts are applicable, whereas for unknown or undefined distribution, nonparametric charts are desirable), 2) aspect(s) of the underlying process distribution (whether to monitor the process location parameter and/or the process dispersion parameter), 3) Case K v.s. Case U (the former referred to the case when the parameters of the underlying distribution are known, whereas the latter referred to the case when the parameters are unknown), 4) sample size (individual observations vs. rational subgroups) and 5) one-sided vs. two-sided charts. Shewhart-type charts are effective and highly sensitive for large shifts in production processes, but less effective and insensitive for detecting small or tiny changes, since the past information is ignored and only the present information of the process is considered. This blind spot allows process shifts smaller than one standard deviation to continue undetected, thereby incurring larger total costs for manufacturers. Many production processes are producing very low levels of

nonconforming items in the manufacturing industry due to the development of technological advancements and automation. Note that the element of time is also essential in deciding to detect a large or small shift in the process. Hence, a small shift that persists for a long time through failing to be detected may incur a larger total cost than detecting a large shift.

To overcome this drawback, the recommendation is to consider time-weighted charts, also known as the memory-type/memory-based control charts. Time-weighted charts use all the information from the start until the most recent sample/observation to decide if a process is in-control (IC) or out-of-control (OOC). These charts include, but not limited to, the Uniformly Weighted Moving Average (UWMA), the Exponentially Weighted Moving Average (EWMA), the Double Exponentially Weighted Moving Average (DEWMA), the Exponentially Generally Weighted Moving Average (EGWMA), the Cumulative Sum (CUSUM) and the Generally Weighted Moving Average (GWMA). These charts have been considered in the SPC literature as alternatives to memory-less charts (i.e., Shewhart-type), and monitor the state of a process by combining present and past information. The memory-saving feature of these charts makes them more efficient and reliable for detecting small or tiny shifts originating from special causes in the production process. Roberts (1959) proposed the EWMA chart for monitoring process location parameter. The CUSUM chart was introduced by Page (1954) for monitoring change detection in the process location parameter based on cumulative sums, instead of individual means. CUSUM charts are useful and sometimes more naturally fitting in the process control environment in view of the sequential nature of data collection. CUSUM was proposed a few years after Wald (1947) developed the sequential probability ratio test (SPRT). The CUSUM chart properties are discussed in detail by Hawkins and Olwell (1998). Hawkins et al. (2003) brought a new perspective to the standards unknown case by the introduction of the change-point model. The full literature review for the time-weighted charts under consideration is provided in Section 1.3.

Sheu and Hsieh (2009) proposed the Double Generally Weighted Moving Average (DGWMA) chart for the normal distribution (denoted by DGWMA-$\bar{X}$) by combining the DEWMA-$\bar{X}$ chart developed by Shamma and Shamma (1992) and the GWMA-$\bar{X}$ chart proposed by Sheu and Lin (2003). The DGWMA chart is a generalized type of time-weighted chart that includes the DEWMA chart as a special case, and the GWMA, EWMA, EGWMA and Shewhart-type charts as limiting cases. The DGWMA chart is more sensitive than other time-weighted charts in detecting small or tiny shifts (i.e., less than one standard deviation in the location) in the process due to the implementation of the double exponential smoothing technique proposed by Brown (1962).

Given the multifaceted structure of SPC, it is essential that a researcher accurately describes the context in-depth and the exact nature of his research with the SPC environment. Hence, the focus of the current thesis is as follows:

By acknowledging that variation is present in process outcomes, and that they are to some extent uncertain, the current thesis is concerned with improving the methodologies of existing control charts , employ methods which take uncertainty explicitly into account and develop new charts; more specially, on univariate parametric and nonparametric DGWMA Phase I and Phase II charts (for sample of size $n > 1$) when process parameters are known and unknown, where the former is known as Case K and the latter is known as Case U in the SPC domain.

It is important to notice that only the key aspects of SPC terminologies are covered in the next section to equip the interested reader with the essential principals to provide an in-depth understanding for the rest of this thesis. Also, note that, new charts are constructed for sample sizes of $n > 1$. In SPC, frequently, the phrases "random sample" and "rational subgroup" are used interchangeably, however strictly speaking, a random sample is not necessarily a rational subgroup. For more information, the interested reader is referred to Montgomery (2013).

Further, the study of the DGWMA chart weighting structure is of extreme importance that is rarely considered in the SPC literature. The shape for the weights is dependent of the type of probability mass function (p.m.f.) under consideration. This implies that different choices for the p.m.fs result in changes in chart's performance in detecting tiny shifts. This area is covered in this thesis (see Chapter 3) in detail. To the best of our knowledge, the discrete Weibull distribution is the only distribution available for the weights of the GWMA and the DGWMA charts in the literature. As a result, the study in Chapter 3 based on the new p.m.fs for the weights can be considered as a pioneer work in SPC.

A brief overview of SPC and all the core concepts and general definitions within this context are furnished in Section 1.2. A literature review for different weighting schemes is provided in Section 1.3 with a bibliometric analysis (1956 – 2019) which also includes the DGWMA chart to illustrate the value and importance of the current research. The scope and main objectives of the thesis are presented and outlined in Section 1.4. A road map and general recommendations in terms of selecting the correct control chart conditional on the magnitude of the shift (large, medium, small or tiny) in the process and given the distributional assumption (i.e., parametric control chart) are laid out for practitioners in Section 1.5. Further to this, the relationship between time-weighted (memory-type) and memory-less (Shewhart) charts are portrayed in Figure 1.2, that is missing from the current SPC literature.

1.2 Preliminaries

In this section, a brief introduction to SPC concepts and fundamentals is provided to aid the interested reader to familiarize and study the preliminaries more thoroughly for the rest of this thesis. Two important concepts, namely, “common causes of variation” and “special causes of variation”, will be discussed.

1.2.1 Statistical process control

SPC is a collection of scientific tools and statistical procedures developed and engineered to execute quality control in a production process. The variation in production processes occurs frequently – for example, during the manufacturing process of fluted stem glass, the length, or the diameter of any two glasses will not be similar. In general, two types of variations exist during the production process, namely chance (or common) causes of variation and assignable (special) causes of variation. The common causes of variation are defined as the variability that is inherent in the process and should be relatively small. Nevertheless, the presence of special causes of variation are extraneous to the process and influence the performance of the underlying process, changing process parameters like location and/or dispersion. There are numerous applications of SPC that can be found in areas outside the classical manufacturing field. In recent times, SPC tools have been applied to enhance network monitoring (Woodall et al., 2017) and data quality (Jones-Farmer et al., 2014). Lizarelli et al. (2016) surveyed the topics about SPC from the Web of Science (WOS) database as: operations research and management science, engineering, business and economics, computer science and mathematical methods in social sciences.

1.2.2 Control charts

Nowadays, it is essential and often of interest to detect any changes in the process location and/or dispersion parameters at the earliest time. To trigger the presence of the special causes of variation in the process and to maintain the stability of a process, SPC possesses some of the most extensively used techniques. Dr. W. A. Shewhart introduced the most commonly used tool in SPC, known as the control chart (Shewhart-type charts), and laid the foundation of SPC (see Shewhart (1931) and Shewhart (1939)). The design and implementation of control charts are effective in detecting changes from an in-control (IC) state to an out-of-control (OOC) state in the process. The control chart is a plot of a sequence of values based on a plotting statistic calculated from a sample of measurements. Thereafter, these points are plotted against three horizontal reference lines: the upper control limit (*UCL*), the centerline (*CL*), and the lower control limit (*LCL*) versus time. The common causes of variation are present in the process if a plotting statistic plots within the control limits (*LCL* and *UCL*), hence the process is considered IC. The special causes of variation exist in the process if a plotting statistic plots on or outside either of the limits, and as a result the process is declared OOC. The underlying process

distribution and the parameter(s) under consideration are two important factors that decide whether to use a one- or two-sided chart.

1.2.3 Control chart properties

The False Alarm Rate (denoted by *FAR*), also known as Type I error (denoted by α), is the probability that an IC data points would appear as an OOC in the process. In SPC literature, the control limits (i.e., *UCL* and *LCL*) are selected in such a way that *FAR* is very small (0.0027 or less). The power of a control chart is defined as the probability of the OOC data points falling outside the control limits. The power of a control chart should be as high as possible in order for a chart to detect the OOC data points.

The most common and well-known measure for evaluating a chart performance is the run length distribution and can be used as an alternative approach to *FAR* for studying the performance of a chart in detecting varying shifts during the monitoring stage of the process parameters. The run length is defined as the number of plotting statistics that must be plotted so that the control chart signals for a shift in the process and is a discrete random variable (denoted by N). The expected value or the average of the run length random variable is symbolized by ARL. Further, the ARL is classified into two different cases: the IC ARL (denoted by ARL_0) and the OOC ARL (labelled as ARL_1). ARL_0 is defined as the expected number of plotting statistics to be plotted until a control chart detects an OOC signal when the process is under statistical control (IC). ARL_1 is defined as the expected number of plotting statistics to be plotted until a control chart detects an OOC signal when the process has shifted to an OOC value. Note that the smaller the value for the FAR, the higher the value for the ARL_1, as the control limits will be wider. For a practitioner to design an optimal control chart, a sufficiently large ARL_0 is required, and on the contrary a sufficiently small ARL_1 so that the chart detects shifts rapidly when the process is OOC. Hence, to find an optimal chart, the ARL_0 and ARL_1 must be balanced. The procedure to design and implement a control chart involves the calculation of the chart parameters (design parameters) to acquire a desired value for the IC ARL labelled as ARL_0^*, such that $ARL_0 \approx ARL_0^*$. Other characteristics of a run length distribution, including the standard deviation of run length (denoted by $SDRL$) and the percentile points (denoted by P_i, i = 5, 25, 50, 75, 95), further describe the behavior of the run length.

1.2.4 Control chart classification

There are various factors involved in choosing a control chart to monitor the output of a production process. These factors could be the type of application, the type of data, the ease and cost of sampling, the process parameters (Case K versus Case U), the number of quality characteristics (individual observations vs. rational subgroups), and the underlying process distribution, amongst others.

Univariate control charts are used to monitor a single quality characteristic in the process, whereas multivariate charts are considered for multiple quality characteristics.

The assumption for the parameter(s) of interest (known or unknown) creates two different scenarios in the SPC literature. If the process parameters are known, the case is referred to as Case K; whereas if the process parameters are unknown, then an estimation is required from an IC reference sample obtained from Phase I. The first case is known as the "standard known" (labelled as Case K) and the other is called the "standard unknown" case (categorized as Case U). Further, control chart process monitoring works under two different phases: Phase I (retrospective phase) and Phase II (prospective phase). Practitioners estimate the unknown parameters from the reference sample (calibration sample) that is time-ordered in Phase I. Then, the determination of the design parameter(s) as well as assessing the stability of a process are considered. The monitoring stage of the process using the estimated control limits obtained from Phase I is performed in Phase II. One of the main differences between Phase I and Phase II is the fact that the FAR is typically used to construct and evaluate Phase II charts, whereas the False Alarm Probability (FAP) is used to construct an evaluate Phase I charts. Phase I charts have been studied by numerous authors; see for example, King (1954), Sullivan and Woodall (1996), Champ and Jones (2004) and Koning (2006).

The control chart can also be classified into variable and attribute charts based on the type of data available in the process. A variable chart is considered if the quality characteristic is continuous – for some examples, see the Shewhart $\bar{X}$, R and S charts (Shewhart, 1931, 1939). An attribute chart is considered if the quality characteristic is discrete – see the p-chart, np-chart, and c-chart for examples. Time-weighted charts are considered for both discrete and continuous quality characteristics, and the advantage is that they use the combination of past and present information to monitor the state of a process.

The underlying process distribution also plays a vital role in the classification of control charts in SPC, which are divided into parametric and nonparametric. Most of the literature in SPC is based on the parametric charts, which implies that the underlying process distribution is known (typically assuming the normal distribution). However, in practice, the distributional assumption and in particular the assumption of normality may not be justified or valid when the observations are from an unknown or non-normal distribution. To overcome the limitation of the parametric charts, nonparametric or distribution-free charts have been proposed as alternatives to monitor a process. In general, if the IC run length distribution is the same for all continuous distributions, the chart is called nonparametric. For an in-depth bibliography on the nonparametric charts, the interested reader may consult the work of Gibbons and Chakraborti (2010), and Chakraborti et al. (2011).

1.2.5 General notation

The general notation for the construction of different charts that will be used in this thesis is discussed in this section. Let X_{ij} denotes the j^{th} observation in the i^{th} observation sample, where $i = 1, 2, \dots, m$ and $j = 1, 2, \dots, n$, where m independent random samples, each size $n \geq 1$ taken sequentially over time from a process with a continuous cumulative distribution function (c.d.f.), denoted by $F\ (x;\ \underline{\theta})$, where F is a known function and $\underline{\theta} = (\theta_1, \theta_2, \dots, \theta_k)$, $k \geq 1$, is a vector of parameters (Case K or Case U), hence $X_{ij} \sim i.i.d\ F\ (x;\ \underline{\theta})$. The sample statistic T_i is a function of the observations with a continuous c.d.f., denoted by $G(.)$, and it depends on the underlying distribution of X_{ij} $(F(.))$. The sample statistic follows an underlying distribution with the mean (target value) μ_T and the variance σ_T^2.

The plotting statistic Z_t is calculated based on the parameter of interest for $t = 1, 2, \dots$, from each sub-group. A plotting statistic Z_t with a continuous c.d.f., denoted by $H(.)$, is used to monitor a process which is typically a function of the observations and a function of the sample statistic. To comment on the state of a process, a comparison is performed between the plotting statistics and the control limits *UCL* and *LCL*. If a plotting statistic plots within the control limits the process is IC, whereas the process is declared to be OOC if a plotting statistic plots on or outside either of the limits.

The properties of a control chart are as follows:

$$\begin{aligned} UCL &= \mu_T + L\sigma_T \\ CL &= \mu_T \\ LCL &= \mu_T - L\sigma_T. \end{aligned} \tag{1.1}$$

where $L > 0$ is the charting constant that determines the distance between the centerline and the exact or steady-state limits.

For a symmetric underlying process distribution, the control limits are based on the tacit assumption of the plotting statistic. However, in the case of asymmetric process distribution, only one-sided charts are applicable since a two-sided chart results in an *ARL*-biased chart. The plotting statistic for the Shewhart-type charts is taken as the subgroup mean or standard deviation. For example, observations from the process being monitored are assumed to be mutually independent and from a normal distribution with mean μ and variance σ^2. Therefore, for a Shewhart $\bar{X}$ chart, the control limits are given by $UCL = \mu + L\frac{\sigma}{\sqrt{n}}$ and $LCL = \mu - L\frac{\sigma}{\sqrt{n}}$, where n denotes the sample size, and $L > 0$ is the charting constant. Note that, for the Shewhart-type charts, $\mu_T = \mu$ and $\sigma_T = \sigma$.

1.2.6 Designing a control chart

The general steps involved in designing a univariate control chart are presented in Figure 1.1.

- Choose or identify the underlying process distribution (F_θ) (parametric chart)
- If the underlying process distribution is unknown or there is no information available, then it is assumed to be continuous (and in some instances symmetric) (nonparametric chart)

Example: Suppose $X_{ij} \sim i.i.d\ F_\theta$, the j^{th} observation in the i^{th} random sample, where $i = 1, 2, \dots, m$ and $j = 1, 2, \dots, n$. Non-i.i.d (autocorrelated) observations are out of scope for this thesis.

- Choose the process characteristic (e.g., the process location and/or dispersion) and the associated sample statistic. If the parameter(s) is(are) known, then Case K is considered; whereas when the parameter(s) is(are) unknown, then Case U is considered, where the parameters are estimated by using a reference sample from Phase I. Thereafter, the monitoring stage of the process using the estimated control limits obtained from Phase I is performed in Phase II.

Example: The sample statistic $T_i \sim$iid G_θ, conditional on the assumption for the underlying process distribution provided in the previous step, where G_θ denotes the distribution function of the sample statistic and $F_\theta \neq G_\theta$.

- Choose the type of a control chart – e.g., time-weighted charts or memory-less charts – that will identify the plotting (charting) statistic to be calculated.

Example: For the time-weighted charts, $Z_t = f\ (T_i)$ and $i = 1, 2, \dots, t$, which is a function of all the sample statistic. Note that, $Z_t \sim H_\theta$, where H_θ denotes the plotting statistic and $F_\theta \neq G_\theta \neq H_\theta$.

Calculate the run length distribution and its characteristics, e.g., $SDRL$ and the percentile points (denoted by P_i, i = 5, 25, 50, 75, 95), by solving for the charting constant $L > 0$ to obtain the desired performance. For evaluation purposes, choose one of these three methods: (i) the exact approach, (ii) the Markov chain method, and (iii) the Monte Carlo simulation.

Figure 1.1. Steps to design a control chart

1.3 Literature review

An increasing volume of research on SPC has emerged. There are various reasons for this growth, including but not limited to, the continuous improvement of manufacturing processes and an increase in global competitiveness generated by innovation. Lizarelli et al. (2016) mentioned that "Data analysis indicates that there was a growth rate of more than 90% in the number of publications on SPC after 1990". Hence, it is extremely important to scrutinize the literature to identify trends in SPC research and its relevance to the current research in this thesis. In this section, a brief literature review on different weighting schemes for time-weighted charts that already exist in the literature is provided. The literature review focuses on the charts exist to monitor the process location and/or dispersion for parametric and nonparametric cases. Note that, the memory-less charts, i.e., Shewhart-type, are defined as the charts that ignore past information. Alternatively, time-weighted charts use all the information from the past (i.e., the initial stage) and present (i.e., the most recent observation) to decide on the state of the process.

1.3.1 Exponential weighting

The EWMA charts have gradually achieved a significant place in SPC literature and keeps growing at a good pace. Numerous designs and innovations have been introduced by the researchers in the structure of EWMA charts for monitoring process location and/or dispersion parameter(s).

The EWMA chart – originally called the geometric moving average (GMA) chart – was introduced by Roberts (1959) to monitor a process location parameter, i.e., process mean. Roberts (1959) assumed an i.i.d normal process and calculated the run length based on the Monte Carlo simulation method. As a result, the author concluded that the EWMA chart cannot improve the Shewhart chart in detecting large shifts in the process parameter. However, the EWMA chart provides greater capability in detecting relatively small shifts (less than one standard deviation). Roberts (1966) also proposed the UWMA chart that was constructed under the assumption of unweighted moving average. Since then, EWMA charts have been investigated and studied extensively by numerous researchers in the SPC literature. Robinson and Ho (1978) presented a numerical procedure based on the exact approach for the calculation of run length and its characteristics for the two-sided EWMA chart when the underlying process distribution is normal. Hunter (1986) exposited an EWMA chart technique that may be of value to both process quality engineers and manufactures. Also, the author explained the difference between the Shewhart, CUSUM, and EWMA charts in terms of weighting to the historical data. Crowder (1987) concluded that computational considerations and ease of use favor the exact approach over the method given by Robinson and Ho (1978). Also, the exact approach can be extended to non-normal distributions. Crowder (1989) reviewed the design strategy of EWMA charts and provided recommendations

for design parameters. Lucas and Saccucci (1990) evaluated the properties of an EWMA chart for monitoring the location parameter of a normally distributed process. A design procedure in terms of using uncommon parameter values in the literature is given. In addition, several enhancements to EWMA charts are developed that include, a fast-initial response feature, a combined Shewhart-EWMA chart that is effective in detecting both large and small shifts in a process, and an EWMA chart that detects outliers in a process. The EWMA chart has received a great deal of attention in the SPC literature. See, for example, Jones et al. (2001), Jones (2002), and Simoes et al. (2010). Lucas and Saccucci (1990) compared the average run length of CUSUM and EWMA charts over a range of parameter values and concluded that there is a little practical difference between the run length properties of the two charts. Numerous studies have compared the performance of the EWMA and CUSUM chart, see for example Hawkins and Wu (2014) and Zwetsloot and Woodall (2017). Zwetsloot and Woodall (2017) concluded that the general belief that the CUSUM and EWMA charts have similar performance no longer holds under estimated parameters. Hawkins and Wu (2014) compared the CUSUM and EWMA charts and concluded that depending on the shift size either the CUSUM or the EWMA chart can provide quicker detection. Steiner (1999) and Abbasi (2010) studied the difference between EWMA charts based on exact and steady-state limits. The interested researcher and practitioner may consult the research conducted by Ruggeri et al. (2007) for an in-depth literature review of EWMA charts. Recently, researchers focused on a mixed type charts to improve the performance of EWMA and CUSUM charts. Abbas et al. (2013) proposed the mixed EWMA-CUSUM for monitoring of the manufacturing process. Authors concluded that this type of chart performs better than existing EWMA and CUSUM charts. Haq (2013) developed a chart using two EWMA statistics, called hybrid EWMA (denoted by HEWMA) chart. More details about the designing and application of other charts can be seen in Lucas (1982), Sparks (2000), Capizzi and Masarotto (2003), Borror et al (2010), Wu et al. (2009) and Aslam et al. (2014).

Nonparametric charts are proposed as opposed to their parametric counterparts when the underlying process distribution is unknown or there is no information available. Distribution-free (nonparametric) versions of the EWMA charts (labelled as NPEWMA) have also been discussed and investigated thoroughly in the literature. Amin and Searcy (1991) introduced the NPEWMA chart for monitoring the median of a symmetric continuous distribution based on the Wilcoxon signed-rank statistic. Li et al. (2010) developed a nonparametric analog of the EWMA chart based on the Wilcoxon signed-rank statistic for monitoring process mean shifts. Graham et al. (2011a) used Markov chain and Monte Carlo simulation approaches to compute the run length distribution and the associated performance characteristics. Detailed recommendations and hints for selecting the design parameters of the proposed chart are provided for practical implementation. Graham (2011b) proposed a two-sided NPEWMA chart for i.i.d individual observations based on the nonparametric sign statistic. Monte Carlo simulation and Markov chain approaches are used to determine the run length distribution and the associated performance characteristics. Guidelines and recommendations are provided in order to aid practical implementation.

Yang et al. (2011) proposed a NPEWMA chart for detecting a shift in the process proportion based on the nonparametric sign statistic. The run length distribution and the associated characteristics of the proposed chart are derived through the Monte Carlo simulation. Haq (2017a) developed a distribution-free EWMA chart for monitoring the shifts in the process variability based on the NPEWMA chart suggested by Yang and Arnold (2015). Extensive Monte Carlo simulations are used to compute the run length distribution of the proposed chart.

The main objective of the scholarly works discussed so far is to monitor the process location parameter. It is important to monitor the process dispersion since in most practical applications a decrease in the process variance leads to an improvement in the process, while an increase in the process variance deteriorates the process. There is a numerous research conducted for the design and implementation of charts that monitor the process dispersion since identifying shifts in a process dispersion is a crucial ingredient of SPC in order to improve process productivity and product quality. Monitoring process variability fall into two categories. The first category utilizes a monotone function to transform the sample variance into a normal distribution. The logarithmic transformation has been widely implemented due to its simplicity. See, for example, Crowder and Hamilton (1992) and Chen et al. (2001). The second category accumulates mean-squared or sample variance from the target by EWMA statistics. The EWMA charts for dispersion have been studied and investigated by Wortham and Heinrich (1972), and Wortham and Ringer (1971). Ng and Case (1989) presented a systematic approach for the EWMA chart for monitoring the process mean and dispersion and the run length is determined by the Monte Carlo simulation. For the individual observations, the Exponentially Weighted Moving Variance (denoted by EWMV) and the Exponentially Weighted Mean Square Error (denoted by EWMS) charts have been advocated by MacGregor and Harris (1993) to monitor the process variability/dispersion. Shu and Jiang (2008) proposed an EWMA chart for monitoring a process variability by using a logarithmic transformation. A Markov chain approach is considered to calculate the run length and its characteristics. Abbasi and Miller (2012) analyzed the performance of different charts based on different estimates for the standard deviation. The performance is investigated under the existence and violation of normality assumption. Abbasi and Miller (2013) proposed an EWMA chart for efficient monitoring of process dispersion based on estimating the process standard deviation using the mean absolute deviation taken from the sample median. A Monte Carlo simulation is considered to calculate the run length of the proposed chart. Abbas et al. (2013) proposed two memory-type charts for monitoring the process dispersion. The *ARL* performance of the charts is evaluated through a Monte Carlo simulation and is also compared with the CUSUM chart. Haq (2017b) proposed EWMA charts using the auxiliary information for monitoring the process dispersion. The run length profiles of proposed charts are computed through an extensive Monte Carlo simulation. Sheu et al. (2009) proposed a chart for monitoring the

process mean and the process variability simultaneously (known as location-scale). Recently, considerable attention has been drawn toward methods that use a single chart for monitoring the process mean and variability. Domangue and Patch (1991) proposed some omnibus EWMA charts for detecting shifts in both the location and the spread. Chen and Cheng (1998) developed the location-scale max chart, which plots maximum absolute values of the standardized mean and standard deviation on a single chart.

1.3.2 Sequential weighting

The CUSUM chart was introduced by Page (1954) for monitoring change detection in the process location parameter based on cumulative sums, instead of individual means. CUSUM charts are useful and sometimes more naturally fitting in the process control environment in view of the sequential nature of data collection. CUSUM was proposed a few years after Wald (1947) developed the sequential probability ratio test (SPRT). In his book, *Sequential Analysis* Wald (1947) gives an approximate formula for the operating characteristic of a sequential test or, equivalently, for the probability that a particle performing a linear random walk between two absorbing barriers is absorbed by a specific barrier. A chart constructed based on a SPRT is effective when the interests is in detecting both small and large shifts in process parameters. Stoumbos and Reynolds (1996) proposed an SPRT chart for monitoring the process mean of a normal distribution. They concluded that the proposed chart outperforms the Shewhart-type and CUSUM charts. For early developments of CUSUM charts, see for example, Gibra (1975), van Dobben de Bruyn (1968) and Wetherill (1969). Zhang et al. (2014) focused on the economic design of the SPRT chart for short-run production. Chou et al. (2006) proposed a SPRT chart to monitor the process dispersion when the underlying process distribution is normal. Ou et al. (2015) proposed a SPRT chart for monitoring the process mean and variance simultaneously (i.e., location-scale). Hawkins and Zamba (2005) mentioned that the CUSUM chart has attractive optimally properties for the detection of step changes in parameters. Early evidence of research in nonparametric SPC mainly capitalized the asymptotic theory of sequential analysis, see, for example, Bhattacharya and Frierson (1981).

Nevertheless, the analogy between the CUSUM control chart and the SPRT provides a useful insight in the theoretical foundations of the CUSUM chart. The SPRT technique is extensively used for system monitoring and early detection of shifts in the process. SPRT is well-known and commonly used for quality control applications, in industries and areas requiring a highly sensitive and especially fast detection of degradation behavior. The mathematical expressions for SPRT are derived under two assumptions: (1) The samples follow a-priori known distribution function and (2) The samples are i.i.d. For example, consider a sequence of values $\{Y_n\} = y_0, y_1, \dots, y_n$ resulting from a stationary process and data follows a normal distribution with mean μ_0 and variance σ_0^2. μ_0 and σ_0^2 are referred to as IC parameters. Since the objective of this research is to monitor a shift in the location parameter, we only

discuss the case when there is a shift occurred in the process and the OOC mean is denoted by μ_1. More explicitly, the null and alternative hypothesis could be written as:

$$H_0: \mu_0 = \mu_1$$

$$H_1: \mu_0 \neq \mu_1$$

The likelihood ration (LR) is the ratio of probabilities for observing the sequence $\{Y_n\}$ under an alternative hypothesis, versus the null hypothesis as follows:

$$LR(n) = \frac{P(y_1, \dots, y_n|H_1)}{P(y_1, \dots, y_n|H_0)}$$

At each step of the $\{Y_n\}$ sequence, SPRT calculates a test index as the natural log of LR, referred to as LLR and compares it to two stopping boundaries:

$$LLR(n) = \log\big(LR(n)\big)$$

$$\log(A) < LLR(n) < \log(B)$$

H_0 is rejected if $LLR \geq \log(B)$. As long as LLR remains between these two boundaries there is not enough evidence to reach a conclusion. The decision boundaries are derived from the following equations:

$$A = \frac{\beta}{1-\alpha} \qquad and \qquad B = \frac{1-\beta}{\alpha};$$

where α and β are referred to as type I error and type II errors, respectively.

For the normal distribution and under condition mentioned above, the expression for LR is as follows:

$$LLR(n) = \frac{(\mu_1 - \mu_0)}{\sigma_0^2} \sum_{i=1}^{n} y_i - \frac{n}{2\sigma_0^2}(\mu_1^2 - \mu_0^2)$$

Note that, for the alternative hypothesis, $H_1: \mu_0 \neq \mu_1$, two cases are possible such as : $H_1: \mu_0 < \mu_1$ and/or $H_1: \mu_0 > \mu_1$. The former case is used when the practitioner is interested in detecting an increase in the process location parameter and as a result an upper-sided chart is constructed. For the latter case, i.e., $H_1: \mu_0 > \mu_1$, the practitioner is interested in detecting a decrease in the process location parameter and as a result a lower-sided chart is constructed. For two sided charts, i.e., $H_1: \mu_0 \neq \mu_1$, the practitioner could detect negative as well as positive changes in the process location parameter. Note that the discussion provided here is only applicable when the practitioner is interested in detecting a shift in the process location parameter.

The *ARL* of all the charts depends on the underlying process distribution, true location parameter, and true standard deviation of the process as well as the values of the chart constants, e.g., reference value and decision interval for CUSUM. Hawkins et al. (2003) brought a new perspective to the standards unknown case by the introduction of the change-point model when the underlying process distribution is normal. Also, there have been developments for the nonparametric case for monitoring the process

location parameter by Hawkins and Deng (2010). Hawkins and Zamba (2005) mentioned that the IC process location and scale parameters are seldom known and recommended modeling a persistent shift in the process location parameter by $X_i \sim \begin{cases} N(\mu_1, \sigma^2) & i \leq \tau \\ N(\mu_2, \sigma^2) & i > \tau \end{cases}$, $X_1, X_2, \ldots, X_i, \ldots$ are the sequential process readings, μ_1 is the IC process mean, μ_2 is the OOC value to which the process mean shifts, τ is the changepoint, and σ is the standard deviation of the process, assumed to be constant. Hawkins and Zamba (2005) developed a chart based on a variance change-point methodology and the likelihood ratio test for detecting a shift in the variance. They concluded that using the change-point model in SPC leads to testing for the presence of a shift and estimating the parameters. Zamba et al. (2008) applied a sequential Bayesian model for early detection of intentional outbreaks. Zamba and Hawkins (2006) developed a multivariate chart based on unknown-parameter change-point approach that outperformed the estimated-parameter T^2 chart and having a much faster response to medium sized shifts as well as large shifts. Zamba and Hawkins (2009) developed a multivariate change-point model to detect shifts for an unknown mean vector and/or covariance based on the generalized likelihood-ratio statistics applied sequentially.

Hawkins (1992) studied the evaluation of *ARL* for CUSUM chart with an arbitrary data distribution. Since then, the CUSUM chart have been studied and developed by numerous researchers. Barnard (1959) suggested a new approach to construct a control chart for industrial processes. Ewan and Kemp (1960) constructed a CUSUM chart for monitoring the location parameter when the underlying process distribution is normal. Johnson (1961) developed a theoretical approach to obtain an approximate formula for the CUSUM chart. Johnson and Leone (1962a) considered simultaneous applications of SPRT to test a null hypothesis against two separate alternative hypotheses and thereafter the decision lines are used to construct a CUSUM chart when the underlying process distribution is normal. Johnson (1966) extended the Johnson and Leone (1962) procedure to a CUSUM chart under the Weibull distribution. Goldsmith and Whitfield (1961) computed the run length distribution of the CUSUM chart when the underlying process distribution is normal and either independent or serially correlated class. Ewan (1963) described and reviewed CUSUM charts by emphasizing on the practical aspects of successful application. Goel and Wu (1971) calculated the run length distribution and its associated characteristics of a CUSUM chart by solving the systems of linear equations to approximate the exact approach. Numerical results are provided for monitoring the process mean when the underlying process distribution is normal by a nomogram and guidelines in terms of design parameters are discussed in detail. Chiu (1974) proposed an economic design of CUSUM charts for monitoring the process mean when the underlying process distribution is normal. A simplified version of the algorithm is devised which is suitable for application purposes. Yang and Cheng (2011) introduced the CUSUM mean chart to illustrate the superiority of the proposed chart compared to other charts when the underlying process distribution is unknown. Li et al. (2016) proposed two CUSUM charts that perform well for the joint

monitoring of the mean and variance when the parameters of the underlying process distribution are unknown (Case U). A comprehensive simulation study is studied to examine the performance of the charts. Also, beneficial recommendations are provided for the practitioners. There is a plethora of research on the joint monitoring charts. Some scholars addressed monitoring the mean and variance simultaneously (i.e., location-scale) on a single chart, see for example, Chen et al (2001), Wu et al. (2010), Zhang et al. (2011), and the references therein. For a more complete exposition of CUSUMs in general, see Hawkins and Olwell (1998). For more literature on the CUSUM charts for monitoring the process dispersion, see Tuprah and Ncube (1987), Chang and Gan (1995), Acosta-Mejia (1999), Knoth (2006), Castagliola et al. (2009), and the references therein.

CUSUM charts discussed thus far are designed for monitoring the process location parameter. However, in several industrial applications it is important to monitor the process variability as well. Hawkins (1981) developed for employing the CUSUM procedure for monitoring the process dispersion parameter. The author has shown that for both normal and heavy-tailed distributions centred around zero, the square root of the absolute value gives a random variable whose distribution is approximately normal. Thus, the quality control on the spread of a process may be carried out effectively through CUSUM methods designed for detecting shifts in the process location parameter when the underlying process distribution is normal. Hawkins (1993) concluded that the EWMA and the CUSUM chart are effective in detecting shifts, however, the CUSUM chart is a little better for the diagnosis of when the shift occurred. Hawkins and Olwell (1997) developed a location-scale CUSUM chart under the inverse Gaussian distribution and evaluates its performance in detecting step shifts in each of the parameters.

McGilchrist and Woodyer (1975) developed a nonparametric CUSUM chart (denoted by NPCUSUM) for detecting a shift in the median of a rainfall distribution when the underlying process distribution is normal, and the process parameter is known. Bakir and Reynolds (1979) proposed a NPCUSUM chart based on Wilcoxon signed-rank statistic for monitoring a shift in the process location parameter. Also, the run length distribution of the new chart is computed for any distribution for which the distribution of the Wilcoxon signed-rank statistic is known. Amin et al. (1995) proposed a NPCUSUM chart based on the sign statistic to monitor the process location parameter. These charts are denoted NPCUSUM-SN and NPCUSUM-SR, respectively. Chakraborti et al. (2004) considered a class of nonparametric Phase II Shewhart-type charts based on the so-called precedence statistics, called the precedence charts, however, the main contribution was covered in the overview paper of Chakraborti et al. (2011). Hence, CUSUM-type charts based on precedence statistics is considered in Mukherjee et al. (2013). Mukherjee et al. (2013) proposed a CUSUM chart based on the exceedance statistic (denoted CUSUM-EX).

1.3.3 Double/dual exponential weighting

The DEWMA chart with a single smoothing parameter was initially introduced by Shamma and Shamma (1992) for the process mean by implementing the double exponential smoothing technique proposed by Brown (1962). The DEWMA chart enhances the performance of the EWMA chart constructed under the single exponential technique. The DEWMA chart with two smoothing parameters was proposed by Zhang and Chen (2005) for the normal distribution to monitor the process mean. Khoo et al. (2010) further investigated the quality characteristic of interest of the DEWMA chart under the normal distribution. Zhang et al. (2003) assumed the Poisson distribution as the underlying process distribution for the DEWMA chart to monitor the process mean. Mahmoud and Woodall (2010) conducted a performance comparison between the DEWMA and EWMA charts. Alkahtani (2013) assessed the robustness of the DEWMA and the EWMA charts to non-normal processes. His study considers several symmetric non-normal distributions such as the t-distribution, and skewed distributions such as the gamma distribution. He concluded that the DEWMA chart is more robust to the non-normality assumption when compared to the EWMA chart.

The nonparametric case of the DEWMA chart (denoted by NPDEWMA) was developed by Riaz and Abbasi (2016) to ensure efficient monitoring of the process location parameter. Tsai et al. (2016) extended the NPEWMA sign chart to a DEWMA sign chart to improve the efficiency and the detection capability of the NPEWMA sign chart. Raza et al. (2015) investigated the performance of the EWMA and the DEWMA charts under censoring for the gamma distribution to monitor the process location and the process variance simultaneously (i.e., location-scale).

1.3.4 General weighting

The extended version of the EWMA chart, called the GWMA chart, was developed by Sheu and Lin (2003) for the normal distribution to monitor the process mean by applying the method of Sheu and Griffith (1996) and Sheu (1998, 199). The weights for the GWMA chart are based on the p.m.f. for the two-parameter discrete Weibull distribution proposed by Nakagawa and Osaki (1975). As a conclusion, the GWMA chart has superior detection, in comparison with the EWMA chart, for small shifts in the process mean. Sheu and Yang (2006) proposed a parametric GWMA chart for the process median. Sheu and Chiu (2007) introduced a GWMA chart by assuming the Poisson distribution as the underlying process distribution. Aslam et al. (2015) proposed a GWMA chart when the underlying process distribution follows an exponential distribution.

Chakraborty et al. (2016) proposed the nonparametric GWMA chart by implementing the signed-rank statistic when the process parameter of interest is known (Case K). An exact approach is considered to calculate the run length distribution for the proposed chart. Areepong (2015) proposed the GWMA chart for the zero-inflated Poisson distribution. Chakraborty et al. (2017) developed the parametric GWMA

chart to monitor the time between events (TBE) for the nonconforming under the gamma distribution. Chakraborty et al. (2018) constructed the nonparametric version of the GWMA chart for the process location parameter based on the exceedance statistic (EX) when the process parameter of interest is unknown (Case U).

The GWMA chart to monitor the process dispersion was proposed by Sheu and Tai (2009). Teh et al. (2012) developed a new max chart to simultaneously detect both the decrease and increase in the mean and/or variability (i.e., location-scale). Huang (2014) proposed a new chart called the sum of squares generally weighted moving average, denoted by SS-GWMA, to simultaneously detect both the increase and decrease in the mean and/or variability (i.e., location-scale).

Mohsin et al. (2016) developed a new single GWMA chart to monitor the process mean and dispersion, i.e., location-scale chart, based on Taguchi's loss function. A Monte Carlo simulation is used to calculate the run length and its associated characteristics. Haq and Ul Abidin (2018) proposed an enhanced version of the GWMA chart (denoted by AIB-GWMA) by using an auxiliary-information-base (AIB) to increase the sensitivity of the AIB-EWMA chart. The AIB-Shewhart introduced by Riaz (2008) and AIB-EWMA proposed by Abbas et al. (2014), are special cases of the AIB-GWMA chart.

1.3.5 Double general weighting

Sheu and Hsieh (2009) developed the DGWMA chart by implementing the double exponential smoothing technique and combining it with the GWMA chart to monitor the process mean for the normal distribution. Chiu (2009) and Chiu and Lu (2015) created a DGWMA chart for monitoring the Poisson observations in the process, later studying the steady-state performance of the Poisson DGWMA chart. Huang et al. (2014) proposed a DGWMA chart based on the sum of squares of the plotting statistic. These authors concluded, in their respective papers, that the DGWMA chart is more sensitive than the GWMA, DEWMA, EWMA, and Shewhart-type charts in detecting small or tiny shifts in the process. Alevizakos et al. (2018) proposed a DGWMA chart for monitoring of time between events when the underlying process distribution is gamma and the chart parameters are set to be equal (i.e., $q_1 = q_2 = q$ and $\alpha_1 = \alpha_2 = \alpha$).

Lu (2018) developed a nonparametric DGWMA sign chart to monitor the process proportion when the process parameter of interest is known (Case K). Masoumi Karakani et al. (2019) proposed a generalized nonparametric DGWMA chart (denoted by DGWMA-EX) to monitor the process median based on the EX when the location parameter of interest is unknown (Case U). The GWMA-EX and EWMA-EX charts are the limiting cases of the DGWMA-EX chart. Also, the DEWMA-EX chart is a special

case of the proposed DGWMA-EX chart. Teh et al. (2011) proposed and investigated a DGWMA chart for individual observations to monitor the process mean and the process variance simultaneously.

1.3.6 Bibliometric analysis for the DGWMA chart

An increasing number of papers on time-weighted charts has emerged in the past decade due to the fundamental role that SPC plays in quality and production processes. In this sense, it is essential to understand what has been done, and identify the research gaps that exist in the current SPC research. The WOS database, is a well-known reliable resource for researchers in scientific fields and it covers research from most of the well-known scientific resources including more than 15 thousand journals and 55 million articles. This database is used in this section to conduct a bibliometric analysis for the DGWMA chart from 1956 to 2019. The main objective of this analysis is to use bibliometrics to analyze the availability and growth of the EWMA, DEWMA, CUSUM, GWMA and DGWMA charts and uncover the areas that require further research. Advanced search methods were used to retrieve the keywords: EWMA, DEWMA, CUSUM, GWMA, and DGWMA. Then, the titles for the results (published papers) were checked to confirm the relativeness of the conducted research and the keywords. The search in the WOS database found 4430 articles regarding the time-weighted charts published from 1956 to 2019. The results are illustrated in Figure 1.2:

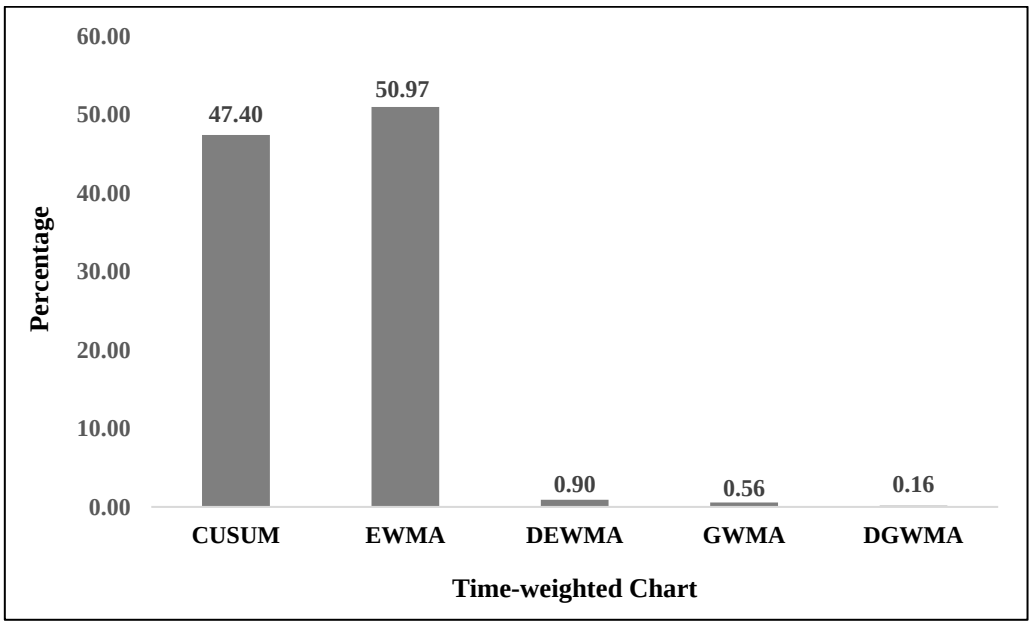

Figure 1.2. Bibliometric analysis for the time-weighted charts (1956 – 2019)

The highest number of publications belong to the EWMA chart (50.97% of the records), which is expected due to the global performance of this chart and popularity amongst researchers and practitioners. The second place is for the CUSUM chart (47.40% of the records). The third place is for the DEWMA chart (0.90% of the records). The GWMA chart, with 0.56% of the records, stays in the fifth place. The DGWMA chart, which is the core and the main objective of the present research, only has 0.16% of the publication records. Therefore, the bibliometric analysis clearly indicates that there are various research

gaps within this domain (DGWMA) that need to be addressed and will be discussed in Sections 1.5 and 1.6 as the contribution of the thesis.

1.4 Small shifts in SPC

In SPC, for an IC manufacturing process, the process produces readings with mean (denoted by μ_0) and a standard deviation (denoted by σ_0). The main objective of constructing a control chart is to identify special causes of variation in the process and make timely decision. These causes can lead to a shift or a change in the process location parameter or a change in the process scale parameter or both, i.e., location-scale. In this thesis, the concentration will be on shifts that will be occurred in the location parameter; however, our recommendations and conclusions apply to shifts in the process scale parameter.

Assume that X_{ij} denotes the j^{th} observation in the i^{th} observation sample, where $i = 1, 2, \dots, m$ and $j = 1, 2, \dots, n$. During the process monitoring, some cause occurred at some time and shifts the IC location parameter value, e.g., mean (μ_0), to an OOC value (denoted by μ_1). The purpose of SPC is to construct charts that are effective in detecting shifts at the earliest time, diagnose the cause, and remove or accommodate it through adjustment of process settings. The importance of detecting small shifts in the process is discussed in this section with the following real-life example.

Assume a toothpaste has a nominal content of 12 ml. The actual fillings assume to follow a distribution, i.e., normal distribution with parameters μ and standard deviation 0.25 ml. The manufacturer aims to set the location parameter high enough to avoid legal problems related to labelling. Hence, only 5% of containers will have a content less than 12 ml (nominal value). The desired IC mean is then $\mu_0 = 12 + 1.28 * 0.25 = 12.32$ ml. Downward shifts in the mean lead to substantial increases in the percentage of underfilled tubes, whereas upward shifts result tubes containing more fillings than is required. The former case will face legal actions due to labelling regulations, whereas the latter case represents wasted spilling from overfilled tubes or a gift to the consumer. Suppose that the toothpaste costs the manufacturer \$0.008 per ml and that the line fills 6000 tuber per hour. Hence, each 1-ml upward shift in the mean costs \$0.008*6000 = \$48 per hour, or \$1152 per day. Hence, a daily loss of \$1152 would correspond to a mean overfill of 0.25 ml, that is given by 12.32 + 0.25 = 12.57 ml. This lost is based on a shift in the mean by one standard deviation which is in fact the definition for a small shift in the process. One might be interested in detecting the shift by two or three standard deviation (large shifts in the process).

Suppose a tube is sampled every 2 hours and the quality practitioner measured its exact content. The cost of running at the process is proportional to the amount by which the mean fill exceed the nominal

level multiplied by the length of time for which the process runs at the shifted mean. Hence, the expected loss will be: $E(L(\mu)) = \$40 * ARL * (\mu_1 - \mu_0),\ \mu_1 > \mu_0$, where ARL is the average number of fillings from the time processes shifts OOC and the IC value is $\mu_0 = 12.37$. Note that the element of time is essential in deciding to detect a large or small shift in the process. Hence, a small shift that persists for a long time through failing to be detected may incur a larger total cost than detecting a large shift.

For example, one can draw a figure to illustrate the expected loss for varying shift sizes in the mean for two schemes – Shewhart chart and a CUSUM chart with the following parameters $d = 0.5$ and $h = 4.77$, where d is a reference value and h is the decision limit

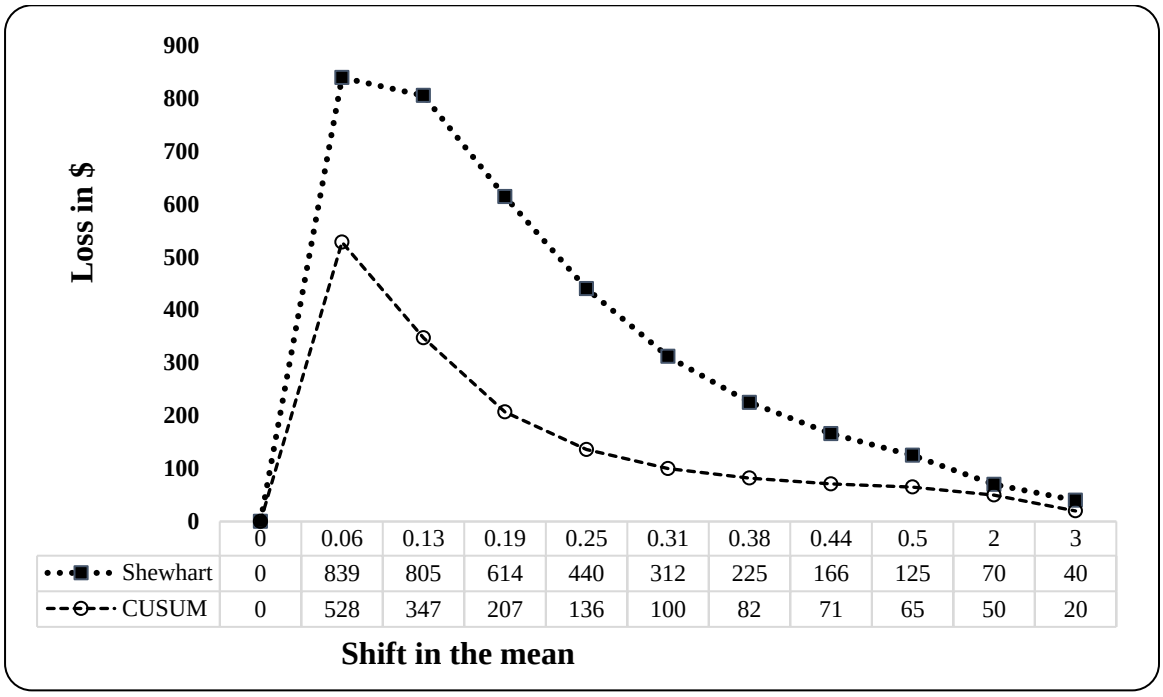

	0	0.06	0.13	0.19	0.25	0.31	0.38	0.44	0.5	2	3
Shewhart	0	839	805	614	440	312	225	166	125	70	40
CUSUM	0	528	347	207	136	100	82	71	65	50	20

Figure 1.3. Comparison of loss between the Shewhart and CUSUM charts

The horizontal axis presents the shift in the mean (in standard deviation) and the vertical axis presented the expected loss measured in US dollars ($) per incident.

These two schemes are based on taking one reading per 2 hours and assuming the IC ARL of 740 readings. These values are taken from the research published by Hawkins and Zamba (2003) which the authors illustrate the importance of small shifts in the production processes. As illustrated, the curve is high for the Shewhart chart for detecting small shifts and a severe blind spot for shifts about 0.3 standard deviation of overfill. On the contrary, the CUSUM chart has much lower expected loss than the Shewhart chart for changes below 2 standard deviation (medium shift) and 1 standard deviation (small shift).

Note that there are numerous research available in SPC who mentioned the term “small shifts”, for example, Hawkins (1978), Bakir and Reynolds (1979), Bhattacharya and Frierson (1981), Amin et al. (1995), Borror et al. (2003), Hawkins and Zamba (2003), Sheu and Lin (2003), Sheu and Hsieh

(2009), Tai and Hsieh (2010), Abbas et al. (2013), Huang et al. (2014), Chiu and Lu (2015), Lu (2018), and the references therein.

1.5 Scope and objectives

This research is based on developing novel generalized time-weighted (memory-type) control charting techniques for the DGWMA chart. Sheu and Hsieh (2009) concluded that the DGWMA chart is superior in detecting small or tiny shifts in the manufacturing processes compared to its counterparts, e.g., the GWMA, the DEWMA and the EWMA charts. The main focus of this thesis is within this domain (i.e., double general weighting) by employing the double exponential smoothing technique – proposed by Brown (1962) – to enhance the performance and the detection capability of the existing memory-type charts.

Since the introduction of the Shewhart chart, time-weighted charts (parametric and nonparametric) have been developed and shown to have improved the performance of the memory-less charts. Amongst these time-weighted charts, the GWMA, EWMA and CUSUM charts are known to be effective in detecting small shifts in the process. However, for example, the performance comparison between the DGWMA chart and the CUSUM chart is not currently available in the SPC literature.

In order to find relevant research gaps for the DGWMA chart and provide motivation for the current research, the following aspects are taken into consideration and compared with other DGWMA charts already exist in the literature: 1) underlying process distribution, 2) one-sided charts vs. two-sided charts, 3) Case K vs. Case U, 4) monitoring objective based on the parameter(s) of the underlying distribution, and 5) calculation methods for the run length distribution. These aspects are monitored for all of the published articles available in SPC related to the DGWMA chart as follows:

1) **Sheu and Hsieh (2009)** – A two-sided DGWMA-$\bar{X}$ chart is constructed to monitor the process location parameter under the normal distribution when the parameter of interest is known (Case K). The Monte Carlo simulation is used to calculate the run length distribution and its associated characteristics. A simulated example is presented.

2) **Tai et al. (2010)** – A two-sided DGWMA chart is constructed to monitor the process mean and process variability simultaneously (i.e., location-scale) under the normal distribution, when parameters of the underlying distribution are known (Case K). The Monte Carlo simulation is considered to calculate the run length distribution and its associated characteristics.

3) **Huang et al. (2014)** – A two-sided DGWMA chart is constructed to monitor the process mean and process variability simultaneously under the normal distribution, when parameters are

known (Case K) and unknown (Case U). The Monte Carlo simulation is used to evaluate the run length distribution and its associated characteristics.

4) **Chiu and Lu (2015)** – A two-sided DGWMA chart is constructed to monitor the process location parameter under the Poisson distribution, when the parameter of interest is known (Case K). The Monte Carlo simulation is used to calculate the run length distribution of the proposed chart.

5) **Lu (2018)** – A two-sided nonparametric DGWMA chart is constructed when the underlying process distribution is unknown for monitoring the process proportion based on the sign statistic. The parameter of interest is assumed to be known (Case K) and the Monte Carlo simulation is considered to calculate the run length distribution.

Table 1.1. provides a broad overview of different types of charts (memory-less versus time-weighted) available in the SPC literature and an illustration of how the contribution of the research studied in this thesis for the DGWMA charts fit into the SPC environment.

Table 1.1. The contribution of the thesis

			Memory-less chart	**Time-weighted charts**			
			Shewhart	EWMA	GWMA	DGWMA	DEWMA
Parametric	**Case K**		×	×	×	× ■	× ■
	Case U	**Phase I**	×	×			
		Phase II	×	×	×	■	■
Nonparametric	**Case K**		×	×	×	×	×
	Case U	**Phase I**	×				
		Phase II	×	×	×	■	■

In summary, Table 1.1 reveals that:

(i) The symbol "×" denotes the existing charts in the SPC literature, whereas "■" represents the contribution of this thesis. Note that, for some cases, both symbols "×" and "■" have been used, since there is already some work available in the literature. The grey blocks represent the charts developed and studied in this research.

(ii) The research conducted in this thesis is only limited to the design and implementation of univariate (parametric and nonparametric) charts. Multivariate harts have been studied by numerous researchers in the SPC literature. Hotelling (1947) proposed a chart for detecting a shift in the mean vector under the multivariate normal distribution. Lowry et al. (1992) extended the original univariate EWMA chart to a multivariate case for monitoring the mean vector under the multivariate normal distribution. Qiu and Hawkins (2003) developed

a nonparametric multivariate CUSUM chart for detecting shifts in all directions. Hence, the multivariate control charts are out of scope for this study. Zamba and Hawkins (2009) provided a multivariate toolkit for practitioners to detect change in the mean vector and/or covariance matrix through the lens of LR statistics.

(iii) Also, both cases when $n = 1$ (individual observations) and $n > 1$ (rational subgroups) are considered. In SPC, frequently, the phrases "random sample" and "rational subgroup" are used interchangeably, however strictly speaking, a random sample is not necessarily a rational subgroup. For more information, the interested reader is referred to the discussion provided in Montgomery (2013).

(iv) Note that these charts are constructed when the observations are assumed to be mutually independently and identically distributed, i.e., i.i.d. The effect of autocorrelation in SPC has been studied by numerous authors. This include but not limited to the following, Johnson and Bagshaw (1974), Schmid (1997), Psarakis and Papaleonida (2007), Alwan and Roberts (1988), amongst others. Furthermore, the following areas indicate the interest in constructing charts with autocorrelated observations: Finance (Frisen, 2007), public health monitoring (Woodall, 2006), and network monitoring (Ye & Chen, 2001). Several other studies consider monitoring the residuals after fitting a time series model to processes that exhibit autocorrelation and may be stationary or non-stationary, for example, Hawkins (1991), Tsiamyrtzis and Hawkins (2008), Kim et al. (2012) and Montgomery and Mastrangelo (1991). Atienza et al. (1998) proposed a chart for detecting shifts in autocorrelated data. Zhang (1981) along with Lu and Reynolds (1999a, 1999b) and Apley and Lee (2003) proposed EWMA based methods to accommodate the lack of independence. Zacks and Kenett (1994) developed a change-point model based on a mixture of normal distributions that could be applied to startup data. For more information, the interested reader is referred to the work by Triantafyllopoulos and Bersimis (2016) and the references therein. Autocorrelated data is out of scope for this study.

(v) For the parametric case, DGWMA charts available in the literature only focus on Case K, where the parameter(s) of interest are known and constructed under the normality assumption. The contribution of the present research is to develop a DGWMA chart for Case K (known parameters) and Case U (unknown parameters) under the non-normal distribution(s) and more specifically for the skewed distributions, e.g., exponential and gamma. A DEWMA-TBE chart, is also constructed and studied for Cases K and U (see Chapter 3).

(vi) From the existing information, it can be deduced that, for the nonparametric case, there is only one research article published for Case K to monitor the process proportion (see Lu, 2018). The contribution of the present research is to construct a nonparametric DGWMA chart based on the nonparametric EX statistic for monitoring the process location parameter. The objective is to monitor the process median which is a more robust location parameter compared to its counterparts. The DGWMA-EX chart and the DEWMA-EX chart are proposed for Case U. The robustness of the proposed DGWMA-EX chart is evaluated under several symmetric and asymmetric distributions (see Chapter 4).

A quick summary of the objectives and the main contributions for this thesis are as follows:

- Construct a generalized type of time-weighted (memory-type) charts (DGWMA) to be effective in detecting small shifts in the process. The proposed charts include other time-weighted charts like the GWMA, DEWMA, EWMA, CUSUM and Shewhart-type charts as special or limiting cases.

- This generalized chart is considered for parametric and nonparametric cases. In the parametric case, a DGWMA chart is proposed when the underlying process distribution follows a gamma distribution. For the nonparametric case, the underlying process distribution is assumed to be symmetric and continuous.

- Both parametric and nonparametric DEWMA charts, which are the special cases of the proposed DGMWA charts (i.e., denoted by DGWMA-TBE and DGWMA-EX), are developed and considered in detail. For the sake of brevity, in the rest of this thesis, the DEWMA chart with two smoothing parameters is denoted by the DEWMA chart (Case 1), whereas the one with a single smoothing parameter is denoted by the DEWMA chart (Case 2).

- Case K (when the parameters of the underlying process distribution are known) and Case U (when the parameters of the underlying process distribution are unknown) have been considered in this thesis for the DGWMA chart, since Case U for the nonparametric is not available in the SPC literature.

- In the existing SPC literature, the majority of researchers only considered the DGWMA chart in the scenario when the chart parameters (i.e., $q_1 = q_2 = q$ and $\alpha_1 = \alpha_2 = \alpha$ are equal, e.g., Sheu and Hsieh (2009)). These authors concluded that the performance of the chart does not differ when all four parameters of the DGWMA chart are included under the normal distribution. However, in this thesis, a comparative study is conducted to evaluate the performance between these two scenarios. For the sake of brevity, in the rest of this thesis, the DGWMA chart with four parameters is denoted by the DGWMA chart (Case 1), whereas the DGWMA chart with two parameters is represented by the DGWMA chart (Case 2).

- The run length distribution will be considered as the chart performance measure in detail for the proposed DGWMA charts. To calculate the run length distribution, there are three different approaches in SPC: (i) an exact approach, (ii) a Markov chain method, and (iii) a Monte Carlo simulation. The Monte Carlo simulation has been implemented and considered as the only method in the SPC environment for the DGWMA chart. In this thesis, the exact and the Markov chain approaches are also studied for the first time for the DGWMA chart
- A constructive discussion is provided in Section 1.6 for the practitioners to provide a road map and general guidelines in selecting the control chart(s) that are efficient in detecting different shift magnitudes (large, medium, small or tiny) in the process, given the distributional assumption. These guidelines are of utmost importance in the present era surrounded by various practical necessities.
- The GWMA charts currently available in the SPC literature are constructed under the assumption that the weights follow a two-parameter discrete Weibull distribution proposed by Nakagawa and Osaki (1975). However, in this thesis, alternative discrete distributions, i.e., discrete Burr and discrete Burr Type III distributions, will be considered to enhance the detection capability and the performance of the existing GWMA charts. A motivation for considering alternative discrete distributions is provided in Chapter 3 in detail.

1.6 Guidelines for practitioners

Numerous control charts have been proposed and developed by researchers in the SPC paradigm for detecting various shift sizes (large, medium, small, or tiny) in the production process as quickly as possible. The number of manuscripts published on SPC topics seems to be growing exponentially, thus keeping full records of advances in the SPC literature is impossible. However, it may be fair to conclude that the advances in the research world of SPC methods have not yet been fully incorporated in practice. Therefore, the crucial step is finding an approach to narrow the gap between the theory developed by academic researchers and the practice applied by practitioners. As Deming (1993, p. 106) mentioned: "Without theory, experience has no meaning. Without theory, one has no questions to ask. Hence, without theory, there is no learning." By reviewing the charts available in statistical packages – e.g., SAS, R, MINITAB, etc. – due to the lack of accessibility of the more advanced charts, they are not used as often as most practitioners would prefer. Therefore, there is a necessity in the SPC literature to provide some hints or recommendations that encourage practitioners to consider advanced charts in practice. Woodall (2017) addressed this problem only for basic charts, such as the $\bar{X}$ chart and the R chart and provides some ideas and suggestions. However, due to various changes in the types of processes

available today (i.e., high-yield processes), there is a lack of discussion on the time-weighted charts that proved to be more efficient in detecting small shifts compared to the basic charts. Hence, we give recommendations for the implementations of these charts as to encourage their use.

The properties for the EWMA, DEWMA charts (Case 1 and Case 2) and CUSUM charts are provided in Appendix A. For the GWMA chart, the interested reader is referred to the work by Sheu and Lin (2003).

Since the novel DGWMA chart proposed in this thesis is a generalized time-weighted chart, the relationship between the proposed chart and other existing charts is portrayed in Figure 1.4.

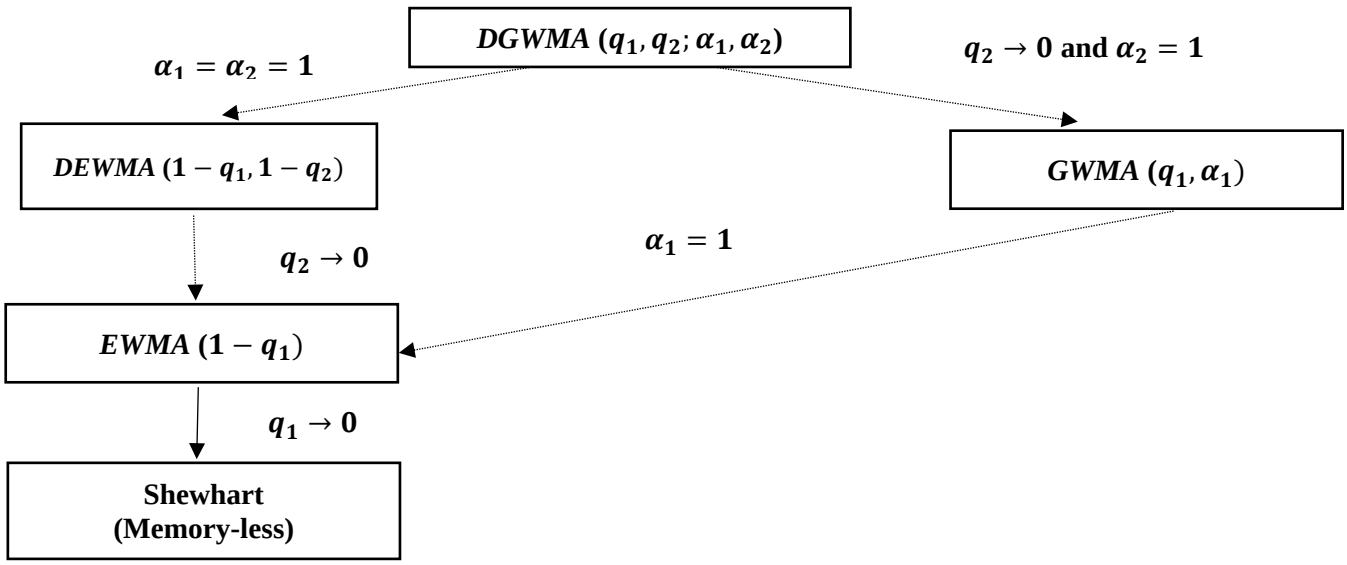

Figure 1.4. Time-weighted (memory-type) and memory-less charts relationship

The guidelines for practitioners are provided in terms of a table, where the columns denoted the type of a control chart (memory-less versus time-weighted) and the rows denote the magnitude of a shift in the production process. The information provided in this table is based on the findings from Chapter 3, which assume the gamma distribution (denoted by $Gamma\ (k, \theta)$) as the underlying process distribution. For illustration purposes, the IC scale parameter is assumed to be one (i.e., $\theta_0 = 1$) and the value for the shape parameter is chosen as $k = 1$. The OOC scale parameter is denoted by θ_1, and the shift is defined as the ratio of the OOC and IC scale parameters as $\delta = \theta_1/\theta_0$. The size of the shift in the process can be classified as tiny ($\delta = 0.975, 0.95, 0.925$), small ($\delta = 0.9, 0.85$), medium ($\delta = 0.8, 0.7$) and large ($\delta = 0.5, 0.25$). The objective of this table is to provide recommendations that, given the process distributional assumption and the size of the shift, assist a practitioner in selecting an optimal time-weighted chart as well as selecting the most efficient chart for detecting tiny shifts. More precisely, an easy-to-use table is provided for the time-weighted chart's design parameters to aid practical implementation.

Table 1.2. Roadmap for practitioners when the underlying process distribution is gamma

	Type of control chart				
	Memory-less	**Time-weighted**			
Magnitude of a shift (δ)	**Shewhart-TBE**	**EWMA-TBE**	**DEWMA-TBE**	**GWMA-TBE**	**DGWMA-TBE**
Large	$q_1, q_2 \to 0$ $\alpha_1 = \alpha_2 = 1$				
Medium		$q_1 = 1 - \lambda = 0.95$	$q_1 = 1 - \lambda_1 = 0.95$ $q_2 = 1 - \lambda_2 = 0.95$		$0.8 \leq q \leq 0.95$ $0.9 \leq \alpha \leq 1$
Small				$0.5 \leq q_1 \leq 0.95$ $0.6 \leq \alpha_1 \leq 1$	$0.5 \leq q \leq 0.95$ $0.6 \leq \alpha \leq 1$
Tiny					$0.5 \leq q \leq 0.95$ $0.6 \leq \alpha \leq 1$

The recommendations for the practitioners with respect to Table 1.2 are summarized as follows:

(i) The general guidelines recommended in Table 1.2 in terms of selecting the chart parameters are only valid when the underlying process distribution is gamma (i.e., parametric paradigm). However, one can extend and construct a similar table for other parametric charts constructed under different types of distributions (normal versus non-normal) as well as nonparametric charts. For more information, the interested reader may consult Montgomery (2013).

(ii) The DGWMA-TBE chart developed and proposed in this thesis (see Chapter 3), outperformed other time-weighted cha, under consideration, in detecting medium, small, and more precisely the tiny shifts in the production processes. The proposed DGWMA-TBE chart is more efficient and better alternative than its counterparts in detecting tiny shifts in the process.

(iii) The Shewhart-TBE charts (memory-less) are known as the limiting cases of the proposed DGWMA-TBE chart. A practitioner can conclude from Table 1.2 that these types of charts are only effective in detecting large shifts in the process.

(iv) The EWMA-TBE chart, which is the limiting case of the proposed DGWMA-TBE chart, is efficient at detecting medium/moderate shifts in the process. Further, the larger value for the parameter q_1 implies a smaller value for the smoothing parameter λ. A similar

recommendation is also given by Montgomery (2013) for the EWMA chart to detect shifts in the process.

(v) The DEWMA-TBE chart is also developed in this thesis (see Chapter 3) – is also efficient in detecting medium shifts in the process. Further, based on the results in Chapter 3, the DEWMA-TBE chart is more effective than the EWMA-TBE and Shewhart-TBE charts in detecting moderate shifts due to the implementation of the double exponential smoothing technique.

(vi) The GWMA-TBE chart proposed by Chakraborty et al. (2016) is the limiting case of the DGWMA-TBE chart constructed in this thesis and is efficient at detecting small shifts in the process. Results from Chapter 3 recommend that the GWMA-TBE chart outperforms the EWMA-TBE and Shewhart-TBE charts in detecting small shifts which line up with the results obtained by Chakraborty et al. (2016).

(vii) A platform or a forum is needed in SPC so that academic researchers and practitioners can use to share their own perspectives from the charts available in the literature. Also, the research papers should be written with practitioners in mind, whenever possible. As Hoerl (2000) stated, "the research community breathes its own exhaust without practitioners' input".

1.7 Outline of the thesis

The structure of the thesis is discussed below.

Chapter 2 provides an overview on the design and implementation of the DGWMA chart. The properties of the DGWMA chart, including the plotting (charting) statistics, the structure for the weights, the properties of the plotting statistic (the expected value and the variance), centerline, and control limits (exact/steady-state) will be considered. The special and limiting cases of the DGWMA chart are also analyzed and the behavior of the weighting structure is discussed through graphical illustrations. Furthermore, three calculation methods for the run length distribution of the DGWMA chart will be investigated and discussed in-depth.

Chapter 3 provides a new parametric time-weighted chart (denoted by DGWMA-TBE) for monitoring the TBE of nonconforming items originating from the high-yield processes for Case K and Case U. The statistical properties of the proposed DGWMA-TBE chart have been studied and a performance analysis based on the Monte Carlo simulation has also been undertaken to execute a comparative study with a number of existing control charting procedures. The special case of the DGWMA-TBE chart (i.e., DEWMA-TBE) is also constructed and considered in this chapter. The Markov chain approach and the exact approach are considered to calculate the run length distribution for the first time in the literature. Alternative discrete distributions (i.e., discrete Burr and discrete Burr Type III distributions) for the

GWMA-TBE chart weights are considered and a performance comparison is conducted with its counterparts. The DGWM-TBE and DEWMA-TBE charts for Case U are also discussed in detail.

Chapter 4 provides a distribution-free (nonparametric) DGWMA chart for Case U based on the two-sample nonparametric statistic EX, denoted as DGWMA-EX. The statistical properties of the proposed DGWMA-EX chart have been studied and a performance analysis based on the Monte Carlo simulation has also been undertaken to make comparisons with a number of existing control charting procedures. The Markov chain approach and the exact approach are considered to calculate the run length distribution for the first time in the literature. The DGWMA-EX chart with four parameters (Case 1) and the DGWMA-EX chart with two parameters (Case 2) are also considered. A distribution-free DEWMA-EX chart is also proposed. Note that, the robustness of the proposed DGWMA-EX chart is evaluated under several symmetric and heavy-tailed distributions. To the best of our knowledge, the robustness study for nonparametric DGWMA charts is not available in the SPC literature and has been addressed in this thesis.

Chapter 5 provides a conclusion and recommendations for an extension of the current research.

Chapter 2 Double Generally Weighted Moving Average control chart – an overview

2.1 Introduction

SPC is a collection of scientific tools and statistical procedures developed and engineered to execute quality control in a production process. The variation in production processes occurs frequently and needs to be detected in timely manner. In general, two types of variations exist during the production process, namely common causes of variation and special causes of variation. The common causes of variation are defined as the variability that is inherent in the process and should be relatively small. Nevertheless, the presence of special causes of variation are extraneous to the process and influence the performance of the underlying process, shifting process parameters like location and/or dispersion.

In the present era, surrounded by innumerable technologically advanced tools, special causes are frequently presented and need to be detected at the earliest time. The main objective of SPC research is to design and implement efficient control charts for detecting small shifts (one standard deviation) originating from the presence of special causes of variation in the process. Note that the element of time is essential in deciding to detect a large or small shift in the process. Hence, a small shift that persists for a long time through failing to be detected may incur a larger total cost than detecting a large shift.

There are numerous charts designed in the SPC literature to detect small shifts that have gained lots of attention amongst researchers. The Shewhart-type charts are well-known as they can be easily implemented in practice and for their global performance in detecting large shifts. However, the blind spot of these charts, also known as memory-less charts, is their weak performance in detecting small or tiny shifts. In contrast, more efficient classes of charts labelled as time-weighted (memory-based or memory-type) charts, such as the UWMA, EWMA, EGWMA, DEWMA, CUSUM and GWMA charts, are more naturally appropriate and effective for detecting small shifts in the production process. These charts use a mixture of past and present information to monitor the state of the process, known as the memory-saving feature.

A time-weighted DGWMA chart, denoted by DGWMA $(q_1, q_2, \alpha_1, \alpha_2)$, was proposed by Sheu and Hsieh (2009) under the normal distribution (denoted by DGWMA-$\bar{X}$) through the combination of the DEWMA-$\bar{X}$ and the GWMA-$\bar{X}$ charts. The authors concluded that the DGWMA chart is superior at detecting small or tiny shifts in comparison with its main counterparts – i.e., the GWMA and the DEWMA charts – due to the implementation of the double or dual exponential smoothing technique proposed by Brown (1962).

The underlying process distribution for the DGWMA chart is assumed to be normal in this chapter. The preliminaries and statistical framework required for the construction of the DGWMA chart are studied and discussed in Section 2.3. The aforementioned information will be used as a baseline in Chapters 3 and 4. Further to this, a brief discussion of exact and steady-state control limits is provided with the key emphasis being on the pros and cons for each of these control limits. Two types of DGWMA charts, namely Case 1 and Case 2, are discussed in Section 2.4. The limiting and special cases of the DGWMA chart are presented in more depth in Section 2.5. Furthermore, the weighting structure and behaviour for time-weighted charts is studied. An informative discussion is provided to link the relationship between the shapes of the weights and the performance of time-weighted charts. In general, there are three methods in SPC literature to calculate and evaluate the run length distribution: (i) the exact approach, (ii) the Markov chain approach, and (iii) the Monte Carlo simulation. These approaches are discussed in detail for the DGWMA chart and its special case the DEWMA chart in Section 2.6. Further to this, the pros, and cons for each of these methods are outlined.

2.2 Motivation

The bibliometric analysis for the time-weighted charts presented in Chapter 1 (see Section 1.3.6) reveals that few researches has been conducted in the SPC literature for the DGWMA chart. From the literature review, most of the existing parametric DGWMA charts are constructed under the normality assumption. Also, parameters of interest based on the underlying distribution are assumed to be known (Case K) in majority of scholar works related to the DGWMA chart. However, a practitioner or researcher might be interested in evaluating the performance of the DGWMA chart under heavy-tailed distributions or non-normal distributions. Frequently, the underlying process distribution is unknown, or no information is available. Also, the parameters of interest are rarely known in practice and there is a necessity to design a DGWMA chart to accommodate this assumption. Sheu and Hsieh (2009) mentioned that the added parameters in the DGWMA plotting statistics slightly adjust the kurtosis of the weight function so that the DGWMA chart becomes more sensitive than other time-weighted charts, under consideration in this thesis, in detecting small shifts. The choice of the DGWMA parameters and the weighting distribution determine the decline of the weights, and thereby the effect of past observations in the computation of weights.

Motivated by these findings, the objective of this thesis is to design a parametric (under normal and non-normal distributions) or nonparametric (under continuous and symmetric distributions) DGWMA chart when the parameters of interest are unknown (Case U) and when the parameters of interest are known (Case K). In this thesis, the DGWMA chart is viewed as a generalized time-weighted chart.

In the published papers within the DGWMA chart domain, the main focus is only on the DGWMA chart (Case 2), where an equality is assumed for the chart parameters, i.e., $q_1 = q_2 = q$ and $\alpha_1 = \alpha_2 = \alpha$. However, one might be interested in the performance of the DGWMA chart when the equality assumption for the chart parameters is not fulfilled. Hence, two types of the DGWMA chart (Case 1 and Case 2) are discussed in this chapter and subsequent chapters.

Further to this, the weighting structure for time-weighted charts plays a vital role in increasing and enhancing the chart's sensitivity in detecting small or tiny shifts. The amount of information allocated to the past and present observations and the shapes for the weights have a direct impact on the performance of a chart. The plots illustrated in this chapter to study the behavior of the weights for the time-weighted charts can be considered as the pioneer work within this field (DGWMA) and based on the findings, the weights possess the properties of a valid probability mass function (p.m.f.).

The run length distribution is the most commonly used performance measure to evaluate and compare different charts. The Monte Carlo simulation is frequently considered in the majority of the published papers and scholarly work as the only approach to calculate the run length distribution of a chart due to its ease of implementation and the increasing access to software packages. In this chapter, the exact approach and the Markov chain approach are discussed in detail for the DGWMA chart and the necessary closed-form expressions are obtained. To the best of our knowledge, there is no scholarly work available to calculate the run length distribution of the DGWMA chart through the Markov chain and exact approaches and address these methodologies in the SPC literature.

2.3 Preliminaries and statistical framework

2.3.1 Assumptions

Let $X_{ij} \sim i.i.d\ F_{\boldsymbol{\theta}}$ for $i = 1, 2, \dots, m$, and $j = 1,2, \dots, n$, denote random samples from a quality characteristic of an arbitrary process, where $n \geq 1$. The vector of parameters is denoted by $\underline{\theta} = (\theta_1, \theta_2, \dots, \theta_k),, k \geq 1$, with the discrete or continuous process c.d.f. $F_{\boldsymbol{\theta}}$. The sample statistic is represented by $T_{\boldsymbol{i}} = f(X_{i1}, X_{i2}, \dots, X_{in})$ based on the i^{th} subgroup observations in Case K.

2.3.2 Plotting statistic

The discrete random variables M_1 and M_2 denote the number of samples until the next occurrence of an event since its last occurrence with the following property:

$$\sum_{i=1}^{\infty} P(M_j = i) = \sum_{i=1}^{t} P\big(M_j = i\big) + P(M_j > t) = 1\ ,\ \ j = 1, 2\ . \qquad (2.1)$$

M_1 and M_2 notations are used to represent weighting schemes for the GWMA and DGWMA charts, respectively. Note that, in Sheu and Lin (2003), since the objective is to construct a GWMA chart, M is used instead of M_1. Also, Sheu and Hsieh (2009) used M and M_1 to distinguish between the weighting

notations for the GWMA and the DGWMA charts. The probability $P(M_j = i)$ is known as the weight (denoted by v_i) for the i^{th} most recent sample statistic T_{t-i+1}, where $i = 1, 2, \ldots, t$. The probability $P(M_j = 1)$ is the weight (denoted by v_1) for the latest observation T_t; the probability $P(M_j = t)$ is the weight (denoted by v_t) for the most outdated observation T_1. Also, $P(M_j > t)$ represents the weight for the starting value (denoted by Z_0^1). For the statistic under consideration, the starting value (Z_0^1) is selected as the IC expected value – i.e., $E(T_i|IC)$ for Case K. The plotting statistic for the GWMA chart is defined as (see Sheu and Lin (2003)):

$$Z_t^1 = \sum_{i=1}^{t} P(M_1 = i)\, T_{t-i+1} + P(M_1 > t) Z_0^1 \,. \tag{2.2}$$

Equation (2.2) can be rewritten in terms of the weights for the GWMA chart as:

$$Z_t^1 = \sum_{i=1}^{t} v_i\, T_{t-i+1} + v_0 Z_0^1 \,, \tag{2.3}$$

where $v_i = P(M_1 = i)$, $v_0 = P(M_1 > t)$, and $\sum_{i=1}^{t} v_i + v_0 = 1$. In Case U, the starting value Z_0^1 will be a random variable that needs to be estimated from the calibration sample or reference sample collected in Phase I.

Note that, the weights are denoted by v_i for the GWMA chart and for the DGWMA chart the weights are denoted by w_i.

The p.m.f. for the discrete variables M_1 and M_2 are:

$$P(M_1 = i) = q_1^{(i-1)^{\alpha_1}} - q_1^{i^{\alpha_1}} \quad \text{for} \quad i = 1, 2, \ldots \tag{2.4}$$

and

$$P(M_2 = i) = q_2^{(i-1)^{\alpha_2}} - q_2^{i^{\alpha_2}} \quad \text{for} \quad i = 1, 2, \ldots, \tag{2.5}$$

where $0 < q_1, q_2 < 1$ and $\alpha_1, \alpha_2 > 0$, are the parameters of the DGWMA chart. Nakagawa and Osaki (1975) proposed and developed the p.m.f. in equations (2.4) and (2.5), which are known as the two-parameter discrete Weibull distribution.

The plotting statistic for the DGWMA chart is defined as follows:

$$Z_t^2 = \sum_{i=1}^{t} P(M_2 = i)\, Z_{t-i+1}^1 + P(M_2 > t) Z_0^2 \,, \tag{2.6}$$

where $Z_0^2 = Z_0^1 = E(T_i|IC) = \mu$ is the expected value of the statistic under consideration, also known as the starting value.

Much like the Sheu and Hsieh (2009) approach, the plotting statistic in equation (2.6) can be presented in terms of weights as:

$$\begin{aligned} Z_t^2 &= P(M_2 = 1)Z_t^1 + P(M_2 = 2)Z_{t-1}^1 + \cdots + P(M_2 = i)Z_1^1 + P(M_2 > i)Z_0^2 \\ &= w_1 T_i + w_2 T_{i-1} + \cdots + w_i T_1 + (1 - \textstyle\sum_{i=1}^{t} w_i)Z_0^2 \ . \end{aligned} \tag{2.7}$$

For the DGWMA chart, the weight at time *t* is defined as:

$$w_t = \textstyle\sum_{j=1}^{t} P(M_1 = j)P(M_2 = t - j + 1) \quad \text{for } t = 1,2,3, \ldots \tag{2.8}$$

The weight function can be written in terms of the two-parameter discrete Weibull distribution p.m.f. by replacing (2.4) and (2.5) into (2.8) as:

$$w_t = \textstyle\sum_{j=1}^{t} \left(q_1^{(j-1)^{\alpha_1}} - q_1^{j^{\alpha_1}}\right)\left(q_2^{(t-j)^{\alpha_2}} - q_2^{(t-j+1)^{\alpha_2}}\right). \tag{2.9}$$

Therefore, the plotting statistic for the DGWMA chart in terms of weights is defined as:

$$Z_t^2 = \textstyle\sum_{i=1}^{t} w_i \, T_{t-i+1} + \left(1 - \sum_{i=1}^{t} w_i\right)Z_0^2 \quad \text{for } t = 1,2,3, \ldots \tag{2.10}$$

Note that the superscripts used to denote the plotting statistics for the GWMA and DGWMA charts (i.e., Z_t^1 and Z_t^2, respectively) also denote the order in which the first-order and second-order "smoothing" of the sample statistic T_i are applied. These superscripts should not be confused with the mathematical concept of raising a number or variable to an arbitrary power.

2.3.3 Control limits

The mean and the variance of the statistic under consideration are defined as $E(T_i) = \mu_0$ and $var(T_i) = \sigma_0^2$, respectively for all $i = 1,2,3, \ldots$. Therefore, the properties of the DGWMA plotting statistic Z_t^2, including the IC expected value and the IC variance, can be obtained as follows:

$$E(Z_t^2|IC) = \textstyle\sum_{i=1}^{t} w_i \, E(T_{t-i+1}) + \left(1 - \sum_{i=1}^{t} w_i\right)E(Z_0^2) = \mu_0 \tag{2.11}$$

and

$$var(Z_t^2|IC) = \textstyle\sum_{i=1}^{t} w_i^2 \, var(T_{t-i+1}) = Q_t' \sigma_0^2 \ , \tag{2.12}$$

where $Q_t' = \sum_{i=1}^{t} w_i^2$.

From equation (2.12), one can observe that the variance of the DGWMA plotting statistic is a convergent function of t, resulting in a finite variance for the plotting statistic. The calculation for this quantity involves selecting the values for the DGWMA chart parameters (i.e., q_1, q_2, α_1, α_2) and the time t. For

illustration purposes, the parameters are selected as $q_1 = q_2 = q$ and $\alpha_1 = \alpha_2 = \alpha$. However, note that there is no necessity to assume an equality assumption for the chart's parameters and Q_t' can also be calculated for the DGWMA chart with four parameters (i.e., Case 1). The parameters are chosen as $q =$ 0.5, 0.7, 0.9, $\alpha =$ 0.5, 0.9, 1.3, and the time is selected as $t =$ 5, 10, 50, and 100. For various combinations of DGWMA parameters (q, α) and different values of t, the values for the quantity Q_t' are illustrated in Table 2.1.

Table 2. 1. $Q_t' = \sum_{i=1}^{t} w_i^2$ values.

t	$q = 0.5, \alpha = 0.5$	$q = 0.7, \alpha = 0.9$	$q = 0.9, \alpha = 1.3$
5	0.0941	0.1632	0.1415
10	0.1002	0.1682	0.1450
50	0.1026	0.1682	0.1457
100	0.1026	0.1682	0.1458
t	$q = 0.5, \alpha = 0.5$	$q = 0.7, \alpha = 0.9$	$q = 0.9, \alpha = 1.3$
5	0.0169	0.1230	0.1340
10	0.0211	0.1245	0.1355
50	0.0261	0.1243	0.1353
100	0.0264	0.1245	0.1340
t	$q = 0.5, \alpha = 0.5$	$q = 0.7, \alpha = 0.9$	$q = 0.9, \alpha = 1.3$
5	0.0533	0.0019	0.0080
10	0.0725	0.0058	0.0085
50	0.0759	0.0188	0.0211
100	0.0759	0.0191	0.0212

We observe that the variance is finite and converges in those settings considered in Table 2.1.

2.3.3.1 Exact control limits

For a two-sided DGWMA chart, the symmetric (exact) control limits (labelled as UCL_e and LCL_e) and the centerline (CL) are given by:

$$LCL_e = \mu_0 - L\,\sigma_0\sqrt{Q_t'} \qquad (2.13)$$
$$UCL_e = \mu_0 + L\,\sigma_0\sqrt{Q_t'}\,,$$

where $L > 0$ is the charting constant that determines the distance between the centerline and the exact limits, and these exact control limits are denoted by the subscript "*e*".

Note that, symmetrically placed control limits defined in equation (2.13) are only applicable if the plotting statistic has a symmetric distribution. In the case of the DGWMA-TBE chart proposed in Chapter 3, the underlying process distribution is gamma (an asymmetric distribution). As a result, a linear combination of gamma random variables is used and, in such a case, a one-sided chart will be constructed,

since a two-sided chart is *ARL*-biased. The biasness terminology for control charts is discussed in detail in Chapter 3. For more information, the interested reader is referred to Chakraborty et al. (2017).

2.3.3.2 Steady-state control limits

It has been observed from Table 2.1 that as $t \to \infty$, the quantity Q_t' converges, which results in an asymptotic and a finite variance that is given by $\lim_{t\to\infty} var(Z_t^2) = Q'\sigma_0^2$, where $Q' = \lim_{t\to\infty} Q_t'$, and $Q_t' = \sum_{i=1}^{t} w_i^2$.

Hence, for a two-sided DGWMA chart, the steady-state control limits (labelled as UCL_s and LCL_s), and the centerline (CL) are given by:

$$LCL_s = \mu_0 - L\,\sigma_0\sqrt{Q'} \qquad (2.14)$$
$$UCL_s = \mu_0 + L\,\sigma_0\sqrt{Q'}\,,$$

where $Q' = \lim_{t\to\infty} Q_t'$, and the subscript "s" denotes the steady-state control limits.

For the DGWMA chart Case U – where the parameter(s) of interest are unknown – in order to find the estimates for the μ_0 and σ_0, the reference sample from Phase I (retrospective phase) is required. Thereafter, these estimates are denoted by $\hat{\mu}_0$ and $\hat{\sigma}_0$, respectively, and substitute for μ_0 and σ_0 in equation (2.14) to obtain the estimated control limits (i.e., denoted by $\widehat{LCL}_s$ and $\widehat{UCL}_s$) that will be used in Phase II (prospective phase) to monitor the state of the process.

2.3.3.3 Exact versus steady-state control limits

In designing a control chart, one of the critical decisions that must be made is specifying and calculating the control limits. The Markov chain approach required the use of steady-state limits to simplify matters, whereas for the Monte Carlo simulation there is no significant difference to distinguish between the exact and the steady-state limits. If the control limits are moved further away from the centerline, the Type I error – defined as a point falling beyond the limits that declares the process is OOC when no assignable cause present – is decreasing. On the contrary, by narrowing the control limits, the and error, defined as the probability of a point falling between the limits when the process is actually OOC, is increasing. The steady-state limits are typically used when the control chart has been running for several time periods and to simplify the calculation of the IC run length distribution through the Markov chain approach. Since the Monte Carlo simulation is the main approach that has been considered through this thesis to calculate the run length distribution and its associated characteristics, the exact control limits are used for calculation and illustration purposes.

Note that, although asymptotic control limits are considered, there are charts available in the SPC literature for small sample. The price paid for considering steady-state limits is that the wider limits reduce the chart's ability to react quickly to early shifts.

For illustration purposes, the DGWMA-$\bar{X}$ chart under the normal distribution for monitoring the process mean is considered here. The subgroup size is set at $n = 1$, and the sample statistic T_t, $t = 1, 2,\ldots$, follows an independent normal distribution with the mean $\mu = 0$, and the variance $\sigma^2 = 1$. Hence, the exact control limits are defined as: $LCL_e = -L\sqrt{Q_t'}$ and $UCL_e = L\sqrt{Q_t'}$. The steady-state control limits will then be: $LCL_s = -L\sqrt{Q'}$ and $UCL_s = L\sqrt{Q'}$, where $Q' = \lim_{t\to\infty} Q_t'$. Two sets of design parameters are selected for the DGWMA-$\bar{X}$ chart to calculate and compare the exact and the steady-state limits.

The results are outlined in Table 2.2.

Table 2. 2. Comparison between the exact and the steady-state control limits

DGWMA parameters	Exact control limits			Steady-state control limits	
$q = 0.9$, $\alpha = 0.7$, $L = 2.188$	$t = 1$	$LCL_e = -0.292$	$UCL_e = 0.292$	$LCL_s = -0.498$	$UCL_s = 0.498$
	$t = 5$	$LCL_e = -0.410$	$UCL_e = 0.410$		
	$t = 10$	$LCL_e = -0.456$	$UCL_e = 0.456$		
	$t = 15$	$LCL_e = -0.478$	$UCL_e = 0.478$		
$q = 0.6$, $\alpha = 0.8$, $L = 2.921$	$t = 1$	$LCL_e = -0.469$	$UCL_e = 0.469$	$LCL_s = -0.630$	$UCL_s = 0.630$
	$t = 5$	$LCL_e = -0.530$	$UCL_e = 0.530$		
	$t = 10$	$LCL_e = -0.577$	$UCL_e = 0.577$		
	$t = 15$	$LCL_e = -0.607$	$UCL_e = 0.607$		

To ensure the validity of the values obtained in Table 2.2, these results are compared to those of Sheu and Hsieh (2009) for the DGWMA-$\bar{X}$ chart under the normal distribution as follows:

- For $q = 0.9$, $\alpha = 0.7$, $L = 2.185$, Sheu and Hsieh (2009) computed the exact control limits for $t = 15$ as $(-0.472, 0.472)$. From Table 2.2, when $q = 0.9$, $\alpha = 0.7$, $L = 2.188$, the control limits are $(-0.478, 0.478)$.
- For $q = 0.6$, $\alpha = 0.8$, $L = 2.917$, Sheu and Hsieh (2009) computed the steady-state control limits as $(-0.624, 0.624)$. From Table 2.2, when $q = 0.9$, $\alpha = 0.7$, $L = 2.921$, the steady-state control limits are $(-0.630, 0.630)$.

The quantity Q' is a convergent function of t, which implies the convergence of exact control limits in (2.13) towards the steady-state control limits in (2.14).

Hereafter, for the sake of brevity, *UCL* and *LCL* are used in the rest of this thesis to represent the steady-state control limits.

2.4 Two types of the DGWMA chart

The DGWMA chart can be classified as two different cases based on the equality or/and inequality of its parameters – i.e., q_1, q_2, α_1, α_2. The general form of this chart (Case 1) includes four parameters – q_1, q_2, α_1 and α_2 – and is denoted by *DGWMA* (q_1, q_2, α_1, α_2). By assuming the equality for the parameters – i.e., $q_1 = q_2 = q$, and $\alpha_1 = \alpha_2 = \alpha$ – then the DGWMA chart reduces into two parameters and is denoted by *DGWMA* (q, α) and will be called Case 2 throughout the entire thesis. Sheu and Hsieh (2009) concluded that the DGWMA chart (Case 1) does not outperform the DGWMA chart (Case 2) under the normal distribution, and only considered Case 2 for the design and implementation of the DGWMA-$\bar{X}$ chart. Contrarily, this thesis discusses both cases in detail for the parametric and nonparametric cases, and the necessary recommendations that would be of interest for practitioners will be provided. The majority of the peer-reviewed articles published in the SPC environment assume the equality of the parameters, and therefore only Case 2 has been considered. However, as stated in Section 1.5, one of the main contributions of this research is to also scrutinize the DGWMA chart (Case 1) and compare the performance with the DGWMA chart (Case 2). This comparative study is performed to evaluate and study the effect of adding extra parameters and their influence on the detection capability of the proposed chart(s). The relationship between these two charts can be portrayed as follows:

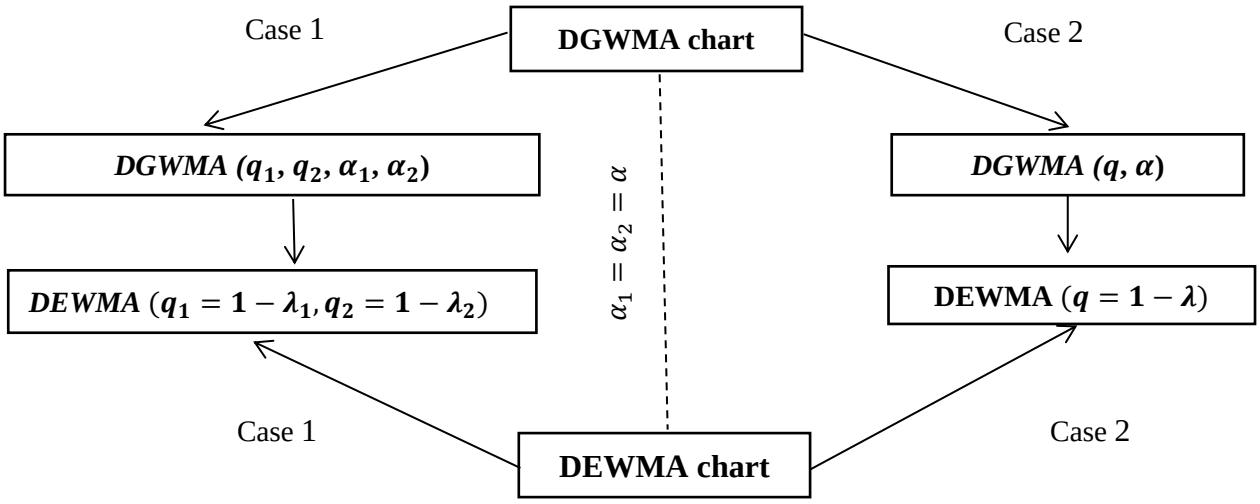

Figure 2.1. Relationship between the DGWMA (Case 1 and Case 2) and the DEWMA (Case 1 and Case 2) charts

In Figure 2.1, two types of the DGWMA chart are illustrated. The DEWMA chart is a special case of the DGWMA chart by assuming $\alpha_1 = \alpha_2 = \alpha$ and also consists of two different cases. The relationship between these cases are also portrayed in the above figure. In Section 2.5, more information is provided with respect to different types of the DEWMA chart.

2.5 Special and limiting cases

In this section, the general steps for obtaining the special and limiting cases of the DGWMA chart (Case 1) are discussed. The limiting cases are the GWMA, EWMA, and Shewhart charts, and the special case is the DEWMA chart. Further, the DEWMA chart is classified as Case 1 and Case 2, dependent on the equality and/or inequality of its parameters. Sheu and Hsieh (2009) were the first authors to use the "special cases" terminology for the DGWMA chart in SPC which only limited to the DGWMA chart (Case 2), EGWMA, and DEWMA (Case 1 and Case 2) charts. Later, Chiu and Lu (2015) also mentioned that the DEWMA chart is the special case of the DGWMA chart and compared the performance of their proposed chart with the GWMA, DEWMA, and EWMA charts. Note that the EWMA chart is a special case of the GWMA chart, as mentioned by Chakraborty et al. (2016), Chakraborty et al. (2017) amongst others.

2.5.1 DGWMA chart (Case 2)

By assuming the equality assumption for the parameters of the DGWMA chart – i.e., $q_1 = q_2 = q$, and $\alpha_1 = \alpha_2 = \alpha$ – the chart simplifies to a DGWMA chart denoted by *DGWMA* (q, α). This chart is the GWMA chart that is weighted sequentially twice by implementing the double exponential smoothing technique proposed by Brown (1962). As a result, the weighting scheme defined in equation (2.9) becomes:

$$w_t = \sum_{j=1}^{t}\left(q^{(j-1)^\alpha} - q^{j^\alpha}\right)\left(q^{(t-j)^\alpha} - q^{(t-j+1)^\alpha}\right). \tag{2.15}$$

Figure 2.2 illustrates the weights for the DGWMA chart. The values for the DGWMA parameters are selected as $q = 0.5$, and $\alpha = 0.5, 0.6, 0.7, 0.8, 0.9, 1.0, 1.2$. The main objective of constructing a graph for the weights is to evaluate the weighting mechanism from the initial stage of the process (i.e., $t = 1$) up to the most recent observation. The shape of the weights play a major role in the performance of the charts. Also, the influence of the parameter α on the weights is studied when the other chart parameter q is equal for all the series. For small values of the parameter α (0.5 to 0.9), less weights are assigned to the initial observations and the weights decrease exponentially. For larger values of the parameter α ($\alpha \geq 1$), more weights are allocated to the past observations. The same interpretation is true by using $q = 0.6$, which is illustrated in Figure 2.2.

The allocation of the weights to observations, i.e., increasing and decreasing patterns, determines the ability of time-weighted charts in detecting shifts in production processes. Since time-weighted charts use the mixture of previous and current information, hence as a result have faster detection capability in detecting small shifts in the process due to the implementation of double exponential smoothing.

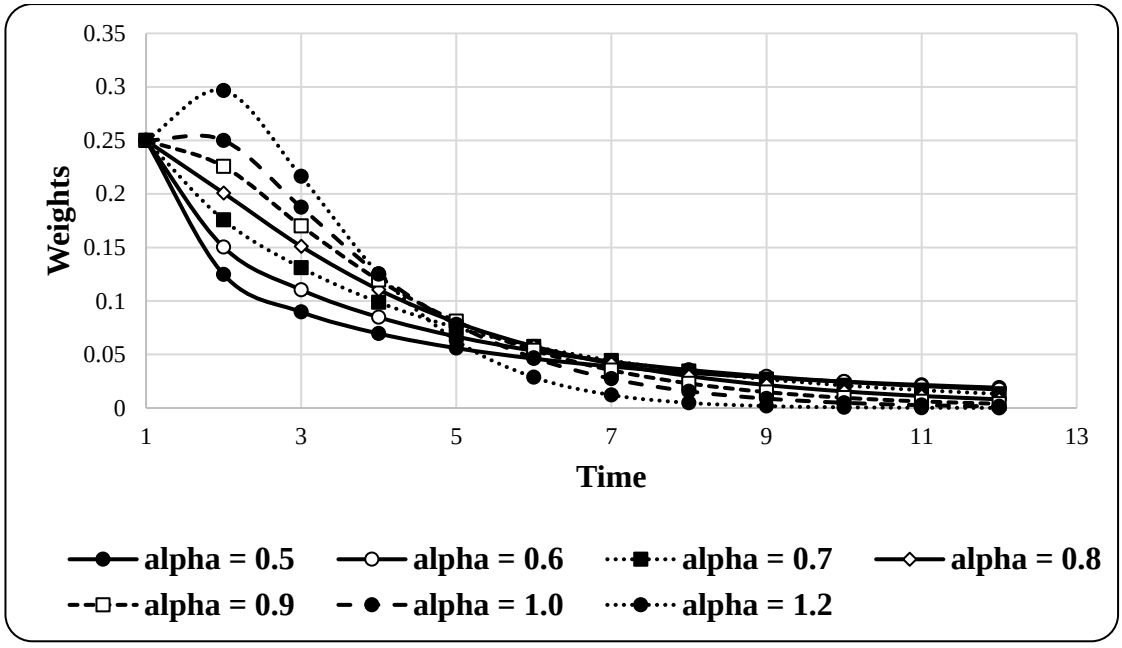

Figure 2.2. Weights for the DGWMA chart when $q = 0.5$

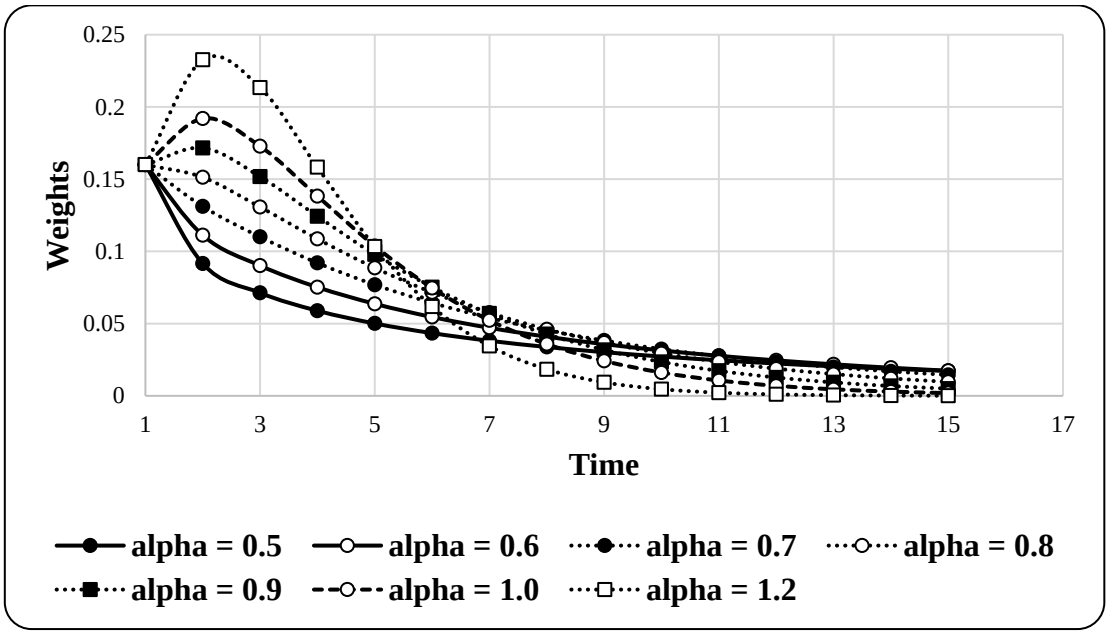

Figure 2.3. Weights for the DGWMA chart when $q = 0.6$

2.5.2 GWMA chart

In the DGWMA chart, by assuming $q_2 \to 0$ and $\alpha_2 = 1$, the chart reduces to the GWMA chart denoted by *GWMA* (q_1, α_1). Note that, theoretically the parameter q_2 cannot be equal to zero, since $q_2 > 0$. Thus, this time-weighted chart is called the "limiting case" of the DGWMA chart.

The weighting scheme for the GWMA chart is illustrated in Figures 2.3 and 2.4, when the parameter q_1 is selected as 0.5 and 0.9, respectively. The value for the parameter α_1 is selected as $0.75, 1, 1.25$

for Figure 2.4, and $0.5, 0.75, 1, 1.25$ for Figure 2.5. These figures illustrate that as the value for the parameter α_1 starts increasing, there are more weights assigned to the initial observations. Furthermore, by increasing the value for the parameter q_1, the weighting structure starts changing as well.

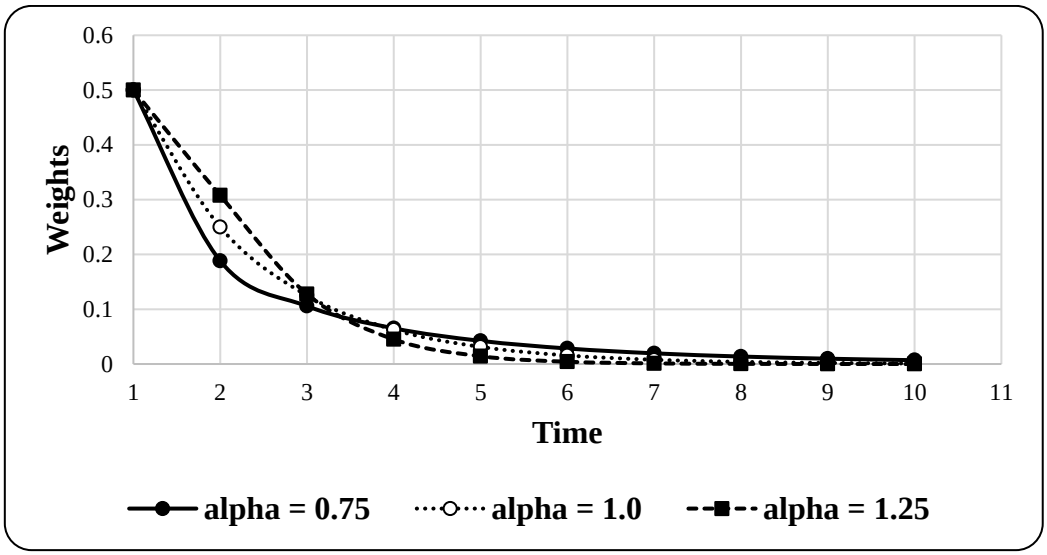

Figure 2.4. Weights for the GWMA chart when $q = 0.5$

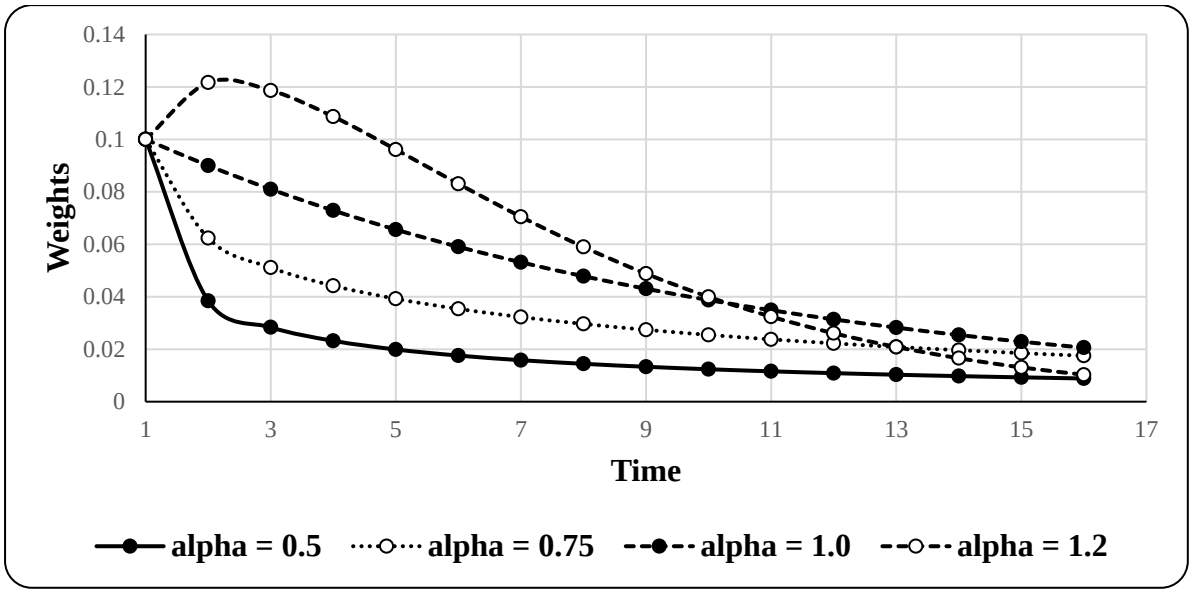

Figure 2.5. Weights for the GWMA chart when $q = 0.9$

2.5.3 EWMA chart

In the GWMA chart, by selecting $\alpha_1 = 1$, then it simplifies to the EWMA chart denoted as $EWMA\ (q_1)$. The same result can be obtained if one selects $\alpha_1 = \alpha_2 = 1$ and $q_2 \to 0$ – the DGWMA chart reduces to the EWMA chart denoted as $EWMA\ (q_1)$. Hence, the EWMA chart can be regarded as a limiting case

of the DGWMA chart, and as a special case of the GWMA chart. Also, Chakraborty et al. (2017) concluded that the EWMA chart is a special case of the GWMA chart. Further, one can briefly show that the EWMA chart reduces to the Shewhart chart when $q_1 \to 0$, which implies that the Shewhart chart is, in fact, a limiting case of the EWMA chart. The EWMA chart introduced by Roberts (1959) is denoted by *EWMA* (λ), where λ is the smoothing parameter. The relationship between the parameter q_1 and the smoothing parameter λ is $q_1 = 1 - \lambda$, and as a result the EWMA chart can also be denoted alternatively by *EWMA* ($q_1 = 1 - \lambda$). The weighting function of the EWMA chart is illustrated in Figure 2.6 when the parameter q_1 is: 0.95, 0.9, 0.8, 0.5 and 0.2, and as a result the weights are decreasing exponentially.

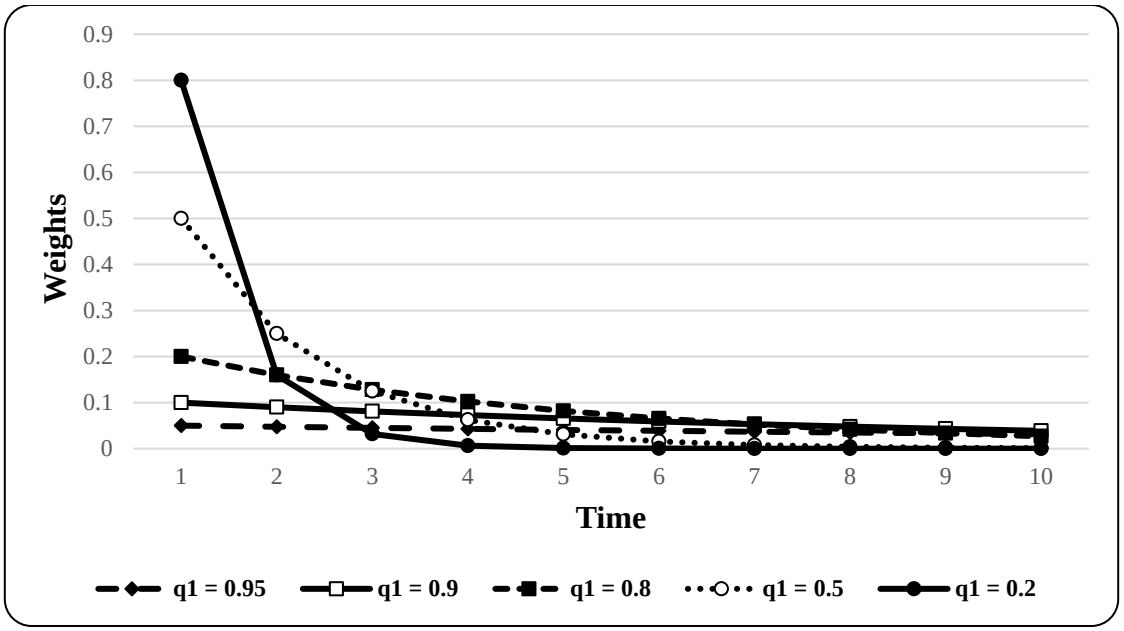

Figure 2.6. Weights for the EWMA chart

From Figure 2.6, the shape of the weights for the EWMA chart are decreasing exponentially quicker than the DGWMA, and the GWMA charts. Further, less weights are assigned to the initial observations for the EWMA chart in comparison with the GWMA and the DGWMA charts. This feature has a significant impact on the detection capability of the EWMA chart. For more information, see the OOC performance of the charts in Chapters 3 and 4.

2.5.4 EGWMA chart

In the DGWMA chart, by selecting $q_1 = q_2 = q$ and $\alpha_2 = 1$, the chart simplifies to the EGWMA chart denoted by *EGWMA* (q, α_1). The EGWMA chart is a combination of the weighted sequences for the EWMA and the GWMA charts. As a result, the weighting scheme defined in equation (2.9) becomes:

$$w_t = (1-q)\left(q^{t-1} - q^{t^{\alpha_1}}\right) + (1-q)^2 \sum_{j=1}^{t-1} q^{(t-j)^{\alpha_1}+j-1} . \qquad (2.16)$$

Sheu and Hsieh (2009) introduced the EGWMA chart as the special case of the DGWMA chart. However, they did not study the design and implementation of this chart in detail. Therefore, this will not be studied further in this thesis and is included in the scope for further research.

2.5.5 DEWMA chart (Case 1)

In general, Zhang and Chen (2005) studied and discussed two different scenarios for the DEWMA chart, depending on the equality and/or inequality of the smoothing parameters i.e., λ_1 and λ_2. By selecting $\alpha_1 = \alpha_2 = 1$, the DGWMA chart simplifies to the DEWMA chart (Case 1) denoted by *DEWMA* $(1 - q_1, 1 - q_2)$. Further to this, the relationship between the smoothing parameters (i.e., λ_1 and λ_2) and the parameters of the DGWMA chart (i.e., q_1 and q_2) can be expressed as $\lambda_1 = 1 - q_1$ and $\lambda_2 = 1 - q_2$. Moreover, by selecting $\lambda_1 \to 1$ and $\lambda_2 \to 1$, then the DEWMA chart reduces to the Shewhart chart. Also, by selecting $\lambda_1 \to 1$ or $\lambda_2 \to 1$, then the DEWMA chart reduces to the EWMA chart. As a conclusion, the EWMA and Shewhart charts are the limiting cases of both the DGWMA and the DEWMA charts.

The weighting scheme defined in equation (2.9) becomes:

$$w_t = (1 - q_1)(1 - q_2)\frac{1-\left(\frac{q_1}{q_2}\right)^t}{1-\frac{q_1}{q_2}} q_2^{t-1}. \tag{2.17}$$

Then, for the DGWMA chart, the plotting statistic can be rewritten as:

$$Z_t^2 = (1 - q_1)(1 - q_2)\sum_{i=1}^{t} \frac{1-\left(\frac{q_1}{q_2}\right)^{t-i+1}}{1-\frac{q_1}{q_2}} q_2^{t-i} T_i + \left(q_2(1 - q_1)\frac{q_2^i - q_1^i}{q_2 - q_1} + q_1^i\right) Z_0^2 \; ; \tag{2.18}$$

where Z_0^2 is the starting value, and T_i is the sample statistic.

The weights for the DEWMA chart are illustrated in Figures 2.7 and 2.8 for different combinations of the parameters q_1 and q_2. In Figure 2.7, $q_1 = 0.5$ and $q_2 = 0.6, 0.8, 0.9$; whereas in Figure 2.7, $q_1 = 0.6, 0.8, 0.9$ and $q_2 = 0.7$. From Figure 2.7, when the parameter q_1 is the same for all of the series, more weight is assigned to the initial observations for smaller values of the parameter q_2. In Figure 2.8, when the parameter q_2 is the same for all of the series, more weights are assigned to the initial observations when $q_1 = 0.8$.

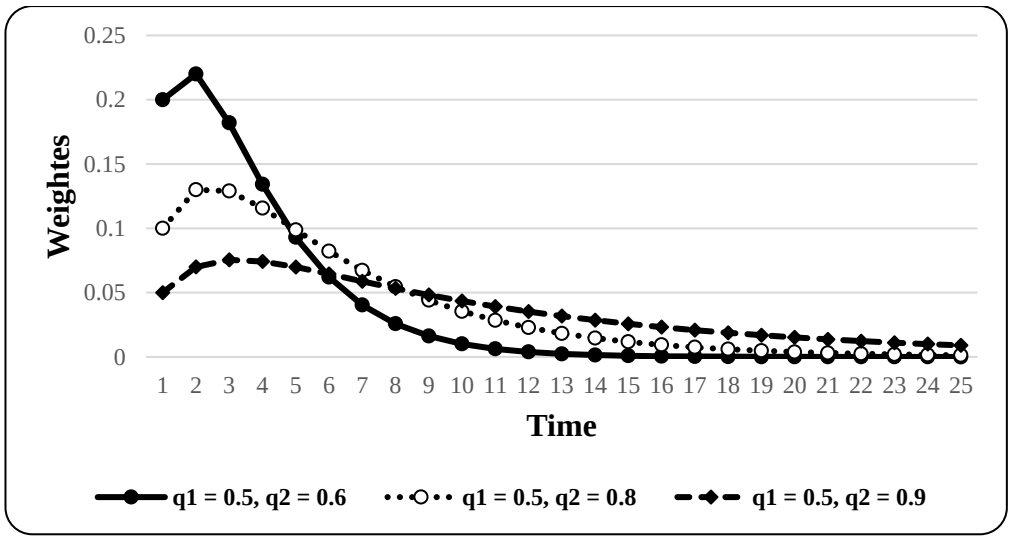

Figure 2.7. Weights for the DEWMA chart (Case 1)

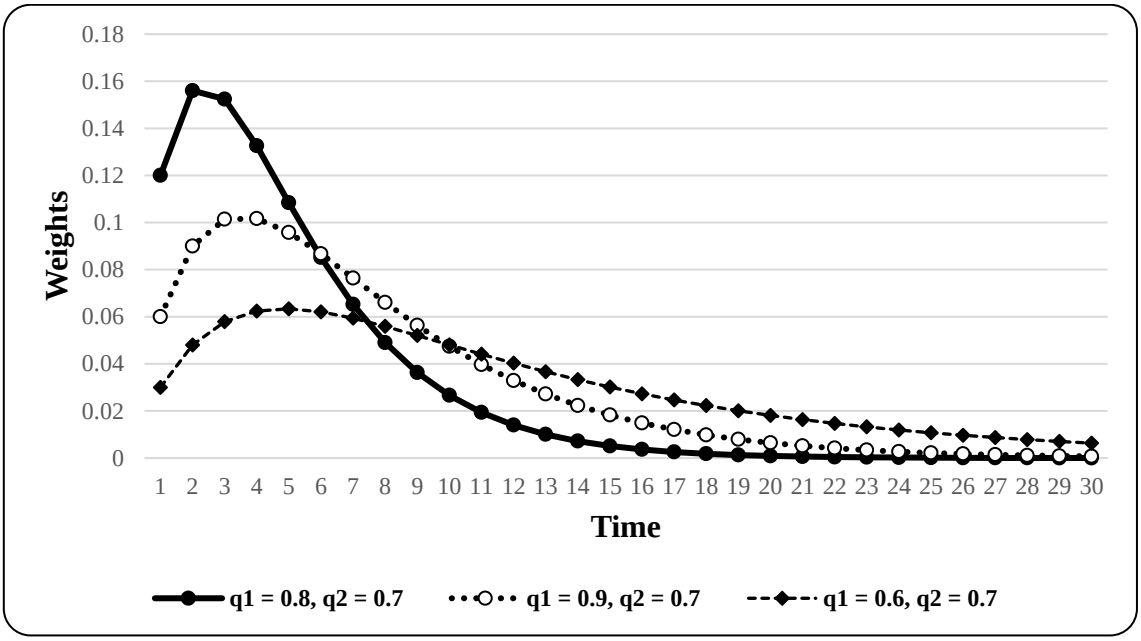

Figure 2.8. Weights for the DEWMA chart (Case 2)

The shape for the DEWMA chart's weights illustrates that more weights are assigned to the initial observations in comparison to the EWMA chart. However, further analysis is required in terms of the design and implementation of the DEWMA chart and the performance comparison with other time-weighted charts.

2.5.6 DEWMA chart (Case 2)

By selecting $q_1 = q_2 = q$ and $\alpha_1 = \alpha_2 = 1$, the DGWMA chart reduces to the DEWMA chart, denoted by *DEWMA* $(1-q)$. As a result, the weighting scheme defined in equation (2.9) becomes:

$$w_t = tq^{t-1}(1-q)^2 \tag{2.19}$$

Then, the plotting statistic is defined as:

$$Z_t^2 = (1-q)^2 \sum_{i=1}^{t}(t-i+1)q^{t-i}\,T_{t-i+1} + q^t(t-tq+1)Z_0^2 \tag{2.20}$$

Shamma and Shamma (1992) introduced and studied the performance of the DEWMA chart denoted by *DEWMA* (λ) with a single smoothing parameter. The DEWMA chart presented in this section is called the DEWMA chart (Case 2) since the smoothing parameters are equal (i.e., $\lambda_1 = \lambda_2 = \lambda$). The relationship between the smoothing parameter (λ) and the DGWMA parameter (q) is equivalent to $q = 1-\lambda$.

The weights for the DEWMA chart are illustrated in Figure 2.9 when the parameter q is selected as $q = 0.6, 0.7, 0.8$. The initial observations are assigned with more weight for the smaller value of the parameter q.

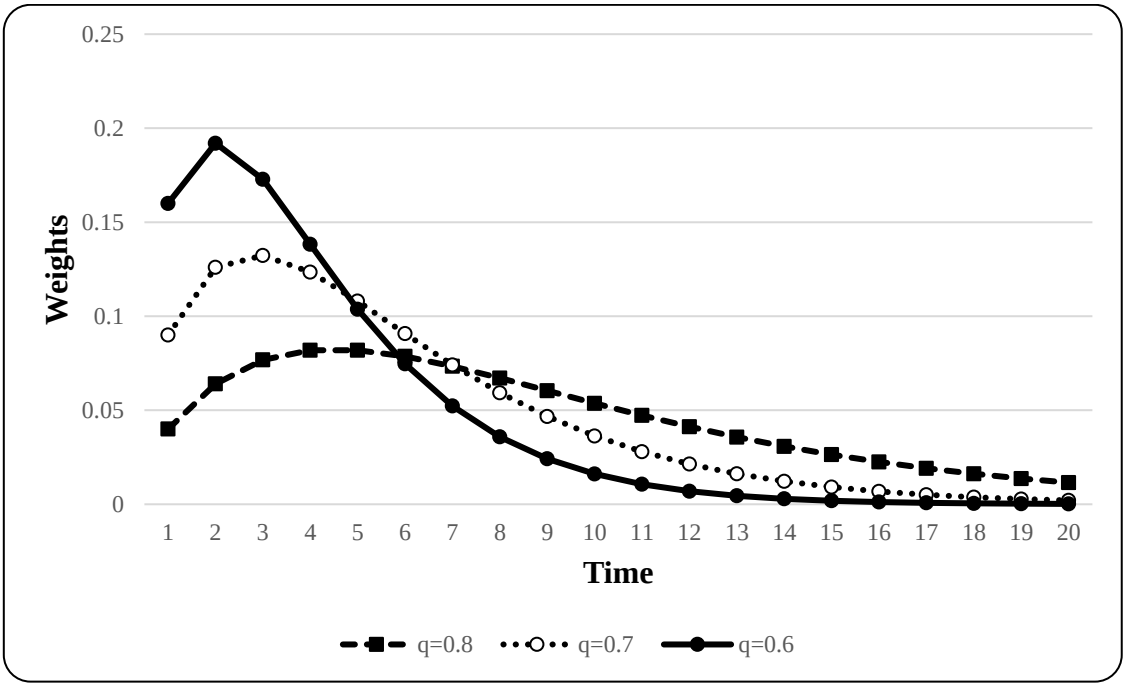

Figure 2.9. Weights for the DEWMA chart (Case 2)

2.6 Run length distribution

There are several measures in the SPC environment to evaluate and compare the performance of competing charts. The recent brief literature review by Nikolaidis and Tagaras (2017), discussed and developed new statistical measures of performance. The most well-known and commonly used measure is the run length distribution, which is defined in Section 1.2 in Chapter 1. The average run length (*ARL*) is the most conventional statistical measure in SPC and other properties of the run length distribution, such as the median of the run length (*MDRL*), the standard deviation of the run length (*SDRL*), and the different percentiles, could be calculated to provide more information and insight on the performance comparison between different charts.

For the DGWMA chart, which is the core of this thesis, a Monte Carlo simulation is considered as the only method in the context of the SPC literature to evaluate the run length distribution. Sheu and Hsieh (2009) and Lu (2018) amongst others concluded that other approaches encounter challenges/obstacles, such as the computational difficulties, and are time-consuming. Overall, there are three methods that are often used to calculate or evaluate the *ARL*: (i) the exact approach introduced by Crowder (1987); (ii) the Monte Carlo simulation; and (iii) the Markov chain approach proposed and developed by Brook and Evans (1972). For more recent developments in the area of computing the *ARL* and related indexes in SPC, the work of Li et al. (2014) is relevant.

In this section, each of these approaches are discussed in more detail for the DGWMA chart and the pros and cons will also be highlighted. As stated in Chapter 1, one of the main contributions of the present research is to calculate the run length distribution for the DGWMA chart by implementing the exact and the Markov chain approaches. For the Markov chain approach, the steady-state limits are used, whereas the exact limits are considered for the exact approach. These methods are generally neglected and dismissed in the SPC literature due to the computational time and other complexities arise during the evaluation of the closed-form expressions. Further to this, for the DEWMA chart, which is the special case of the DGWMA chart, the Markov chain approach is used to obtain the closed-form expressions for the *ARL* and other properties of the run length distribution. This is due to the fact that the DEWMA chart can be viewed as a first-order Markov chain as opposed to the DGWMA chart.

2.6.1 Exact approach

The idea of computing the *ARL* through the exact approach by evaluating the integral equations is originally proposed for the EWMA chart by Crowder (1987). Moreover, he used numerical quadrature methods to solve the exact integral equations for the normal distribution. Let N denote the run length for the DGWMA chart, and the p.m.f. of N is called the run length distribution, denoted as $P[N = n]$, where $n = 1, 2, 3, \ldots$. The signaling event at the i^{th} sample is denoted by A_i, whereas the non-signaling event is denoted by A_i^c, and given by $A_i^c = [LCL < Z_i^2 < UCL]$ for $i = 1, 2, \ldots$. The run length

distribution can be written as $\mathrm{P}[N = n] = \mathrm{P}[\{\cap_{i=1}^{n-1} A_i^c\} \cap A_n]$, for $n = 1, 2, \ldots$. The plotting statistic plots below the *UCL* for $\forall t > 1$, can be written as:

$$Z_t^2 < UCL \Leftrightarrow \left(\sum_{i=1}^{t} w_t\, T_{t-i+1} + \left(1 - \sum_{i=1}^{t} w_i\right) Z_0^2\right) < UCL$$
$$\Leftrightarrow T_t < \frac{UCL - \left(\sum_{i=2}^{t} w_t T_{t-i+1} + \left(1 - \sum_{i=1}^{t} w_i\right) Z_0^2\right)}{(1-q_1)(1-q_2)}.$$

The plotting statistic plots above the *LCL* for $\forall i > 1$, can be written as:

$$Z_t^2 > LCL \Leftrightarrow T_t > \frac{LCL - \left(\sum_{i=2}^{t} w_t T_{t-i+1} + \left(1 - \sum_{i=1}^{t} w_i\right) Z_0^2\right)}{(1-q_1)(1-q_2)}.$$

The following notations are defined for $t = 2, 3, \ldots$ as follows:

$$U_t = \frac{UCL - \left(\sum_{i=2}^{t} w_t\, T_{t-i+1} + \left(1 - \sum_{i=1}^{t} w_i\right) Z_0^2\right)}{(1-q_1)(1-q_2)},$$
$$L_t = \frac{LCL - \left(\sum_{i=2}^{t} w_t\, T_{t-i+1} + \left(1 - \sum_{i=1}^{t} w_i\right) Z_0^2\right)}{(1-q_1)(1-q_2)}, \tag{2.21}$$

where $U_1 = \frac{UCL-(1-w_1)Z_0^2}{(1-q_1)(1-q_2)}$ and $L_1 = \frac{LCL-(1-w_1)Z_0^2}{(1-q_1)(1-q_2)}$.

The plotting statistics T_t are dependent on the control limits defined in (2.21). Hence, this dependency arises complexity to use the exact approach and obtain the closed-form expressions for the run length distribution. As an alternative, the joint distribution of a sequence of independent sample statistics T_i is considered and then compared with the limits defined in equation (2.21). Hence, the non-signaling event are equivalent to: $A_i^c = [LCL < Z_i^2 < UCL] \equiv [L_i < T_i < U_i]$. This implies that the calculation for the run length distribution depends on the distribution of the sample statistic T_i.

The probability of run length equal to 1 is equivalent to:

$$\mathrm{P}[\mathrm{N} = 1] = \mathrm{P}[A_1] = 1 - \mathrm{P}[L_1 < T_1 < U_1]. \tag{2.22}$$

By implementing the unconditional/conditional approach, the probability that the run length distribution is equal to *n*, i.e., $\mathrm{P}[N = n]$, can be written as:

$$\mathrm{P}[N = n] = \mathrm{P}\left[\{\cap_{i=1}^{n-1} A_i^c\} \cap A_n\right]$$
$$= \mathrm{P}\left[\cap_{i=1}^{n-1} \{T_i \in (U_i, L_i)\} \cap \{Z_n^2 \notin (UCL, LCL)\}\right]$$
$$= \int_{L_1}^{U_1} \int_{L_2}^{U_2} \ldots \int_{L_{n-1}}^{U_{n-1}} \mathrm{P}\left[\{Z_n^2 \notin (UCL, LCL)\} \mid \cap_{i=1}^{n-1} \{T_i \in (U_i, L_i)\}\right] g(t_1, t_2, \ldots, t_{n-1}) dt_n dt_{n-1} \ldots dt_1$$

In Section 2.3, it is assumed that the observations are independent, which results in the independency of the sample statistics T_i. Hence, the joint distribution of $T_1, T_2, \ldots, T_n$ can be written as

$g(t_1, t_2, \dots, t_n) = \prod_{i=1}^{n} g(t_i)$, when $T_i \sim G_{\boldsymbol{\theta}}$ $(\forall\, i)$, and for some continuous c.d.f. $G_{\boldsymbol{\theta}}$. Hence, $\mathrm{P}[N = n]$ can be written as:

$$\mathrm{P}[N = n] = \int_{L_1}^{U_1} \int_{L_2}^{U_2} \dots \int_{L_{n-1}}^{U_{n-1}} \mathrm{P}[\{Z_n^2 \notin (UCL, LCL)\} \mid \cap_{i=1}^{n-1} \{T_i \in (U_i, L_i)\}] \prod_{i=1}^{n-1} g(t_i)\, dt_n dt_{n-1} \dots dt_1,$$

where g(.) is the probability density function of the plotting statistic.

This approach requires calculation of all the sample statistics T_i values so that $T_i \in (U_i, L_i)$, $\forall i$ and as the number of run length i.e., *n* increases, the computation of the integrals becomes cumbersome and time-consuming.

An alternative approach would be to write the run length probability as follows:

$\mathrm{P}[N = n] = \mathrm{P}\left[\{\cap_{i=1}^{n-1} A_i^c\} \cap A_n\right] = \mathrm{P}\left[\cap_{i=1}^{n-1} A_i^c\right] - \mathrm{P}\left[\{\cap_{i=1}^{n-1} A_i^c\} \cap A_n^c\right]$

$= \mathrm{P}\left[\cap_{i=1}^{n-1} A_i^c\right] - \mathrm{P}[\cap_{i=1}^{n} A_i^c]$.

Therefore, for $n = 2,3,\dots$:

$$\mathrm{P}[N = n] = \mathrm{P}\left[\cap_{i=1}^{n-1} A_i^c\right] - \mathrm{P}[\cap_{i=1}^{n} A_i^c]; \tag{2.23}$$

where A_i^c is the non-signalling event at the i^{th} sample, and is defined as $A_i^c = [L_i < T_i < U_i]$.

Equation (2.23) is equivalent to:

$$\mathrm{P}[N = n] = I_{n-1} - I_n,\ n = 2,3,\dots \tag{2.24}$$

where $I_n = \mathrm{P}[\cap_{i=1}^{n} A_i^c]$ and $\mathrm{P}[N = 1] = \mathrm{P}[A_1] = 1 - I_1$.

In Section 2.3, it is assumed that the observations are independent, which results in the independency of the sample statistics T_i. Hence, the joint distribution of $T_1, T_2, \dots, T_n$ can be written as $g(t_1, t_2, \dots, t_n) = \prod_{i=1}^{n} g(t_i)$, when $T_i \sim G_{\boldsymbol{\theta}}$ $(\forall\, i)$, and for some continuous c.d.f. $G_{\boldsymbol{\theta}}$.

Therefore,

$$I_n = \mathrm{P}[\cap_{i=1}^{n} A_i^c] = \int_{L_1}^{U_1} \int_{L_2}^{U_2} \dots \int_{L_n}^{U_n} \prod_{i=1}^{n} g(t_i)\ dt_i. \tag{2.25}$$

The expression in equation (2.25) implies that for any p.d.f. $g(t_i)$, a DGWMA control chart can be designed. However, the design for the DGWMA chart depends on the availability of an efficient algorithm, which can evaluate expression (2.25) without any simulation involved.

The *ARL* can be obtained as follows:

$ARL = E(N) = \sum_{n=1}^{\infty} n\, \mathrm{P}[N = n]$

$= \mathrm{P}[N = 1] + \sum_{n=2}^{\infty} n\, \mathrm{P}[N = n] = \mathrm{P}[A_1] + \sum_{n=2}^{\infty} n(I_{n-1} - I_n) = 1 - I_1 + I_1 + \sum_{n=1}^{\infty} I_n$

$= 1 + \sum_{n=1}^{\infty} I_n$.

The variance for the run length distribution denoted as *VRL* can be obtained as:

$$VRL = var(N) = E(N^2) - (E(\mathrm{N}))^2$$

$$= \sum_{n=1}^{\infty} n^2 \, \mathrm{P}[N = n] - ARL^2 = \mathrm{P}[N = 1] + \sum_{n=2}^{\infty} n^2 \, \mathrm{P}[N = n] - ARL^2$$
$$= 1 - I_1 + \sum_{n=2}^{\infty} (n(n-1) + n) \, \mathrm{P}[N = n] - ARL^2$$

$$= 1 - I_1 + \sum_{n=2}^{\infty} n(n-1)(I_{n-1} - I_n) + \sum_{n=2}^{\infty} n(I_{n-1} - I_n) - ARL^2$$
$$= 1 + 2I_1 + 2\sum_{n=2}^{\infty} nI_n + \sum_{n=1}^{\infty} I_n - ARL^2$$
$$= 1 + 2\sum_{n=1}^{\infty} nI_n + \sum_{n=1}^{\infty} I_n - ARL^2$$
$$= 1 + \sum_{n=1}^{\infty} (2n+1) I_n - ARL^2 \, .$$

The p.d.f. of the run length *N*, denoted by $F_N(n)$ for $n = 1,2,3, \ldots$, can be obtained as follows:

$$F_N(n) = \sum_{i=1}^{n} \mathrm{P}[N = i] = \mathrm{P}[N = 1] + \sum_{i=2}^{n} (I_{i-1} - I_i)$$
$$= 1 - I_1 + (I_1 - I_2) + (I_2 - I_3) + \cdots + (I_{n-1} - I_n) = 1 - I_n.$$

Hence, the closed-form expressions for the *ARL*, *VRL*, SDRL, and $F_N(n)$ for the DGWMA chart obtained from the exact approach are:

$$ARL = 1 + \sum_{n=1}^{\infty} I_n \tag{2.26}$$

$$VRL = 1 + \sum_{n=1}^{\infty} (2n+1) I_n - ARL^2 \tag{2.27}$$

$$SDRL = \sqrt{1 + \sum_{n=1}^{\infty} (2n+1) I_n - ARL^2} \tag{2.28}$$

$$F_N(n) = 1 - I_n, \text{ for } n = 1,2, \ldots \tag{2.29}$$

where I_n is defined in equation (2.25).

Although the properties of the run length distribution are provided in terms of closed-form expressions, the evaluation of these equations is cumbersome and time-consuming due to the following reasons:

(i) In equation (2.25), the lower bounds in the integrals are functions of the preceding statistics $X_1, X_2, \ldots, X_{i-1}$, and mutually dependent, which makes the exact method a computationally inefficient approach.

(ii) Since calculating equations (2.26) to (2.29) depends on finding the integrals in (2.25), the calculation process is complex.

(iii) As n increases, the number of integrals in equation (2.25) that needs to be evaluated increases. As a result, a high-dimensional integral equation need to be evaluated and the computation process becomes time-consuming and intensive.

However, by using the Mathematica software package and by assuming a specific type of distribution, equation (2.25) can be evaluated and calculated for $n = 1,2,3,4$. The results are presented in Chapter 3 for the proposed DGWMA-TBE chart under the gamma distribution.

2.6.2 Markov chain approach

Brook and Evans (1972) proposed the Markov chain approach for the first time in the SPC literature. For the EWMA chart, Lucas and Saccucci (1990) implemented the Markov chain approach for the normal distribution. This approach is easily adjustable to various time-weighted charts exist in the literature and simplify solutions to the particular cases to which they are applied. The complexities of implementing the Markov chain method for the DGWMA chart have been raised and noted by Sheu and Hsieh (2009), Chiu and Lu (2015), amongst others. This section includes a brief discussion on the general steps involved in applying the Markov chain method for the DGWMA chart, as well as for its special case, the DEWMA chart.

Fu and Lou (2003) provided a detailed discussion on the general results of the Markov chain approach. The approach entails that the run length can be written in terms of a finite Markov chain. As a result, the run length random variable *N* can be demonstrated by the probability that the Markov chain resides in a specific subset *S* that belongs to a state-space (denoted by Ω), and **M** that is a transition probability matrix. The state-step defined as the set of values that the random variable *N* can take, consists of two types of states – (i) ν non-absorbing states (i.e., the region between the control limits); and (ii) one absorbing state (i.e., the region on or above/below the control limits) – so that in total there are $\nu + 1$ states. The transition probability matrix **M** is defined as:

$$\boldsymbol{M}_{(\nu+1)\times(\nu+1)} = \begin{pmatrix} \boldsymbol{Q}_{\nu\times\nu} & q_{\nu\times 1} \\ 0_{1\times\nu} & \mathbf{1}_{\boldsymbol{\nu}\times\mathbf{1}} \end{pmatrix}.$$

The expressions for the *ARL*, *SDRL*, and $F_N(n)$, based on the theorems from Fu and Lou (2003) are as follows:

$$ARL = \boldsymbol{\xi}(\boldsymbol{I} - \boldsymbol{Q})^{-1}\mathbf{1} \tag{2.30}$$

$$SDRL = \sqrt{\boldsymbol{\xi}(\boldsymbol{I} + \boldsymbol{Q})(\boldsymbol{I} - \boldsymbol{Q})^{-2}\mathbf{1} - ARL^2} \tag{2.31}$$

$$F_N(n) = 1 - \boldsymbol{\xi}\boldsymbol{Q}^{\boldsymbol{n}}\mathbf{1}, \text{ for } n = 1,2, \dots, \tag{2.32}$$

where the sub-matrix $\boldsymbol{Q}_{\nu\times\nu} = \boldsymbol{Q}$ is called the essential transient probability sub-matrix with order ν, $q_{\nu\times 1}$ is a column vector defined as $q_{\nu\times 1} = (\boldsymbol{I}_\nu - \boldsymbol{Q}_{\nu\times\nu})\mathbf{1}_{\nu\times 1}$, where $\mathbf{1}_{\nu\times 1}$ is a unit vector, $\boldsymbol{I}_\nu$ is an identity matrix with order ν, $0_{1\times\nu}$ is a row vector, and $\boldsymbol{\xi}_{1\times\nu} = \boldsymbol{\xi} = (1,0,0, \dots, 0)$ is the initial distribution**.**

The procedures of constructing the state-space Ω and the essential transition probability sub-matrix $\boldsymbol{Q}_{v\times v}$ are the fundamental parts and main objectives of employing the Markov chain approach to calculate the run length distribution.

(i) DGWMA chart

Each plotting statistic Z_t^2 for the DGWMA chart depends on all the previous plotting statistics. From equation (2.10) the plotting statistic is:

$$Z_t^2 = \sum_{i=1}^{t} w_t\, T_{t-i+1} + \left(1 - \sum_{i=1}^{t} w_i\right) Z_0^2 \quad \text{for} \quad t = 1,2,3, \dots , \tag{2.33}$$

where $w_t = \sum_{j=1}^{t} \left(q_1^{(j-1)^{\alpha_1}} - q_1^{j^{\alpha_1}}\right)\left(q_2^{(t-j)^{\alpha_2}} - q_1^{(t-j+1)^{\alpha_2}}\right)$, are the weights.

The plotting statistic for different values of t can be expanded as follows:

$$Z_1^2 = (1-q_1)(1-q_2)T_1 + (q_1 + q_2 - q_1 q_2) Z_0^2$$

$$Z_2^2 = (1-q_1)\left(q_2 - q_2^{2^{\alpha_2}}\right)T_2 + \left(q_1 - q_1^{2^{\alpha_1}}\right)(1-q_2)T_1 + \left(1 - q_1 + q_2^{2^{\alpha_2}} + q_1^{2^{\alpha_1}} - q_2 q_1^{2^{\alpha_1}} + 2q_1 q_2 - q_2\right) Z_0^2$$

$$Z_3^2 = (1-q_1)\left(q_2^{2^{\alpha_2}} - q_2^{3^{\alpha_2}}\right)T_3 + \left(q_1 - q_1^{2^{\alpha_1}}\right)\left(q_2 - q_2^{2^{\alpha_2}}\right)T_2 + \left(q_1^{2^{\alpha_1}} - q_1^{3^{\alpha_1}}\right)(1-q_2)T_1 + (1 - q_2^{2^{\alpha_2}} + q_2^{3^{\alpha_2}} + q_1 q_2^{2^{\alpha_2}} - q_1 q_2^{3^{\alpha_2}} - q_1 q_2 + q_1 q_2^{2^{\alpha_2}} + q_2 q_1^{2^{\alpha_1}} - q_1^{2^{\alpha_1}} q_2^{2^{\alpha_2}} - q_1^{2^{\alpha_1}} + q_2^{2^{\alpha_2}} + q_1^{3^{\alpha_1}} - q_2 q_1) Z_0^2$$

.

.

.

$$Z_t^2 = (1-q_1)\left(q_2^{(t-1)^{\alpha_2}} - q_2^{t^{\alpha_2}}\right)T_t + \cdots + \left(q_1^{(t-1)^{\alpha_1}} - q_1^{t^{\alpha_1}}\right)(1-q_2)T_1 + \left(1 - q_2^{(t-1)^{\alpha_2}} + q_1^{t^{\alpha_1}} + q_2 q_1^{(t-1)^{\alpha_1}} - q_1 q_2^{t^{\alpha_2}} + q_2^{t^{\alpha_2}}\right) Z_0^2. \tag{2.34}$$

The $(t+1)^{th}$ plotting statistic is given by:

$$Z_{t+1}^2 = (1-q_1)\left(q_2^{t^{\alpha_2}} - q_2^{(t+1)^{\alpha_2}}\right)T_{t+1} + \cdots + \left(q_1^{t^{\alpha_1}} - q_1^{(t+1)^{\alpha_1}}\right)(1-q_2)T_1 + \left(1 - q_2^{t^{\alpha_2}} + q_1^{(t+1)^{\alpha_1}} + q_2 q_1^{t^{\alpha_1}} - q_1 q_2^{(t+1)^{\alpha_2}} + q_2^{(t+1)^{\alpha_2}}\right) Z_0^2 . \tag{2.35}$$

The first t equations in (2.34) can be written in a matrix format as follows:

$$\underset{\sim}{\boldsymbol{Z}}_t^2 = \boldsymbol{\mathcal{A}}_t \, \underset{\sim}{\boldsymbol{T}}_t + Z_0^2 \, \underset{\sim}{\boldsymbol{Q}}_t;$$

(2.36)

where $\underset{\sim}{\boldsymbol{Z}}_t^2$ is representing a column vector for plotting statistics (order t), i.e., $\underset{\sim}{\boldsymbol{Z}}_t^2 = (Z_1^2, Z_2^2, \dots, Z_t^2)^T$, $\underset{\sim}{\boldsymbol{T}}_t = (T_1, T_2, T_3, \dots, T_t)^T$ is a column vector for the test statistics (order t), $\underset{\sim}{\boldsymbol{Q}}_t = \Big(q_1 + q_2 - q_1 q_2, 1 - q_1 + q_2^{2^{\alpha_2}} + q_1^{2^{\alpha_1}} - q_2 q_1^{2^{\alpha_1}} + 2q_1 q_2 - q_2, \dots, 1 - q_2^{t^{\alpha_2}} + q_1^{(t+1)^{\alpha_1}} + q_2 q_1^{t^{\alpha_1}} - q_1 q_2^{(t+1)^{\alpha_2}} + q_2^{(t+1)^{\alpha_2}}\Big)^T$, and $\boldsymbol{\mathcal{A}}_t$ is a $(t \times t)$ lower triangular matrix given by:

$$\boldsymbol{\mathcal{A}}_t = \begin{pmatrix} (1-q_1)(1-q_2) & 0 & 0 & & 0 \\ (q_1 - q_1^{2^{\alpha_1}})(1-q_2) & (1-q_1)(q_2 - q_2^{2^{\alpha_2}}) & 0 & \cdots & 0 \\ (q_1^{2^{\alpha_1}} - q_1^{3^{\alpha_1}})(1-q_2) & (q_1 - q_1^{2^{\alpha_1}})(q_2 - q_2^{2^{\alpha_2}}) & (1-q_1)(q_2^{2^{\alpha_2}} - q_2^{3^{\alpha_2}}) & & 0 \\ & \vdots & & \ddots & \vdots \\ \left(q_1^{(t-1)^{\alpha_1}} - q_1^{t^{\alpha_1}}\right)(1-q_2) & q^{(t-2)^{\alpha}} - q^{(t-1)^{\alpha}} & & \cdots & (1-q_1)(1-q_2) \end{pmatrix}.$$

The $(t+1)^{th}$ plotting statistic defined in equation (2.35) can be rewritten as:

$$Z_{t+1}^2 = (1-q_1)\left(q_2^{t^{\alpha_2}} - q_2^{(t+1)^{\alpha_2}}\right) T_{t+1} + \left(\left(q_1^{t^{\alpha_1}} - q_1^{(t+1)^{\alpha_1}}\right)(1-q_2), \dots, \left(q_2^{t^{\alpha_2}} - q_2^{(t+1)^{\alpha_2}}\right)\left(q_1^{t^{\alpha_1}} - q_1^{(t+1)^{\alpha_1}}\right)\right) \underset{\sim}{\boldsymbol{T}}_t + \left(1 - q_2^{t^{\alpha_2}} + q_1^{(t+1)^{\alpha_1}} + q_2 q_1^{t^{\alpha_1}} - q_1 q_2^{(t+1)^{\alpha_2}} + q_2^{(t+1)^{\alpha_2}}\right) Z_0^2.$$

Equation (2.36) is equivalent to:

$$\underset{\sim}{\boldsymbol{T}}_t = \boldsymbol{\mathcal{A}}_t^{-1} \left(\underset{\sim}{\boldsymbol{Z}}_t^2 - Z_0^2 \, \underset{\sim}{\boldsymbol{Q}}_t\right).$$

By replacing the above equation into Z_{t+1}^2 in equation (2.35), the result is as follows:

$$Z_{t+1}^2 = (1-q_1)\left(q_2^{t^{\alpha_2}} - q_2^{(t+1)^{\alpha_2}}\right) T_{t+1} + \underset{\sim}{\boldsymbol{q}}_t \, \boldsymbol{\mathcal{A}}_t^{-1} \left(\underset{\sim}{\boldsymbol{Z}}_t^2 - Z_0^2 \, \underset{\sim}{\boldsymbol{Q}}_t\right) + \left(1 - q_2^{t^{\alpha_2}} + q_1^{(t+1)^{\alpha_1}} + q_2 q_1^{t^{\alpha_1}} - q_1 q_2^{(t+1)^{\alpha_2}} + q_2^{(t+1)^{\alpha_2}}\right) Z_0^2 ;$$

(2.37)

where $\underset{\sim}{\boldsymbol{q}}_t = \left(\left(q_1^{t^{\alpha_1}} - q_1^{(t+1)^{\alpha_1}}\right)(1-q_2), \dots, (1-q_1)(1-q_2)\right)$ is a row vector of order t.

From equations (2.36) and (2.37), it can be observed that for each plotting statistic, the order of dependency varies as a new observation enters the process. The order of dependency is $(t-1)$ for Z_t^2, whereas for Z_{t+1}^2 the order is t. Hence, for the DGWMA plotting statistics, the order of dependency is varying, and all plotting statistics contain information from the initial stage of the process. Thus, if changes are made at the starting point of the process, all the future plotting statistics are affected accordingly. In other words, from the practical point of view this implies that the DGWMA chart combines information from the past and present which increases the sensitivity of the chart in detecting tiny shifts in the process.

The order of dependency is varying for the DGWMA chart, and as a result the charting statistic cannot be viewed as a first-order Markov chain. Hence, the derivation of the closed-form expressions becomes cumbersome. Further to this, Chakraborty et al. (2017) concluded the same outcome for the GWMA chart which is a limiting case of the DGWMA chart.

Alternatively, in order to make the Markov chain approach more convenient and obtain the closed-form expressions for the *ARL* and other properties of the run length distribution, the special case of the DGWMA chart, the DEWMA chart, will be discussed next.

(ii) DEWMA chart

The Markov chain approach can be considered for Case 1 and Case 2 of the DEWMA chart, see Figure 2.1. However, since Case 1 is a generalized form of the DEWMA chart involving two smoothing parameters, i.e., λ_1 and λ_2, the Markov chain methodology is discussed for this case. Note that, the results can be obtained for Case 2 in a similar manner.

The run length distribution of a DEWMA chart can be approximated by the Markov chain approach, which entails that the plotting statistic – i.e., Z_t defined as $Z_t = \lambda_2 C_t + (1-\lambda_2)Z_{t-1}$ for $t \geq 1$, where $C_t = \lambda_1 T_t + (1-\lambda_1)C_{t-1}$ for $t \geq 1$ – can be considered as a first-order Markov chain with Ω as a state-space, and a transition probability matrix $\boldsymbol{M}$. Since the present value of the plotting statistics Z_t depends on the current plotting statistic C_t and one previous plotting statistic Z_{t-1}, it is possible to implement the Markov chain approach. A crucial point that needs to be employed first is to discretize the range of the plotting statistic within the control limits. As a result, each subinterval can be taken as a state of the Markov chain, since the plotting statistics are generally continuous random variables. For a two-sided DEWMA chart, half of the width for the subinterval is defined as $\gamma = (UCL - LCL)/2\nu$, where ν is defined as the number of subintervals between the control limits. The area outside the control limits represents the absorbing state (one absorbing state), while each subinterval within the control limits is called a non-absorbing state (ν transient states), so that there are $\nu + 1$ states in total. The process is said to be OOC when the plotting statistic is in an absorbing state, while the process is declared to be IC if the plotting statistic is in a non-absorbing state. The midpoint of the i^{th} subinterval denoted by S_i is defined as $S_i = LCL + (2i-1)\,\gamma$ for $i = 1, 2, \ldots, \nu$.

The t^{th} plotting statistic is in state i if Z_t is in the i^{th} subinterval. The transition probability p_{ij} is defined as $p_{ij} = P\left[S_j - \gamma < Z_t < S_j + \gamma \middle| Z_{t-1} = S_i\right]$ (see Evan and Brooks (1972)). For the DEWMA chart, the transition probability can be written as:

$$P\left[S_j - \gamma < Z_t < S_j + \gamma \middle| Z_{t-1} = C_{t-1} = S_i\right]$$
$$= P\left[S_j - \gamma < \lambda_2 C_t + (1-\lambda_2)Z_{t-1} < S_j + \gamma \middle| Z_{t-1} = C_{t-1} = S_i\right]$$

$$= P\left[S_j - \gamma < \lambda_2 C_t + (1-\lambda_2)S_i < S_j + \gamma \middle| Z_{t-1} = C_{t-1} = S_i\right]$$
$$= P\left[S_j - \gamma < \lambda_2(\lambda_1 T_t + (1-\lambda_1)C_{t-1}) + (1-\lambda_2)S_i < S_j + \gamma \middle| Z_{t-1} = C_{t-1} = S_i\right]$$
$$= P\left[S_j - \gamma < \lambda_1\lambda_2 T_t + \lambda_2(1-\lambda_1)S_i + (1-\lambda_2)S_i < S_j + \gamma \middle| Z_{t-1} = C_{t-1} = S_i\right]$$
$$= P\left[\frac{S_j-\gamma-\lambda_2(1-\lambda_1)S_i-(1-\lambda_2)S_i}{\lambda_1\lambda_2} < T_t < \frac{S_j+\gamma-\lambda_2(1-\lambda_1)S_i-(1-\lambda_2)S_i}{\lambda_1\lambda_2}\right]$$
$$= P\left[\frac{S_j-\gamma-S_i(1-\lambda_1\lambda_2)}{\lambda_1\lambda_2} < T_t < \frac{S_j+\gamma-S_i(1-\lambda_1\lambda_2)}{\lambda_1\lambda_2}\right]$$
$$= F_G\left(\frac{S_j+\gamma-S_i(1-\lambda_1\lambda_2)}{\lambda_1\lambda_2}\right) - F_G\left(\frac{S_j-\gamma-S_i(1-\lambda_1\lambda_2)}{\lambda_1\lambda_2}\right). \quad (2.38)$$

The above expression can be calculated and evaluated for any c.d.f. F_G.

The performance of the Markov chain approach hinges on the number of transient states, and the larger its value, the smaller the number of transient states of γ (i.e., the width for the subinterval). As a result, the plotting statistic falls closer to the midpoint. For the Markov chain approach, when the number of subintervals is sufficiently large, it provides an effective method to accurately approximate the run length properties of a chart. Yu (2007) mentioned that in practice, values of ν around 100 yield satisfactory approximations. However, the author compared simulation results with the Markov chain approach and suggest that the discrepancies between values obtained from these approaches can be somewhat large for $\nu \leq 100$. For larger values of ν, i.e., greater than 100, the discrepancies are small and particularly small when an even larger value, such as $\nu = 1001$, is employed. However, note that in principle, taking larger values of subintervals should result in more accurate results while implementing the Markov chain approach, but in doing so, some run length characteristics could not be computed within a practical period of time. For more information, the interested reader is referred to Graham and Chakraborti (2019) and references therein. The first step is to obtain the transition probabilities, and after this the essential transition probability matrix of order ν can be constructed and is defined as $\boldsymbol{Q}_{\nu\times\nu} = \left(\left(\boldsymbol{p}_{ij}\right)\right)$. A submatrix of the transition probability matrix $\boldsymbol{M}_{(\nu+1)\times(\nu+1)}$ is called an essential transition probability matrix that contains the transition probabilities for the non-absorbing states.

The *ARL*, *SDRL*, and the c.d.f. of the run length *N* for the DEWMA chart can be obtained by implementing expressions (2.30), (2.31) and (2.32), respectively.

2.6.3 Monte Carlo simulation approach

The advent of more complicated control charts – e.g., the DGWMA chart – and the cumbersome calculation of the run length distribution by implementing the exact approach and/or the Markov chain approach, has necessitated the application of the Monte Carlo simulation. The computational time plays a major role in designing and implementing a control chart. In practice, a shorter computational time chart in most cases due to various reasons. In this thesis, 10,000 iterations are used to calculate the run length and its properties for the Monte Carlo simulation. The reason behind choosing this specific value is that without losing much information, the computational time is reduced. More information regarding

the number of simulations is provided in Chapter 3 (see Section 3.6.4), where a comparative study is conducted to weigh up the IC *ARL* and *SDRL* values for 10,000 and 100,000 simulations. Each simulation for the results provided in Chapter 3 and Chapter 4 were run with 10,000 iterations, and given an IC *ARL* (ARL_0) of 370, the approximate standard error of the simulation is thus $370/\sqrt{10{,}000} \cong 3.7$.

The Monte Carlo simulation algorithm differs for varying cases (Case K versus Case U) in terms of the parameter(s) of interest in the process. The simulation's algorithm for Case K is described first, and thereafter the algorithm for Case U can easily be modified.

The Monte Carlo simulation algorithm for the DGWMA chart (Case K) is described as follows:

(i) Specify a process c.d.f. $F_X(x)$, the sample size n, the IC distribution parameter(s) of interest, the magnitude of the shift denoted by δ, and the chart design parameters $(q_1, q_2, \alpha_1, \alpha_2, L)$.

(ii) Z_0^2 is equivalent to the IC expected value of the statistic under consideration – i.e., $Z_0^2 = E(T_i|IC)$ – and is known as the starting value.

(iii) Calculate the quantity $Q' = \lim_{t\to\infty} Q_t' = \lim_{t\to\infty} \sum_{i=1}^{t} w_i^2$ by considering a large value for t given the combination of parameters (see Table 2.1). Then, calculate the control limits (exact or steady-state) according to equations (2.13) and/or (2.14).

(iv) The plotting statistic is calculated according to equation (2.10) with the $Z_0^2 = E(T_i|IC)$.

(v) The run length is incremented if the plotting statistic calculated in step (iv) is within the control limits worked out in step (iii) – i.e., $LCL < Z_t^2 < UCL$.

(vi) Steps (iii) to (v) are repeated until a signal is given (OOC state), which is $Z_t^2 \leq LCL$ or $Z_t^2 \geq UCL$, and then the run length is recorded.

(vii) For a large number of iterations (i.e., 10,000), steps (i) to (vi) are repeated.

The simulation algorithm for Case U differs in step (ii) since the plotting statistic Z_t^2 becomes a random variable. As a result, the estimated control limits are required, which are obtained from a reference sample in Phase I (retrospective phase). For more information on Case U and an overview of Phase I control procedures, refer to Chakraborti et al. (2008).

The Monte Carlo simulation algorithm for the DGWMA chart (Case U) is as follows:

(a) Specify a process c.d.f. $F_X(x)$, the sample size n, the reference sample size m, the IC distribution parameter of interest, the magnitude of the shift denoted by δ, and the chart design parameters $(q_1, q_2, \alpha_1, \alpha_2, L)$.

(b) From the underlying process distribution $F_X(x)$, a Phase I reference sample is drawn, and then the process distribution parameter(s) of interest is estimated by using the Phase I reference sample.

(c) Steps (i) to (vii) of the simulation algorithm for Case K are performed as mentioned above, with the only difference being that the estimation of the process distribution parameter(s) is used in the calculation, which results in an estimated control limit.

(d) The *ARL* or other characteristics of a DGWMA chart for Case U are obtained by repeating steps (a) and (c).

Note that, the Monte Carlo simulation algorithm provides a general guideline and platform for practitioners, and since the DGWMA chart is a generalized type of time-weighted chart, which includes the GWMA, the EWMA, and Shewhart-type charts as limiting cases, and the DEWMA chart as a special case, the same algorithm can also be applied for these charts by modifying the algorithms discussed above.

2.7 Concluding remarks

An overview for the generalized type of time-weighted (memory-type or memory-based) chart known as the DGWMA chart is discussed in detail. The necessary preliminaries and statistical framework for the construction of this chart as well as its properties – e.g., the plotting statistic and control limits (exact and steady-state) – are provided and investigated. A brief discussion in terms of the exact and steady-state limits are also provided. The limiting cases of the DGWMA chart, which includes the GWMA, EWMA, and Shewhart-type charts as well as the special case which is the DEWMA chart (Case 1 and Case 2) are all discussed. The general behavior of the weighting mechanism for the time-weighted charts are investigated in terms of graphical representation. As a result, it is concluded that the shape of the weights has a direct impact on the performance of a chart in detecting different types of shifts in the process. Three main procedures exist in the SPC literature to calculate and evaluate the run length distribution are discussed and the pros and cons for each approach are provided. These methods include (i) the exact approach, (ii) the Markov chain approach, and (iii) the Monte Carlo simulation. The closed-form expressions for the *ARL* and other properties of the run length distribution, i.e., *SDRL*, *VRL*, etc. for the DGWMA chart are obtained. The obstacles and challenges of obtaining the closed-form expressions for the DGWMA chart through the Markov chain approach are highlighted. Furthermore, since the DEWMA chart can be viewed as a first-order Markov chain, a detailed description, and the necessary steps for implementing the Markov chain for this chart are provided. The Monte Carlo simulation is explained and the algorithms for Case K and Case U are also provided for the DGWMA chart.

Chapter 3 A Double Generally Weighted Moving Average control chart for time between events

3.1 Introduction

High-yield processes are in more demand nowadays since the accessibility to new technology for process monitoring purposes is increasing. In general, an item that does not comply with standards is known as a nonconforming or defective item. For high-yield processes, the occurrence rate is usually very low – i.e., one in a million or one in a billion (for instance, in manufacturing processes like airplane generators, automobile engines, etc., see Ali et al. (2016) and references therein). In these processes, shifts are usually tiny, but may lead to large financial losses due to the nature of the process.

Shewhart-type attributes control charts use the present information of the process and ignore the past information. As a result, these types of charts are less sensitive and ineffective in detecting small or tiny changes, but highly sensitive and effective when it comes to large shifts in the process. To overcome this shortcoming, the recommendation is to monitor the time between events (TBE), which observes the inter-arrival times of nonconforming items. As in the case of a high-yield process, where the failure rate is very low, TBE charts are effective and efficient. The Shewhart-type C-chart or U-chart monitor the proportion or number of occurrences within a specific sampling interval, whereas TBE charts track the inter-arrival time between successive occurrences of events.

The underlying assumption in most TBE chart is the exponential data-generating process of the inter-arrival time. However, numerous researchers revealed that in-control (IC) average run length of the TBE charts for the exponential distribution does not reach its maximum level. This type of behavior is known as biasness of a control chart. To circumvent this bias, a one-sided chart based on the gamma distribution has been considered as an alternative.

SPC researchers recommend the use of time-weighted (memory-type or memory-based) control charts to increase the sensitivity of a chart in detecting small or tiny shifts in the process. A one-sided DGWMA chart (Case K and Case U) under the assumption of a gamma distribution for monitoring TBE data, known as the DGWMA-TBE chart, is proposed in this chapter. The proposed chart is effective in detecting a deterioration – i.e., when a sustained downward step shift in a process is investigated. The proposed one-sided DGWMA-TBE chart is run length unbiased, due to the consideration of a one-

sided chart constructed under the gamma distribution assumption. Furthermore, the DEWMA-TBE chart (Case K and Case U) chart is introduced and discussed in detail. The shape for the weights has a direct impact on improving the performance of a chart in detecting tiny shifts. Alternative discrete distributions are considered as the p.m.f. for the weights of the GWMA-TBE chart.

The structure for this chapter is as follows: Section 3.2 provides a literature review for time-weighted TBE charts available in SPC. Section 3.3 presents the rationale for constructing the DGWMA-TBE chart and the methodologies used in the entire thesis are discussed in detail. In Section 3.5, the preliminaries and statistical framework concerning the DGWMA-TBE chart are provided. Discussions on two types of the DGWMA-TBE chart and the DEWMA-TBE chart are supplied in Sections 3.6 and 3.7, respectively. The run length distribution and its calculation approaches are discussed in Section 3.8. The design and implementation of the proposed charts are presented in Section 3.9. The OOC performance evaluation of the proposed charts and their counterparts are given for Case K in Section 3.10. The optimal design as well as the near optimal design are considered in Section 3.11. Alternative discrete distributions for the weights of the GWMA-TBE chart are discussed in detail in Section 3.12. Also, the usefulness of these alternative discrete distributions for practitioners is discussed in detail. Further, the IC design and the OOC performance of the new charts are investigated as well. The implementation of the DGWMA-TBE and DEWMA-TBE charts in Phase II are provided in Sections 3.13 and 3.14, respectively. Two illustrative examples in the form of simulated data and real-life data is provided in Section 3.15.

3.2 Literature review

There are numerous TBE charts available in the SPC literature. Note that, in this section, only research articles related to TBE charts are discussed. For an overview of time-weighted charts and their weighting schemes, the reader is referred to the literature review provided in Section 1.3. TBE charts ae introduced as alternatives for monitoring high quality processes when nonconforming items are rarely observed. The TBE charts observe the time between successive occurrences of events instead of monitoring the number of events occurring in a certain sampling interval. These charts can be used for monitoring any processes with TBE random variables that includes, time between medical errors (Dogu, 2012), time between two consecutive radiation pulses (Lu et al., 2012) and time between asthma attacks (Alemi and Neuhauser, 2004).

Calvin (1983) monitored the cumulative number of conforming items between two nonconforming items and developed the first TBE chart based on probability limits and further studied by Goh (1987). Scariano & Calzada (2003) proposed synthetic chart based on the exponential data and the zero-state *ARL* performance of the chart was studied using a direct formulation method. Authors concluded that the exponential EWMA and CUSUM charts are still superior to their proposed charts in detecting small shifts in the process, except for large shifts. Vardeman and Ray (1985) extended the work so-called

TBE charts for the CUSUM chart when the underlying process distribution is exponential. Authors showed that for the case of exponentially distributed observations, Page (1954) integral equation for the run length can be solved without resorting to approximations. Radaelli (1998) developed the one-sided and two-sided Shewhart TBE charts when the TBE is exponentially distributed. Gan (1998) developed an EWMA chart based on the inter-arrival times for monitoring the rate of occurrences of rare events. Benneyan (2001) developed Shewhart-TBE charts based on the negative binomial and geometric distributions. The TBE charts based on the CUSUM or EWMA charts have also been proposed to monitor both variables and attributes TBE data. These include the Poisson CUSUM and exponential CUSUM charts proposed by Vardeman and Ray (1985) and Gan (1994), respectively; geometric CUSUM and geometric EWMA charts proposed and discussed by Xie et al. (1998), Bourke (2001), Sun and Zhang (2000); exponential EWMA chart proposed by Gan (1998), exponential EWMA chart with estimated parameters by Ozsan et al. (2010) and the references therein. Gan (1998) indicated that based on a performance comparison, the exponential CUSUM and the exponential EWMA charts have similar performance. Xie et al. (2002) developed a TBE chart to monitor the TBE based on the exponential distribution. Borror et al. (2003) proposed an exponential CUSUM-TBE chart and investigated the robustness of the chart for the lognormal and Weibull distributions. Liu et al. (2006) compared the performance of EWMA-TBE chart and the CUSUM-TBE chart when the underlying process distribution is exponential. Zhang et al. (2007) developed a gamma chart for monitoring the TBE. Pehlivan and Testik (2010) evaluated the sensitivity of lower-sided exponential EWMA charts in detecting mean shifts and a detailed analysis is carried out to evaluate the robustness of the chart when the distribution departs from the exponential distribution. The Markov chain approach is considered to compute the run length and its associated characteristics. Xie et al. (2010) discussed the development of TBE charts and their applications in health sector. Cheng and Chen (2011) proposed TBE charts with run rules. Shafae et al. (2014) assesses the performance of three CUSUM-TBE charts and the robustness of the ECUSUM chart is evaluated by a comparative study with two CUSUM charts that are designed based on the Weibull distribution. These two charts include the Weibull CUSUM (denoted by WCUSUM) that was discussed by Hawkins and Olwell (1998) and an adjusted ECUSUM chart. Chakraborty et al. (2016) developed a chart labelled as GWMA-TBE, constructed under the assumption of a gamma distribution when the parameters of the underlying distribution are known (Case K) and unknown (Case U). The Markov chain and the integral equation methodologies are considered for obtaining a closed-form expression for the run length distribution.

3.3 Motivation

The inefficiency of Shewhart-type attributes charts, i.e., C-chart or U-chart, in detecting small or tiny shifts in the high-yield processes provide a platform for the construction of the TBE charts. These charts monitor the time between the consecutive occurrences of the failure. Ali et al. (2016) provided a detailed literature review related to the high-quality or TBE concept. Authors concluded that most of researchers in SPC arena constructed their proposed charts for TBE data based on the assumption that the process parameters are known (i.e., Case K). Hence, proposed charts with estimated parameters is carried out in this thesis to increase the competitiveness of DGWMA-TBE charts and to enhance the chart's practical advantages.

Also, the underlying assumption in most TBE charts is the exponential data-generating process of the inter-arrival times. Zhang et al. (2007) revealed that the IC average run length (*ARL*) of the TBE charts based on the exponential distribution only reaches a maximum once a shift in the process occurs. In the context of the SPC literature, this type of behavior is known as biasness of a control chart. Also, Knoth and Morais (2015) mentioned that, for example, the S^2-chart recommended by most SPC textbooks, to effectively detect the occurrence of both increase and decrease in the standard deviation – is an *ARL*-biased chart. To circumvent this bias, a one-sided chart based on the gamma distribution has been considered as an alternative for the inter-arrival times by Zhang et al. (2007). The performance of the Shewhart-type TBE chart for the gamma distribution is evaluated by Zhang et al. (2007). The authors revealed that the TBE charts constructed under the gamma distribution are more sensitive to small shifts than the TBE charts based on the exponential distribution.

In the context of TBE, there is a need to develop new parametric DGWMA charts under different distributional assumptions. Utilization of the current and past information makes DGWMA charts more sensitive to small shifts in the process parameters. Limited number of researches is available in the literature to address the performance of DGWMA charts under positively skewed or heavy-tailed distributions, such as exponential, gamma and Weibull distributions. In real applications, the underlying process distribution is frequently not normally distributed.

Further, an optimal design of a control chart is an important concept by itself when it comes to the performance of time-weighted charts. The weights behavior of time-weighted charts has a direct impact on the performance of a chart. The discrete Weibull distribution is the only distribution considered in SPC for the weights of the GWMA chart. A research question could be raised about alternative discrete distributions that can be substituted and considered to aid the optimal design and near optimal design of time-weighted charts. A response to this question is also provided in this chapter by considering other alternative distributions for the weights of the GWMA-TBE chart to aid the optimal design of a control chart.

Motivated by these findings and a growth in the development of the TBE charts, it is recommended that practitioners and quality managers conduct further research for DGWMA charts within the TBE domain, which is the main objective of the current chapter. Hence, a one-sided DGWMA-TBE chart is proposed in this chapter (to overcome the biasness issue) constructed under the gamma distribution assumption and for both Case K and Case U to assess the performance and behavior of the aforementioned chart to non-normal processes, i.e., positively skewed distributions. Moreover, the DEWMA-TBE chart that is the special case of the proposed DGWMA-TBE chart is constructed in this chapter. The presented work for the DEWMA-TBE can be considered as the pioneering body that will cover Case K and Case U. A real-life example and a simulated dataset are considered for addressing the application of the proposed chart to practitioners.

3.4 Methodology

We use a Markov chain approach, see Fu and Lou (2003), to derive the run length distribution and its associated characteristics for our proposed DGWMA-TBE and DEWMA-TBE charts. This approach provides a more unified and compact view of the derivations. Balakrishnan and Koutras (2004) stated that, "The Markov techniques possess a great advantage (over the classical combinatory methods) as they are easily adjustable to many problems; they often simplify the solutions to specific problems they are applied on and remain valid even for cases involving non-identical or dependent trials". Also, a novel algorithm based on this approach is developed in R in order to provide a platform to compare the results with other approaches, e.g., the exact approach and the Monte Carlo simulation. The computational time (in seconds) is captured for the calculation of the run length. This methodology is novel in SPC for the DGWMA chart, since Sheu and Hsieh (2009), Lu (2018) and Chiu and Lu (2015) concluded that the implementation of the Markov chain approach encounter challenges such as the complexity to obtain expressions and the calculation is time-consuming.

The exact approach utilizes mathematical derivations and combinatorics to obtain a closed-form expression of the run length distribution. This approach is commonly discarded in the literature for the DGWMA chart since the process of obtaining expressions is cumbersome or difficult to evaluate numerically. However, we also use this methodology to obtain the closed-form expressions for the proposed DGWMA-TBE chart. Further, by using integration and functional tools available in Mathematica, the run length is calculated for some arbitrary values and the computational is captured as well.

We also developed a Monte Carlo simulation algorithm to calculate the run length distribution of the proposed charts. This approach has been considered as the only numerical method by various authors in the SPC literature for the DGWMA chart. The popularity of the Monte Carlo simulation stems from

the fact that computer simulations can almost always be implemented to calculate the run length distribution fairly accurately, provided the simulation size is big enough.

There is a lack of proper guidance to the practitioner on the design and implementation of time-weighted charts and more specifically the DGWMA chart. There is multiple combination of the chart parameters that will yield the desired result when the process is IC. A research question will be answered in this chapter is that which combination of the design parameters is able to detect a shift in the process quicker? This question is answered by using the optimal design and near optimal design concepts and assuming alternative discrete distributions for the weights of the GWMA-TBE chart without the implementation of the double exponential technique.

3.5 The DGWMA-TBE chart

3.5.1 Assumptions

The inter-arrival times between consecutive failure rates are denoted by $Y_j \sim i.i.d\ Exp(\theta), j = 1,2,3, \ldots$, and $1/\theta$ is the rate parameter. $X = \sum_{j=1}^{k} Y_j$ denotes the sum of the inter-arrival times of k consecutive failures. It can be shown that X follows a $Gamma(k, \theta)$ distribution with the p.d.f. given by:

$$f(x; k, \theta) = \frac{e^{-x/\theta} x^{k-1}}{\Gamma(k)\theta^k},\ x > 0\ , \theta > 0 \text{ and } k > 0; \tag{3.1}$$

where θ and k are the parameters known as the scale and shape parameters, respectively.

The following points are crucial with respect to equation (3.1) and the strategies to construct the proposed parametric chart:

i. The properties of the continuous random variable X are $E(X) = k\theta$ and $var(X) = k\theta^2$, which are known as the expected value and variance, respectively.

ii. In practice, the value for the shape parameter ($k > 0$) is selected by the practitioner, and in this research, is assumed to be known – i.e., $k = 1,2,3, \ldots$, where k is the number of consecutive events.

iii. By setting up the shape parameter $k = 1$, equation (3.1) becomes an exponential distribution with the scale parameter θ. Thus, the exponential distribution that monitors the time until one failure is regarded as a special case of the gamma distribution.

iv. The gamma distribution with an integer shape parameter (k) is also known as the Erlang distribution. The Erlang random variable describes the time interval between any event and the k^{th} following event.

v. In general, two cases are considered in SPC depend on the parameter(s) of interest. If the scale parameter θ is unknown, then it is estimated from an IC reference sample from Phase I

(retrospective phase). If the scale parameter is known, θ_0 is assumed to denote the known value of the parameter θ. The first case is known as the "standard unknown" (Case U), and the latter is called the "standard known" (Case K). In this chapter, both of these scenarios are considered for the DGWMA-TBE and DEWMA-TBE charts.

vi. The main objective is to construct a one-sided generalized time-weighted control chart that monitors the scale parameter θ to detect a deterioration in the process (i.e., a sustained downward step shift). The proposed time-weighted chart will be employed to detect small or tiny shifts in the process at the earliest possible time.

3.5.2 Plotting statistics

The DGWMA-TBE chart is a generalization of the GWMA-TBE chart proposed and studied by Chakraborty et al. (2016). The major advantage of the DGWMA-TBE chart over the GWMA-TBE chart is the implementation of dual or double exponential smoothing technique proposed by Brown (1962) which increases the DGWMA chart capability in detecting small shifts in the process (see, Sheu and Hsieh, 2009). The plotting statistic for the DGWMA-TBE chart can be obtained following a similar approach described in Section 2.3. Since the gamma distribution is considered in this chapter as the underlying process distribution, the starting values are defined as $Z_0^2 = Z_1^2 = E(X_i|\text{IC}) = k\theta_0$. As a result, the plotting statistic for the DGWMA-TBE chart is defined as:

$$Z_t^2 = \sum_{i=1}^{t} w_t\, X_{t-i+1} + (1 - \sum_{i=1}^{t} w_i)k\theta_0 \quad \text{for } t = 1,2,\ldots; \tag{3.2}$$

where $w_t = \sum_{j=1}^{t} \left(q_1^{(j-1)^{\alpha_1}} - q_1^{j^{\alpha_1}}\right)\left(q_2^{(t-j)^{\alpha_2}} - q_2^{(t-j+1)^{\alpha_2}}\right)$ is the weighting function, and has the following property; $\sum_{i=1}^{t} w_t + \left(1 - \sum_{i=1}^{t} w_i\right) = 1$. Hence, the weights possess the properties of a valid p.m.f. For a detailed discussion on the weighting scheme for time-weighted charts under consideration, see Section 2.5.

The properties of the plotting statistic Z_t^2, including the IC expected value and IC variance, are:

$$E(Z_t^2|IC) = \sum_{i=1}^{t} w_i\, E(X_{t-i+1}) + \left(1 - \sum_{i=1}^{t} w_i\right)k\theta_0 = k\theta_0 \tag{3.3}$$

and

$$var(Z_t^2|IC) = \sum_{i=1}^{t} w_i^2\, var(X) = k\theta_0^2 \sum_{i=1}^{t} w_i^2 \tag{3.4}$$

respectively.

3.5.3 Control limits

In the SPC environment, it is vital to detect a deterioration or an improvement in a process, where the former is defined as a small sustained downward shift, and the latter is seen as a small sustained upward shift. In this section, the concept of bias in SPC is discussed in detail in the next section as the motivation for designing a one-sided chart in this chapter. Also, the exact control limits and steady-state control limits are discussed in subsequent sections.

3.5.3.1 Bias in SPC

The objective of this chapter is to focus on the gamma distribution as the underlying process distribution. It is important to bear in mind that most of the TBE charts available in the SPC literature are ARL-biased. Pignatiello et al. (1995) introduced the term *ARL*-unbiased in SPC and Acosta-Mejia et al. (1999) conducted the first attempt to overcome the bias of the *ARL* function of the np-chart.

The *ARL* is defined as the average number of samples that must be plotted until and OOC signal is detected in the process. A well-designed chart should ensure that the *ARL* curves reach their maximum or nominal values at their IC occurrence rates. In other words, the chart is set in such a way that the *ARL* curve attains a maximum in the IC situation, i.e., the chart is *ARL*-unbiased; and when the IC *ARL* (denoted by ARL_0) or attained *ARL* is equal to or close to a pre-specified or nominal value (denoted by ARL_0^*). The pre-specified value for ARL_0^* is typically selected as 370 or 500.

Symmetrically placed control limits are only applicable if the plotting statistic has a symmetric distribution or, a downward/upward shift is equally important. These limits are calculated based on the equal-tail probability limits that are often used in the literature to calculate the control limits of gamma charts. However, for charts constructed based on symmetrically places limits, their *ARL* curves will not reach their maximum values at their pre-specified value. For more information, see Knoth and Morais (2015) and the references therein.

Hence, in the case of the DGWMA-TBE chart proposed in this chapter, since the underlying process distribution is gamma (an asymmetric distribution), then a linear combination of gamma random variables is used. As a result, a one-sided chart will be utilized as the two-sided chart is *ARL*-biased.

On the one hand an increase in the process location parameter means process deterioration and on the other hand, a decrease in the process location parameter can indicate process improvement. Controlling both increase and decrease in a parameter, i.e., process location parameter, by using a plotting statistic with an asymmetrical distribution, e.g., gamma, frequently leads to an *ARL*-biased chart and as a result it takes longer to detect shifts in the parameter. Although a one-sided DGWMA-TBE chart is constructed to detect a deterioration in the process, a one-sided DGWMA-TBE chart for detecting an improvement in the process can be designed, which would require only an upper limit. For example, in the medical field, psychologists may be interested in monitoring the maximum reaction time to a

stimulus, hence, the upper control limit becomes more critical in this case. Since, the data for these scenarios have positively skewed distributions, such as exponential, gamma, etc, then an appropriate one-sided chart needs to be carefully designed to detect an improvement in the process. Another example, electronic components are subjected to life tests about their failure rates. The failure rates of these parts need to be monitored carefully to maintain below a maximum acceptable level. The upper limit becomes more critical in this case. Hence, an appropriate one-side chart needs to be designed.

3.5.3.2 Exact control limits

For a two-sided DGWMA-TBE chart, the exact symmetrically placed control limits, and the centerline (CL) are given by:

$$LCL_e = k\theta_0 - L\sqrt{k\theta_0^2 \sum_{i=1}^{t} w_i^2}$$

$$CL = k\theta_0$$

$$UCL_e = k\theta_0 + L\sqrt{k\theta_0^2 \sum_{i=1}^{t} w_i^2}; \tag{3.5}$$

where $L > 0$ is the charting constant that determines the distance between the centerline and the exact limits.

3.5.3.3 Steady-state control limits

For a two-sided DGWMA-TBE chart, the steady-state (asymptotic) control limits and the centerline are given by:

$$LCL_s = k\theta_0 - L\sqrt{k\theta_0^2 Q'}$$

$$CL = k\theta_0$$

$$UCL_s == k\theta_0 + L\sqrt{k\theta_0^2 Q'}; \tag{3.6}$$

where $Q' = \lim_{t\to\infty} \sum_{i=1}^{t} w_i^2$.

Table 2.1 shows that for different choices of the parameters (q, α), and various values of t, the quantity Q' is a convergent function of t. This implies the convergence of exact control limits in (3.5) towards the steady-state control limits given in (3.6). The steady-state control limits are used for the implementation of the proposed chart and for illustration purposes. Note that, as discussed in Chapter 2, there is no prerequisite to use the steady-state limits and the exact control limits can be considered alternatively.

As this research is primarily interested in detecting a deterioration in the process location parameter – i.e., a decrease in the waiting times between failures – only an *LCL* is considered for the design and implementation of the proposed DGWMA-TBE chart. The lower steady-state control limit is defined as:

$$LCL_s = LCL = k\theta_0 - L\sqrt{k\theta_0^2 Q'} \tag{3.7}$$

If the plotting statistic for the DGWMA-TBE chart Z_t^2 plots on or below the LCL in (3.7), the process is declared OOC and a search for assignable causes is started. Otherwise, the process is considered to be IC, which implies no change occurred in the scale parameter θ, and the charting procedure continues.

3.6 Two types of the DGWMA-TBE chart

The special and/or limiting cases of the generalized time-weighted DGWMA chart are discussed in Chapter 2 in detail. For the TBE data, the DGWMA chart with four parameters (Case 1) denoted by *DGWMA-TBE* $(q_1, q_2, \alpha_1, \alpha_2)$ are dismissed and unavailable in the current SPC literature. To fill the gap in relation to this matter, the DGWMA-TBE chart (Case 1) will be considered in this chapter and a performance comparison is conducted to investigate the detection capability due to adding extra parameters to the chart. The results for the DGWMA-TBE chart, including the design parameters, the IC *ARL* (ARL_0), and the OOC *ARL* (ARL_1) are calculated and discussed in detail in the subsequent sections. The relationship between the DGWMA-TBE chart and its special case, the DEWMA-TBE chart is illustrated in Figure 3.1. Further, the connection between different cases of these charts are also presented.

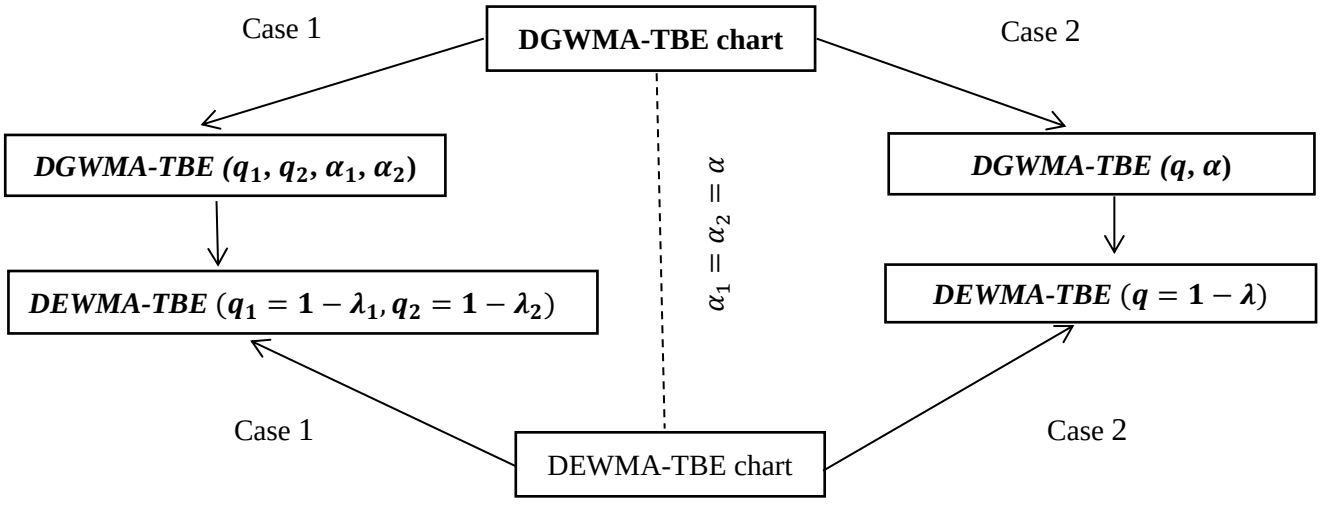

Figure 3.1. Relationship between the DGWMA-TBE and the DEWMA-TBE charts

The DEWMA-TBE chart, a special case of the DGWMA-TBE chart, is discussed in the ensuing section in more detail. The main difference between the DGWMA-TBE and DEWMA-TBE charts is the assumptions made for the chart parameters, i.e., q_1, q_2, α_1, α_2. Hence, the control limits defined for the

DGWMA-TBE chart are valid for the DEWMA-TBE chart by considering an assumption that result in the special case, i.e., $\alpha_1 = \alpha_2 = \alpha$.

3.7 DEWMA-TBE chart as special case

The DEWMA chart is introduced for the TBE data, labelled as the DEWMA-TBE chart in this research, which is a special case of the proposed DGWMA-TBE chart.

Zhang and Chen (2005) state that two different scenarios exist for the DEWMA chart, depending on the equality and/or inequality of the smoothing parameters ($\lambda_1 = 1 - q_1$, $\lambda_2 = 1 - q_2$). These two cases for the DEWMA-TBE chart are denoted as *DEWMA-TBE* ($\lambda = 1 - q$) and *DEWMA-TBE* ($\lambda_1 = 1 - q_1$, $\lambda_2 = 1 - q_2$), respectively. In the DGWMA-TBE chart, if one selects $\alpha_1 = \alpha_2 = 1$, the result is the DEWMA-TBE chart with parameters q_1 and q_2, denoted as *DEWMA-TBE* $(1 - q_1, 1 - q_2)$. To illustrate this, consider the plotting statistic of the DGWMA-TBE chart in equation (3.2) as follows:

$$
\begin{aligned}
Z_t^2 &= (1-q_2)\sum_{i=0}^{t-1} q_2^i Z_{t-i}^1 + q_2^t k\theta_0 \qquad (3.8)\\
&= (1-q_2)\sum_{i=0}^{t-1} q_2^i((1-q_1)\sum_{k=0}^{t-i+1} q_1^k X_{t-i-k} + q_1^{t-i}k\theta_0) + q_2^t k\theta_0\\
&= (1-q_1)(1-q_2)\sum_{i=0}^{t-1} q_2^i \sum_{k=0}^{t-i+1} q_1^k X_{t-i-k} + (1-q_2)\sum_{i=0}^{t-1} q_2^i q_1^{t-i}k\theta_0 + q_2^t k\theta_0\\
&= (1-q_1)(1-q_2)\sum_{i=1}^{t}(q_1^{t-i}\sum_{k=0}^{t-i}({}^{q_2}/_{q_1})^k)X_i + (1-q_2)\sum_{i=0}^{t-1} q_2^i q_1^{t-i}k\theta_0 + q_2^t k\theta_0\\
&= (1-q_1)(1-q_2)\sum_{i=1}^{t}\frac{1-({}^{q_2}/_{q_1})^{t-i+1}}{1-({}^{q_2}/_{q_1})} q_1^{t-i}X_i + (q_1(1-q_2)\frac{q_1^t-q_2^t}{q_1-q_2} + q_2^t)k\theta_0 \,.
\end{aligned}
$$

The DEWMA-TBE defined as above is referred to as Case 1 for the rest of this chapter for frequently used purposed. For more information, see Figure 3.1.

If it is assumed that $q_1 = q_2 = q$ and $\alpha_1 = \alpha_2 = 1$, then the plotting statistic in (3.2) is written as follows:

$$Z_t^2 = (1-q)^2\sum_{j=1}^{t}(t-j+1)q^{t-j}X_i + q^t(t-tq+1)\,k\theta_0 \,. \qquad (3.9)$$

The plotting statistic Z_t^2 in equation (3.9) is the plotting statistic of the DEWMA-TBE and is named as Case 2 for the rest of this chapter for frequently used purposed. For more information, see Figure 3.1.

3.8 Run length distribution

There are different types of measures available in the SPC literature that can be considered when designing and comparing the performance of the competing chart. The most well-known and commonly used measure is the run length distribution. The design and implementation as well as the OOC performance for the proposed DGWMA-TBE chart are based on the *ARL* measure that is commonly used in SPC.

The procedure for designing and implementing the proposed DGWMA-TBE chart typically involves the calculation of the chart parameters to acquire a desired value for the IC ARL labelled as ARL_0^* – i.e., one has to solve for q_1, q_2, α_1, α_2 and L such that $ARL_0 \approx ARL_0^*$. The computational aspects (i.e., time, complexity, etc.) need to be carefully considered and investigated. For the DGWMA-TBE chart, all of the four parameters are included; whereas for the other case, the parameters are set equal to each other, i.e., $q_1 = q_2 = q$ and $\alpha_1 = \alpha_2 = \alpha$ to reduce the computational time. Contrarily, as discussed previously, the limiting cases for the DGWMA-TBE chart – i.e., the GWMA-TBE, EWMA-TBE, and Shewhart-TBE charts – are obtained by selecting specific values for the parameters of the proposed DGWMA-TBE chart. Since the GWMA-TBE and the EWMA-TBE charts are the limiting cases of the proposed DGWMA-TBE chart, the parameters q_2 and q_1 are selected as 0 and 1, respectively. However, since the parameters (q_1 and q_2) for the DGWMA-TBE chart lie between 0 and 1 (i.e., $0 < q_1, q_2 < 1$), the weights tend to be zero mathematically.

There are numerous approaches available to evaluate the run length distribution of a control chart. These methods are discussed in Chapter 2 in detail for the DGWMA chart under the normal distribution. For the DGWMA-TBE chart constructed under the gamma distribution assumption (parametric control chart), some modifications such as considering a one-sided chart is required in terms of the methods discussed in Chapter 2. These methods are: (i) the exact approach; (ii) the Markov chain approach; and (iii) the Monte Carlo simulation algorithm and each of these approaches are considered for the one-sided DGWMA-TBE chart and its special case, which is the DEWMA-TBE chart.

3.8.1 Exact approach

Let N denote the run length for the DGWMA-TBE chart and the signaling event at the i^{th} sample is denoted by A_i. The non-signaling event is denoted by A_i^C and given by $A_i^C = [Z_i^2 > LCL]$ for $i = 1,2,3, \ldots$. The non-signaling event can be rewritten as $A_i^C = [X_i > L_i]$ for $\forall i \geq 1$, where $L_1 = \frac{LCL-(1-w_1)k\theta_0}{(1-q_1)(1-q_2)}$, and:

$$L_i = \frac{LCL - \sum_{j=2}^{i} w_j X_{i-j+1} - \left(1 - \sum_{j=2}^{t} w_j\right)k\theta_0}{(1-q_1)(1-q_2)}, i = 2,3,4, \ldots \tag{3.10}$$

From equation (2.24), the run length distribution can be written as:

$$P[N=1] = 1 - P[X_1 > L_1] \quad \text{and} \quad P[N=n] = I_{n-1} - I_n; \tag{3.11}$$

where $I_n = P\left[\bigcap_{i=1}^{n} A_i^C\right] = P[\bigcap_{i=1}^{n}\{X_i > L_i\}]$ for $n = 2,3,4, \ldots$

The continuous random variables X_i's are assumed to follow an independent $Gamma\ (k,\theta)$. Hence, I_n can be written as:

$$I_n = \int_{L_1}^{\infty}\int_{L_2}^{\infty}\ldots\int_{L_n}^{\infty}\prod_{i=1}^{n} f(x_i;k,\theta)dx_i\ ; \tag{3.12}$$

where $f(x_i;k,\theta)$ is defined in (3.1), which is the p.d.f. for the gamma distribution.

Similar to equation (2.26), an alternative expression for the ARL is as follows:

$$ARL = 1 + \sum_{n=1}^{\infty} I_n\ . \tag{3.13}$$

The scaled random variable X/θ_1 follows a gamma distribution with the parameters k and $1/\delta$ ($X \sim Gamma(k,\frac{1}{\delta})$). The continuous random variable X follows a $Gamma(k,\theta_0)$ distribution with p.d.f. defined in (3.1), where θ_1, which is the OOC scale parameter is defined as $\theta_1 = \delta\theta_0$, θ_0 is the IC scale parameter, and $\delta > 0$ is the shift size. Similarly, the continuous random variable $Y = X/\theta_0$ also follows a gamma distribution ($Y \sim Gamma(k,1)$), and as a result the IC scale parameter can be taken as $\theta_0 = 1$. Thus, irrespective of the value for the IC scale parameter i.e., θ_0, the ratios X/θ_1 and Y/δ have the same distribution and can be denoted as $\frac{X}{\theta_1} \overset{d}{=} \frac{Y}{\delta} \sim Gamma\left(k,\frac{1}{\delta}\right)$. For the DGWMA-TBE chart, the IC scale parameter is taken as $\theta_0 = 1$, so that the chart is applicable for any IC scale parameter when the process is IC, and the shift is taken as the ratio so that it is applicable for any θ_0 and θ_1. To obtain the IC run length distribution, the magnitude for the shift is selected as $\delta = 1$; whereas for the OOC run length, the shift is selected as $\delta \neq 1$.

Equations (3.12) and (3.13) can be used to calculate the exact value for the ARL. Equation (3.12) consists of multiple integrals, and as n increases, the number of integrals rise accordingly. Furthermore, the lower bounds (i.e., L_1, L_2,…, L_n) in equation (3.12) are mutually dependent based on the sequence of statistics $X_1, X_2, \ldots, X_{i-1}$. Hence, the evaluation of the aforementioned equation is computationally cumbersome and time-consuming. However, as previously discussed in Section 2.6, the run length is calculated for the DGWMA-TBE for $n = 1,2,3,4$ by using Mathematica software package and the results are presented in Section 3.8.4.

3.8.2 Markov chain approach

The Markov chain approach provides a unified method to calculate the run length distribution and its characteristics for a control chart. The general steps involved in calculating the run length distribution through the Markov chain method are provided for the DGWMA and DEWMA charts in Chapter 2 in details. The challenges or obstacles involved in implementing this approach in the case of a DGWMA chart were highlighted. In this section, the Markov chain method is used to calculate the run length distribution for a one-sided DEWMA-TBE chart.

As discussed previously, a one-sided DEWMA-TBE chart is a special case of the proposed DGWMA-TBE chart when $\alpha_1 = \alpha_2 = 1$. Further to this, the parameters for the DEWMA-TBE chart are $q_1 = 1 - \lambda_1$ and $q_2 = 1 - \lambda_2$, where λ_1 and λ_2 are the smoothing parameters (i.e., $0 < \lambda_1, \lambda_2 \leq 1$). Thus, the steady-state control limit defined in (3.7) is simplified to $LCL_s = k\theta_0 - L\theta_0\sqrt{k\frac{q_2}{q_1 - q_2}}$ for the DEWMA-TBE chart, and the value for the scale parameter is selected as $\theta_0 = 1$ for illustration purposes. The DEWMA-TBE plotting statistic, i.e., Z_t is defined as:

$$\begin{aligned} C_t &= \lambda_1 X_t + (1 - \lambda_1) C_{t-1} \quad t \geq 1 \\ Z_t &= \lambda_2 C_t + (1 - \lambda_2) Z_{t-1} \quad t \geq 1 \end{aligned} \tag{3.14}$$

The plotting statistic for the DEWMA-TBE chart can be viewed as a first-order Markov chain. Two types of states exist in the state-space: (i) υ non-absorbing states; and (ii) one absorbing state (the region on or below the *LCL*). Therefore, there are $\upsilon + 1$ states in total.

For a one-sided DEWMA-TBE chart proposed in this chapter, since the upper limit does not exist, the construction of transient states is challenging. U' is assumed as the *UCL* for the DEWMA-TBE chart, such that $P[Z_t \geq U' | IC] \leq \varepsilon$, when ε is very small. The Lugananni-Rice saddlepoint approximation method proposed by Lugananni and Rice (1980) can be used to approximate the upper-tail probability $P[Z_t \geq U' | IC]$. A similar approach is explained and implemented by Chakraborty (2017) for a one-sided EWMA-TBE chart, which is a special case of the GWMA-TBE chart.

The plotting statistic Z_t depends on the previous plotting statistic C_t and Z_{t-1}, which depends on all of the previous sample statistics. From equation (2.17), the weights for the DEWMA-TBE chart are as follows: $w_i = (1 - q_1)(1 - q_2)\frac{1 - \left(\frac{q_1}{q_2}\right)^i}{1 - \frac{q_1}{q_2}} q_2^{i-1}$ for $0 < q_1, q_2 < 1$. Hence, the plotting statistic for the DGWMA-TBE chart (as the general form of the DEWMA-TBE) in this case can be written as follows: $Z_t^2 = (a)(b)\sum_{i=1}^{t} \frac{1 - \left(\frac{q_1}{q_2}\right)^{t-i+1}}{1 - \frac{q_1}{q_2}} q_2^{t-i} X_i + \left(q_2(a)\frac{q_2^i - q_1^i}{q_2 - q_1} + q_1^i\right) Z_0^2$, where $a = (1 - q_1)$ and $b = (1 - q_2)$. As illustrated in Chapter 2, the weights are descending as time increases. As a result the plotting statistic

can be approximated by $Z_t^2 \approx \sum_{i=1}^{M} w_i X_{t-i+1}$, where M is chosen as $w_i \sim 0$ for $i > M$. This procedure simplifies the calculation of the upper-tail probability. The value of M can be approximated by the following expression $M = \left(\left[\left(\frac{\log \varepsilon}{\log q}\right)\right] + 1\right)$ as recommended by Chakraborty (2017), where $[x]$ is the largest integer less than or equal to x, and ε is a very small number (i.e., $\varepsilon = 10^{-5}$), such that $w_i < \varepsilon$.

Jensen (1995) defined the saddlepoint equation as $\frac{d}{ds}k(s) = U'$, where $k(s)$ is the cumulant generating function of the DEWMA-TBE plotting statistic Z_t and is equivalent to $k(s) = logM_{Z_t}(s)$. The moment-generating function (m.g.f.) for the plotting statistic Z_t in the case of the gamma distribution is given by $M_{Z_t}(s) = \prod_{i=1}^{M} M_X(sw_i) = \prod_{i=1}^{M}(1 - \theta sw_i)^{-k}$, and as a result the cumulant generating function is $k(s) = -\sum_{i=1}^{M} klog(1 - \theta sw_i)$. The solution of the first derivative for the cumulant generating function, $k'(s) = -\sum_{i=1}^{M} \frac{k\theta w_i}{1-\theta sw_i} = U'$, will provide the saddlepoint γ, which can be obtained through available software packages. In the current thesis, R programming language is used to approximate the saddlepoint. Consequently, the upper-tail probability based on this methodology is approximated by $P[Z_t \geq U'|IC] \sim 1 - \Phi(r) + \phi(r)\left(\frac{1}{b} - \frac{1}{r}\right)$, where $\phi(.)$ and $\Phi(.)$ are standard normal p.d.f. and c.d.f., respectively; $r = sign(\gamma) = \sqrt{\left[2\left(\gamma U' - k(\gamma)\right)\right]}$, and $b = (1 - e^{-\gamma})\sigma(\gamma)$. The initial value to obtain U' is taken as $k\theta$ and increased by 0.001 increment, such that $P[Z_t \geq U'|IC] \leq \varepsilon$. Once U' is obtained, the transient states correspond to υ equal-length subintervals are obtained by dividing the interval between LCL and U'.

As in Chapter 2, the half of the width of a subinterval is defined as $\gamma = (U' - LCL)/2\upsilon$, and the midpoint of the i^{th} subinterval is seen as $S_i = LCL + (2i - 1)\gamma$ for $i = 1,2, \ldots, \upsilon$. The expression for the S_υ is equal to $S_\upsilon = LCL + (2\upsilon - 1)\gamma = LCL + \left(\frac{U'-LCL}{\gamma} - 1\right)\gamma = (U' - LCL) + LCL - \gamma = U' - \gamma$. The properties of the run length distribution can be obtained through the expressions (2.30), (2.31), and (2.32) provided in Chapter 2 (see, Fu & Lou, 2003).

The next step is to calculate the transition probabilities p_{ij} – i.e., the probability that the plotting statistic Z_t falls in state j at time t conditional on Z_{t-1} in state i at time $t - 1$, hence this probability is defined as: $p_{ij} = P\left(Z_t = S_j \middle| Z_{t-1} = S_i\right)$. For the DEWMA-TBE chart, the transition probability can be written as:

$$P\left[S_j - \gamma < Z_t < S_j + \gamma \middle| Z_{t-1} = C_{t-1} = S_i\right]$$
$$= P\left[S_j - \gamma < \lambda_2 C_t + (1 - \lambda_2)Z_{t-1} < S_j + \gamma \middle| Z_{t-1} = C_{t-1} = S_i\right]$$
$$= P\left[S_j - \gamma < \lambda_2 C_t + (1 - \lambda_2)S_i < S_j + \gamma \middle| Z_{t-1} = C_{t-1} = S_i\right]$$

$$= P\left[S_j - \gamma < \lambda_2(\lambda_1 X_t + (1-\lambda_1)C_{t-1}) + (1-\lambda_2)S_i < S_j + \gamma \middle| Z_{t-1} = C_{t-1} = S_i\right]$$
$$= P\left[S_j - \gamma < \lambda_1\lambda_2 X_t + \lambda_2(1-\lambda_1)S_i + (1-\lambda_2)S_i < S_j + \gamma \middle| Z_{t-1} = C_{t-1} = S_i\right]$$
$$= P\left[\frac{S_j - \gamma - \lambda_2(1-\lambda_1)S_i - (1-\lambda_2)S_i}{\lambda_1\lambda_2} < X_t < \frac{S_j + \gamma - \lambda_2(1-\lambda_1)S_i - (1-\lambda_2)S_i}{\lambda_1\lambda_2}\right]$$
$$= P\left[\frac{S_j - \gamma - S_i(1-\lambda_1\lambda_2)}{\lambda_1\lambda_2} < X_t < \frac{S_j + \gamma - S_i(1-\lambda_1\lambda_2)}{\lambda_1\lambda_2}\right].$$

(3.15)

Since $\lambda_1 = 1 - q_1$ and $\lambda_2 = 1 - q_2$, equation (3.15) can be rewritten as:

$$P\left[\frac{S_j - \gamma - S_i\big(1-(1-q_1)(1-q_2)\big)}{(1-q_1)(1-q_2)} < X_t < \frac{S_j + \gamma - S_i\big(1-(1-q_1)(1-q_2)\big)}{(1-q_1)(1-q_2)}\right]$$
$$= F_G\left(\frac{S_j + \gamma - S_i\big(1-(1-q_1)(1-q_2)\big)}{(1-q_1)(1-q_2)}\right) - F_G\left(\frac{S_j - \gamma - S_i\big(1-(1-q_1)(1-q_2)\big)}{(1-q_1)(1-q_2)}\right);$$

(3.16)

where F_G is the c.d.f. of the gamma distribution defined in (3.1). The approximation of the run length distribution through the Markov chain approach provides better results as the number of subintervals is large. However, by increasing the number of states v, the computational time increased as well, which causes the software to run slowly. In this study, $v = 2001$ is considered, as recommended by Graham et al. (2011a) and Chakraborty et al. (2018). The motivation behind selecting the number of states is provided in detail in Section 2.6.2. For more information related to the saddlepoint approximation, refer to the book by Butler (2007).

Note that, the EWMA chart is the limiting case of the DEWMA chart when $\lambda_1 \to 1$ or $\lambda_2 \to 1$, or alternatively $q_1 \to 0$ or $q_2 \to 0$. Hence, the one-sided EWMA-TBE chart is also the limiting case of the proposed DEWMA-TBE chart. To ensure the validity of expression (3.16), one can replace $q_1 \to 0$ in equation (3.16) and the result is:

$$P\left[\frac{S_j - \gamma - S_i\big(1-(1-q_1)(1-q_2)\big)}{(1-q_1)(1-q_2)} < X_t < \frac{S_j + \gamma - S_i\big(1-(1-q_1)(1-q_2)\big)}{(1-q_1)(1-q_2)}\right]$$
$$= F_G\left(\frac{S_j + \gamma - S_i\big(1-(1-q_2)\big)}{(1-q_2)}\right) - F_G\left(\frac{S_j - \gamma - S_i\big(1-(1-q_2)\big)}{(1-q_2)}\right).$$

(3.17)

Since $\lambda_2 = 1 - q_2$, equation (3.17) can be written as:

$$F_G\left(\frac{S_j + \gamma - S_i\big(1-(1-q_2)\big)}{(1-q_2)}\right) - F_G\left(\frac{S_j - \gamma - S_i\big(1-(1-q_2)\big)}{(1-q_2)}\right)$$
$$= F_G\left(\frac{S_j + \gamma - S_i(1-\lambda_2)}{\lambda_2}\right) - F_G\left(\frac{S_j - \gamma - S_i(1-\lambda_2)}{\lambda_2}\right).$$

(3.18)

By assuming $\lambda_2 = \lambda = 1 - q$, equation (3.18) can be written as:

$$F_G\left(\frac{S_j + \gamma - S_i(1-\lambda_2)}{\lambda_2}\right) - F_G\left(\frac{S_j - \gamma - S_i(1-\lambda_2)}{\lambda_2}\right)$$

$$= F_G\left(\frac{S_j + \gamma - qS_i}{1-q}\right) - F_G\left(\frac{S_j - \gamma - qS_i}{1-q}\right).$$

(3.19)

Expression (3.19) is identical to equation (3.13) obtained by Chakraborty (2017) for a one-sided EWMA-TBE chart as expected, since the EWMA-TBE chart is the limiting case of the proposed DEWMA-TBE chart.

Furthermore, if $\lambda_1 \to 1$ and $\lambda_2 \to 1$ or equivalently $q_1 \to 0$ and $q_2 \to 0$, then the DEWMA-TBE chart reduces to the Shewhart-TBE chart, and can be considered as the limiting case of the proposed DEWMA-TBE chart. Therefore, equation (3.16) reduces to:

$$F_G\left(\frac{S_j + \gamma - S_i\big(1-(1-q_1)(1-q_2)\big)}{(1-q_1)(1-q_2)}\right) - F_G\left(\frac{S_j - \gamma - S_i\big(1-(1-q_1)(1-q_2)\big)}{(1-q_1)(1-q_2)}\right)$$

$$= F_G\big(S_j + \gamma - S_i\big) - F_G\big(S_j - \gamma - S_i\big) \tag{3.20}$$

As a conclusion, the closed-form expression derived in this chapter through the Markov chain approach – equation (3.16) – can be used alternatively for the limiting cases of a one-sided DEWMA-TBE chart – i.e., a one-sided EWMA-TBE and Shewhart-TBE charts.

Note that, the saddlepoint approximation is considered only for the Markov chain approach since the upper control limit is required to construct the transient state. However, for the Monte Carlo simulation that will be discussed in the next section, the availability of the upper control limit is not mandatory for numerical calculations.

3.8.3 Monte Carlo simulation

The evaluation of the run length distribution for the DGWMA chart by implementing the exact or the Markov chain approaches is extremely challenging and difficult (see Section 2.6). In this chapter, a numerical Monte Carlo simulation has been implemented to estimate the ARL values of the DGWMA-TBE chart. Further, the algorithm developed for this aim can also be employed for the limiting and special cases of the proposed DGWMA-TBE chart by modifying and selecting specific values for the chart parameters – i.e., $q_1, q_2, \alpha_1, \alpha_2$. The general algorithm is constructed under the assumption that

all four parameters of the DGWMA chart are included for the computational purposes. For more information, see Figure 3.1.

The following steps elaborates the simulation algorithm for the DGWMA-TBE chart:

i. Select a combination of the design parameters – i.e., $(q_1, q_2, \alpha_1, \alpha_2, L)$ – the shift to be detected (δ), the IC scale parameter set as $\theta_0 = 1$, and calculate the *LCL* defined in equation (3.7).

ii. Use statistical software R package to generate individual gamma observations ($Gamma(k, 1)$, $k = 1,2,3,4,5$), and use equation (3.2) to calculate the DGWMA-TBE plotting statistic Z_t^2 by selecting the starting value as $Z_0^2 = k$.

iii. If the plotting statistic is plotted above the steady-state control limit in equation (3.7) – i.e., $Z_t^2 > LCL$ – the process is declared to be IC and a run length counter is incremented.

iv. By running steps (i) to (iii) for 10,000 iterations, the number of samples until the first plotting statistic falls on or outside the steady-state limit, known as the run length, is calculated for each of the interactions corresponding to the specific process k and $(q_1, q_2, \alpha_1, \alpha_2, L)$ combination. These 10,000 empirical run length values are then used to calculate the average run length and other characteristics for the run length.

v. The charting constant ($L > 0$) corresponding to the desired ARL_0^* is obtained through the "grid search" method by repeating steps (i) to (iv) under the process IC scale parameter ($\theta_0 = 1$). The grid search will be discussed in the subsequent sections.

vi. All the ARL_1s for the given OOC parameter can be calculated by repeating steps (i) to (iii) under the exact combination of $(q_1, q_2, \alpha_1, \alpha_2, L)$, which corresponds to ARL_0^*.

Other characteristics of the run length distribution, including the $SDRL$ and percentile points (denoted by P_i, i = 5, 25, 50, 75, 95), are also computed to further describe the behavior of the run length, and are provided in the Appendix.

3.8.4 Comparative study

In the previous sections, numerical methods to calculate the run length distribution for the proposed DGWMA-TBE chart are discussed in detail and the pros and cons for each approach are provided, too. In this section, a comparative study between these three methods – (i) the exact approach, (ii) the Markov chain approach, and (iii) the Monte Carlo simulation – are performed. For the DGWMA-TBE chart, the comparison study is conducted between the Monte Carlo simulation and the exact approaches. For the DEWMA-TBE chart that is the special case of the DGWMA-TBE chart, the comparison is done between the Markov chain approach and Monte Carlo simulation (10,000 versus 100,000). Further to this, an assessment is also conducted in terms of the number of simulations (10,000 versus 100,000) to

observe whether there are any significant differences for the computation of the ARL_0 and IC *SDRL*. These results are illustrated in Tables 3.1. and 3.2. for the DGWMA-TBE and the DEWMA-TBE charts, respectively.

Table 3.1. The run length distribution for the DGWMA-TBE chart when $n = 1, 2, 3, 4$

Run length	$q_1 = q_2 = q$	$\alpha_1 = \alpha_2 = \alpha$	L	10, 000	100, 000	Exact approach
$P(N = 1)$	0.9	0.8	1.552	0.032	0.035	0.031
$P(N = 2)$	0.9	0.8	1.552	0.037	0.038	0.036
$P(N = 3)$	0.9	0.8	1.552	0.040	0.039	0.043
$P(N = 4)$	0.9	0.8	1.552	0.043	0.045	0.042

Table 3.2. IC *ARL* and *SDRL* values for the Markov chain approach, 10,000 and 100,000 simulations for the DEWMA-TBE chart

Scale parameter	$q_1 = q_2 = q$	$\alpha_1 = \alpha_2 = \alpha$	L	10, 000	100, 000	Markov chain approach
$k = 1$	0.95	1.0	1.405	370.11 (353.84)	374.40 (357.30)	372.65 (355.45)
$k = 2$	0.95	1.0	1.418	370.40 (354.17)	374.35 (358.09)	373.20 (356.78)
$k = 3$	0.95	1.0	1.417	369.64 (355.60)	370.78 (355.30)	370.35 (355.08)
$k = 4$	0.95	1.0	1.414	370.39 (358.07)	368.14 (355.60)	369.12 (356.14)
$k = 5$	0.95	1.0	1.420	369.51 (350.86)	371.00 (355.52)	370.78 (354.90)

The following points are worth mentioning in relation to the above tables:

i. A quick comparison between the 10,000 and 100,000 simulations reveals that the 10,000 simulation results are providing estimates as good as the 100,000 simulation results. Thus, the 10,000 simulation is used in the throughout this thesis to reduce the computational time without losing much information.

ii. Table 3.1 shows the IC *ARL* and *SDRL* results for a one-sided DGWMA-TBE chart through the exact approach and the Monte Carlo simulation. The aforementioned values approximated by the Monte Carlo simulation with 10,000 and 100,000, and exact approach are close.

iii. Table 3.2 illustrates the IC *ARL* and *SDRL* values for a one-sided DEWMA-TBE chart by implementing the Markov chain approach and the Monte Carlo simulation. These values approximated by the Markov chain approach and Monte Carlo simulation with 10,000 and 100,000 are close.

Next, the computational time (in seconds) of the IC *ARL* through the Markov chain and the Monte Carlo simulation for the proposed charts are calculated with a central processing unit (CPU) of 2.7 GHz Core i5 (MacBook Pro) system. The results are presented in Table 3.3.:

Table 3.3. CPU time (in seconds) of the IC *ARL* for the DGWMA-TBE and DEWMA-TBE charts

Time-weighted chart	Markov chain approach	Monte Carlo simulation (10,000)	Monte Carlo simulation (100,000)
DGWMA-TBE chart	91.899	100.156	693.963
DEWMA-TBE chart	83.529	91.415	667.763

From Table 3.3., the computational time for the Markov chain approach is less than the Monte Carlo simulation (10,000) for both the DGWMA-TBE and the DEWMA-TBE charts. As a result, one can also consider using the Markov chain approach as an alternative to calculate the run length distribution.

3.9 The IC design

For the proposed DGWMA-TBE chart, the IC design consists of the calculation for the charting constant ($L > 0$) based on a chosen value for the shape parameter k, and a combination of the DGWMA-TBE design parameters $(q_1, q_2, \alpha_1, \alpha_2, L)$, so that the attained ARL is close to the pre-specified value ARL_0^*. The pre-specified value is typically selected as 370 or 500, and the former is taken into consideration for this study. Furthermore, to enhance and increase the sensitivity of the shift detection ability for the DGWMA-TBE chart in the case of the small shift occurrence in the process, the parameters are selected from the following intervals; $0.5 \leq q \leq 0.9$ and $0.5 \leq \alpha \leq 1$. Similar range of values are defined and recommended by Huang et al. (2014), Sheu and Hsieh (2009), and Tai et al. (2010). Chakraborty et al. (2016) considered the ranges $q = 0.5, 0.6, 0.7, 0.8, 09, 095$ and $\alpha = 0.5, 0.6, 0.7, 0.8, 0.9, 1.0, 1.3$ for the GWMA-TBE chart. Since the GWMA-TBE chart is the main counterpart of the DGWMA-TBE chart amongst other time-weighted charts, the range for the selected parameters should be the same to make the comparison valid. Hence, the shape parameter is selected as $k = 1, 2, 3, 4, 5$, and the chart parameters are chosen as $q = 0.5, 0.6, 0.7, 0.8, 09, 095$, and $\alpha = 0.5, 0.6, 0.7, 0.8, 0.9, 1.0, 1.3$. There are various combinations for the DGWMA-TBE chart (Case 1) parameters – i.e., q_1, q_2, α_1, α_2 – that can be used to compare the performance and the detection capability with the DGWMA-TBE chart (Case 2). For the DGWMA-TBE chart (Case 1), the chart parameters are selected as $q_1 = 0.7, 0.8, 0.9$, $q_2 = 0.5, 0.6, 0.8, 0.9, 0.95$, $\alpha_1 = 0.5, 0.6, 0.7, 0.8, 0.9, 1, 1.3$, and $\alpha_2 = 0.5, 0.6, 0.7, 0.8, 0.9, 1, 1.3$. For the DEWMA-TBE chart (Case 1), the chart parameters are chosen as $q_1 = 0.5, 0.6, 0.7, 0.8, 0.9$, and $q_2 = 0.6\ 0.7, 0.8, 0.9, 0.95$. For the DEWMA-TBE chart (Case 2), the chart parameters are selected as $q = 0.5, 0.6, 0.7, 0.8, 0.9, 0.95$. For more information in terms of different cases of the DGWMA-

TBE and the DEWMA-TBE charts, refer to Figure 3.1. The grid search procedure for obtaining the charting constant $L > 0$ is as follows:

- **Input:** The chart parameters are selected as follows, q_1: 0.7(0.1)0.95, q_2: 0.5(0.1)0.95, α_1: 0.5(0.1)1, α_2: 0.5(0.1)1, and the shape parameter is selected as $k = 1(1)5$, where the values given in the parentheses are representing the step size (grid size). The starting values for the parameters q_1, q_2, α_1, and α_2 are selected as 0.7, 0.5, 0.5, and 0.5, respectively and incremented based on the given step size for other combinations. The starting value for the shape parameter is selected as 1 and incremented by 1.
- **Output:** For the chosen $(q_1, q_2, \alpha_1, \alpha_2, k)$ as an input, the algorithm searches for the combination of (L, ARL_0) under the desired $ARL_0^* = 370$. Thereafter, the charting constants $L > 0$ are obtained such that the attained ARL_0 is approximately equal to the desirable value of $ARL_0^* = 370$.

By implementing the grid search method in the simulation algorithm, the charting constant $L > 0$ are obtained for the chosen $(q_1, q_2, \alpha_1, \alpha_2, L)$ combination, and the value of the shape parameter k has been specified, so that the attained ARL_0 is approximately equal to the desirable value of $ARL_0^* = 370$. The values of L determined through this approach are presented in Tables A.3.1 to A.3.5 (Appendix for Chapter 3) for the DGWMA-TBE (Case 2), GWMA-TBE, EWMA-TBE (highlighted row), and Shewhart-TBE charts. Furthermore, the ARL_0^* values and the charting constant $L > 0$ for the DGWMA-TBE chart (Case 1) are presented in Table A.3.6 (Appendix for Chapter 3). For the DEWMA-TBE chart (Cases 1 and 2), the ARL_0^* and $L > 0$ values are presented in Table A.3.7 (Appendix for Chapter 3). Note that, the first value in each cell is the charting constant L and the second value in each cell is the ARL_0. The charting constants presented in these tables will be useful for the design and implementation of time-weighted charts under consideration.

A comparative study is conducted to ensure the validity of the results obtained by an algorithm developed in R with the simulation results obtained by Chakraborty et al. (2016). The comparison is reasonable and valid since the GWMA-TBE, EWMA-TBE, and Shewhart-TBE charts are the limiting cases of the proposed DGWMA-TBE chart. For example, consider the following two cases:

i. When $k = 1$, $q_1 = 0.9$, $q_2 = 0, \alpha_1 = 0.5$, and $\alpha_2 = 1$ from Table A.3.1, the value for the charting constant and the IC ARL are $L = 1.620$ and $ARL_0 = 371.34$, respectively. In Chakraborty et al. (2016), the GWMA-TBE chart with $q_1 = q = 0.9$ and $\alpha_1 = \alpha = 0.5$ and $L = 1.620$ has an attained $ARL_0 = 371.32$.

ii. When $k = 2$, $q_1 = 0.95$, $q_2 = 0, \alpha_1 = 0.7$ and $\alpha_2 = 1$ from Table A.3.2, the value for the charting constant and the IC ARL are $L = 1.802$ and $ARL_0 = 370.61$, respectively. In Chakraborty et al. (2016), the GWMA-TBE chart with $q_1 = q = 0.95$ and $\alpha_1 = \alpha = 0.7$ and $L = 1.802$ has an attained $ARL_0 = 370.62$.

3.10 The OOC performance

To evaluate the OOC performance for different charts, the first step is to ensure that the ARL_0s for all the competing charts are close to 370 ($\delta = 1$), so that all the charts are on an equal footing. Since the main objective is to detect a downward step shift in the process, i.e., deterioration, the magnitude of the shifts is selected as $\delta < 1$ ($\delta = 0.975, 0.95, 0.925, 0.9, 0.85, 0.8, 0.7, 0.5$, and 0.25) as recommended and considered by Chakraborty et al. (2016).

The OOC performance results are shown in Tables A.3.8 to A.3.12 for the DGWMA-TBE (Case 2); Tables A.3.13 to A.3.17 for the GWMA-TBE, the EWMA-TBE, and the Shewhart-TBE charts; Tables A.3.18 to A.3.22 for the DGWMA-TBE (Case 1) chart, and Tables A.3.23 to A.3.27 for the DEWMA-TBE (Case 1 and Case 2), and when $k = 1, 2, 3, 4, 5$. Note that all these tables are included in the Appendix for Chapter 3. For the CUSUM-TBE charts, the tables are embedded within the text in Chapter 3.

The OOC performance comparison between time-weighted charts under consideration for the TBE data can be conducted in terms of a chart's detection superiority and ability in detecting small or tiny shifts in the production process. The comparative study is divided into multiple parts dependents on the type of a chart, and a brief discussion is provided for each part. Tables that contain the relevant results are presented in the Appendix for Chapter 3. The essential discussion points that are necessary to design and implement a time-weighted chart are summarized in this section which highlight practical advantages of the proposed chart that are useful for practitioners.

(i) DGWMA-TBE (Case 2) versus GWMA-TBE, EWMA-TBE, and Shewhart-TBE

The first comparison is conducted between the proposed DGWMA-TBE chart and its main counterparts the GWMA-TBE, the EWMA-TBE and the Shewhart-TBE charts. The simulation results advocate the following:

i. The DGWMA-TBE chart outperforms the EWMA-TBE and Shewhart-TBE charts for all values of the shape parameter k, and all shifts irrespective of the values for the parameters q and α.

ii. For tiny, small, and moderate shifts ($\delta \geq 0.7$), the DGWMA-TBE chart outperforms the GWMA-TBE chart. For example, consider Tables A.3.8 and A.3.13 from the Appendix, with

the results for $k = 1$, where $q = 0.8$: all DGWMA-TBE charts with $\alpha = 0.5$, 0.6, 0.7, 0.8, 0.9, 1, and 1.3 outperform the GWMA-TBE charts. The same is applicable for other values of the shape parameter k and different parameter combinations.

iii. For large shifts ($\delta \leq 0.5$), the GWMA-TBE chart outperforms the DGWMA-TBE chart. For example, consider Tables A.3.9 and A.3.14, with the results for $k = 2$, where $q = 0.95$: all GWMA-TBE charts with $\alpha = 0.5$, 0.6, 0.7, 0.8, 0.9, 1, and 1.3 outperform the DGWMA-TBE charts in detecting large shifts. Also, the GWMA-TBE chart outperforms the EWMA-TBE and Shewhart-TBE charts in detecting small to large shifts irrespective of the values for the parameters. Note that, same conclusions obtained in Chakraborty et al. (2016).

iv. The performance for both the DGWMA-TBE and GWMA-TBE charts improves as the k value increases. For example, from Table A.3.8, when $k = 1$ and $\delta = 0.925$, the ARL_1 for a DGWMA-TBE chart with $q = 0.95$, $\alpha = 0.5$, $L = 0.595$ is 92.49; while from Table A.3.9, the ARL_1 for a DGWMA-TBE chart when $k = 2$ and $\delta = 0.925$, and $q = 0.95$, $\alpha = 0.5$, $L = 0.608$ is 72.06. The improvement and increase in sensitivity of a chart for higher values of k is due to the fact that as the shape parameter k increases, more failures need to be collected. However, practitioners will choose the specific value for the shape parameter k.

In the following figures, different aspects of the DGWMA-TBE, the GWMA-TBE, and the EWMA-TBE charts are illustrated and discussed. The optimal values for the chart's parameters, the chart's ability in detecting different shift sizes as well as the effect of chart's parameters in increasing or decreasing chart performance are discussed.

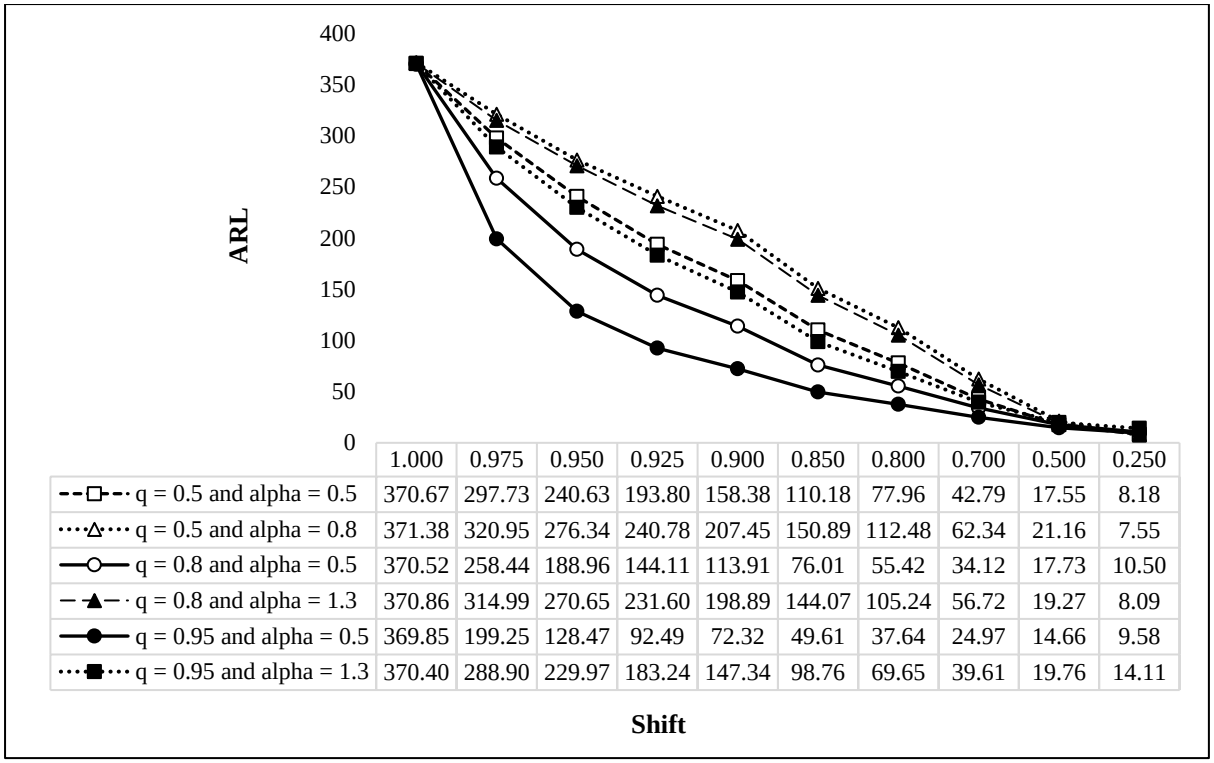

	1.000	0.975	0.950	0.925	0.900	0.850	0.800	0.700	0.500	0.250
q = 0.5 and alpha = 0.5	370.67	297.73	240.63	193.80	158.38	110.18	77.96	42.79	17.55	8.18
q = 0.5 and alpha = 0.8	371.38	320.95	276.34	240.78	207.45	150.89	112.48	62.34	21.16	7.55
q = 0.8 and alpha = 0.5	370.52	258.44	188.96	144.11	113.91	76.01	55.42	34.12	17.73	10.50
q = 0.8 and alpha = 1.3	370.86	314.99	270.65	231.60	198.89	144.07	105.24	56.72	19.27	8.09
q = 0.95 and alpha = 0.5	369.85	199.25	128.47	92.49	72.32	49.61	37.64	24.97	14.66	9.58
q = 0.95 and alpha = 1.3	370.40	288.90	229.97	183.24	147.34	98.76	69.65	39.61	19.76	14.11

Figure 3.2. DGWMA-TBE chart with different parameter combinations

In Figure 3.2, different parameter combinations for the DGWMA-TBE chart are illustrated. The parameter q is selected as 0.5, 0.8, 0.95 and the values selected for the parameter α are 0.5, 0.8, and 1.3. Note that the shape parameter k is selected as 1 for all the combinations, and different range of values are considered for the parameters to identify the impact of varying parameters on the chart's detection capability. These values are extracted from Table A.3.8, see, Appendix for Chapter 3. The chart constant L, values are selected as 1.692, 1.747, 1.703, 1.837, 0.595, 1.677, respectively. The $(q = 0.95, \alpha = 0.5)$ combination provides the best performance in detecting tiny to medium shifts in comparison to other combinations. The $(q = 0.5, \alpha = 0.8)$ combination provided the worse performance in detecting tiny to medium shifts in the process. Practitioners could use this graph as a guideline to select optimal values for the DGWMA-TBE chart parameters for detecting small shifts in the process. For large values of the parameter q (close to 0.95) and small values of the parameter α (close to 0.5), the DGWMA-TBE provides optimal performance in detecting small shifts in the production process. Note that parameters q and α are selected in the following intervals, $(0 < q < 1)$ and $(\alpha > 0)$, respectively.

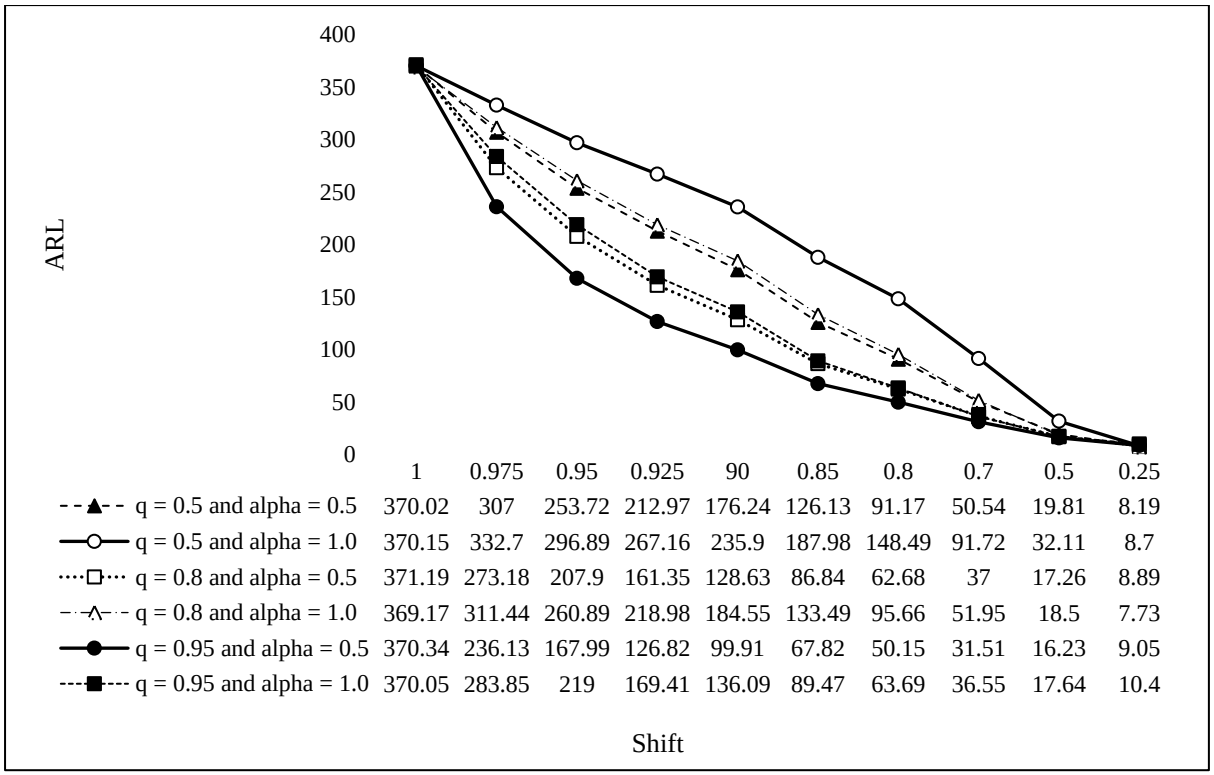

Figure 3.3. GWMA-TBE and EWMA-TBE charts with different parameter combinations.

In Figure 3.3, different parameter combinations are selected for the GWMA-TBE and the EWMA-TBE charts. Note that, these charts are the limiting cases of the proposed DGWMA-TBE chart and Chakraborty et al. (2016) mentioned that the EWMA-TBE chart is the special case of the GWMA-TBE chart. The parameter q is selected as 0.5, 0.8, 0.95 and the values selected for the parameter α are 0.5, and 1.0. From Table A.3.13, the chart constant L, values are selected as 1.345, 1.451, 1.594, 1.812, 1.552, 1.859, respectively. The $(q = 0.95, \alpha = 0.5)$ combination which corresponds to the GWMA-TBE chart, provides the best performance in detecting tiny to medium shifts in comparison to other combinations. The worse performance is for the combination $(q = 0.5, \alpha = 1.0)$ which corresponds to the EWMA-TBE chart. For large values of the parameter q (close to 0.95) and small values of the parameter α (close to 0.5), the GWMA-TBE provides optimal performance in detecting small shifts in the production process. Note that, when $\alpha = 1.0$, the GWMA-TBE chart reduces to the EWMA-TBE chart.

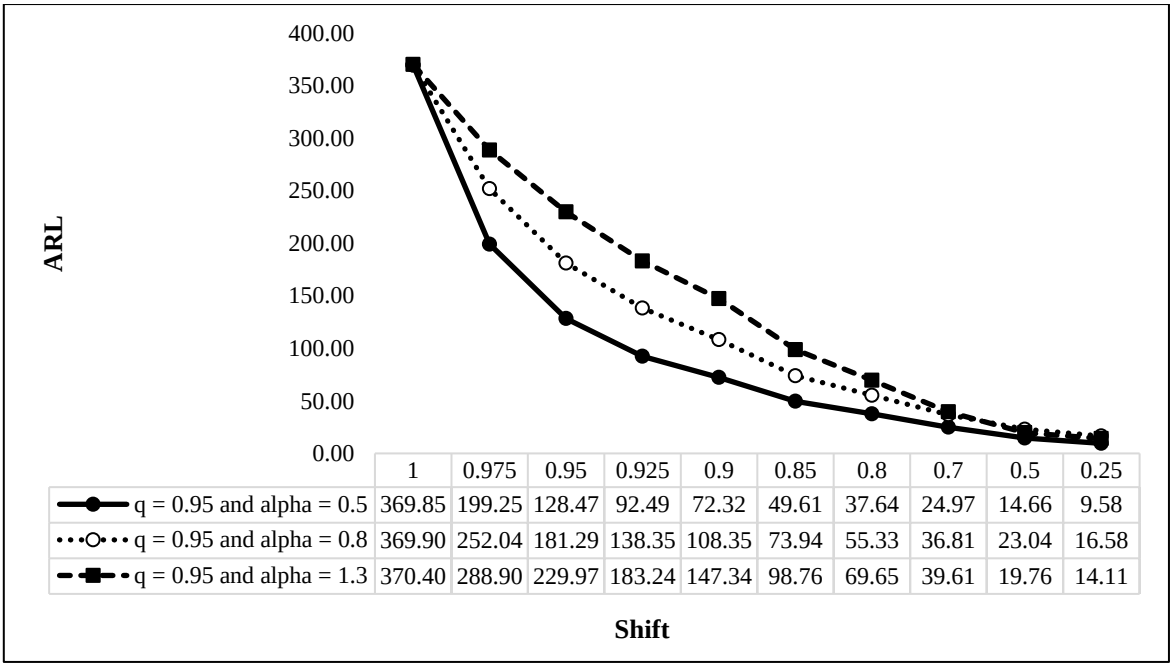

	1	0.975	0.95	0.925	0.9	0.85	0.8	0.7	0.5	0.25
q = 0.95 and alpha = 0.5	369.85	199.25	128.47	92.49	72.32	49.61	37.64	24.97	14.66	9.58
q = 0.95 and alpha = 0.8	369.90	252.04	181.29	138.35	108.35	73.94	55.33	36.81	23.04	16.58
q = 0.95 and alpha = 1.3	370.40	288.90	229.97	183.24	147.34	98.76	69.65	39.61	19.76	14.11

Figure 3.4. The effect of the parameter α on the DGWMA-TBE chart

In Figure 3.4, the effect of the parameter α on the DGWMA-TBE is investigated and illustrated. Different values for the parameter α are considered 0.5, 0.8, 1.3, when the parameter q is constant ($q = 0.95$). For small values of the parameter α, the DGWMA-TBE performs best in detecting small to large shifts in the process. The chart's detection capability in detecting small to large shifts deteriorated when the value for the parameter α increased. Hence, the combination ($q = 0.95, \alpha = 1.3$) has the worse case scenario in detection small shifts in the process.

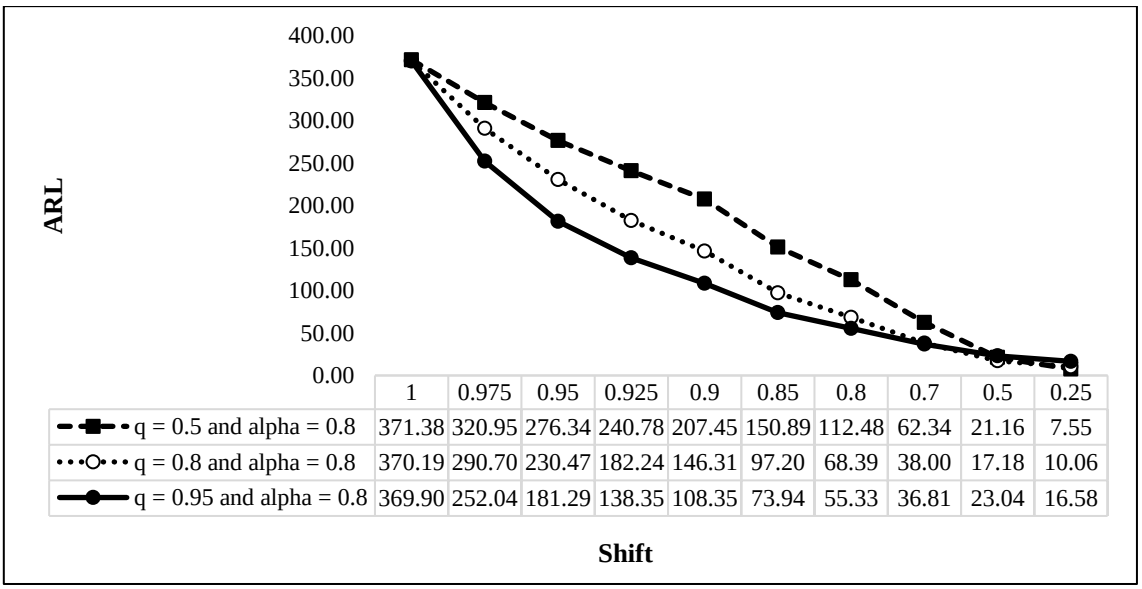

	1	0.975	0.95	0.925	0.9	0.85	0.8	0.7	0.5	0.25
q = 0.5 and alpha = 0.8	371.38	320.95	276.34	240.78	207.45	150.89	112.48	62.34	21.16	7.55
q = 0.8 and alpha = 0.8	370.19	290.70	230.47	182.24	146.31	97.20	68.39	38.00	17.18	10.06
q = 0.95 and alpha = 0.8	369.90	252.04	181.29	138.35	108.35	73.94	55.33	36.81	23.04	16.58

Figure 3.5. The effect of the parameter q on the DGWMA-TBE chart

The effect of the parameter q on the performance of the DGWMA-TBE chart is illustrated in Figure 3.5. When the parameter α is constant (0.8), different values for the parameter q are selected such as

0.5, 0.8 and 0.95. For large values of the parameter q, the DGWMA-TBE chart performs best in detecting small shifts in the process. The chart's detection capability in detecting small to large shifts deteriorated when the value for the parameter q decresed. Hence, the combination $(q = 0.5, \alpha = 0.8)$ has the worst-case scenario in detection small shifts in the process.

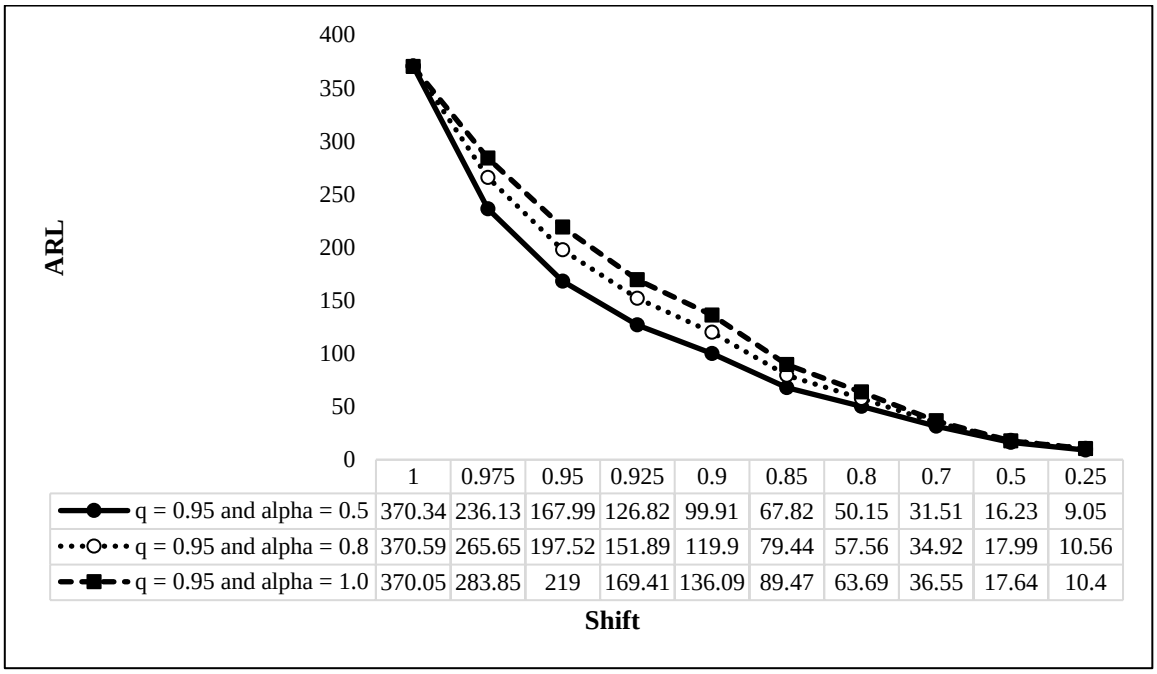

	1	0.975	0.95	0.925	0.9	0.85	0.8	0.7	0.5	0.25
q = 0.95 and alpha = 0.5	370.34	236.13	167.99	126.82	99.91	67.82	50.15	31.51	16.23	9.05
q = 0.95 and alpha = 0.8	370.59	265.65	197.52	151.89	119.9	79.44	57.56	34.92	17.99	10.56
q = 0.95 and alpha = 1.0	370.05	283.85	219	169.41	136.09	89.47	63.69	36.55	17.64	10.4

Figure 3.6. The effect of the parameter α on the GWMA-TBE and EWMA-TBE charts

The effect of the parameter α on the detection capability of the GWMA-TBE and the EWMA-TBE charts are illustrated in Figure 3.6. Different values for the parameter α are selected such as 0.5, 0.8, 1.0 when the parameter q is constant (0.95). For small values of the parameter α, the GWMA-TBE chart performs best in detecting small shifts in the process. The GWMA-TBE and EWMA-TBE charts performance deteriorated in detection small shifts in the process when the value for the parameter α increased. The combination $(q = 0.95, \alpha = 0.5)$ has the best performance in detecting small shifts in the process.

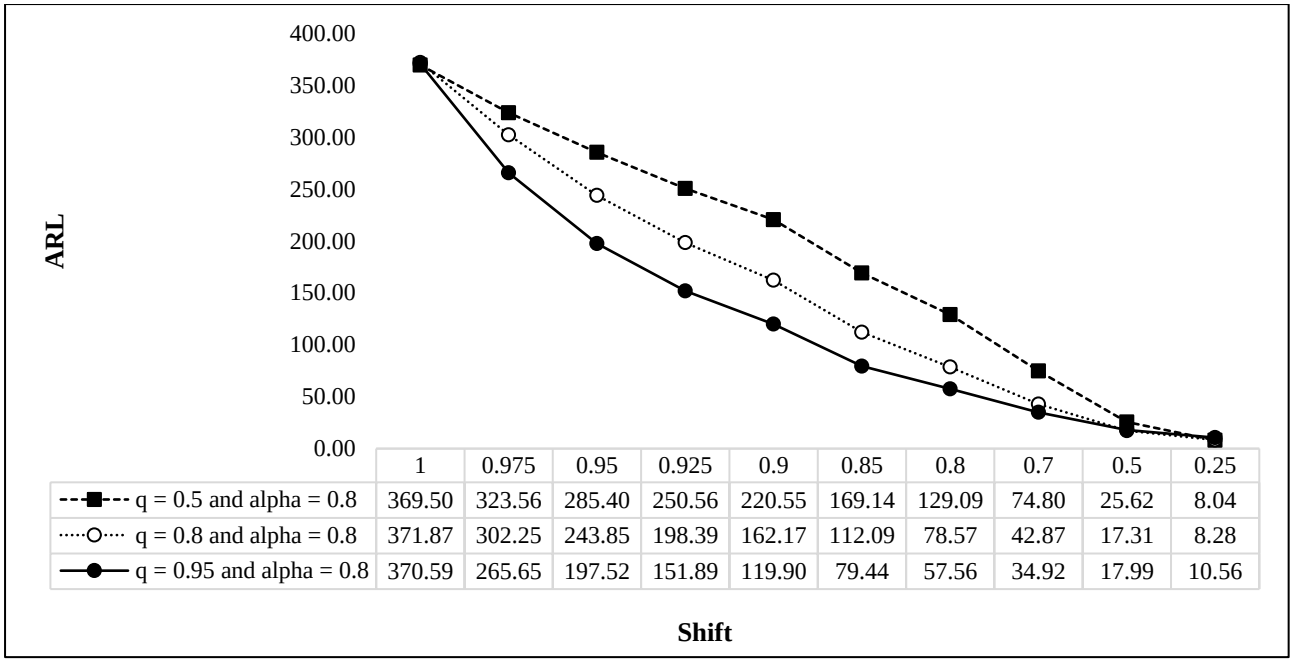

	1	0.975	0.95	0.925	0.9	0.85	0.8	0.7	0.5	0.25
q = 0.5 and alpha = 0.8	369.50	323.56	285.40	250.56	220.55	169.14	129.09	74.80	25.62	8.04
q = 0.8 and alpha = 0.8	371.87	302.25	243.85	198.39	162.17	112.09	78.57	42.87	17.31	8.28
q = 0.95 and alpha = 0.8	370.59	265.65	197.52	151.89	119.90	79.44	57.56	34.92	17.99	10.56

Figure 3.7. The effect of the parameter q on the GWMA-TBE and EWMA-TBE charts

The effect of the parameter q on the detection capability of the GWMA-TBE and the EWMA-TBE charts are illustrated in Figure 3.7. Different values for the parameter q are selected such as 0.5, 0.8, 0.95 when the parameter α is constant (0.8). For large values of the parameter q, the GWMA-TBE chart performs best in detecting small shifts in the process. The GWMA-TBE and EWMA-TBE charts performance deteriorated in detection small shifts in the process when the value for the parameter q decreased. The combination $(q = 0.95, \alpha = 0.8)$ has the best performance in detecting small shifts in the process.

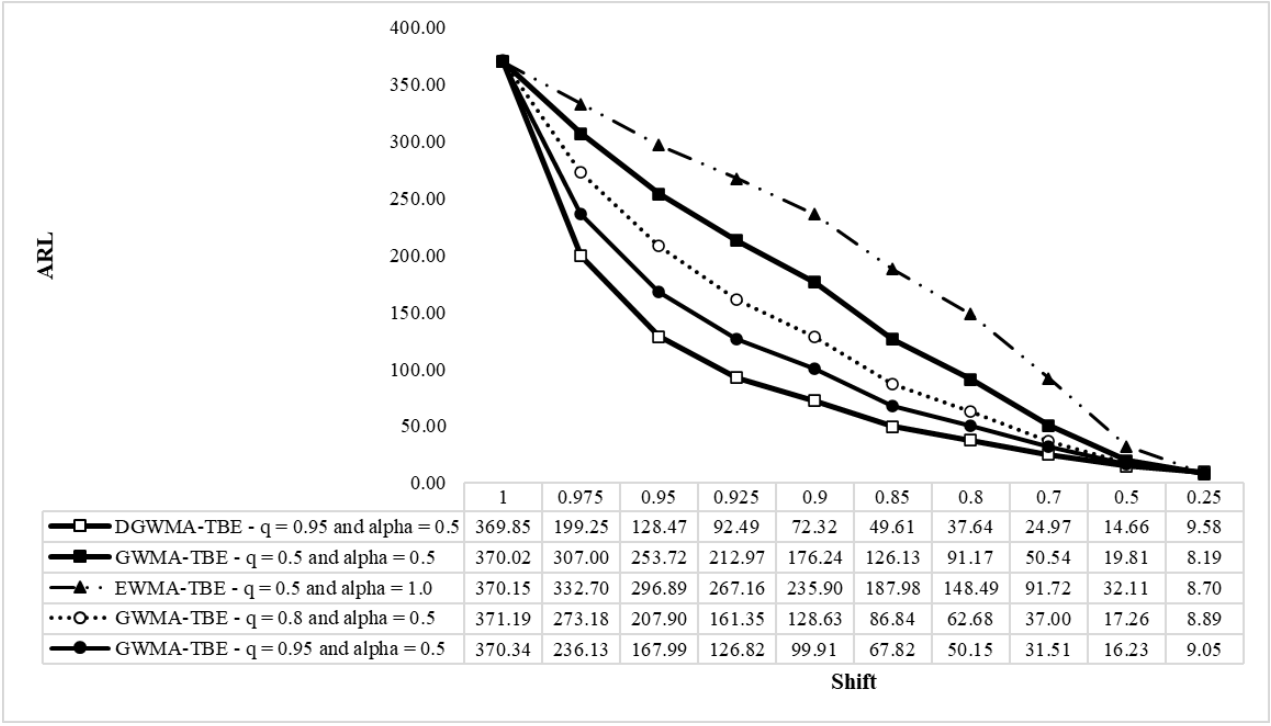

	1	0.975	0.95	0.925	0.9	0.85	0.8	0.7	0.5	0.25
DGWMA-TBE - q = 0.95 and alpha = 0.5	369.85	199.25	128.47	92.49	72.32	49.61	37.64	24.97	14.66	9.58
GWMA-TBE - q = 0.5 and alpha = 0.5	370.02	307.00	253.72	212.97	176.24	126.13	91.17	50.54	19.81	8.19
EWMA-TBE - q = 0.5 and alpha = 1.0	370.15	332.70	296.89	267.16	235.90	187.98	148.49	91.72	32.11	8.70
GWMA-TBE - q = 0.8 and alpha = 0.5	371.19	273.18	207.90	161.35	128.63	86.84	62.68	37.00	17.26	8.89
GWMA-TBE - q = 0.95 and alpha = 0.5	370.34	236.13	167.99	126.82	99.91	67.82	50.15	31.51	16.23	9.05

Figure 3.8. DGWMA-TBE vs GWMA-TBE vs EWMA-TBE

In Figure 3.8, the proposed DGWMA-TBE chart is compared with the GWMA-TBE and the EWMA-TBE charts. The parameters for the DGWMA-TBE chart are selected as 0.95 and 0.5, respectively. Different sets of parameters are selected for the GWMA-TBE chart and the EWMA-TBE chart. These values are extracted from Tables available in the Appendix for Chapter 3. The DGWMA-TBE chart outperforms the GWMA-TBE and the EWMA-TBE charts in detecting small to medium shifts in the process. Also, the proposed DGWMA-TBE chart is competitive for detecting large shifts. The GWMA-TBE chart outperforms the EWMA-TBE chart and as discussed in the previous sections, the GWMA-TBE chart with large value for the parameter q and small value for the parameter α, performs better than the GWMA-TBE chart with other parameter combinations.

(ii) DGWMA-TBE (Case 1) versus DGWMA-TBE (Case 2)

Sheu and Hsieh (2009) concluded that the DGWMA chart with four parameters does not perform better than the DGWMA chart with two parameters under the normal distribution. However, it was discovered based on the calculations in this chapter that there are DGWMA-TBE charts (Case 1) that outperform the DGWMA-TBE chart (Case 2) in detecting small shifts in the process when the underlying process distribution is gamma. The results are presented in Tables A.3.18 to A.3.22 (see, Appendix for Chapter 3) for different values of the shape parameter k. Note that, the first step before conducting the comparison between these two charts or any other types of time-weighted chart is to compute the ARL_0 first,

to ensure that the competing charts are on an equal footing. The simulation results advocate the following:

i. There are various combinations of the DGWMA-TBE chart (Case 1) that outperform the DGWMA-TBE chart (Case 2). The ARL_0 of the *DGWMA-TBE* $(q_1, q_2, \alpha_1, \alpha_2)$ is 369.58, and for the *DGWMA* (q, α) it is 370. For example, from Table A.3.18, for $k = 1$, q_1 = 0.9, q_2 = 0.95, α_1 = 0.5, α_2 = 0.6, and L = 0.865, the OOC ARL is equal to ARL_1 = 225.32, and ARL_1 = 45.32, for shift sizes (δ) 0.975 and 0.8, respectively. From Table A.3.11, for $q_1 = q_2 = q = 0.9$, $\alpha_1 = \alpha_2 = \alpha = 0.5$, and L = 1.140, the OOC ARL is equal to ARL_1 = 232.01, and ARL_1 = 47.27, for shift sizes 0.975 and 0.8, respectively.

ii. The performance for the DGWMA-TBE charts (Cases 1 and 2) improves as the value of k increases. For example, from Table A.3.9, when $k = 2$ and $\delta = 0.9$, the ARL_1 for a DGWMA-TBE chart (Case 2) with $q = 0.9$, $\alpha = 0.5$, $L = 1.173$ is 69.72; while from Table A.3.10, the ARL_1 when $k = 3$, $\delta = 0.9$, $q = 0.9$, $\alpha = 0.5$, and $L = 1.177$ is 55.98. For the DGWMA-TBE chart (Case 1), from Table A.3.18, when $k = 1$ and $\delta = 0.9$, the ARL_1 with $q_1 = 0.7$, $q_2 = 0.8$, $\alpha_1 = 0.5$, $\alpha_2 = 0.6$, $L = 1.833$ is 126.02; while from Table A.3.19, the ARL_1 when $q_1 = 0.7$, $q_2 = 0.8$, $\alpha_1 = 0.5$, $\alpha_2 = 0.6$, $L = 1.935$ for $k = 2$ and $\delta = 0.9$ is 92.39.

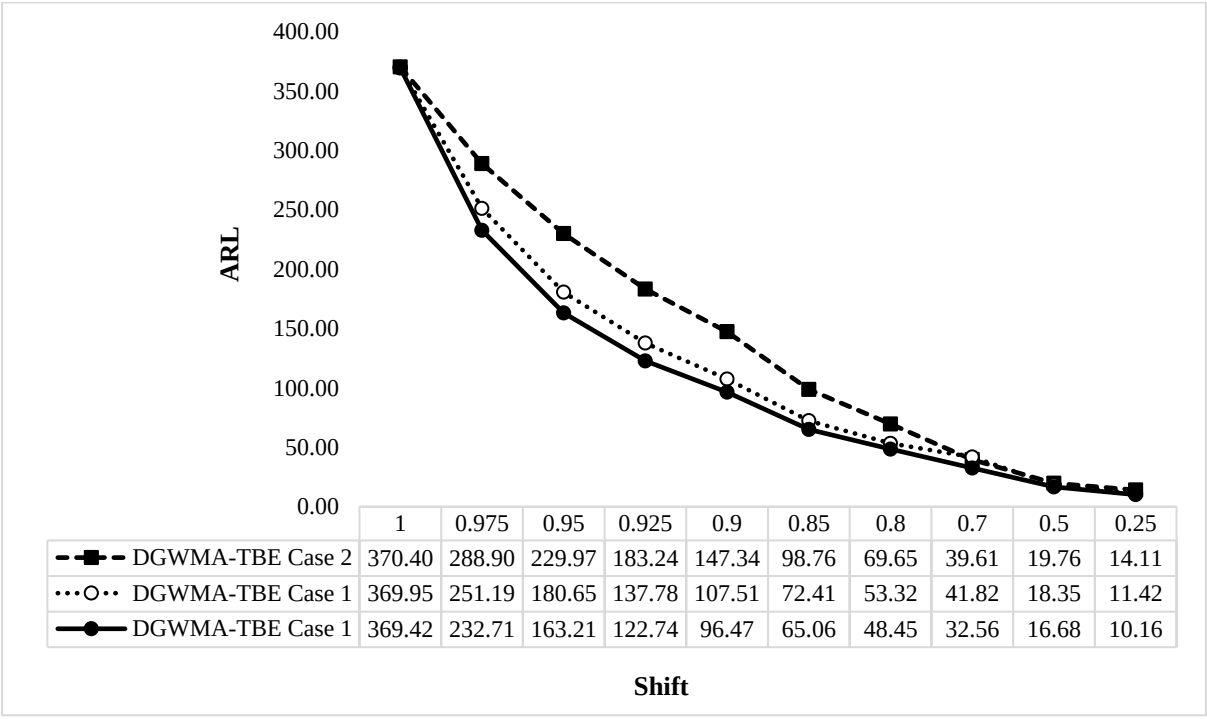

	1	0.975	0.95	0.925	0.9	0.85	0.8	0.7	0.5	0.25
DGWMA-TBE Case 2	370.40	288.90	229.97	183.24	147.34	98.76	69.65	39.61	19.76	14.11
DGWMA-TBE Case 1	369.95	251.19	180.65	137.78	107.51	72.41	53.32	41.82	18.35	11.42
DGWMA-TBE Case 1	369.42	232.71	163.21	122.74	96.47	65.06	48.45	32.56	16.68	10.16

Figure 3.9. Comparison between the DGWMA Case 1 vs DGWMA Case 2

A comparative plot is illustrated in Figure 3.9 to compare the performance between different cases of the proposed DGWMA-TBE chart. From Table A.3.8, when $q = 0.95$, $\alpha = 1.3$, $L = 1.677$, the

$ARL_1 = 288.90$ and 229.97, for small shifts ($\delta \geq 0.95$). From Table A.3.18, when $q_1 = 0.8$, $q_2 = 0.9$, $\alpha_1 = 0.5$, $\alpha_2 = 0.6$, $L = 1.500$, the $ARL_1 = 251.19$ and 180.65, for small shifts ($\delta \geq 0.95$). Also, from Table A.3.18, when $q_1 = 0.7$, $q_2 = 0.95$, $\alpha_1 = 0.5$, $\alpha_2 = 0.5$, $L = 1.401$, the $ARL_1 = 232.71$ and 163.21, for small shifts ($\delta \geq 0.95$). Hence, the DGWMA-TBE chart (Case 1) outperformed the DGWMA-TBE charts (Case 2) in detecting small shifts in the process. For medium to large shifts, the DGWMA-TBE chart (Case 1) is competitive with the DGWMA-TBE chart (Case 2).

(iii) DEWMA-TBE versus GWMA-TBE, EWMA-TBE, and Shewhart-TBE

The DEWMA-TBE chart is also proposed and discussed in Section 3.7. For the DEWMA-TBE chart, there are two different cases that are dependent on the equality and/or inequality of the smoothing parameters. For more information, see Figure 3.1 in Section 3.6. In this part, the performance of the DEWMA-TBE chart (Case 1 and Case 2) with the GWMA-TBE, EWMA-TBE, and Shewhart-TBE charts are considered in detail as follows:

i. Zhang and Chen (2005) mentioned that the DEWMA-TBE chart with two smoothing parameters does not outperform the DEWMA-TBE chart with a single smoothing parameter under the normal distribution. However, it was discovered that there are some cases, where the latter (Case 2) is outperformed by the former (Case 1). For example, from Table A.3.23, the ARL_0 is calculated first to ensure that both of the DEWMA-TBE cases are on an equal footing, and the IC *ARL* is equal to $ARL_0 = 370.79$ (Case 1) and $ARL_0 = 371.85$ (Case 2). For the DEWMA-TBE chart (Case 1), when $k = 1$, $q_1 = 0.5$, $q_2 = 0.6$, $\alpha_1 = 1.0$, $\alpha_2 = 1.0$, L = 1.773 and $\delta = 0.975$, ARL_1 is equal to 324.18; whereas for the DEWMA-TBE (Case 2), when $k = 1$, $q_1 = q_2 = q = 0.5$, $\alpha_1 = \alpha_2 = 1$, L = 1.719 and $\delta = 0.975$, ARL_1 is equal to 327.37.

ii. For small or tiny shifts, some combinations of the parameters exist, where the DEWMA-TBE chart (Case 1) outperforms the GWMA-TBE chart. The ARL_0 for these two charts is equal to 370 and 369.50, respectively. For example, from Table A.3.23, when $k = 1$, $q_1 = 0.5$, $q_2 = 0.8$, $\alpha_1 = 1.0$, $\alpha_2 = 1.0$, L = 1.874 and $\delta = 0.975$, ARL_1 is equal to 310.30; whereas for the GWMA-TBE chart from Table A.3.13, when $k = 1$, $q_1 = 0.5$, $q_2 = 0$, $\alpha_1 = 0.8$, $\alpha_2 = 1.0$, L = 1.433 and $\delta = 0.975$, ARL_1 is equal to 323.56.

iii. For larger shifts, in most cases the GWMA-TBE chart outperforms the DEWMA-TBE chart for all the values of the shape parameter k.

iv. The DEWMA-TBE chart (Cases 1 and 2) outperforms the EWMA-TBE and Shewhart-TBE charts for all values of the shape parameter k, and all shifts irrespective of the values for the parameters q and α.

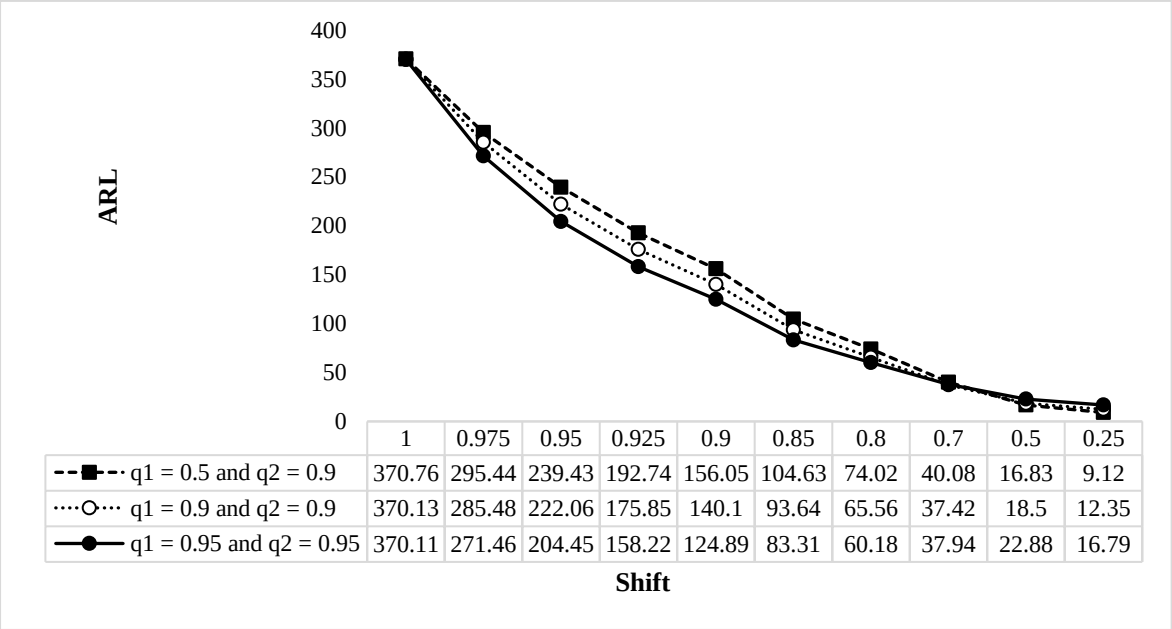

	1	0.975	0.95	0.925	0.9	0.85	0.8	0.7	0.5	0.25
q1 = 0.5 and q2 = 0.9	370.76	295.44	239.43	192.74	156.05	104.63	74.02	40.08	16.83	9.12
q1 = 0.9 and q2 = 0.9	370.13	285.48	222.06	175.85	140.1	93.64	65.56	37.42	18.5	12.35
q1 = 0.95 and q2 = 0.95	370.11	271.46	204.45	158.22	124.89	83.31	60.18	37.94	22.88	16.79

Shift

Figure 3.10. DEWMA-TBE chart with different parameter combinations

In Figure 3.10, different parameter combinations for the DEWMA-TBE chart are illustrated. Different cases of the DEWMA-TBE charts are illustrated based on the equality or inequality of the parameters. From Table A.3.23, the chart constant L values are selected as 1.889, 1.713 and 1.405 for combinations $(q_1 = 0.5, q_2 = 0.9)$, $(q_1 = 0.9, q_2 = 0.9)$, and $(q_1 = 0.95, q_2 = 0.95)$, respectively. From the above plot, one can conclude that, the DEWMA-TBE chart with equal parameters, i.e., $q_1 = q_2 = q = 0.95$, outperformed the DEWMA-TBE chart with inequal parameters. Also, by comparing two cases of the DEWMA-TBE chart with different parameters, one can also comment on the optimal combination of the chart's parameters. For example, when $q_2 = 0.9$, and for different values for the parameter q_1, 0.5 and 0.9, the DEWMA-TBE chart with larger q_1 outperformed the latter one in detecting small shifts in the process.

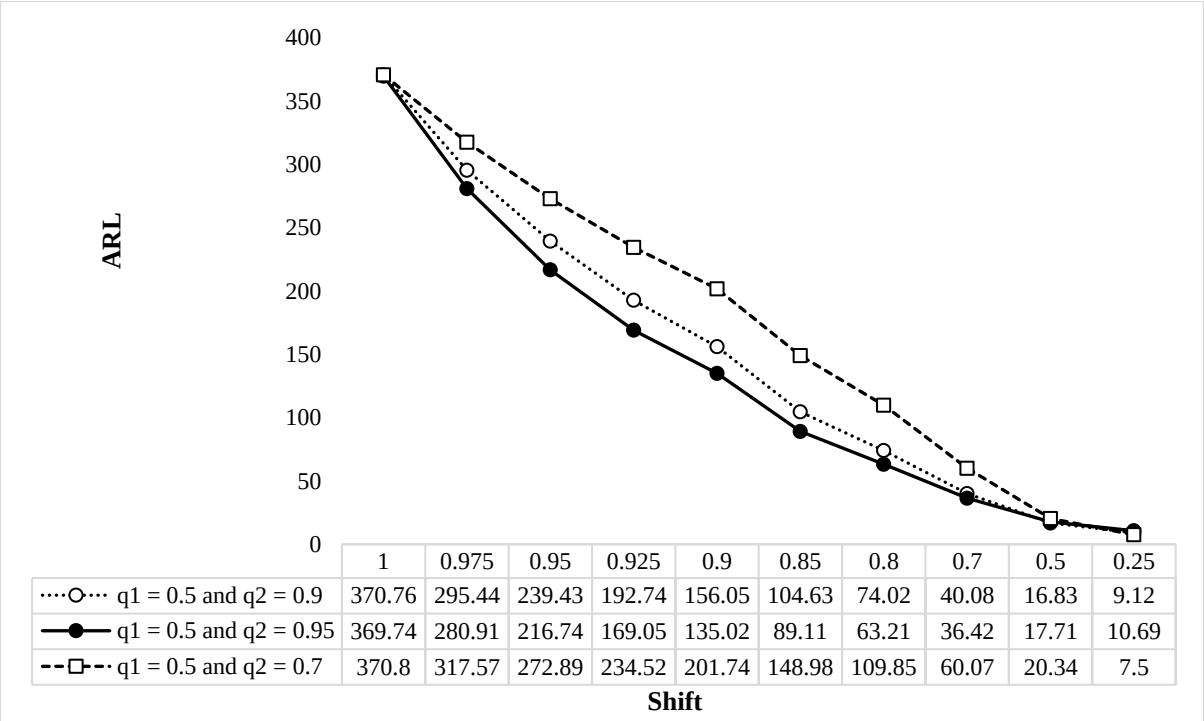

	1	0.975	0.95	0.925	0.9	0.85	0.8	0.7	0.5	0.25
q1 = 0.5 and q2 = 0.9	370.76	295.44	239.43	192.74	156.05	104.63	74.02	40.08	16.83	9.12
q1 = 0.5 and q2 = 0.95	369.74	280.91	216.74	169.05	135.02	89.11	63.21	36.42	17.71	10.69
q1 = 0.5 and q2 = 0.7	370.8	317.57	272.89	234.52	201.74	148.98	109.85	60.07	20.34	7.5

Figure 3.11. The effect of the parameter q_2 on the DEWMA-TBE chart

The effect of the parameter q_2 on the detection capability of the DEWMA-TBE chart is illustrated in Figure 3.11. Different values for the parameter q_2 are selected such as 0.9, 0.95, 0.7 when the parameter q_1 is constant (0.5). For large values of the parameter q_2, the DEWMA-TBE chart performs best in detecting small shifts in the process. The DEWMA-TBE chart performance deteriorated in detection small shifts in the process when the value for the parameter q_2 decreased. The combination ($q_1 = 0.5, q_2 = 0.95$) has the best performance in detecting small shifts in the process.

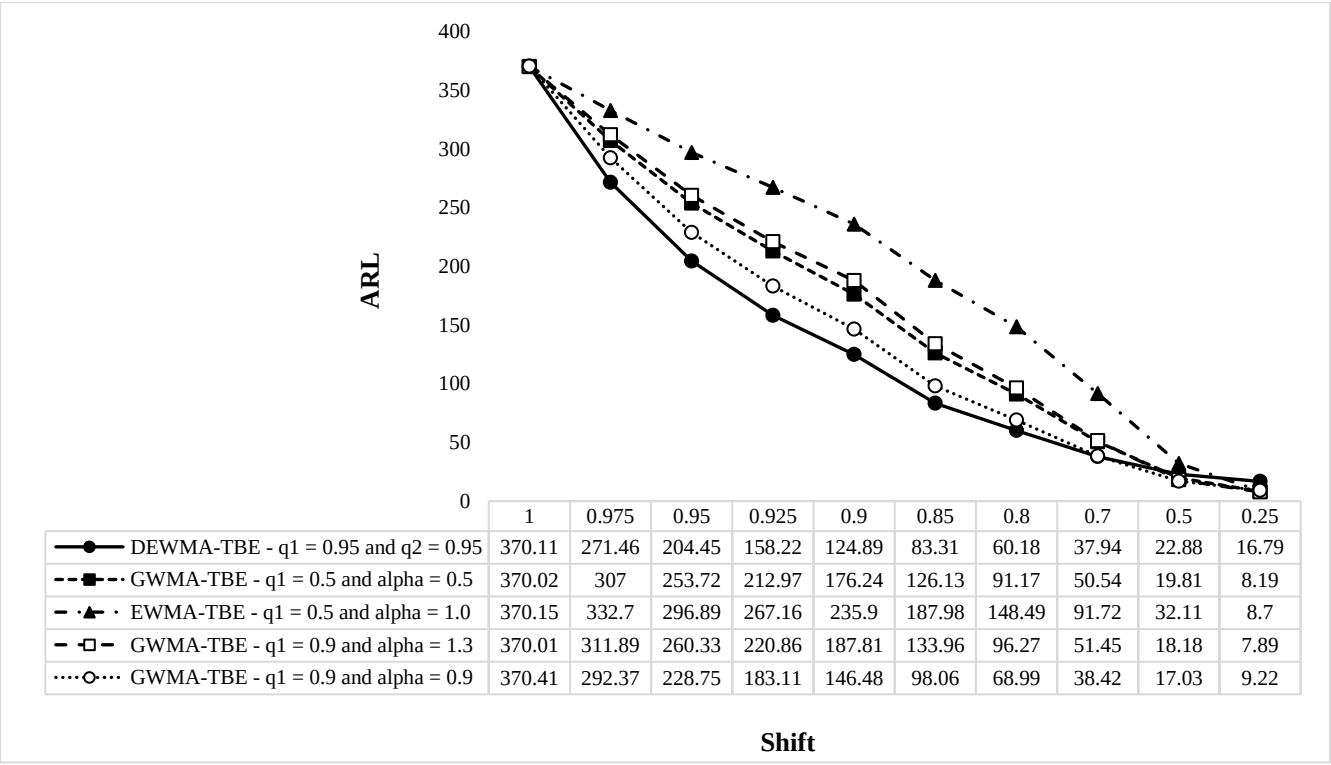

	1	0.975	0.95	0.925	0.9	0.85	0.8	0.7	0.5	0.25
DEWMA-TBE - q1 = 0.95 and q2 = 0.95	370.11	271.46	204.45	158.22	124.89	83.31	60.18	37.94	22.88	16.79
GWMA-TBE - q1 = 0.5 and alpha = 0.5	370.02	307	253.72	212.97	176.24	126.13	91.17	50.54	19.81	8.19
EWMA-TBE - q1 = 0.5 and alpha = 1.0	370.15	332.7	296.89	267.16	235.9	187.98	148.49	91.72	32.11	8.7
GWMA-TBE - q1 = 0.9 and alpha = 1.3	370.01	311.89	260.33	220.86	187.81	133.96	96.27	51.45	18.18	7.89
GWMA-TBE - q1 = 0.9 and alpha = 0.9	370.41	292.37	228.75	183.11	146.48	98.06	68.99	38.42	17.03	9.22

Figure 3.12. DEWMA-TBE vs GWMA-TBE vs EWMA-TBE

The performance between different charts in detecting shifts is evaluated in terms of comparing their ARL_1 values. In Figure 3.12, the DEWMA-TBE chart is compared with different GWMA-TBE charts. The ARL_0 for all the charts are set equal so that the charts are at an equal footing and then the chart with the minimum value for ARL_1 performs best in detecting small shifts compared to its counterparts. For the DEWMA-TBE chart and from Table A.3.23, $q_1 = q_2 = q = 0.95$ and $L = 1.405$; for the GWMA-TBE chart and from Table A.3.13, $(q = 0.5, \alpha = 0.5, L = 1.345), (q = 0.9, \alpha = 0.9, L = 1.898), (q = 0.5, \alpha = 1.3, L = 1.880)$, and for the EWMA-TBE chart, $(q = 0.5, \alpha = 1.0, L = 1.451)$ are selected. The DEWMA-TBE chart outperformed the GWMA-TBE charts and the EWMA-TBE chart in detecting small to moderate shifts in the process. Note that, the DEWMA-TBE chart is a special case of the proposed DGWMA-TBE chart and also proposed in this chapter. The GWMA-TBE chart outperformed the EWMA-TBE chart in detecting small to large shifts.

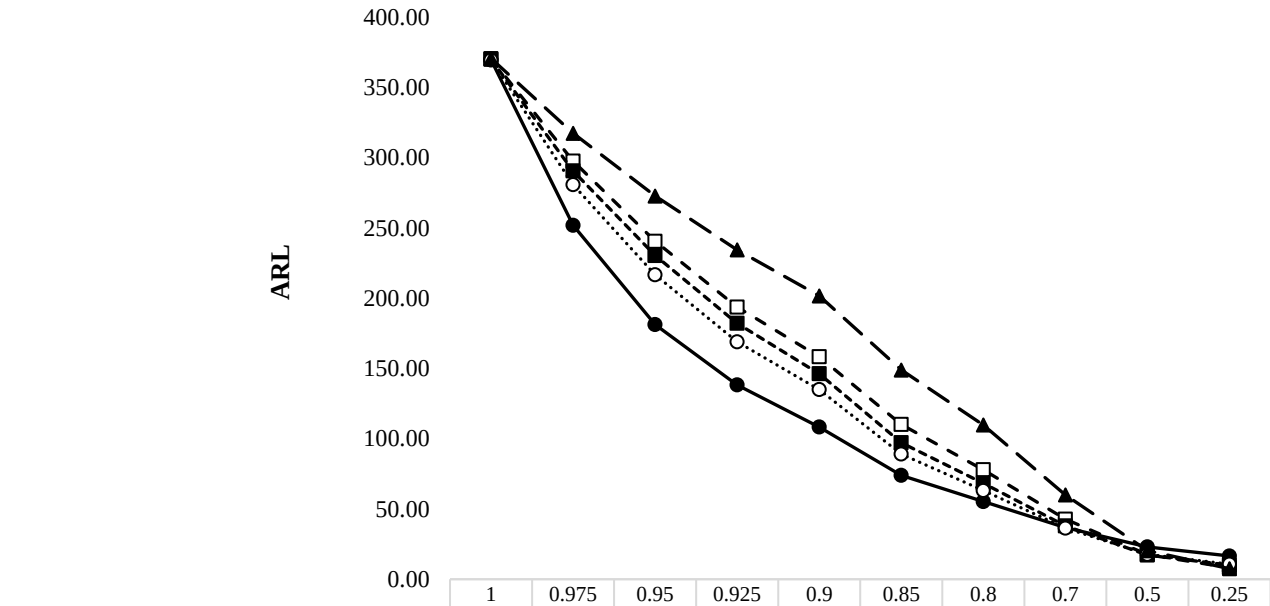

	1	0.975	0.95	0.925	0.9	0.85	0.8	0.7	0.5	0.25
GWMA-TBE q1 = 0.5 and alpha = 0.5	370.67	297.73	240.63	193.80	158.38	110.18	77.96	42.79	17.55	8.18
GWMA-TBE q1 = 0.8 and alpha = 0.8	370.19	290.70	230.47	182.24	146.31	97.20	68.39	38.00	17.18	10.06
GWMA-TBE q1 = 0.95 and alpha = 0.8	369.90	252.04	181.29	138.35	108.35	73.94	55.33	36.81	23.04	16.58
DEWMA-TBE q1 = 0.5 and alpha = 0.95	369.74	280.91	216.74	169.05	135.02	89.11	63.21	36.42	17.71	10.69
DEWMA-TBE - q1 = 0.5 and alpha = 0.7	370.80	317.57	272.89	234.52	201.74	148.98	109.85	60.07	20.34	7.50

Figure 3.13. DEWMA-TBE vs GWMA-TBE vs EWMA-TBE

Different cases of the DEWMA-TBE chart based on the equality and/or inequality of the parameters are compared with different GWMA-TBE charts in Figure 3.13. The parameters for the GWMA-TBE chart are selected from Table A.3.13 as follows: $(q = 0.5, \alpha = 0.5, L = 1.345)$, $(q = 0.8, \alpha = 0.5, L = 1.594)$ and $(q = 0.95, \alpha = 0.8, L = 1.764)$. The parameters for the DEWMA chart are selected from Table A.3.23 as follows: $(q_1 = 0.5, q_2 = 0.95, L = 1.800)$ and $(q_1 = 0.5, q_2 = 0.7, L = 1.827)$. The GWMA-TBE chart with $(q = 0.95, \alpha = 0.8, L = 1.764)$ outperformed other charts in detecting small to medium shifts in the process. The DEWMA-TBE chart with $(q_1 = 0.5, q_2 = 0.7, L = 1.827)$ performed worse in detecting small shifts in the process. However, the DEWMA-TBE chart with $(q_1 = 0.5, q_2 = 0.95, L = 1.800)$ outperformed other GWMA-TBE charts in detecting small to medium shifts. One can conclude that from Figures 3.12 and 3.13, different cases exist where in some cases the DEWMA-TBE chart outperformed the GWMA-TBE chart and in other cases the GWMA-TBE chart outperformed the DEWMA-TBE. Hence, a roadmap is necessary to provide guidelines for practitioners to select optimal design parameters for detecting small shifts in the production processes.

(iv) DGWMA-TBE versus DEWMA-TBE

A performance comparison is conducted to measure the detection capability of these two charts, i.e., the DGWMA-TBE as the general case and the DEWMA-TBE chart as its special case, for different shift sizes, specifically in detecting small or tiny shifts in the process. The findings for these charts reveal that:

i. For small to moderate shifts ($\delta \geq 0.8$), the DGWMA-TBE chart with four parameters outperforms the DEWMA-TBE chart with two smoothing parameters, for all values of the shape parameter k irrespective of the values for the chart parameters – i.e., q_1, q_2, α_1, α_2. The ARL_0 for these two charts is equal to 369.95 and 370.10, respectively. For example, from Table A.3.18, when $k = 1$, $q_1 = 0.8$, $q_2 = 0.9$, $\alpha_1 = 0.5$, $\alpha_2 = 0.6$, L = 1.500 and $\delta \geq 0.8$, the DGWMA-TBE chart (Case 1) outperforms the DEWMA-TBE (Case 1) chart.

ii. For large shifts ($\delta \leq 0.7$), the DEWMA-TBE chart (Case 1) outperforms the DGWMA-TBE chart (Case 1) for some values of the chart parameters q_1, q_2, α_1, α_2. The ARL_0 for these two charts is equal to 370.30 and 369.75, respectively. For example, from Table A.3.24, when $k = 2$, $q_1 = 0.7$, $q_2 = 0.8$, $\alpha_1 = 1.0$, $\alpha_2 = 1.0$, L = 2.013 and $\delta = 0.5$, the ARL_1 for the DEWMA-TBE (Case 1) chart is equal to 10.52; whereas f, when $k = 2$, $q_1 = 0.7$, $q_2 = 0.8$, $\alpha_1 = 0.5$, $\alpha_2 = 0.6$, L = 1.833 and $\delta = 0.5$, the ARL_1 for the DGWMA-TBE chart (Case 1) is equal to 17.50.

iii. The DGWMA-TBE chart with two parameters outperforms the DEWMA-TBE chart with a single smoothing parameter for all the shift size in the shift range $\delta \geq 0.5$, and for all from Table 3.22, values of the shape parameter k, irrespective of the values for the parameter q and when $\alpha \leq 1$.

iv. The DEWMA-TBE chart with a single smoothing parameter outperforms the DGWMA-TBE chart with two parameters when $\delta = 0.25$ (i.e., large shift). Further to this, the DEWMA-TBE chart always outperforms the DGWMA-TBE chart with $\alpha = 1.3$, regardless of the shift sizes. The ARL_0 for these two charts is equal to 370.24 and 370.51, respectively. For example, from Table A.3.23, when $k = 1$, $q_1 = 0.6$, $q_2 = 0.6$, $\alpha_1 = 1.0$, $\alpha_2 = 1.0$, L = 1.813 and $\delta = 0.25$, the ARL_1 for the DEWMA-TBE chart is equal to 7.46; whereas from Table A.3.8, when $k = 1$, $q_1 = 0.6$, $q_2 = 0.6$, $\alpha_1 = 0.7$, $\alpha_2 = 0.7$, L = 1.856 and $\delta = 0.25$, the ARL_1 for the DGWMA-TBE chart is equal to 8.05.

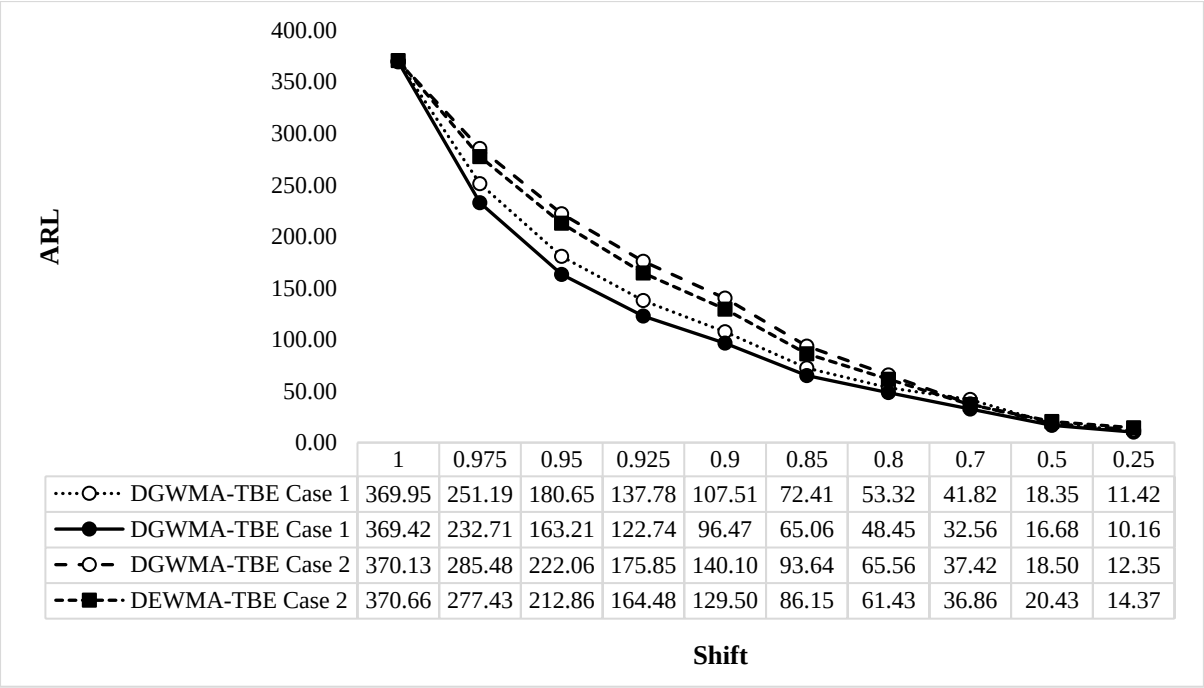

	1	0.975	0.95	0.925	0.9	0.85	0.8	0.7	0.5	0.25
DGWMA-TBE Case 1	369.95	251.19	180.65	137.78	107.51	72.41	53.32	41.82	18.35	11.42
DGWMA-TBE Case 1	369.42	232.71	163.21	122.74	96.47	65.06	48.45	32.56	16.68	10.16
DGWMA-TBE Case 2	370.13	285.48	222.06	175.85	140.10	93.64	65.56	37.42	18.50	12.35
DEWMA-TBE Case 2	370.66	277.43	212.86	164.48	129.50	86.15	61.43	36.86	20.43	14.37

Figure 3.14. DGWMA-TBE vs DEWMA-TBE

A comparative study is illustrated in Figure 3.14 to compare the performance between the DGWMA-TBE chart and the DEWMA-TBE chart. For the DGWMA-TBE chart and from table A.3.18, the parameters are selected as follows: $(q_1 = 0.7, q_2 = 0.95, \alpha_1 = 0.5, q_2 = 0.5, L = 1.401)$, $(q_1 = 0.8, q_2 = 0.9, \alpha_1 = 0.5, q_2 = 0.6, L = 1.500)$. For the DGWMA-TBE chart (Case 2) and from Table A.3.8, the parameters are selected as $(q = 0.9, \alpha = 1.0, L = 1.713)$. The DGWMA-TBE chart (Case 1) outperforms the DGWMA-TBE chart (Case 2) and the DEWMA-TBE chart in detecting small to medium shifts in the process. The DEWMA-TBE chart outperforms the DGWMA-TBE chart (Case 2) in detecting small to medium shifts in the process. Hence, in some cases the DEWMA-TBE chart outperforms the DGWMA-TBE chart and in other cases the latter outperforms the former.

The visual presentations of the findings discussed so far provide more insights on the detection capability and superiority of a chart in detecting different shift sizes, and more specifically for the small or tiny shifts, which is the main objective of the thesis. The design parameters selected for illustration purposes are as follows: $q_1 = 0.9$, $q_2 = 0.95$, $\alpha_1 = 0.5$, $\alpha_2 = 0.9$, L = 1.208 for the DGWMA-TBE chart (Case 1); $q_1 = 0.9$, $q_2 = 0.9$, $\alpha_1 = 0.6$, $\alpha_2 = 0.6$, L = 1.285 for the DGWMA-TBE chart (Case 2); $q_1 = 0.9$, $q_2 = 0$, $\alpha_1 = 0.5$, $\alpha_2 = 1.0$, L = 1.808 for the GWMA-TBE chart; $q_1 = 0.9$, $q_2 = 0$, $\alpha_1 = 1.0$, $\alpha_2 = 1.0$, L = 2.045 for the EWMA-TBE chart; $q_1 = 0.9$, $q_2 = 0.95$, $\alpha_1 = 1.0$, $\alpha_2 = 1.0$, L = 1.590 for the DEWMA-TBE chart (Case 1), and $q_1 = 0.9$, $q_2 = 0.9$, $\alpha_1 = 1.0$, $\alpha_2 = 1.0$, L = 1.756 for the DEWMA-TBE chart (Case 2). A comparative plot between the proposed DGWMA-TBE chart

(Cases 1 and 2) as the generalized time-weighted chart, the special case (i.e., the DEWMA-TBE chart), and the limiting cases (i.e., the GWMA-TBE, EWMA-TBE, and Shewhart-TBE charts) is illustrated in the following figure:

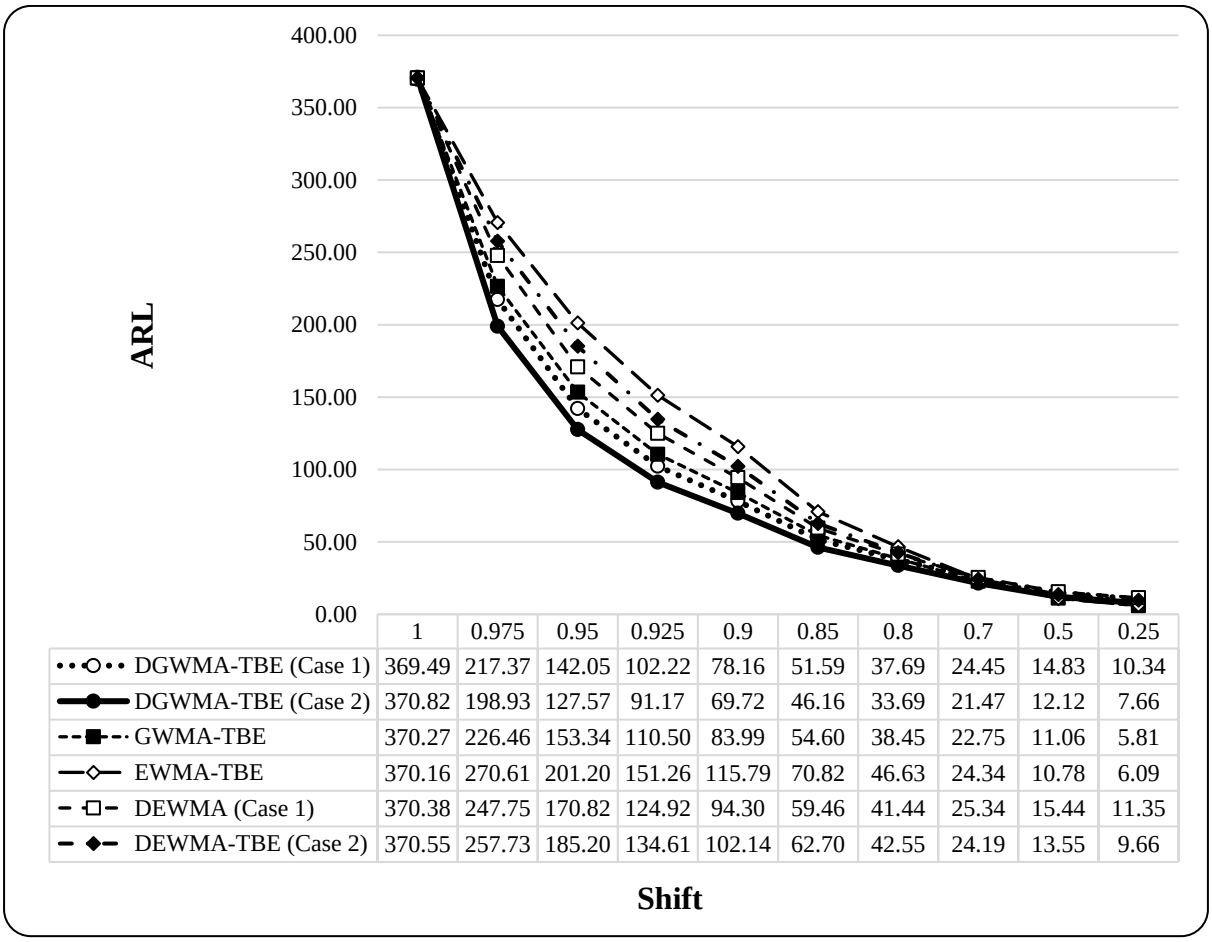

	1	0.975	0.95	0.925	0.9	0.85	0.8	0.7	0.5	0.25
DGWMA-TBE (Case 1)	369.49	217.37	142.05	102.22	78.16	51.59	37.69	24.45	14.83	10.34
DGWMA-TBE (Case 2)	370.82	198.93	127.57	91.17	69.72	46.16	33.69	21.47	12.12	7.66
GWMA-TBE	370.27	226.46	153.34	110.50	83.99	54.60	38.45	22.75	11.06	5.81
EWMA-TBE	370.16	270.61	201.20	151.26	115.79	70.82	46.63	24.34	10.78	6.09
DEWMA (Case 1)	370.38	247.75	170.82	124.92	94.30	59.46	41.44	25.34	15.44	11.35
DEWMA-TBE (Case 2)	370.55	257.73	185.20	134.61	102.14	62.70	42.55	24.19	13.55	9.66

Figure 3.15. Comparative plot between time-weighted charts

From the above plot, one can easily observe that the proposed DGWMA-TBE chart outperforms other time-weighted charts in detecting small or tiny shifts. Further to this, the DGWMA-TBE chart is competitive in terms of detecting moderate shifts compared to its counterparts. Also, the GWMA-TBE chart outperforms the DEWMA-TBE and the EWMA-TBE chart in detecting small shifts in the process dependent on the parameters under consideration in this case.

The effect of the shape parameter k and the effects of the chart parameters q, α for the DGWMA-TBE chart (Case 2) are investigated as well. The results are presented in Figures 3.16, 3.17 and 3.18. Note that, one can plot the same type of figures for the special and the limiting cases of the DGWMA-TBE chart to study the effect of the aforementioned parameters on the chart's performance.

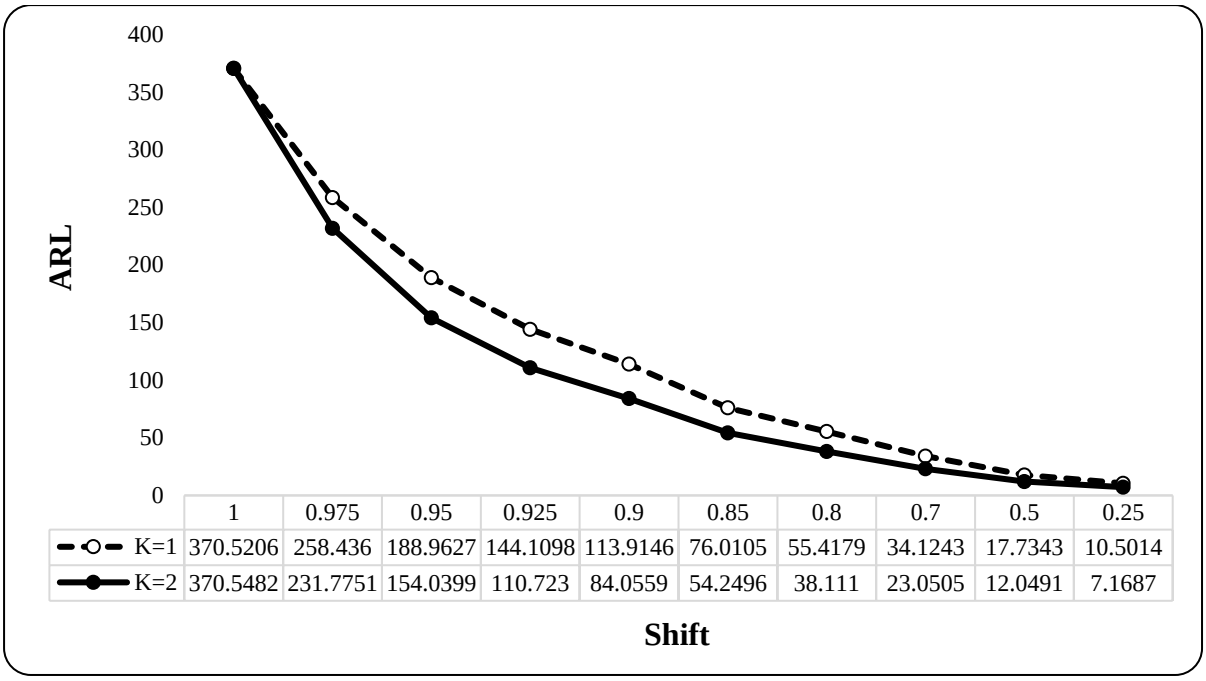

	1	0.975	0.95	0.925	0.9	0.85	0.8	0.7	0.5	0.25
K=1	370.5206	258.436	188.9627	144.1098	113.9146	76.0105	55.4179	34.1243	17.7343	10.5014
K=2	370.5482	231.7751	154.0399	110.723	84.0559	54.2496	38.111	23.0505	12.0491	7.1687

Figure 3.16. The effect of the parameter *k* on the performance of the DGWMA-TBE chart

The performance of the DGWMA-TBE chart for larger values of the shape parameter k is illustrated in Figure 3.16. This caused by an increase in the shape parameter, resulting in more failures needing to be collected. In other words, the performance of the proposed DGWMA-TBE chart improves as the k value increases. The improvement and increase in sensitivity of a chart for higher values of k is due to the fact that as the shape parameter k increases, more failures need to be collected. However, practitioners will choose the specific value for the shape parameter k.

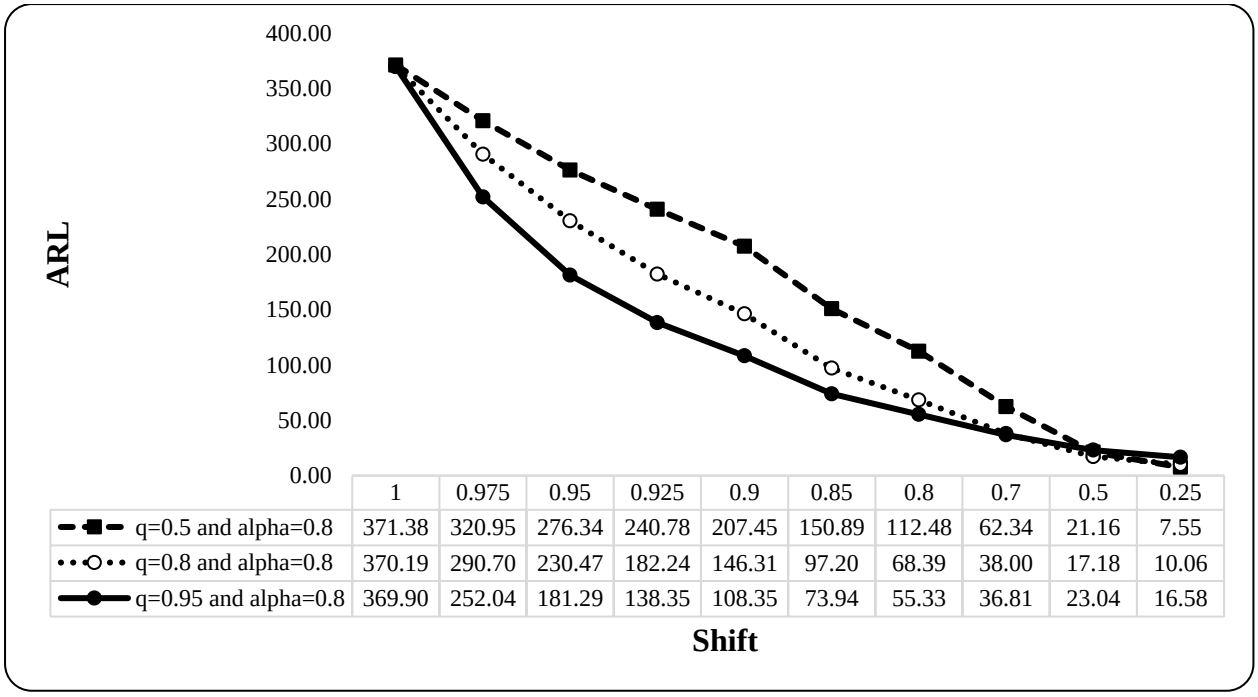

	1	0.975	0.95	0.925	0.9	0.85	0.8	0.7	0.5	0.25
q=0.5 and alpha=0.8	371.38	320.95	276.34	240.78	207.45	150.89	112.48	62.34	21.16	7.55
q=0.8 and alpha=0.8	370.19	290.70	230.47	182.24	146.31	97.20	68.39	38.00	17.18	10.06
q=0.95 and alpha=0.8	369.90	252.04	181.29	138.35	108.35	73.94	55.33	36.81	23.04	16.58

Figure 3.17. The effect of the parameter q on the performance of the DGWMA-TBE chart

In Figure 3.17, for $\alpha = 0.8$, three different values for the parameter q (0.5, 0.8, and 0.95) are selected, and based on the results, a larger value of q has better OOC performance for the DGWMA-TBE chart as a consequence. As the value for the parameter q starts decreasing, the performance of the DGWMA-TBE chart deteriorated.

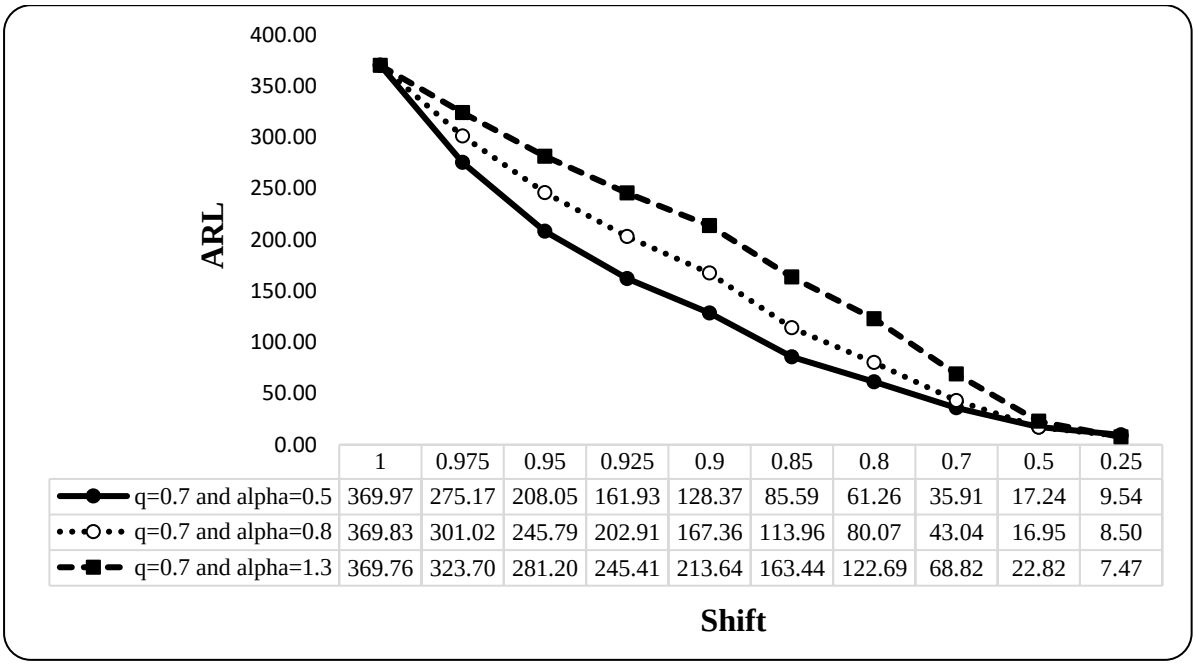

	1	0.975	0.95	0.925	0.9	0.85	0.8	0.7	0.5	0.25
q=0.7 and alpha=0.5	369.97	275.17	208.05	161.93	128.37	85.59	61.26	35.91	17.24	9.54
q=0.7 and alpha=0.8	369.83	301.02	245.79	202.91	167.36	113.96	80.07	43.04	16.95	8.50
q=0.7 and alpha=1.3	369.76	323.70	281.20	245.41	213.64	163.44	122.69	68.82	22.82	7.47

Figure 3.18. The effect of the parameter α on the performance of the DGWMA-TBE chart

In Figure 3.18, for $q = 0.7$, three different values for the parameter α (0.5, 0.8, and 1.3) are considered and the conclusion is that the smaller values of α lead to better OOC performance of the DGWMA-TBE chart.

(v) DGWMA-TBE versus CUSUM-TBE

Numerous CUSUM charts have been developed in SPC to monitor the time between failures for non-conforming items in the process, including the CUSUM chart, denoted by CUSUM-TBE, developed, and studied by Vardeman and Ray (1985), Lucas (1985) and Borror et al. (2003) when the underlying process distribution is exponential and the geometric CUSUM chart proposed by Bourke (2001). For more information regarding the research conducted for CUSUM charts to monitor TBE data, the interested reader is referred to the literature review in Section 3.2. In most of the research conducted for the CUSUM-TBE chart, the TBE is assumed to follow an exponential distribution. Lucas (1985) proposed a two-sided CUSUM chart which consists of two one-sided charts: a lower-sided CUSUM chart for decreasing shifts for the parameters of the exponential distribution and an upper-sided CUSUM chart for detecting increasing shifts.

Various methods have been proposed to calculate the run length distribution and its associated characteristics for the CUSUM chart. Goel and Wu (1971) obtained approximate *ARL* values through an exact approach. Lucas and Crosier (1982) considered both exact and Markov chain approaches to calculate the run length distribution. Woodall (1983) calculated the run length distribution for the CUSUM chart by considering a geometric distribution for the underlying process distribution. Huang et al. (2014) evaluated the run length distribution of CUSUM charts when the underlying process distribution is gamma. A performance comparison is conducted in this part for comparing the results for the CUSUM-TBE chart and the proposed chart, the DGWMA-TBE chart based on the Monte Carlo simulation. The design of CUSUM-TBE charts involve the choices of d and h, which are known as reference value and decision interval, respectively. Note that the choice for the parameter d is dependent on the IC shape and scale parameters and the target OOC scale parameter.

Note that, Borror et al. (2013) and Pehlivan and Testik (2009) concluded that the CUSUM-TBE and the EWMA-TBE charts are very robust to departures from the exponential distribution to the Weibull distribution regardless of the value of the shape parameter. Gan (1998) indicated that based on a performance comparison, the exponential CUSUM and the exponential EWMA charts have similar performance in detecting shifts in the process. For our comparison purposes, the proposed DGWMA-TBE chart is compared with the CUSUM-TBE chart for three different scenarios: (i) the underlying process distribution is gamma, (ii) the underlying process distribution is exponential, and (iii) the underlying process distribution is Weibull. The CUSUM-TBE chart proposed by Shafae et al. (2014) is considered

when the underlying process distribution is Weibull. In order to make the comparison sensible and equivalent, charts are compared based on similar conditions, hence, the proposed DGWMA-TBE is modified when the underlying process distribution is Weibull and the results are obtained. Also, since the exponential distribution is the special case of both gamma and Weibull distributions, the DGWMA-TBE chart and the CUSUM-TBE chart based on the exponential distribution are also compared. The *ARL* is used as a performance metric in order to compare the IC and OOC characteristic of the DGWMA-TBE and the CUSUM-TBE chart. The GWMA-TBE chart and its special case the EWMA-TBE chart are also included in the comparative study since no previous comparison is available in the literature between the GWMW-TBE and the CUSUM-TBE charts. For the comparison under the Weibull distribution, the pre-specified value for the *ARL* is assumed to be 100, since this is the value considered in Shafae et al. (2014) and Borror et al. (2003). For more information related to the CUSUM chart under both the exponential and the Weibull distribution, the interested reader is referred to the discussion provided by Shafae et al. (2014) and the references therein. The relative performance of these charts is investigated in detecting a decreasing shift in the process. Shafae et al. (2014) mentioned that the comparison is based on detecting a decrease in the IC TBE mean, denoted by μ_0 to the OOC TBE mean denoted by μ_1. This corresponds to detecting a shift in the scale parameter, θ of the gamma and Weibull distribution for a fixed value of the shape parameter, *k*. The comparison is divided into three different parts based on the underlying process distribution and the results and recommendations for practitioners are provided. Note that, for the parametric CUSUM chart, the decision interval is typically selected as $d = \frac{1}{2} * \delta$, where δ represents the size of the shift. Hawkins and Olwell (1998) recommended that $d = 0.25$ for shift sizes in the mean less than 0.73. Mukherjee et al. (2013) concluded that when there is no prior information available regarding the size of the shift, then a smaller value of d is recommended.

a. Gamma distribution

In this section the performance of the proposed DGWMA-TBE chart is compared with the CUSUM-TBE, GWMA-TBE and EWMA-TBE charts when the underlying process distribution is gamma. The parameters for the DGWMA-TBE chart are selected as $(q = 0.95, \alpha = 0.5, L = 0.595)$, the parameters for the GWMA-TBE chart are selected as $(q = 0.95, \alpha = 0.5, L = 1.552)$ and the parameters for the EWMA-TBE chart are selected as $(q = 0.95, \alpha = 1.0, L = 1.859)$. The parameters for the CUSUM-TBE chart are selected from the references available in the literature. These results are provided in Table 3.4. Also, different combination of parameters is selected in order to provide sensible comparative study between charts. For this purpose, the parameters for the DGWMA-TBE chart are selected as $(q = 0.9, \alpha = 0.6, L = 1.285)$, the parameters for the GWMA-TBE chart are selected as $(q = 0.9, \alpha = 0.5, L = 1.893)$ and the parameters for the EWMA-TBE chart are selected as $(q = 0.9, \alpha = 1.0, L = 2.045)$. These results are presented in Table 3.5.

Table 3.4. ARL_0 and ARL_1 values for the DGWMA-TBE, GWMA-TBE, CUSUM-TBE and EWMA-TBE chart when $k = 1$ and $ARL_0^* = 370$ under the gamma distribution

δ	DGWMA-TBE	GWMA-TBE	CUSUM-TBE	EWMA-TBE
1.000	369.85	370.08	370.80	370.05
0.975	199.25	236.13	245.96	283.85
0.950	128.47	167.99	160.28	219.00
0.925	92.49	126.82	64.10	169.41
0.900	72.32	99.91	41.20	136.09
0.850	49.61	67.82	26.60	89.47
0.800	37.64	50.15	17.80	63.69
0.700	24.97	31.51	12.60	36.55
0.500	14.66	16.23	9.40	17.64
0.250	9.58	9.05	7.30	10.40

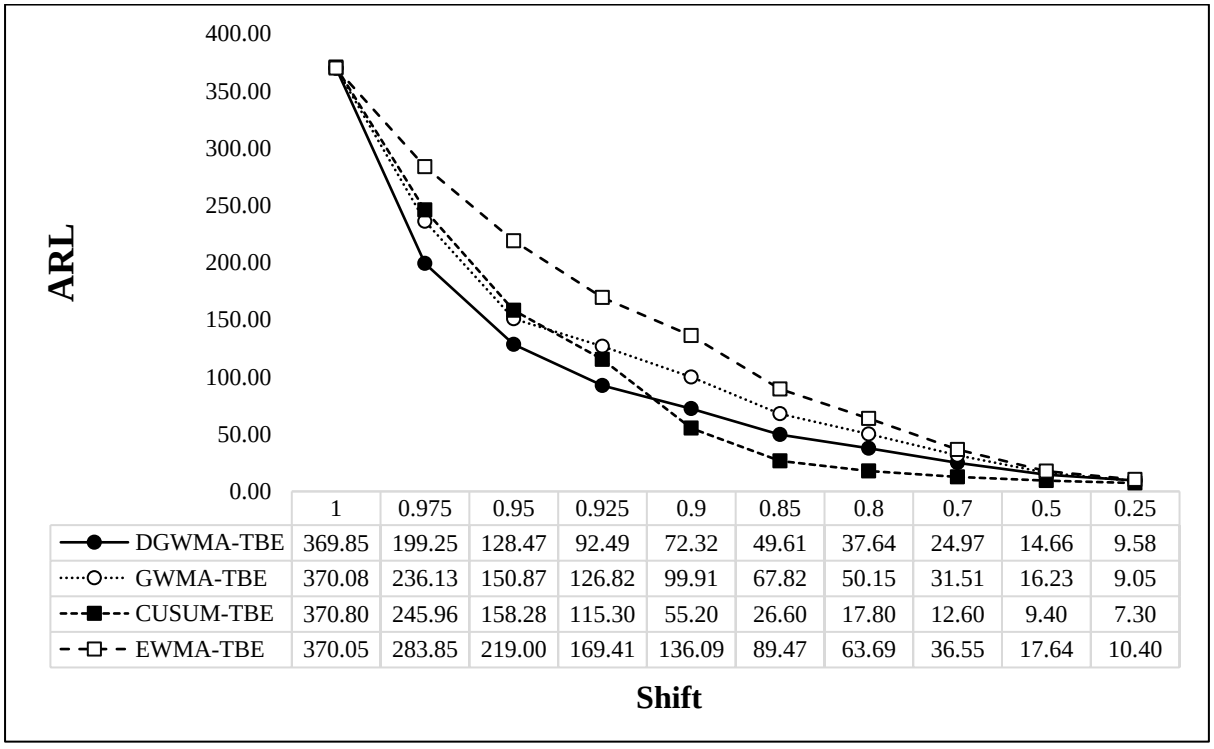

	1	0.975	0.95	0.925	0.9	0.85	0.8	0.7	0.5	0.25
DGWMA-TBE	369.85	199.25	128.47	92.49	72.32	49.61	37.64	24.97	14.66	9.58
GWMA-TBE	370.08	236.13	150.87	126.82	99.91	67.82	50.15	31.51	16.23	9.05
CUSUM-TBE	370.80	245.96	158.28	115.30	55.20	26.60	17.80	12.60	9.40	7.30
EWMA-TBE	370.05	283.85	219.00	169.41	136.09	89.47	63.69	36.55	17.64	10.40

Figure 3.19. Comparison between the DGWMA-TBE, GWMA-TBE, CUSUM-TBE and EWMA-TBE charts

The above plot illustrates a comparative study between the proposed DGWMA-TBE chart with its counterparts, the GWMA-TBE and the CUSUM-TBE charts. For tiny shifts in the process ($\delta \geq 0.925$), the proposed DGWMA-TBE chart outperforms the CUSUM-TBE, GWMA-TBE, and EWMA-TBE charts. For medium to large shifts ($0.9 \leq \delta \leq 0.25$), the CUSUM-TBE chart outperforms the

DGWMA-TBE, GWMA-TBE and EWMA-TBE charts. Also, the GWMA-TBE chart outperforms the CUSUM-TBE chart in detecting small shifts in the process and outperforms the EWMA-TBE charts for all shift sizes. The CUSUM-TBE chart outperforms the EWMA-TBE chart for all shift sizes under consideration. Note that, Gan (1998) indicated that based on a performance comparison, the exponential CUSUM and the exponential EWMA charts have similar performance in detecting shifts in the process. However, based on the results obtained in this chapter, the CUSUM-TBE chart outperforms the EWMA-TBE chart in detecting shifts in the process under the gamma distribution. The performance between these charts under the exponential distribution will be discussed later in this section.

Table 3.5. ARL_0 and ARL_1 values for the DGWMA-TBE, GWMA-TBE, CUSUM-TBE and EWMA-TBE chart when $k = 2$ and $ARL_0^* = 370$ under the gamma distribution

δ	DGWMA-TBE	GWMA-TBE	CUSUM-TBE	EWMA-TBE
1.000	370.18	370.59	370.80	370.16
0.975	216.67	236.86	245.96	256.15
0.950	141.35	170.85	160.28	200.80
0.925	101.38	116.36	64.10	131.96
0.900	77.36	88.63	41.20	99.40
0.850	51.14	56.56	26.60	61.10
0.800	37.12	39.42	17.80	41.32
0.700	23.65	23.16	12.60	23.58
0.500	13.71	11.29	9.40	11.98
0.250	9.04	6.11	7.30	7.32

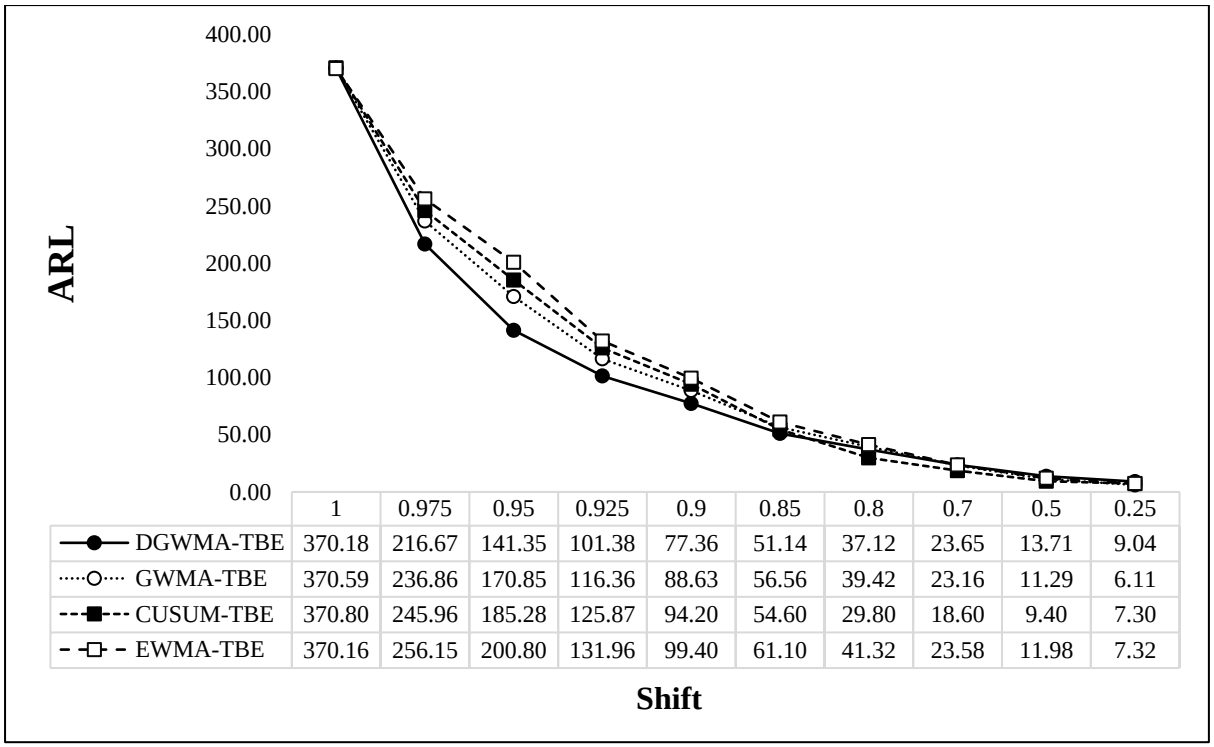

	1	0.975	0.95	0.925	0.9	0.85	0.8	0.7	0.5	0.25
DGWMA-TBE	370.18	216.67	141.35	101.38	77.36	51.14	37.12	23.65	13.71	9.04
GWMA-TBE	370.59	236.86	170.85	116.36	88.63	56.56	39.42	23.16	11.29	6.11
CUSUM-TBE	370.80	245.96	185.28	125.87	94.20	54.60	29.80	18.60	9.40	7.30
EWMA-TBE	370.16	256.15	200.80	131.96	99.40	61.10	41.32	23.58	11.98	7.32

Figure 3.20. Comparison between the DGWMA-TBE, GWMA-TBE, CUSUM-TBE and EWMA-TBE charts

The above plot demonstrated a comparative study between the DGWMA-TBE, GWMA-TBE, CUSUM-TBE and EWMA-TBE charts when $k = 2$. Also, in order to make the comparison more sensible and reliable, different values are selected for the parameters of the time-weighted charts under consideration. From the above plot, one can conclude that, the DGWMA-TBE chart outperformed all its counterparts in detecting small shifts in the process, i.e., $\delta \geq 0.925$. Also, the performance of the DGWMA-TBE chart is competitive in detecting medium shifts in the process. The GWMA-TBE charts outperforms the CUSUM-TBE chart in detecting small shifts i.e., $\delta \geq 0.925$. Also, the GWMA-TBE chart outperforms the EWMA-TBE chart in detecting all shift sizes in the process. Further, the CUSUM-TBE chart outperforms the EWMA-TBE chart for all shift sizes and outperforms the DGWMA-TBE and the GWMA-TBE charts in detecting large shifts in the process.

b. Exponential distribution

In this part, the performance of the DGWMA-TBE chart is compared with the GWMA-TBE and CUSUM-TBE charts when the underlying process distribution is exponential. Note that, the values for the CUSUM-TBE chart are extracted from Shafae et al. (2014). Also, the parameter values for the DGWMA-TBE chart and the GWMA-TBE chart are obtained from tables available in the Appendix. The shift size in this case is considered as $\delta = 1.0, 0.975, 0.950, 0.9, 0.850, 0.5, 0.25$.

Table 3.6. ARL_0 and ARL_1 values for the DGWMA-TBE, GWMA-TBE, CUSUM-TBE and EWMA-TBE chart when $k = 1$ and $ARL_0^* = 100$ under the exponential distribution

δ	DGWMA-TBE	GWMA-TBE	CUSUM-TBE	EWMA-TBE
1.000	99.92	98.72	101.10	100.20
0.975	46.35	50.73	64.10	75.64
0.950	26.90	30.33	41.20	55.23
0.900	18.30	21.89	26.60	35.82
0.850	11.15	10.40	12.60	18.55
0.5	9.87	8.30	9.40	12.25
0.25	8.24	6.20	7.30	9.81

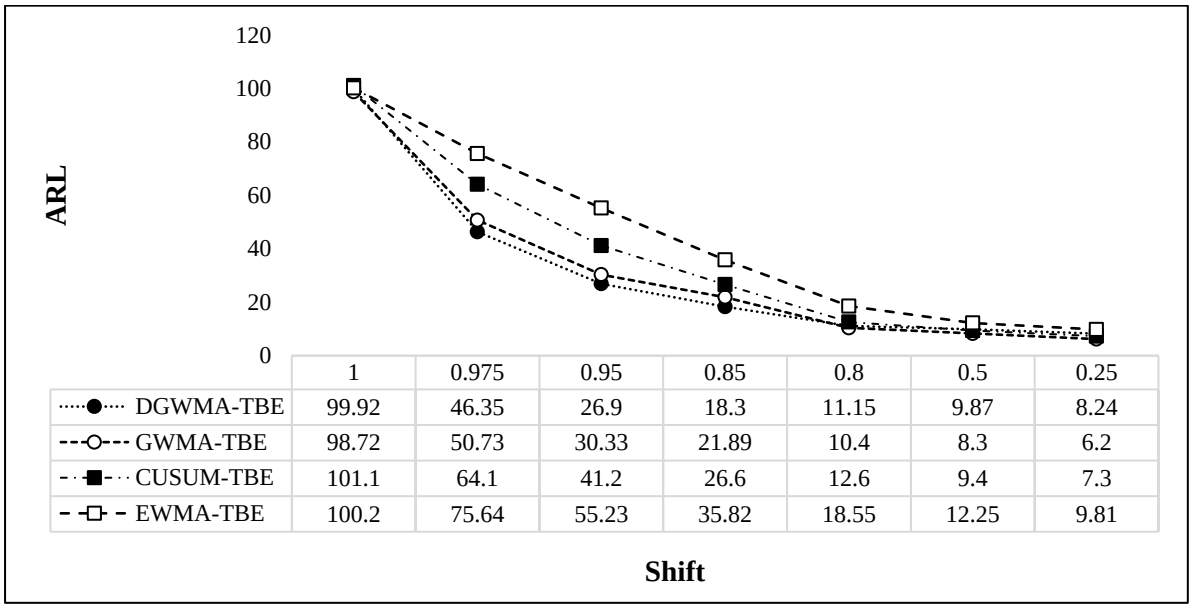

	1	0.975	0.95	0.85	0.8	0.5	0.25
DGWMA-TBE	99.92	46.35	26.9	18.3	11.15	9.87	8.24
GWMA-TBE	98.72	50.73	30.33	21.89	10.4	8.3	6.2
CUSUM-TBE	101.1	64.1	41.2	26.6	12.6	9.4	7.3
EWMA-TBE	100.2	75.64	55.23	35.82	18.55	12.25	9.81

Figure 3.21 Comparison between the DGWMA-TBE, GWMA-TBE, CUSUM-TBE and EWMA-TBE charts

From Figure 3.21, one can conclude that, for small shifts $0.95 \leq \delta \leq 0.975$, the proposed DGWMA-TBE chart outperforms the CUSUM-TBE, GWMA-TBE and EWMA-TBE charts under the exponential distribution. For medium shifts, the performance of the DGWMA-TBE chart is competitive with its counterparts. Also, the GWMA-TBE chart outperforms the CUSUM-TBE charts in detecting small shifts in the process. The CUSUM-TBE chart also outperforms the EWMA-TBE chart when the underlying process distribution is exponential.

c. Weibull distribution

In this part, the performance of the proposed DGWMA-TBE chart is compared with the GWMA-TBE and CUSUM-TBE charts when the underlying process distribution is Weibull. Note that, the values for the CUSUM-TBE chart are extracted from Shafae et al. (2014). The shift size in this case is considered as $\delta = 1.0, 0.975, 0.950, 0.9, 0.850, 0.5, 0.25$. Note that, in this chapter, the DGWMA-TBE and the

GWMA-TBE charts are constructed under the gamma distribution. In order to provide a reliable comparison with equivalent CUSUM-TBE chart, the results for these charts are recalculated by replacing the gamma distribution with the Weibull distribution. Shafae et al. (2014) discussed the CUSUM-TBE chart when the underlying process distribution is Weibull. The results are provided in Table 3.7.

Table 3.7. ARL_0 and ARL_1 values for the DGWMA-TBE, GWMA-TBE, CUSUM-TBE and EWMA-TBE chart when $ARL_0^* = 100$ under the Weibull distribution

Shift	DGWMA-TBE	GWMA-TBE	CUSUM-TBE	EWMA-TBE
1.000	101.20	100.62	96.40	99.80
0.9	35.70	40.76	50.40	60.89
0.8	17.80	22.90	26.30	35.45
0.7	10.30	13.31	14.20	22.91
0.5	8.10	7.80	5.50	12.87
0.4	6.32	5.67	4.10	8.77
0.3	5.08	4.63	3.40	5.34

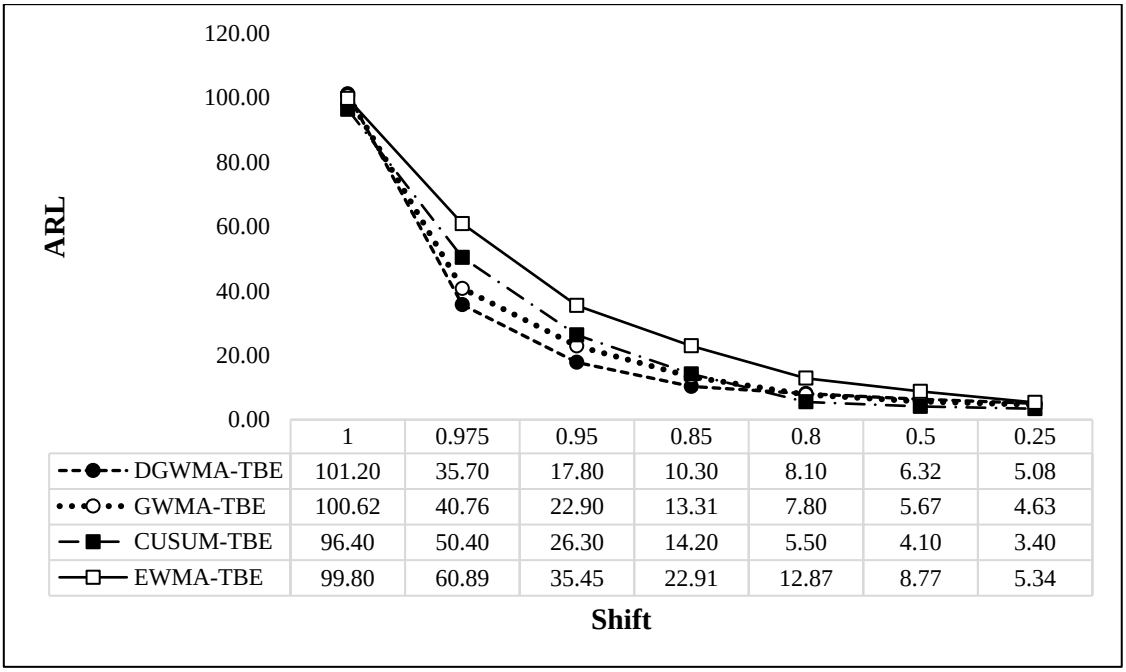

Figure 3.22. Comparison between the DGWMA-TBE, GWMA-TBE, CUSUM-TBE and EWMA-TBE charts

The performance between the DGWMA-TBE chart with its counterparts under consideration in this study is illustrated in Figure 3.22 when the underlying process distribution is Weibull. The DGWMA-TBE chart outperforms the CUSUM-TBE, GWMA-TBE and EWMA-TBE charts in detecting small shifts in the process, i.e., $0.95 \leq \delta \leq 0.975$. The GWMA-TBE charts outperforms the CUSUM-TBE

chart in detecting small shifts and the EWMA-TBE chart in detecting all shift sizes in the process. Also, the CUSUM-TBE chart outperforms the EWMA-TBE chart in detecting all shift sizes in the process. The CUSUM-TBE chart outperforms the GWMA-TBE and DGWMA-TBE charts in detecting large shifts in the process.

From the results provided in this section to compare the performance of the DGWMA-TBE chart with the CUSUM-TBE, GWMA-TBE and EWMA-TBE charts, one can conclude that the DGWMA-TBE chart outperformed its main counterparts in detecting small shifts in the production processes under the exponential, gamma, and Weibull distribution. For medium to large shifts, the CUSUM-TBE chart outperformed other charts. Also, the CUSUM-TBE chart outperforms the EWMA-TBE chart for all shift sizes.

3.11 The optimal design

For the DGWMA-TBE chart (Case 2), the optimal design required the magnitude of the shift (δ) as well as the specification of the desired ARL_0 and ARL_1 values, with the combination of design parameters (q, α, L) then being selected that provides the desired ARL performance. On the other hand, the "near optimal" design consists of the combination of the design parameters (q, α, L) that yield the smallest ARL_1 for a specified shift size (δ) given the $ARL_0 = 370$. The "near optimal" combinations of the parameters (q, α, L) as well as the ARL_1 values for different δ, and k = 1, 2, 3, 4, 5 are provided in Table 3.1.

Table 3.8. Near optimal (q, α, L) combinations with corresponding ARL values for the DGWMA-TBE chart

	k = 1				k = 2				k = 3				k = 4				k = 5			
No constraint	ARL_1	q	α	L	ARL_1	q	α	L	ARL_1	q	α	L	ARL_1	q	α	L	ARL_1	q	α	L
0.975	199.25	0.95	0.5	0.595	168.20	0.95	0.5	0.608	145.30	0.95	0.5	0.601	128.67	0.95	0.5	0.600	122.11	0.95	0.5	0.613
0.95	128.47	0.95	0.5	0.595	101.69	0.95	0.5	0.608	83.98	0.95	0.5	0.601	73.05	0.95	0.5	0.600	68.13	0.95	0.5	0.613
0.925	92.49	0.95	0.5	0.595	72.06	0.95	0.5	0.608	58.25	0.95	0.5	0.601	50.04	0.95	0.5	0.600	46.48	0.95	0.5	0.613
0.9	72.32	0.95	0.5	0.595	54.89	0.95	0.5	0.608	44.16	0.95	0.5	0.601	37.92	0.95	0.5	0.600	34.81	0.95	0.5	0.613
0.85	49.61	0.95	0.5	0.595	36.73	0.95	0.5	0.608	29.23	0.95	0.5	0.601	25.43	0.95	0.5	0.600	23.02	0.95	0.5	0.613
0.8	37.64	0.95	0.5	0.595	27.24	0.95	0.5	0.608	21.74	0.95	0.5	0.601	18.87	0.95	0.5	0.600	17.12	0.95	0.5	0.613
0.7	24.97	0.95	0.5	0.595	17.98	0.95	0.5	0.608	14.25	0.95	0.5	0.601	12.32	0.95	0.5	0.600	11.21	0.95	0.5	0.613
0.5	14.66	0.95	0.5	0.595	10.43	0.7	0.9	2.041	7.6	0.6	0.9	2.121	6.20	0.6	1.0	2.169	5.17	0.5	1.0	2.202
0.25	7.46	0.6	1	1.813	4.37	0.5	1.3	1.923	3.40	0.5	1.3	2.046	3.08	0.5	1.3	2.124	2.85	0.5	1.3	2.180

This table reveals that, for smaller shifts values (δ closer to 1), a larger value of the parameter q (closer to 1) and a smaller value of the parameter α (closer to 0.5) works best. On the other hand, for larger shifts, a smaller value of q (closer to 0.5) and larger value of α ($\geq$1) works best.

Chan and Zhang (2000) investigated the standard deviation relativeness to the ARL, to find the "near optimal" combinations of an EWMA chart. Hence, the near optimal design for the proposed DGWMA-TBE chart (Case 2) subject to the constraint that $SDRL \leq ARL$ is also provided in Table 3.9.

Table 3.9. Near optimal (q, α, L) combinations with corresponding ARL values for the DGWMA-TBE chart when $SDRL \leq ARL$

	k = 1				k = 2				k = 3				k = 4				k = 5			
$SDRL \leq ARL$	ARL_1	q	α	L	ARL_1	q	α	L	ARL_1	q	α	L	ARL_1	q	α	L	ARL_1	q	α	L
0.975	199.25	0.95	0.5	0.595	168.20	0.95	0.5	0.608	183.80	0.95	0.7	0.805	177.89	0.9	0.6	1.288	157.21	0.95	0.7	0.803
0.95	128.47	0.95	0.5	0.595	101.69	0.95	0.5	0.608	96.42	0.95	0.6	0.623	73.05	0.95	0.5	0.600	68.13	0.95	0.5	0.613
0.925	92.49	0.95	0.5	0.595	72.06	0.95	0.5	0.608	58.25	0.95	0.5	0.601	50.04	0.95	0.5	0.600	46.48	0.95	0.5	0.613
0.9	72.32	0.95	0.5	0.595	54.89	0.95	0.5	0.608	44.16	0.95	0.5	0.601	37.92	0.95	0.5	0.600	34.81	0.95	0.5	0.613
0.85	49.61	0.95	0.5	0.595	36.73	0.95	0.5	0.608	29.23	0.95	0.5	0.601	25.43	0.95	0.5	0.600	23.02	0.95	0.5	0.613
0.8	37.64	0.95	0.5	0.595	27.24	0.95	0.5	0.608	21.74	0.95	0.5	0.601	18.87	0.95	0.5	0.600	17.12	0.95	0.5	0.613
0.7	24.97	0.95	0.5	0.595	17.98	0.95	0.5	0.608	14.25	0.95	0.5	0.601	12.32	0.95	0.5	0.600	11.21	0.95	0.5	0.613
0.5	14.66	0.95	0.5	0.595	10.43	0.7	0.9	2.041	7.6	0.6	0.9	2.121	6.20	0.6	1.0	2.169	5.17	0.5	1.0	2.202
0.25	7.46	0.6	1	1.813	4.37	0.5	1.3	1.923	3.40	0.5	1.3	2.046	3.08	0.5	1.3	2.124	2.85	0.5	1.3	2.180

3.12 Alternative discrete distributions for the weights

In Section 2.5, a brief discussion was provided for the behaviour and shape of the weights for the time-weighted charts. There is a connection between the shape for the weights and the detection capability of charts in detecting small or tiny shifts in the process. A distribution is characterized by different measures that will provide different information about its structure. Some of the well-known measures include, but not limited to, scale, location, dispersion, symmetry, among others. The weighting structure for time-weighted charts contain specific information about the shape of a distribution. The shape for the weights is dependent on the type of p.m.f. under consideration. This implies that different choices for the p.m.f. impact the chart's performance in detecting shifts in the production processes. To the best of our knowledge, the discrete Weibull distribution is the only distribution considered for the weights of the GWMA and the DGWMA charts in the SPC literature. A two-parameter discrete Weibull distribution is proposed by Nakagawa and Osaki (1975) and it referred to as type I discrete Weibull. Stein and Dattero (1984) proposed a type II discrete Weibull distribution. Padgett and Spurrier (1985) developed a type III discrete Weibull distribution. Barbiero (2013) mentioned that the discrete Weibull distribution can be used in reliability analysis for modelling failure data such as the number of cycles or runs a component can overcome before failing.

The p.m.f. for the two-parameter discrete Weibull distribution is given by Nakagawa and Osaki (1975) as follows:

$$P(X = x; q_1, \alpha_1) = q_1^{(x-1)^{\alpha_1}} - q_1^{x^{\alpha_1}} \quad \text{for} \quad x = 1, 2, \dots ;$$

where $0 < q_1 < 1$ and $\alpha_1 > 0$, referred to as the scale and shape parameters, respectively.

By assuming $\alpha_1 = 1$, the geometric distribution, which is the discrete analogue of the exponential distribution is obtained. The p.m.f. for the geometric distribution is as follows:

$$P(X = x; q_1) = q_1^{x-1} - q_1^x = q_1^x(1 - q_1) \text{ for } x = 1, 2, \dots .$$

Note that, for $\alpha_1 = 1$, the GWMA chart is also reduced to the EWMA chart as its special case. Note that, the EWMA chart is a limiting case of the DGWMA chart.

Also, by assuming $\alpha_1 = 2$, the discrete version of the Rayleigh distribution proposed by Roy (2004) is obtained and its p.m.f. is as follows:

$$P(X = x; q_1) = q_1^{(x-1)^2} - q_1^{x^2} \quad \text{for} \quad x = 1, 2, \dots .$$

Krishna and Pundir (2009) mentioned that the discretization of a continuous lifetime distribution retains the same functional form of the survival function, hence, many reliability characteristics and properties shall remain unchanged.

Krishna and Pundir (2009) introduced the discrete analogue of the continuous Burr distribution, namely as the discrete Burr distribution and denoted by *DBD* (φ_1, β_1). The probability mass function (p.m.f.) is defined in their paper as:

$$P(X = x; \varphi_1, \beta_1) = \varphi_1^{\log(1+x^{\beta_1})} - \varphi_1^{\log(1+(1+x)^{\beta_1})}; \quad x = 0, 1, 2, \dots$$

where $0 < \varphi_1 < 1$ and $\beta_1 > 0$ are the parameters.

AL-Huniti and AL-Dayian (2012) proposed the discrete Burr Type III distribution by implementing the general approach of discretization of a continuous distribution and denoted by *DBDIII* (φ_2, β_2). The p.m.f. of this distribution is defined as:

$$P(X = x; \varphi_2, \beta_2) = \varphi_2^{\log(1+(1+x)^{-\beta_2})} - \varphi_2^{\log(1+x^{-\beta_2})}; \quad x = 0, 1, 2, \dots$$

where $0 < \varphi_2 < 1$ and $\beta_2 > 0$ are the parameters.

AL-Huniti and Al-Diyan (2012) concluded that if $X \sim DBDIII(\varphi_2, \beta_2)$, then $Y = [log(1 + x^{-\varphi_2})^{-1}] \sim Geo(\frac{1}{\beta_2})$. Also, if $X \sim DBDIII(\varphi_2, \beta_2)$, then $Y = [\sqrt{X}]$ follows a discrete Rayleigh distribution. Further, when $\beta_2 = 1$, the discrete Burr type III distribution is reduced to the discrete Pareto distribution. Hence, the discrete Weibull distribution, the geometric distribution, and the Rayleigh distribution are the special cases of the discrete Burr type III distribution considered in this thesis.

The relationship between these discrete distributions is demonstrated in the following figure:

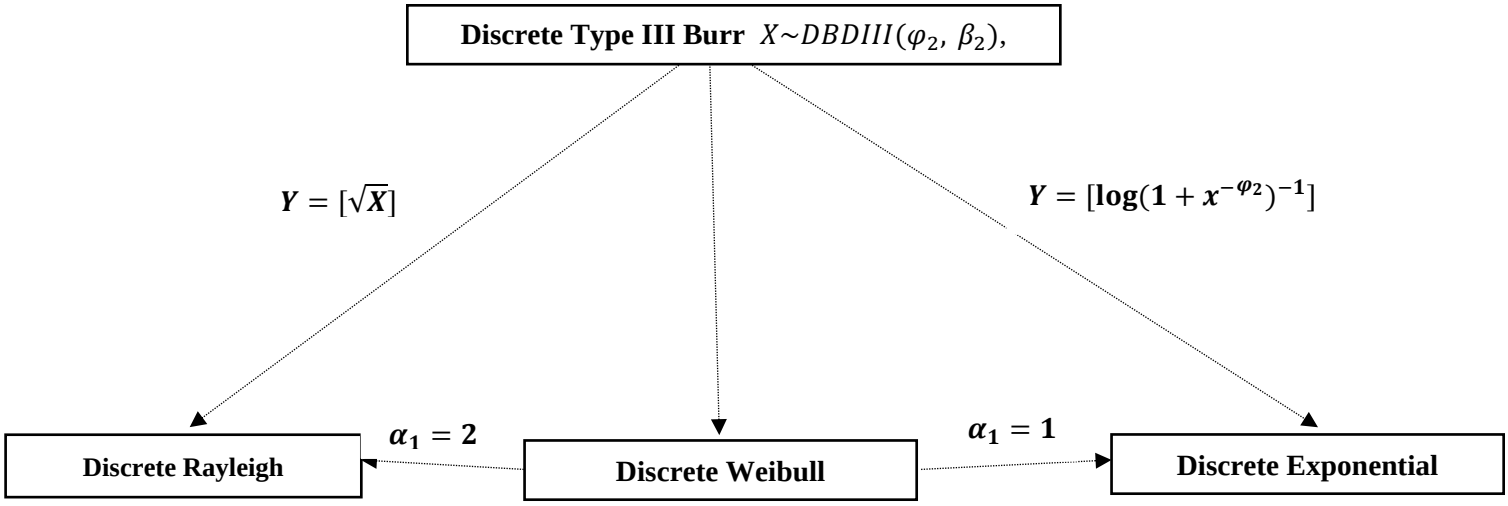

Figure 3.23. The relationship between discrete type III distribution and its special cases

The main objective of assuming alternative discrete distributions for the weights is aiding practitioners in finding the optimal discrete distribution and ultimately finding an optimal design for a time-weighted chart to detect a tiny shift in the process.

Note that, to the best of our knowledge, there are no scholarly works available in the SPC literature that consider alternative discrete distributions for the weights and investigate the effect of the weights on increasing the performance of a time-weighted chart. Hence, the discussion and study provided in this thesis can be considered as a pioneer research. Two discrete distributions namely, the discrete Burr distribution proposed by Krishna and Pundir (2009) and the discrete Burr Type III distribution developed by Al-Huniti and Al-Diyan (2012) are considered as possible candidates. The Burr distribution is proposed by Burr (1942) in the distribution theory literature and it includes the exponential and Weibull distribution as limiting cases. The plots for weights between the discrete Weibull distribution and the discrete Burr distributions are discussed next.

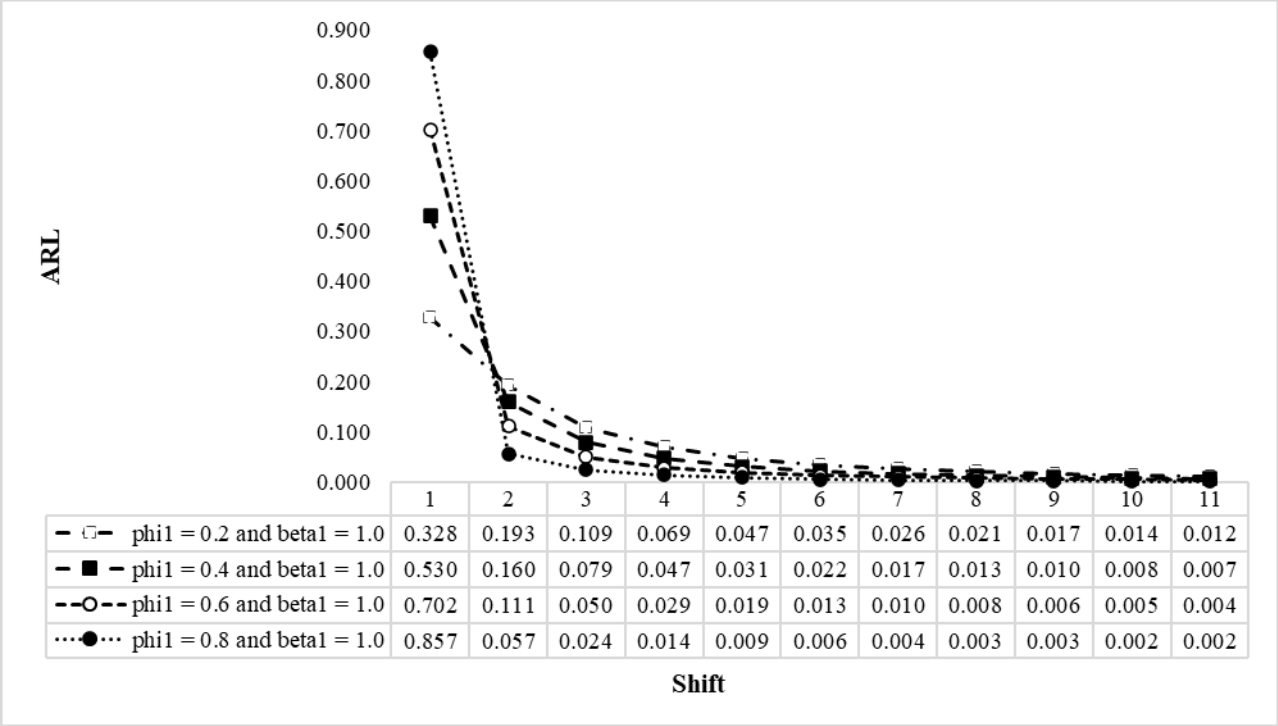

	1	2	3	4	5	6	7	8	9	10	11
phi1 = 0.2 and beta1 = 1.0	0.328	0.193	0.109	0.069	0.047	0.035	0.026	0.021	0.017	0.014	0.012
phi1 = 0.4 and beta1 = 1.0	0.530	0.160	0.079	0.047	0.031	0.022	0.017	0.013	0.010	0.008	0.007
phi1 = 0.6 and beta1 = 1.0	0.702	0.111	0.050	0.029	0.019	0.013	0.010	0.008	0.006	0.005	0.004
phi1 = 0.8 and beta1 = 1.0	0.857	0.057	0.024	0.014	0.009	0.006	0.004	0.003	0.003	0.002	0.002

Figure 3.24. Weights for the discrete Burr Distribution

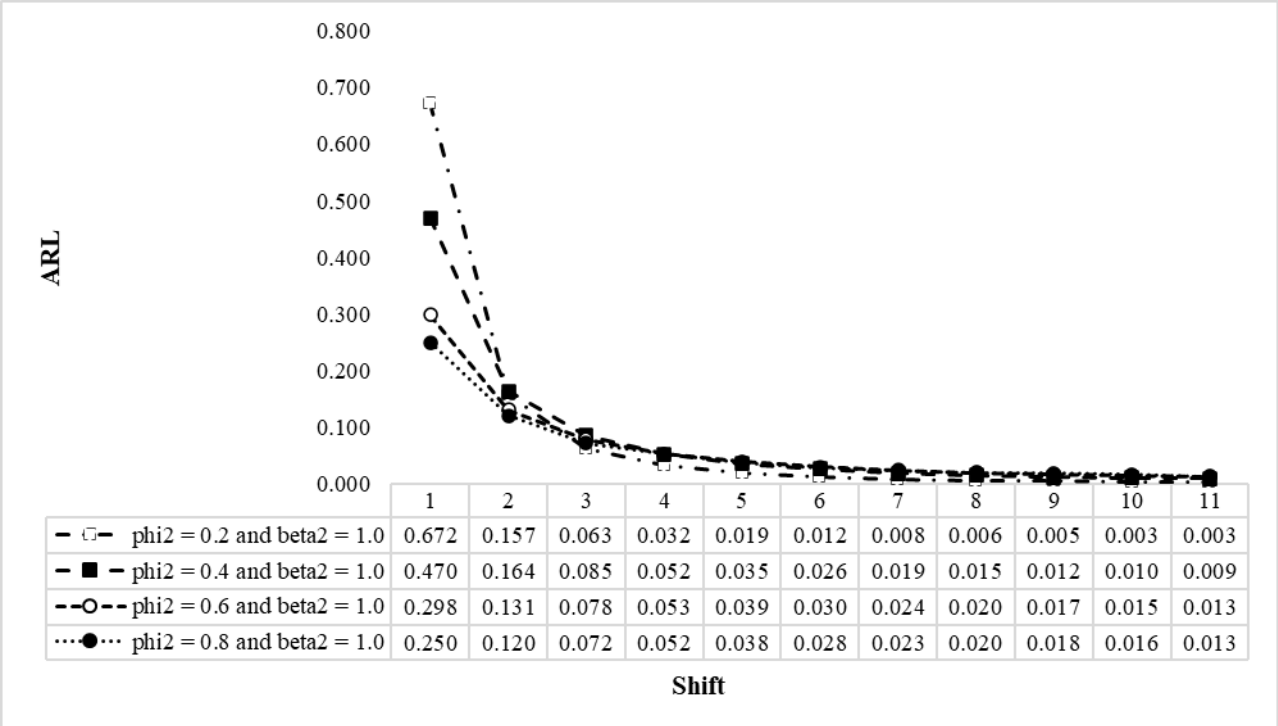

	1	2	3	4	5	6	7	8	9	10	11
phi2 = 0.2 and beta2 = 1.0	0.672	0.157	0.063	0.032	0.019	0.012	0.008	0.006	0.005	0.003	0.003
phi2 = 0.4 and beta2 = 1.0	0.470	0.164	0.085	0.052	0.035	0.026	0.019	0.015	0.012	0.010	0.009
phi2 = 0.6 and beta2 = 1.0	0.298	0.131	0.078	0.053	0.039	0.030	0.024	0.020	0.017	0.015	0.013
phi2 = 0.8 and beta2 = 1.0	0.250	0.120	0.072	0.052	0.038	0.028	0.023	0.020	0.018	0.016	0.013

Figure 3.25. Weights for the discrete Burr Type III Distribution

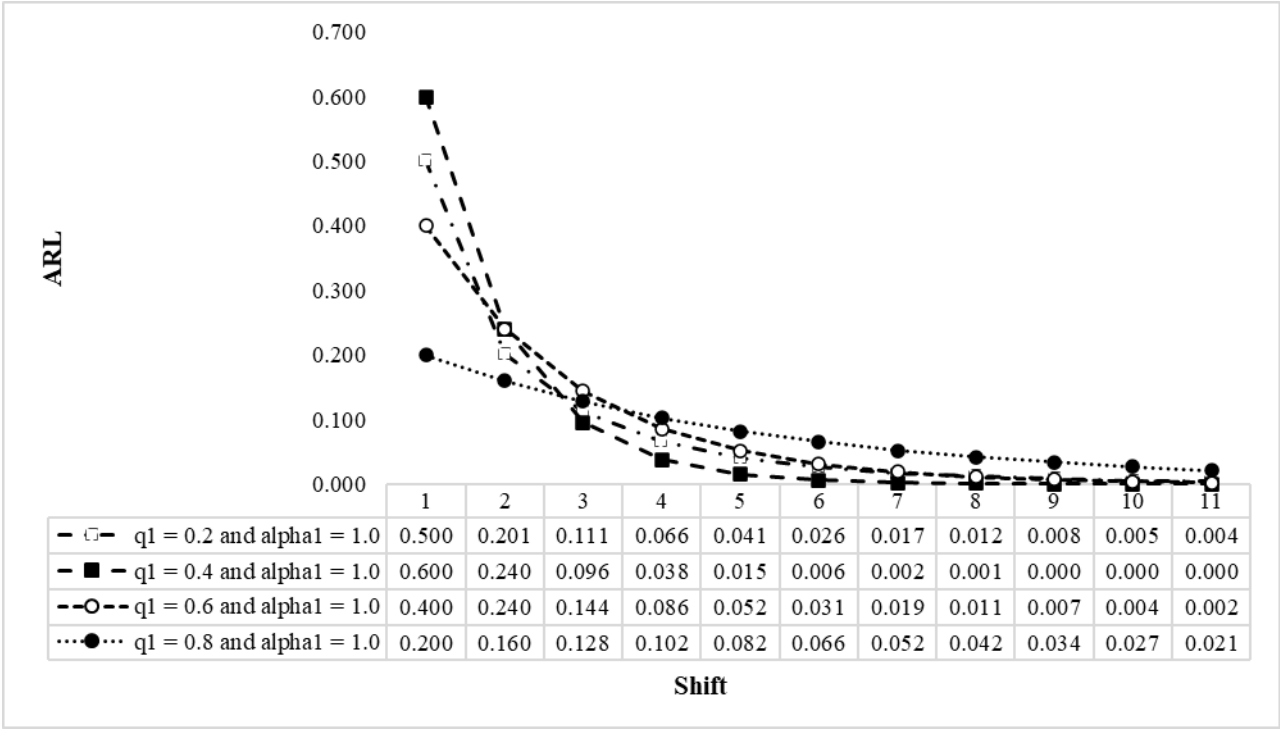

	1	2	3	4	5	6	7	8	9	10	11
q1 = 0.2 and alpha1 = 1.0	0.500	0.201	0.111	0.066	0.041	0.026	0.017	0.012	0.008	0.005	0.004
q1 = 0.4 and alpha1 = 1.0	0.600	0.240	0.096	0.038	0.015	0.006	0.002	0.001	0.000	0.000	0.000
q1 = 0.6 and alpha1 = 1.0	0.400	0.240	0.144	0.086	0.052	0.031	0.019	0.011	0.007	0.004	0.002
q1 = 0.8 and alpha1 = 1.0	0.200	0.160	0.128	0.102	0.082	0.066	0.052	0.042	0.034	0.027	0.021

Figure 3.26. Weights for the discrete Weibull Distribution

For the above plots, see Figures 3.24 to 3.26, the value for the parameters φ_1, φ_2, q_1 is selected as 0.2, 0.4, 0.6 and 0.8 and the value β_1, β_2, α_1 is selected as 1. Hence, the main objective is to observe the influence of the first set of parameters on the weights when the second set of parameters is constant. The weights are plotted for the discrete Burr distribution, discrete Burr Type III distribution and discrete Weibull distributions, respectively. All the weights sum to one, hence the weights possess one of the properties of a valid p.m.f. For large values of φ_1, the discrete Burr distributions assigns more weights to the initial observations. This means that the memory-saving feature (mixture of past and present information) for the weights of the discrete Burr distribution enables this distribution to result an optimal design of a GWMA chart in comparison to the Weibull distribution for the DGWMA chart in detecting small shifts in the process.

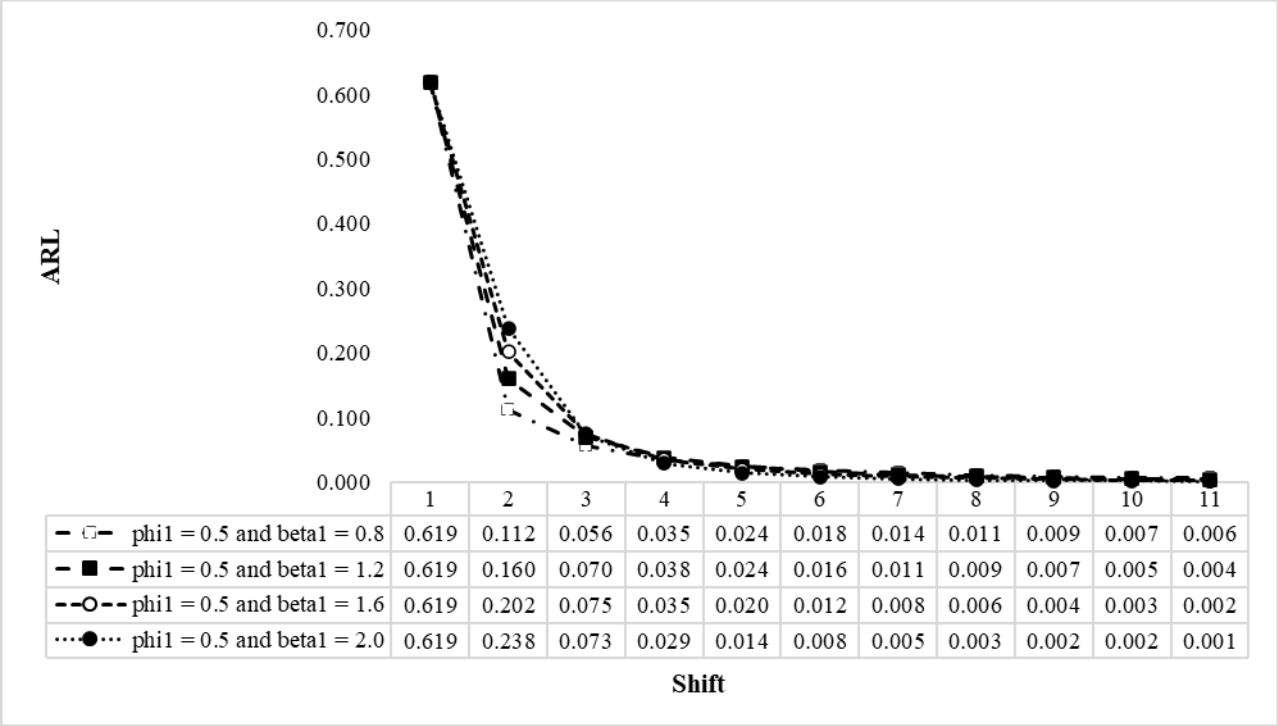

	1	2	3	4	5	6	7	8	9	10	11
phi1 = 0.5 and beta1 = 0.8	0.619	0.112	0.056	0.035	0.024	0.018	0.014	0.011	0.009	0.007	0.006
phi1 = 0.5 and beta1 = 1.2	0.619	0.160	0.070	0.038	0.024	0.016	0.011	0.009	0.007	0.005	0.004
phi1 = 0.5 and beta1 = 1.6	0.619	0.202	0.075	0.035	0.020	0.012	0.008	0.006	0.004	0.003	0.002
phi1 = 0.5 and beta1 = 2.0	0.619	0.238	0.073	0.029	0.014	0.008	0.005	0.003	0.002	0.002	0.001

Figure 3.27. Weights for the discrete Burr distribution

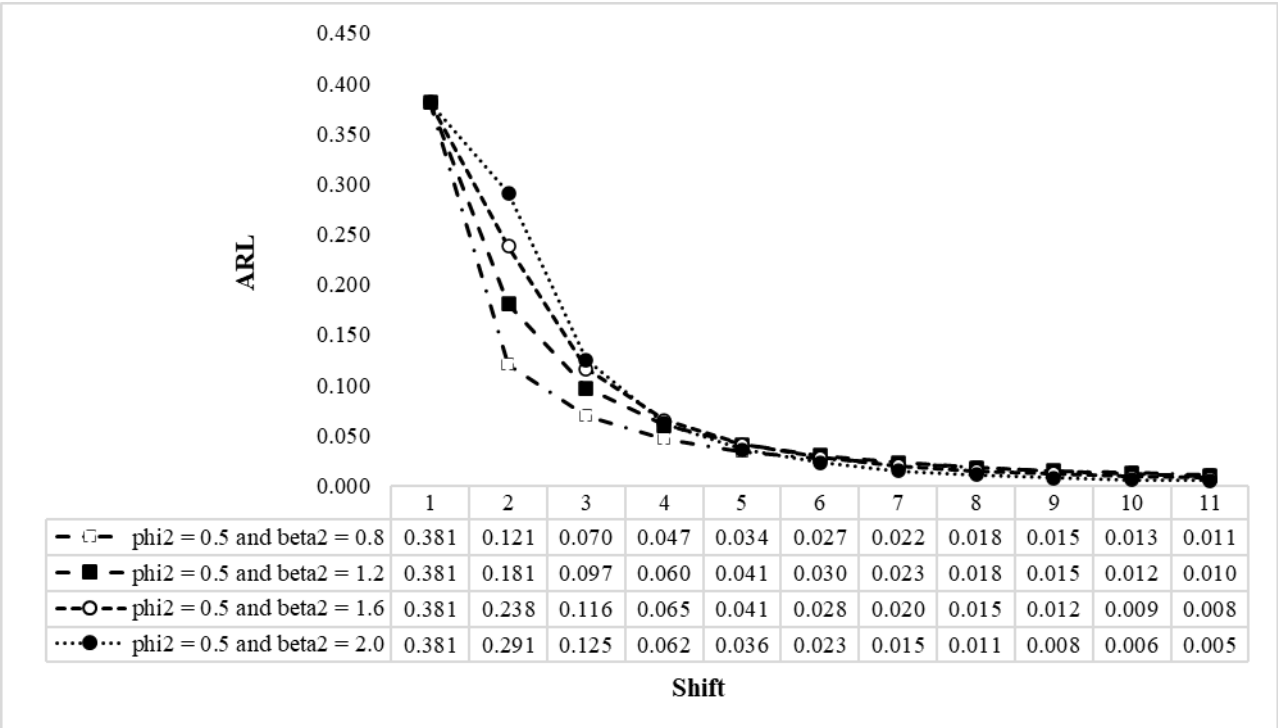

	1	2	3	4	5	6	7	8	9	10	11
phi2 = 0.5 and beta2 = 0.8	0.381	0.121	0.070	0.047	0.034	0.027	0.022	0.018	0.015	0.013	0.011
phi2 = 0.5 and beta2 = 1.2	0.381	0.181	0.097	0.060	0.041	0.030	0.023	0.018	0.015	0.012	0.010
phi2 = 0.5 and beta2 = 1.6	0.381	0.238	0.116	0.065	0.041	0.028	0.020	0.015	0.012	0.009	0.008
phi2 = 0.5 and beta2 = 2.0	0.381	0.291	0.125	0.062	0.036	0.023	0.015	0.011	0.008	0.006	0.005

Figure 3.28. Weights for the discrete Burr Type III distribution

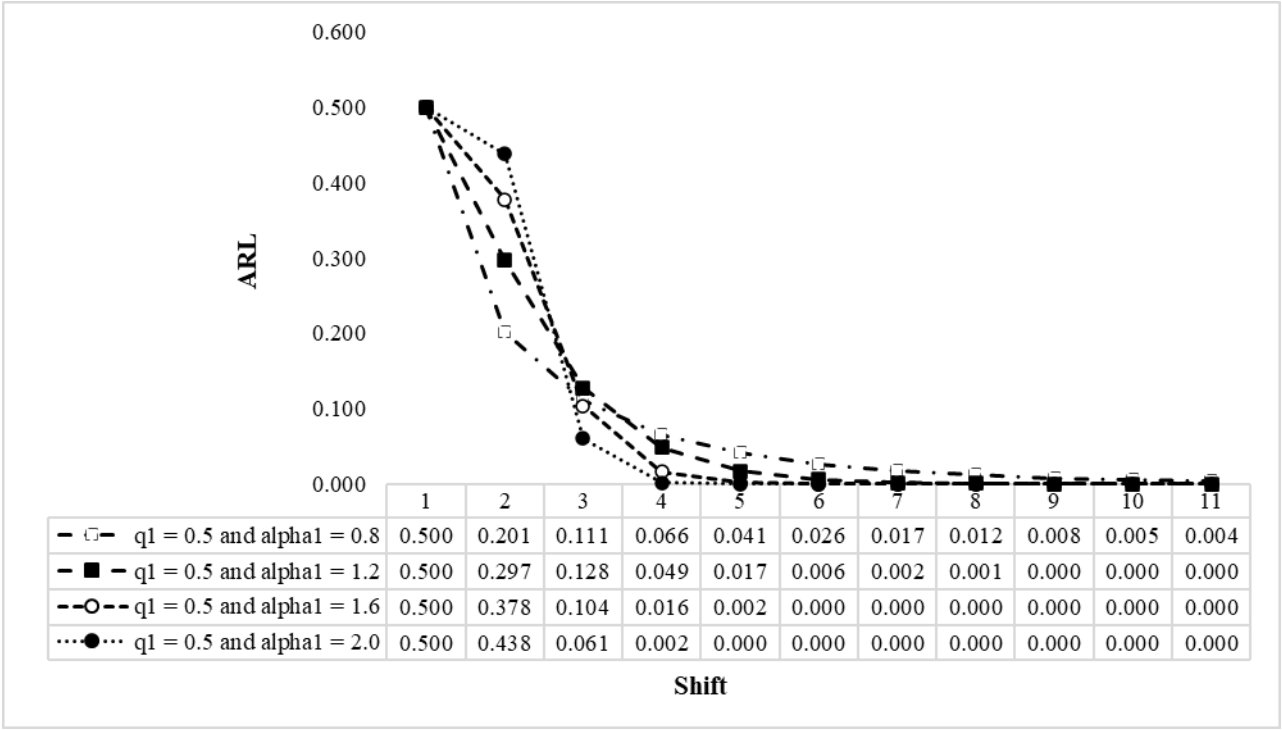

	1	2	3	4	5	6	7	8	9	10	11
q1 = 0.5 and alpha1 = 0.8	0.500	0.201	0.111	0.066	0.041	0.026	0.017	0.012	0.008	0.005	0.004
q1 = 0.5 and alpha1 = 1.2	0.500	0.297	0.128	0.049	0.017	0.006	0.002	0.001	0.000	0.000	0.000
q1 = 0.5 and alpha1 = 1.6	0.500	0.378	0.104	0.016	0.002	0.000	0.000	0.000	0.000	0.000	0.000
q1 = 0.5 and alpha1 = 2.0	0.500	0.438	0.061	0.002	0.000	0.000	0.000	0.000	0.000	0.000	0.000

Figure 3.29. Weights for the discrete Weibull distribution

For the above plots, see Figures 3.27 to 3.29, the value for the parameters φ_1, φ_2, q_1 is selected 0.5 and the value for the parameters β_1, β_2, α_1 is selected as 0.8, 1.2, 1.6 and 2.0. Hence, the main objective is to observe the influence of the second set of parameters, i.e., β_1, β_2, α_1 on the weights when the first set of parameters, i.e., φ_1, φ_2, q_1 is constant. The weights are plotted for the discrete Burr distribution, discrete Burr Type III distribution and discrete Weibull distributions, respectively. All the weights sum to one, hence the weights possess one of the properties of a valid p.m.f.

Hence, in summary, from the performance comparison conducted in terms of weights structure between these three discrete distributions, the motivation and advantage of using the discrete Burr distribution from practitioners' point of view and be summarized as follows:

1) The tails for the distributions converge to zero, however, the rate of convergence is faster for the discrete Weibull distribution in comparison to the discrete Burr distribution. In other words, tails of the discrete Burr distribution have some information that impact the performance of a chart. Note that, tails or extreme values contain specific information about the shape of a distribution (in this case the weights structure for time-weighted charts). The behaviour of these values can be measured by the concept of tail weight to classify distributions into high tail and low tail weight. The tail weight is out of scope of this thesis; however, the concept is applicable in different practical scenarios such as telecommunications network analysis (Heyde and Kou,

2004), stock returns (Peiro, 1992), among others. Several studies propose different measure to quantify the tail weight in a distribution, for example, Hoaglin et al. (1983) proposed the index of tail weight, Schuster (1984) and Haas and Pigorsch (2011) considered the tail exponent measure and the references therein.

2) The discrete Burr distribution can be considered as a generalized case or the general form of distributions for the weights of time-weighted charts. Krishna and Pundir (2009) and Al-Huniti and Al-Diyan (2012) stated the same conclusion in their research papers. This discrete distribution includes the discrete Weibull distribution, the discrete Pareto distribution, the discrete exponential (geometric) distribution and the discrete Rayleigh distribution as special cases. Note that, although the main comparison in this thesis is conducted between the discrete Burr and the discrete Weibull distribution, however, we concluded that other discrete distributions such as the discrete exponential, discrete Pareto and discrete Rayleigh can also be considered as alternatives to the Weibull distribution. The discrete exponential is already considered in this chapter, and the same procedure can be followed to design a chart when the weights follow the discrete Rayleigh or the discrete Pareto distribution.

3) There is a necessity in the SPC literature to provide hints or recommendations that encourage practitioners to consider advanced charts, e.g., GWMA, DGWMA, in practice. By replacing the discrete Weibull distribution with the Burr distribution, we provide a new methodology or path for the optimal design of a GWMA chart that outperforms the DGWMA chart. This means that, by changing the distribution of the weights, one can design a GWMA chart with optimal parameters to be applied in practice by practitioners that outperforms the DGWMA chart without the implementation of double exponential smoothing technique. Tadikamalla (1980) mentioned that the Burr distribution can be used to fit almost any given unimodal lifetime data because of its two shape parameters and tail weights and the results obtained in the next section also supports the applicability of Burr distribution because of its tail weights and rate of convergence.

3.12.1 GWMA-TBE chart under the discrete Burr distribution

Krishna and Pundir (2009) introduced and proposed the discrete analogue of the continuous Burr distribution, namely as the discrete Burr distribution and denoted by *DBD* $(\varphi_1,\ \beta_1)$. The p.m.f. is defined as:

$$P(X = x;\ \varphi_1,\ \beta_1) = \varphi_1^{\log(1+x^{\beta_1})} - \varphi_1^{\log(1+(1+x)^{\beta_1})};\quad x = 0, 1, 2, \ldots \tag{3.21}$$

where $0 < \varphi_1 < 1$ and $\beta_1 > 0$ are the parameters.

By replacing (3.21) into equation (2.2), the plotting statistic for the GWMA-TBE can be written as:

$$Z_t^1 = \sum_{i=1}^{t} v_i T_{t-i+1} + v_0 k\theta_0 ; \tag{3.22}$$

where $v_i = \varphi_1^{\log(1+i^{\beta_1})} - \varphi_1^{\log(1+(1+i)^{\beta_1})}$ are the weights. The GWMA-TBE chart constructed under the discrete Burr distribution is denoted by *GWMA-TBE-DBD* (φ_1, β_1).

3.12.2 GWMA-TBE chart under the discrete Burr Type III distribution

Al-Huniti and Al-Diyan (2012) proposed the discrete Burr Type III distribution by implementing the general approach of discretization of a continuous distribution and denoted by *DBDIII* (φ_2, β_2). The p.m.f. is defined as:

$$P(X = x;\ \varphi_2, \beta_2) = \varphi_2^{\log(1+(1+x)^{-\beta_2})} - \varphi_2^{\log(1+x^{-\beta_2})};\quad x = 0, 1, 2, \ldots \tag{3.23}$$

where $0 < \varphi_2 < 1$ and $\beta_2 > 0$ are the parameters.

By replacing (3.23) into equation (2.2), the plotting statistic for the GWMA-TBE can be written as:

$$Z_t^1 = \sum_{i=1}^{t} v_i T_{t-i+1} + v_0 k\theta_0; \tag{3.24}$$

where $v_i = \varphi_2^{\log(1+(1+i)^{-\beta_2})} - \varphi_2^{\log(1+i^{-\beta_2})}$ are the weights. The GWMA-TBE chart constructed under the discrete Burr Type III distribution is denoted by *GWMA-TBE-DBDIII* (φ_2, β_2).

3.12.3 The IC design

For the GWMA-TBE chart, the IC design consists of the calculation for the charting constant $(L > 0)$ based on a chosen value for the shape parameter k, and a combination of the GWMA-TBE design parameters. For the GWMA-TBE-DBD the design parameters are (φ_1, β_1, L) and for the GWMA-TBE-DBDIII the design parameters are (φ_2, β_2, L). The design parameters are selected so that the attained ARL is close to the pre-specified value ARL_0^*. The pre-specified value is selected as 370. The parameters are selected from the following intervals: $\varphi_1, \varphi_2 = 0.5, 0.7, 0.9, 0.95$ and $\beta_1, \beta_2 = 0.5, 0.7, 0.9, 1.0$. The shape parameter is selected as $k = 1$ and the size for the shift is selected as $\delta = 0.975, 0.950, 0.925, 0.9, 0.85, 0.8, 0.7, 0.5, 0.25$.

By implementing the grid search method in the simulation algorithm, the charting constant $L > 0$ are obtained for the chosen combination of the parameters, and the value of the shape parameter k has been specified, so that the attained ARL_0 is approximately equal to the desirable value of $ARL_0^* = 370$. The

values of L determined through this approach are presented in Tables A.3.28 and A.3.29, see Appendix for Chapter 3.

The value for the charting statistic ($L > 0$) for the GWMA-TBE-DBD chart (see Table A.3.28) is generally larger than the charting statistic for the GWMA-TBE-DBDIII chart (see Table A.3.29). For the DGWMA-TBE and the GWMA-TBE charts, the value for the charting statistic is larger than the GWMA-TBE-DBD and the GWMA-TBE-DBDIII charts when $\beta_1, \beta_2 = 0.5$ and irrespective of the values for the parameters φ_1 and φ_2. As the value for the parameters β_1, β_2 starts increasing, the charting statistic values for the GWMA-TBE-DBD and the GWMA-TBE-DBDIII are larger than the ones for the GWMA-TBE and the DGWMA-TBE charts. Note that, the charting statistics values for the GWMA-TBE and the DGWMA-TBE charts are presented in Table A.3.1 when $k = 1$.

3.12.4 The OOC performance

The main objective is to detect a sustained downward shift in the process. The magnitude of the shifts is selected as $\delta < 1$. The GWMA-TBE charts constructed under the discrete Burr and the discrete Burr Type III distributions are compared with the GWMA-TBE chart proposed by Chakraborty et al. (2016) and the DGWMA-TBE chart proposed in this chapter. To ensure that all the charts are on an equal footing, the ARL_0s for all the competing charts are set close to 370 ($\delta = 1$). The IC *ARL* (i.e., ARL_0) and the OOC *ARL* (i.e., ARL_1) values are presented in Tables A.3.30 and A.3.31.

Note that the notation for the parameters is excluded from Tables A.3.30 and A.3.31 since each of the TBE charts presented have different parameter notation. The range of the parameters for these charts are the same to make a fair comparison. Further, the values for the charting constant (i.e., $L > 0$) are not presented since for each combination of parameters and different control chart there will be different values. However, these values can be obtained from Tables A.3.28 and A.3.29 for the GWMA-TBE-DB and the GWMA-TBE-DBIII charts, and for the GWMA-TBE and the DGWMA-TBE charts the results are presented in Table A.3.1.

The OOC performance is divided into three different parts. The performance comparison between the GWMA-TBE-DB chart and the GWMA-TBE and the DGWMA-TBE charts is considered in the first part. The performance comparison between the GWMA-TBE-DBDIII and the GWMA-TBE and the DGWMA-TBE charts is conducted in the second part. The last part includes the performance comparison between the GWMA-TBE-DB and the GWMA-TBE-DBDIII charts. Note that for all the comparisons performed in this section, the IC *ARL* values are set equal so that the charts are at an equal footing. The results presented in Tables A.3.30 and A.3.31 reveal the following:

(i) GWMA-TBE-DB chart versus GWMA-TBE and DGWMA-TBE charts

i. For small shifts ($\delta \geq 0.925$), the GWMA-TBE-DB chart outperforms the GWMA-TBE and the DGWMA-TBE charts. For example, from Table A.3.30, when $\varphi_1 = 0.5$, $\beta_1 =$

0.7, and L= 1.704, the OOC *ARL*, i.e., ARL_1 is equal to 280.76 for the GWMA-TBE-DB chart. For the GWMA-TBE chart and when $q_1 = 0.5$, $\alpha_1 = 0.7$, and L= 1.414, the ARL_1 is equal to 319.59. For the DGWMA-TBE chart, when $q = 0.5$, $\alpha = 0.7$, and L= 1.747, the ARL_1 is equal to 315.36.

ii. For medium shifts ($0.8 \leq \delta \leq 0.9$), the GWMA-TBE-DB chart outperforms the GWMA-TBE and the DGWMA-TBE charts. For example, from Table A.3.31, when $\varphi_1 = 0.9$, $\beta_1 = 1.0$, and L= 1.770, the OOC *ARL*, i.e., ARL_1 is equal to 58.95 for the GWMA-TBE-DB chart. For the GWMA-TBE chart and when $q_1 = 0.9$, $\alpha_1 = 1.0$, and L= 1.909, the ARL_1 is equal to 74.86. For the DGWMA-TBE chart, when $q = 0.9$, $\alpha = 1.0$, and L= 1.713, the ARL_1 is equal to 65.56.

iii. For large shifts ($0.25 \leq \delta \leq 0.7$), the DGWMA-TBE chart outperforms the GWMA-TBE-DB and the GWMA-TBE charts. For example, from Table A.3.31, when $\varphi_1 = 0.95$, $\beta_1 = 0.5$, and L= 1.737, the OOC *ARL*, i.e., ARL_1 is equal to 16.38 for the GWMA-TBE-DB chart. For the GWMA-TBE chart and when $q_1 = 0.95$, $\alpha_1 = 0.5$, and L= 1.552, the ARL_1 is equal to 16.23. For the DGWMA-TBE chart, when $q = 0.95$, $\alpha = 0.5$, and L= 0.595, the ARL_1 is equal to 14.66.

iv. The DGWMA-TBE chart outperforms the GWMA-TBE and GWMA-TBE-DB charts when $q = 0.95$ and $\alpha = 0.5$ and 0.7, for all the shift sizes.

v. The performance of the GWMA-TBE chart under the discrete Weibull distribution is increased by considering the discrete Burr distribution for the weights. This improvement effects the detection ability of the GWMA-TBE chart as well as providing alternatives in finding an optimal design of a chart.

vi. As a result, by changing the type of distribution for the weights in the GWMA-TBE chart, the performance of the chart increase significantly. This implies that without implementing the double exponential smoothing technique, one can construct a GWMA-TBE chart that outperforms the DGWMA-TBE chart in detecting small shifts in the process. Hence, the type of discrete distribution for the weights plays a major role in improving the detection capability of a chart and aiding in finding an optimal design for a chart.

(ii) GWMA-TBE-DBDIII chart versus GWMA-TBE and DGWMA-TBE charts

i. For small shifts ($\delta \geq 0.925$), the GWMA-TBE-DBDIII chart outperforms the GWMA-TBE and the DGWMA-TBE charts. For example, from Table A.3.30, when $\varphi_2 = 0.5$, $\beta_2 = 0.7$, and $L = 1.620$, the OOC *ARL*, i.e., ARL_1 is equal to 290.46 for the GWMA-TBE-DBDIII chart. For the GWMA-TBE chart and when $q_1 = 0.5$, $\alpha_1 = 0.7$, and $L = 1.414$, the ARL_1 is equal to 319.59. For the DGWMA-TBE chart, when $q = 0.5$, $\alpha = 0.7$, and $L = 1.747$, the ARL_1 is equal to 315.36.

ii. For medium shifts ($0.8 \leq \delta \leq 0.9$), the DGWMA-TBE chart outperforms the GWMA-TBE-DBDIII and the GWMA-TBE charts. For example, from Table A.3.31, when $\varphi_2 = 0.9$, $\beta_2 = 1.0$, and $L = 1.475$, the OOC *ARL*, i.e., ARL_1 is equal to 87.55 for the GWMA-TBE-DBIII chart. For the GWMA-TBE chart and when $q_1 = 0.9$, $\alpha_1 = 1.0$, and $L = 1.909$, the ARL_1 is equal to 74.86. For the DGWMA-TBE chart, when $q = 0.9$, $\alpha = 1.0$, and $L = 1.713$, the ARL_1 is equal to 65.56.

iii. For large shifts ($0.25 \leq \delta \leq 0.7$), the DGWMA-TBE chart outperforms the GWMA-TBE-DBDIII and the GWMA-TBE charts. For example, from Table A.3.31, when $\varphi_2 = 0.95$, $\beta_2 = 0.5$, and $L = 1.620$, the OOC *ARL*, i.e., ARL_1 is equal to 17.68 for the GWMA-TBE-DBDIII chart. For the GWMA-TBE chart and when $q_1 = 0.95$, $\alpha_1 = 0.5$, and $L = 1.552$, the ARL_1 is equal to 16.23. For the DGWMA-TBE chart, when $q = 0.95$, $\alpha = 0.5$, and $L = 0.595$, the ARL_1 is equal to 14.66.

iv. As a result, the GWMA-TBE-DBDIII chart outperforms the GWMA-TBE and the DGWMA-TBE charts in detecting small shifts. For the medium and large shifts, the DGWMA-TBE chart outperforms the GWMA-TBE and the GWMA-TBE-DBDIII charts.

(iii) GWMA-TBE-DB chart versus GWMA-TBE-DBIII chart

The GWMA-TBE-DB chart outperforms the GWMA-TBE-DBDIII chart in most of the cases irrespective of the values for the parameters. The only case where the GWMA-TBE-DBDIII chart outperforms the GWMA-TBE-DB chart is when $\varphi_2 = 0.5$ and $\beta_2 = 0.5$ and 1 and for shift size 0.5, i.e., $\delta = 0.5$.

Next, different comparative graphs are provided to compare the performance between the charts discussed in this section. These graphs will provide better insights than numerical results presented in Tables A.3.30 and A.3.31, since these tables are too informative, whereas a visual presentation always provide better guidelines to select the best performing control chart. Different values are selected for the chart's parameters.

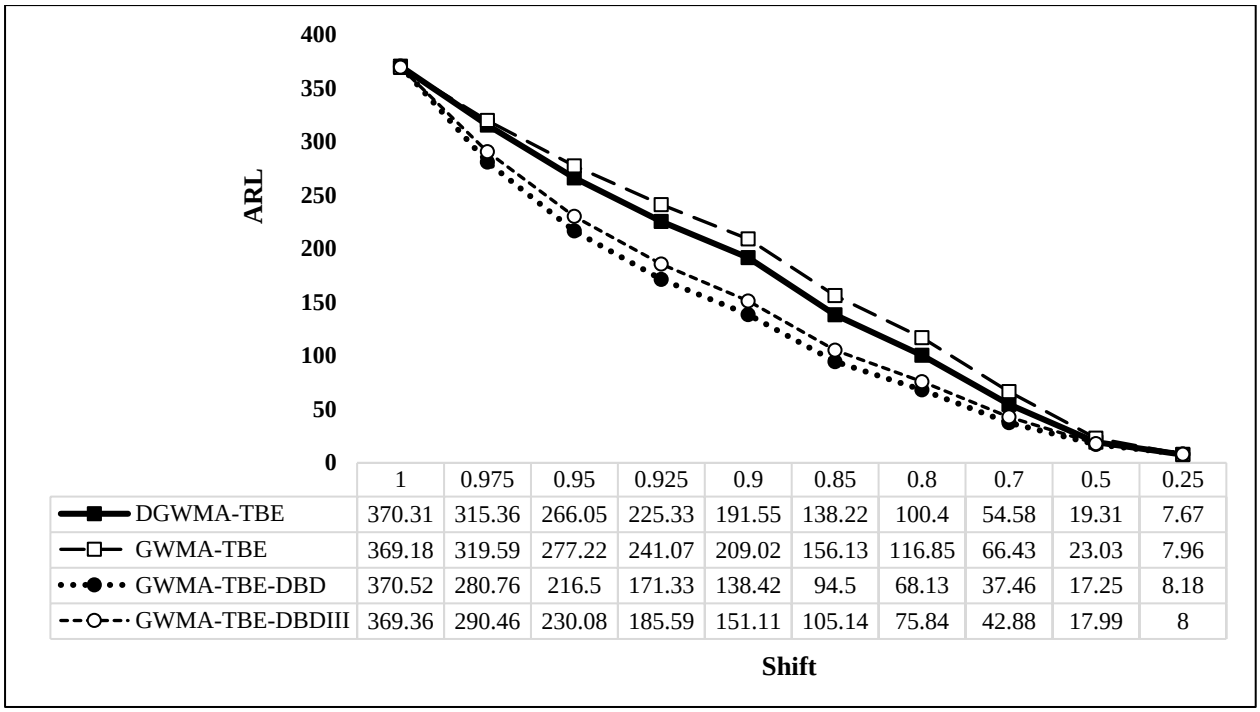

	1	0.975	0.95	0.925	0.9	0.85	0.8	0.7	0.5	0.25
DGWMA-TBE	370.31	315.36	266.05	225.33	191.55	138.22	100.4	54.58	19.31	7.67
GWMA-TBE	369.18	319.59	277.22	241.07	209.02	156.13	116.85	66.43	23.03	7.96
GWMA-TBE-DBD	370.52	280.76	216.5	171.33	138.42	94.5	68.13	37.46	17.25	8.18
GWMA-TBE-DBDIII	369.36	290.46	230.08	185.59	151.11	105.14	75.84	42.88	17.99	8

Figure 3.30. Comparative graph between the DGWMA-TBE, GWMA-TBE (under discrete Weibull distribution) and GWMA-TBE-DBD, and the GWMA-TBE-DBDIII (under discrete Burr distribution)

The chart parameters are selected as follows: $q = 0.5$ and $\alpha = 0.7$ for the DGWMA-TBE chart, $q_1 = 0.5$, $\alpha_1 = 0.7$ for the GWMA-TBE chart, $\varphi_1 = 0.5$, $\beta_1 = 0.7$ for the GWMA-TBE-DBD chart, and $\varphi_2 = 0.5$, $\beta_2 = 0.7$ for the GWMA-TBE-DBDIII chart. From the above plot one can conclude that the GWMA-TBE-DBD chart outperforms other time-weighted charts in detecting tiny shifts in the process and is competitive in detecting moderate to large shifts in the process. Note that, there is no need to implement the double exponential smoothing to enhance the detection capability of the GWMA-TBE chart and by changing the type of the distribution for the weights, one can design a GWMA-TBE chart that outperforms the DGWMA-TBE chart.

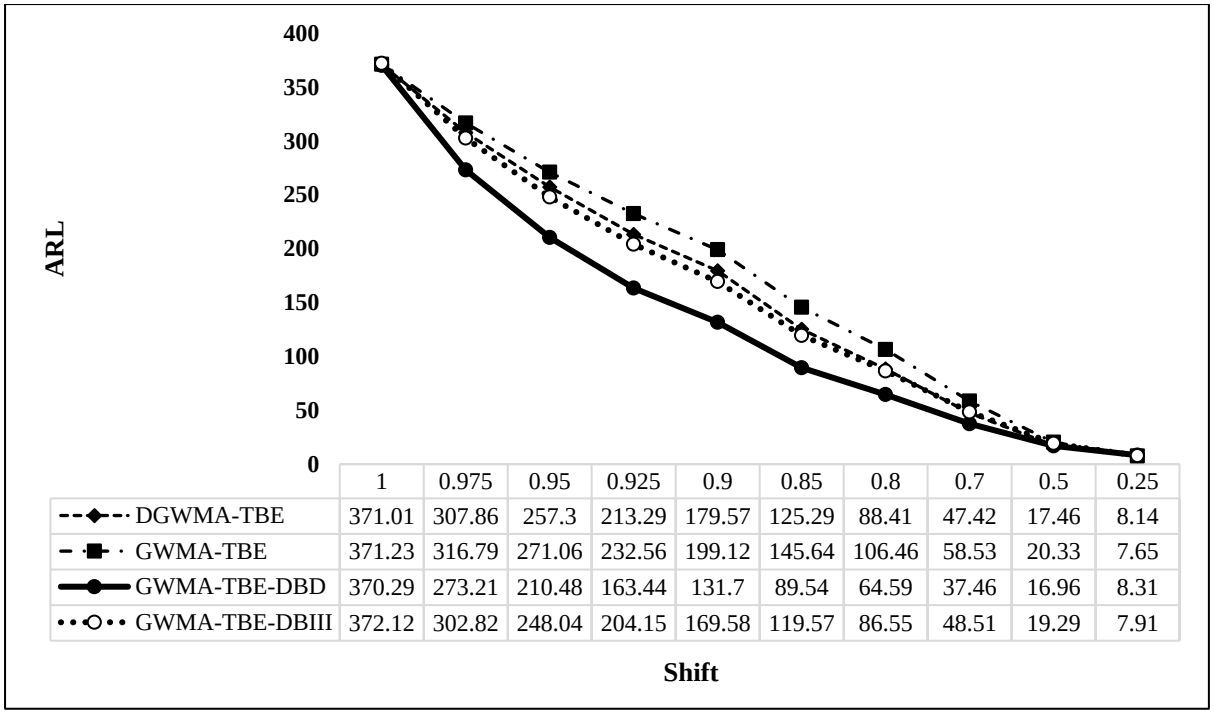

	1	0.975	0.95	0.925	0.9	0.85	0.8	0.7	0.5	0.25
DGWMA-TBE	371.01	307.86	257.3	213.29	179.57	125.29	88.41	47.42	17.46	8.14
GWMA-TBE	371.23	316.79	271.06	232.56	199.12	145.64	106.46	58.53	20.33	7.65
GWMA-TBE-DBD	370.29	273.21	210.48	163.44	131.7	89.54	64.59	37.46	16.96	8.31
GWMA-TBE-DBIII	372.12	302.82	248.04	204.15	169.58	119.57	86.55	48.51	19.29	7.91

Figure 3.31. Comparative graph between the DGWMA-TBE and GWMA-TBE (under discrete Weibull distribution) and GWMA-TBE-DBD, and the GWMA-TBE-DBDIII (under discrete Burr distribution)

The chart parameters are selected as follows: $q = 0.7$ and $\alpha = 0.9$ for the DGWMA-TBE chart, $q_1 = 0.7$, $\alpha_1 = 0.9$ for the GWMA-TBE chart, $\varphi_1 = 0.7$, $\beta_1 = 0.9$ for the GWMA-TBE-DBD chart, and $\varphi_2 = 0.7$, $\beta_2 = 0.9$ for the GWMA-TBE-DBDIII chart. From the above plot one can conclude that the GWMA-TBE-DBD chart outperforms other time-weighted charts in detecting tiny shifts in the process and is competitive in detecting moderate to large shifts in the process. Also, the GWMA-TBE-DBDIII outperforms the DGWMA-TBE and the GWMA-TBE charts in detecting tiny shifts in the process. The DGWMA-TBE chart proposed in this chapter outperforms the GWMA-TBE chart for tiny shifts and its competitive in detecting medium to large shifts.

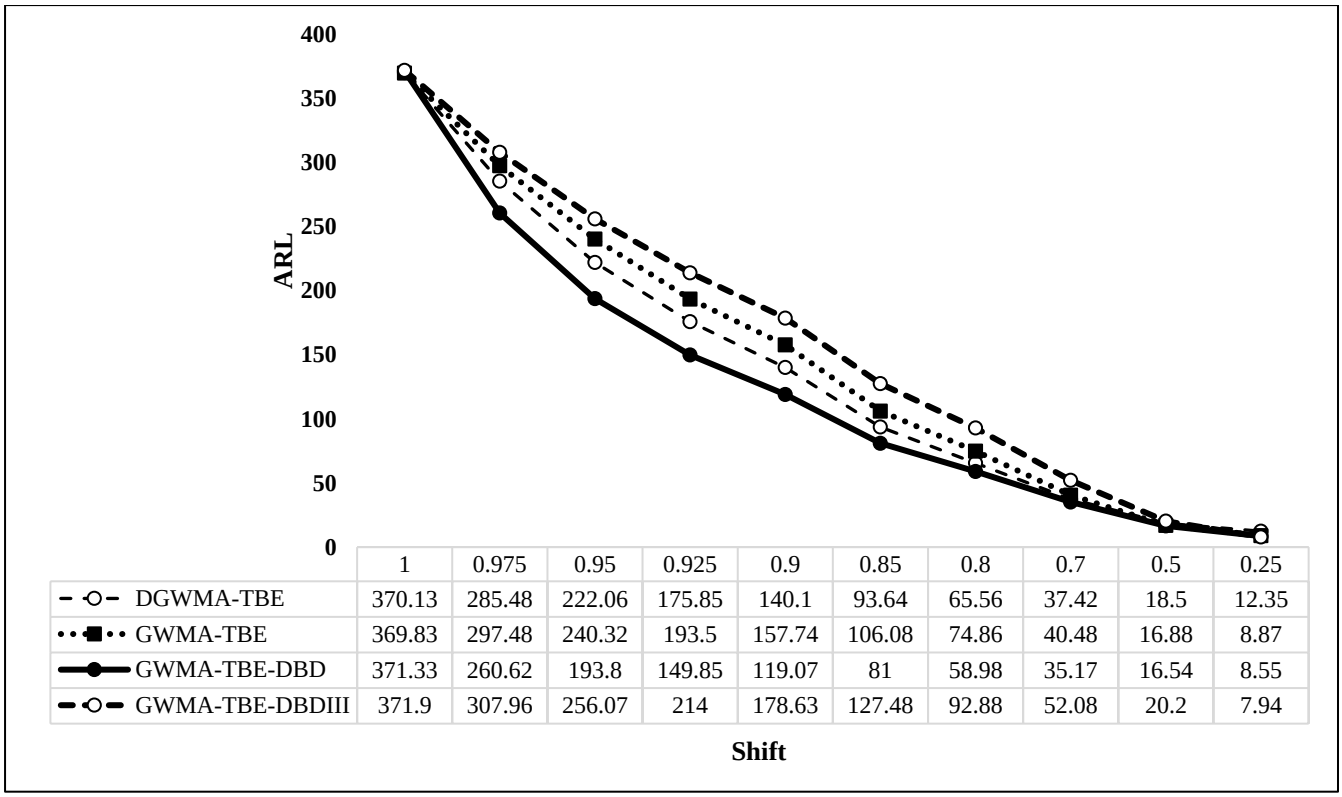

	1	0.975	0.95	0.925	0.9	0.85	0.8	0.7	0.5	0.25
DGWMA-TBE	370.13	285.48	222.06	175.85	140.1	93.64	65.56	37.42	18.5	12.35
GWMA-TBE	369.83	297.48	240.32	193.5	157.74	106.08	74.86	40.48	16.88	8.87
GWMA-TBE-DBD	371.33	260.62	193.8	149.85	119.07	81	58.98	35.17	16.54	8.55
GWMA-TBE-DBDIII	371.9	307.96	256.07	214	178.63	127.48	92.88	52.08	20.2	7.94

Figure 3.32. Comparative graph between the DGWMA-TBE and GWMA-TBE (under discrete Weibull distribution) and GWMA-TBE-DBD, and the GWMA-TBE-DBDIII (under discrete Burr distribution)

The chart parameters are selected as follows: $q = 0.9$ and $\alpha = 1.0$ for the DGWMA-TBE chart, $q_1 = 0.9$, $\alpha_1 = 1.0$ for the GWMA-TBE chart, $\varphi_1 = 0.9$, $\beta_1 = 1.0$ for the GWMA-TBE-DBD chart, and $\varphi_2 = 0.9$, $\beta_2 = 1.0$ for the GWMA-TBE-DBDIII chart. From the above plot one can conclude that the GWMA-TBE-DBD chart outperforms other time-weighted charts in detecting tiny shifts in the process and is competitive in detecting moderate to large shifts in the process. Also, the DGWMA-TBE chart outperforms the GWMA-TBE and the GWMA-TBE-DBDIII charts in detecting tiny shifts in the process.

3.13 Phase II DGWMA-TBE chart

Control chart process monitoring works under two different phases; Phase I (retrospective phase) and Phase II (prospective phase). Practitioners estimate the unknown parameters from the reference sample (calibration sample) that is time-ordered in Phase I. Then, the determination of the design parameter(s) and the assessment of a process's stability are considered in Phase I. Phase II focuses on the monitoring of the process using estimated control limits obtained from Phase I, which is known as Case U. For the

DGWMA-TBE chart, the point estimate of the scale parameter denoted by $\hat{\theta}$ is used to estimate the Phase II *LCL* denoted by $\widehat{LCL}$, and the starting value Z_0^2 that is equal to; $Z_0^2 = k\hat{\theta}$. Hence, for a one-sided DGWMA-TBE chart (Case U), the plotting statistic and estimated *LCL* are defined as:

$$\mathrm{Z_t^2} = \sum_{i=1}^{t} w_i \, \mathrm{X_{t-i+1}} + \left(1 - \sum_{i=1}^{t} w_i\right) k\hat{\theta}; \tag{3.25}$$

and:

$$\widehat{LCL} = k\hat{\theta} - L\sqrt{k\hat{\theta}^2 Q'}. \tag{3.26}$$

The process is declared OOC if a point falls on or below the $\widehat{LCL}$ defined in equation (3.26), which is an indication of the deterioration in the process.

For the retrospective phase, the main assumption is that an IC Phase I reference sample is available. An informative literature review on univariate control charts in Phase I is provided by Chakraborti et al. (2009). For the broader review on different types of Phase I charts, refer to the work of Jones-Farmer et al. (2014). To estimate the unknown value of the scale parameter θ, the MLE method is used. The IC Phase I reference sample is denoted as $X_1, X_2, \ldots, X_m \sim i.i.d\ Gamma\ (k.\theta)$. $m \geq 1$. Then, the MLE estimator for the unknown scale parameter is $\hat{\theta} = \sum_{i=1}^{m} X_i / km$, which follows a gamma distribution with the scale parameter of km and the shape parameter of $\frac{\theta}{km}$ denoted as $Gamma(km, \frac{\theta}{km})$. The estimated values of the IC parameters depend on the number of observations available for a Phase I analysis. Zhang et al. (2013) concluded that the size of the Phase I sample must often be quite large to be confident that the performance of the control chart will achieve the performance under the assumption of known IC parameters.

For the DGWMA-TBE control chart Case U, the starting value and the lower control limit are random variables. Hence, it is extremely important to evaluate the effects of parameter estimation on the Phase II run length distribution. This is a valid criteria robustness of the proposed DGWMA-TBE chart using the design parameters of Case K. The conditional Phase II run length is defined as the run length distribution conditional on a given point estimate $\hat{\theta}$, the performance is evaluated under a specific IC Phase I sample. Since Phase I's IC sample is different for each practitioner, the conditional performance does not provide suitable information on the overall performance of the chart. Hence, the unconditional run length distribution is considered to gain more insight about the effects of parameter estimation. The unconditional average run length is defined as:

$$UARL = E_{\hat{\theta}}\left(E\left(N\middle|\hat{\theta}\right)\right) = \int_0^{\infty} E\left(N\middle|\hat{\theta}\right) f\left(\hat{\theta}\right) d\hat{\theta}\ ; \tag{3.27}$$

where $E\left(N\middle|\hat{\theta}\right)$ denotes the conditional ARL given a point estimate $\hat{\theta}$, and $f\left(\hat{\theta}\right)$ denotes the distribution of estimated parameter $\hat{\theta}$.

3.13.1 Performance analysis

For the Phase II DGWMA-TBE chart, a simulation study is performed to calculate the IC and OOC ARL to test the validity of the design parameters obtained in Case K. The IC Phase I sample is generated from a gamma distribution with the shape parameter $k = 1, 2$, and the scale parameter $\theta = 1$. The values for the reference sample m are set as 50, 100, 500, 1000, and two sets of design parameters were considered:

a) $(k = 1, q = 0.95, \alpha = 0.5, L = 0.595)$
b) $(k = 2, q = 0.95, \alpha = 0.5, L = 0.608)$

The graphs for these sets of design parameters consist of a vertical axis that represent the ARL, and a horizontal axis that represent the magnitude of the shift (δ). The ARL values for Case K are compared with the ARL values obtained for Case U. These graphs are displayed in Figures 3.32 and 3.33 for the set of design parameters presented in a) and b), respectively.

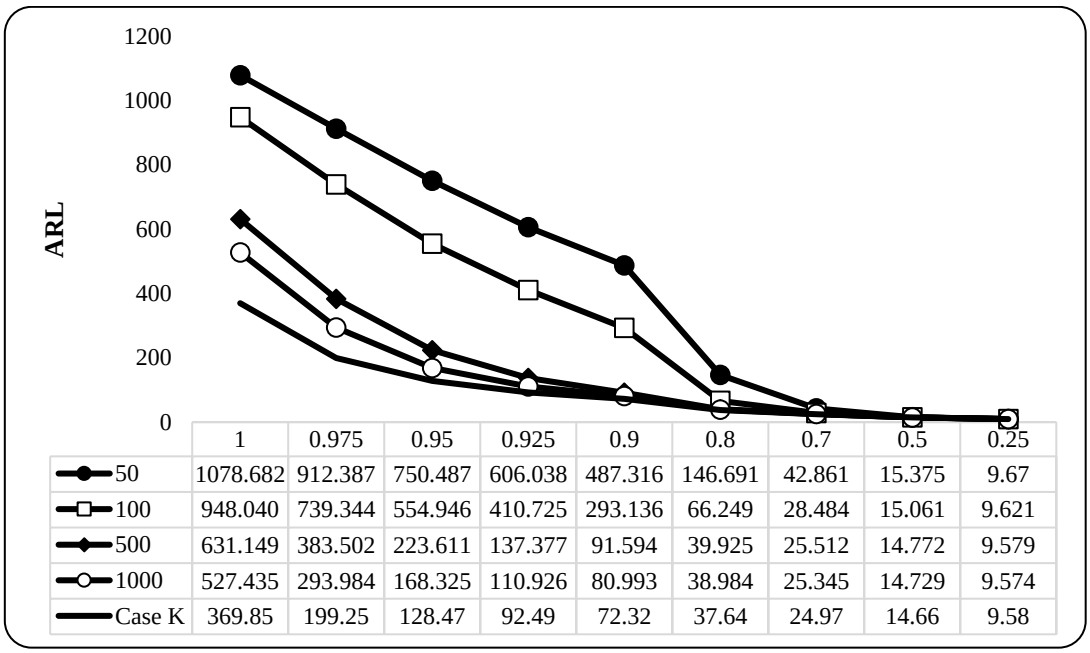

	1	0.975	0.95	0.925	0.9	0.8	0.7	0.5	0.25
50	1078.682	912.387	750.487	606.038	487.316	146.691	42.861	15.375	9.67
100	948.040	739.344	554.946	410.725	293.136	66.249	28.484	15.061	9.621
500	631.149	383.502	223.611	137.377	91.594	39.925	25.512	14.772	9.579
1000	527.435	293.984	168.325	110.926	80.993	38.984	25.345	14.729	9.574
Case K	369.85	199.25	128.47	92.49	72.32	37.64	24.97	14.66	9.58

Figure 3.33. ARL values for the Phase II DGWMA-TBE chart (Case U) for unknown θ when $k = 1$, $q = 0.95$, $\alpha = 0.5$, and $L = 0.595$

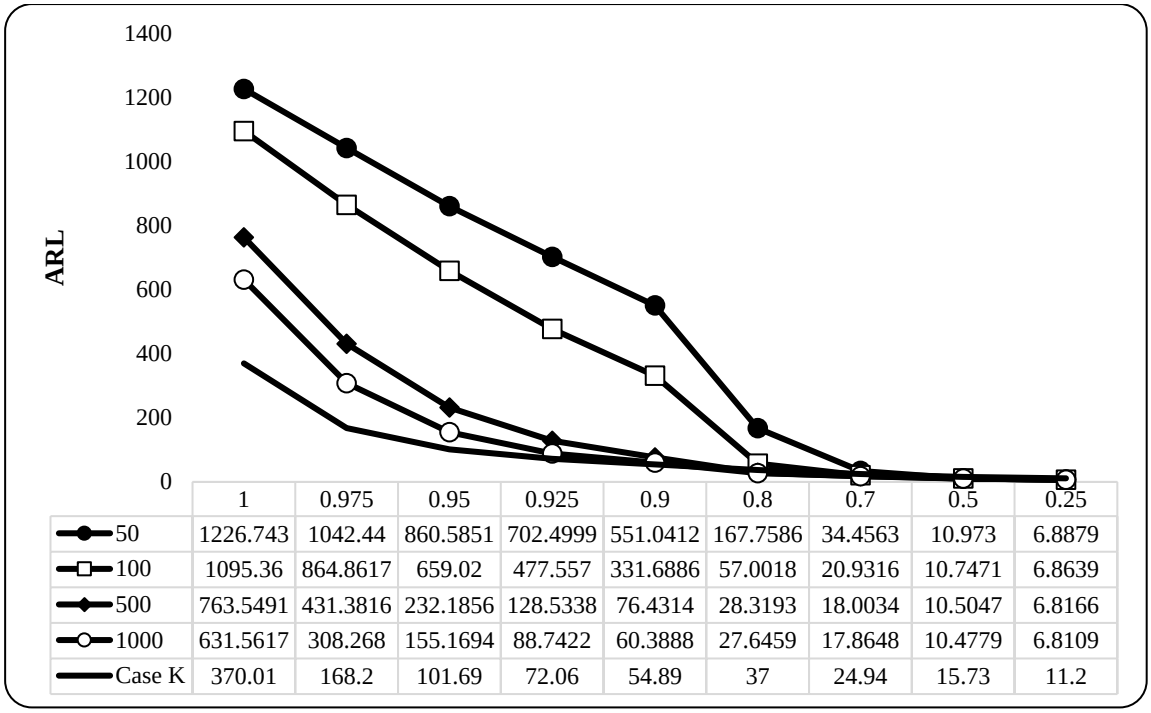

	1	0.975	0.95	0.925	0.9	0.8	0.7	0.5	0.25
50	1226.743	1042.44	860.5851	702.4999	551.0412	167.7586	34.4563	10.973	6.8879
100	1095.36	864.8617	659.02	477.557	331.6886	57.0018	20.9316	10.7471	6.8639
500	763.5491	431.3816	232.1856	128.5338	76.4314	28.3193	18.0034	10.5047	6.8166
1000	631.5617	308.268	155.1694	88.7422	60.3888	27.6459	17.8648	10.4779	6.8109
Case K	370.01	168.2	101.69	72.06	54.89	37	24.94	15.73	11.2

Figure 3.34. ARL values for the Phase II DGWMA-TBE chart (Case U) for unknown θ when $k = 2$, $q = 0.95$, $\alpha = 0.5$, and $L = 0.608$

The following is worth mentioning concerning the above figures:

i. For larger values of shifts ($\delta \leq 0.5$), the charts for Case K and Case U perform similarly. However, for other magnitude of shifts, the IC and OOC ARL in Case U are larger than the corresponding ARLs in Case K.

ii. In terms of the value for the reference sample m, to get a similar performance for Case U and Case K. more than 1.000 Phase I observations are required. Zhang et al. (2013) noted that since the event of interest is rare with the TBE data, the requirement for Phase II sample sizes can be prohibitively large.

3.13.2 The IC design

For the Phase II DGWMA-TBE chart, the IC design requires the implementation of equation (3.26) and the width of the $\widehat{LCL}$ so that the IC $UARL$ is equal to 370. For some combinations of (q, α), the value of the charting constant $(L > 0)$ is obtained by implementing a grid search technique that satisfies $\frac{1}{N}\sum_{j=1}^{N} E\left(N\middle|\hat{\theta}, IC\right) \approx 370$. Table 3.3, displays these values along with the value of L for Case K. It is observed that the value of L converges to the Case K value as the number of observations increases. The values for the parameters q and α are selected as $q = 0.5, 0.6, 0.7, 0.95$, $\alpha = 0.5, 0.6, 0.7, 0.8, 0.9, 1$ and 1.3, and the shape parameter is chosen as $k = 1, 2, 3$. The charting constant $(L > 0)$ for the

DGWMA-TBE chart and Case K are obtained from Tables A.3.8, A.3.9, and A.3.10 for $k = 1, 2, 3$, respectively.

Table 3.10. Design parameters for the Phase II DGWMA-TBE chart (Case 2) in Case U

			m				
k	q	α	50	100	500	1000	Case K
1	0.95	0.5	0.119	0.180	0.374	0.447	0.595
	0.95	0.8	0.118	0.326	0.806	0.920	1.037
	0.95	1	0.590	0.910	1.282	1.340	1.406
	0.6	1	1.743	1.770	1.802	1.808	1.813
	0.6	1.3	1.697	1.713	1.727	1.731	1.734
2	0.95	0.5	0.172	0.273	0.425	0.585	0.608
	0.95	0.8	0.025	0.100	0.640	0.820	1.041
	0.95	1	0.158	0.553	1.167	1.288	1.418
	0.7	0.9	1.708	1.852	1.997	2.017	2.041
	0.5	1.3	1.845	1.885	1.908	1.913	1.923
3	0.95	0.5	0.040	0.090	0.240	0.360	0.601
	0.95	0.6	0.015	0.045	0.190	0.300	0.623
	0.95	0.7	0.010	0.030	0.270	0.445	0.805
	0.6	0.9	1.810	1.945	2.080	2.097	2.121
	0.5	1.3	1.910	1.970	2.035	2.040	2.046

3.14 Phase II DEWMA-TBE chart

As discussed in the previous sections, the DEWMA-TBE chart, proposed and studied in this chapter, is known as the special case of the proposed DGWMA-TBE chart. Since this chart was constructed for both cases (Case 1 and Case 2) when the parameters of the underlying process distribution are known (Case K), there is a necessity to construct the DEWMA-TBE chart for Case U. In the current SPC literature, the majority of the researchers developed and proposed the DEWMA chart for Case K. However, in many practical situations, the parameters of interest are unknown, which emphasizes the important role of Case U charts. The procedure and general steps to obtain the design parameters for the DEWMA-TBE chart is exactly the same as the one explained in Section 3.11 for the DGWMA-TBE chart. Hence, only the design parameters for the DEWMA-TBE chart (Case 1 and Case 2) are presented in Tables 3.11 and 3.12.

Table 3.11. Design parameters for the Phase II DEWMA-TBE (Case 1) chart in Case U

					m				
k	q_1	q_2	α_1	α_2	50	100	500	1000	Case K
1	0.9	0.95	1.0	1.0	0.900	1.180	1.468	1.516	1.569
	0.8	0.95	1.0	1.0	1.120	1.363	1.602	1.642	1.687
	0.7	0.95	1.0	1.0	1.208	1.437	1.665	1.700	1.742
	0.6	0.95	1.0	1.0	1.262	1.480	1.700	1.735	1.776
	0.5	0.95	1.0	1.0	1.296	1.511	1.725	1.756	1.800
2	0.9	0.95	1.0	1.0	0.445	0.882	1.396	1.487	1.590
	0.8	0.95	1.0	1.0	0.710	1.118	1.563	1.638	1.729
	0.7	0.95	1.0	1.0	0.828	1.215	1.640	1.715	1.794
	0.6	0.95	1.0	1.0	0.900	1.272	1.688	1.755	1.835
	0.5	0.95	1.0	1.0	0.950	1.316	1.720	1.787	1.865
3	0.9	0.95	1.0	1.0	0.212	0.654	1.322	1.433	1.595
	0.8	0.95	1.0	1.0	0.448	0.908	1.500	1.600	1.735
	0.7	0.95	1.0	1.0	0.578	1.015	1.585	1.680	1.807
	0.6	0.95	1.0	1.0	0.652	1.084	1.640	1.730	1.852
	0.5	0.95	1.0	1.0	0.706	1.132	1.677	1.767	1.887

Table 3.12. Design parameters for the Phase II DEWMA-TBE chart (Case 2) in Case U

					m				
k	q_1	q_2	α_1	α_2	50	100	500	1000	Case K
1	0.5	0.5	1.0	1.0	1.678	1.696	1.712	1.714	1.719
	0.6	0.6	1.0	1.0	1.746	1.776	1.804	1.808	1.813
	0.7	0.7	1.0	1.0	1.761	1.809	1.858	1.865	1.871
	0.8	0.8	1.0	1.0	1.660	1.754	1.845	1.856	1.873
	0.95	0.95	1.0	1.0	0.592	0.918	1.283	1.336	1.405
2	0.5	0.5	1.0	1.0	1.852	1.908	1.952	1.957	1.965
	0.6	0.6	1.0	1.0	1.845	1.921	1.996	2.006	2.021
	0.7	0.7	1.0	1.0	1.760	1.883	1.998	2.015	2.032
	0.8	0.8	1.0	1.0	1.527	1.725	1.917	1.950	1.975
	0.95	0.95	1.0	1.0	0.148	0.553	1.165	1.280	1.418
3	0.5	0.5	1.0	1.0	1.894	1.975	2.058	2.068	2.078
	0.6	0.6	1.0	1.0	1.844	1.960	2.075	2.091	2.111
	0.7	0.7	1.0	1.0	1.695	1.870	2.044	2.068	2.100
	0.8	0.8	1.0	1.0	1.390	1.636	1.927	1.965	2.020
	0.95	0.95	1.0	1.0	0.043	0.324	1.076	1.215	1.417

3.15 Illustrative example

3.15.1 Simulated data

Zhang et al. (2007) simulated a dataset for a paper manufacturing process, where the defects in the formed paper are referred to high velocity and become unstable. The known value of the IC process failure rate of paper defects is maintained at $1/\theta_0$ = 1/5000 = 0.0002 ($X\sim$ Gamma$(k, 5000)$) defects per square meter. Fifty random observations were simulated from a Gamma$(k = 2, 4000)$

distribution, which is an OOC process following a shift of $\delta = 4000/5000 = 0.8$. This represents a deterioration in the process – i.e., the failure rate increases to 0.00025 defects per square meter. Since $k = 2$, the total time between two consecutive failures will be monitored. Two different sets of design parameters were used: ($q = 0.5$, $\alpha = 0.9$, $L = 1.975$) and ($q_1 = 0.5$, $q_2 = 0.0$, $\alpha_1 = 0.9$, $\alpha_2 = 1.0$, $L = 1.736$). The first set corresponds to a DGWMA-TBE chart, whereas the second one results in a GWMA-TBE chart. Note that any other combination of the design parameters can be chosen, but these values were selected only for illustrative purposes. The IC ARL (i.e., ARL_0) for both charts are approximately 370. From Table 3.12, it is observed that the DGWMA-TBE chart has an OOC ARL of 78.35; while from Table 3.17, it can be seen that the GWMA-TBE chart has an OOC ARL of 96.41. Therefore, the expectation is that the DGWMA-TBE chart will detect a shift in the process before the GWMA-TBE chart does. The LCLs are calculated using equation (3.7) and are equal to 0.854 and 0.607, respectively.

Figure 3.11 displays the DGWMA-TBE and GWMA-TBE charts. It is concluded that the DGWMA-TBE chart signals at time 22, whereas the GWMA-TBE chart signals at time 39.

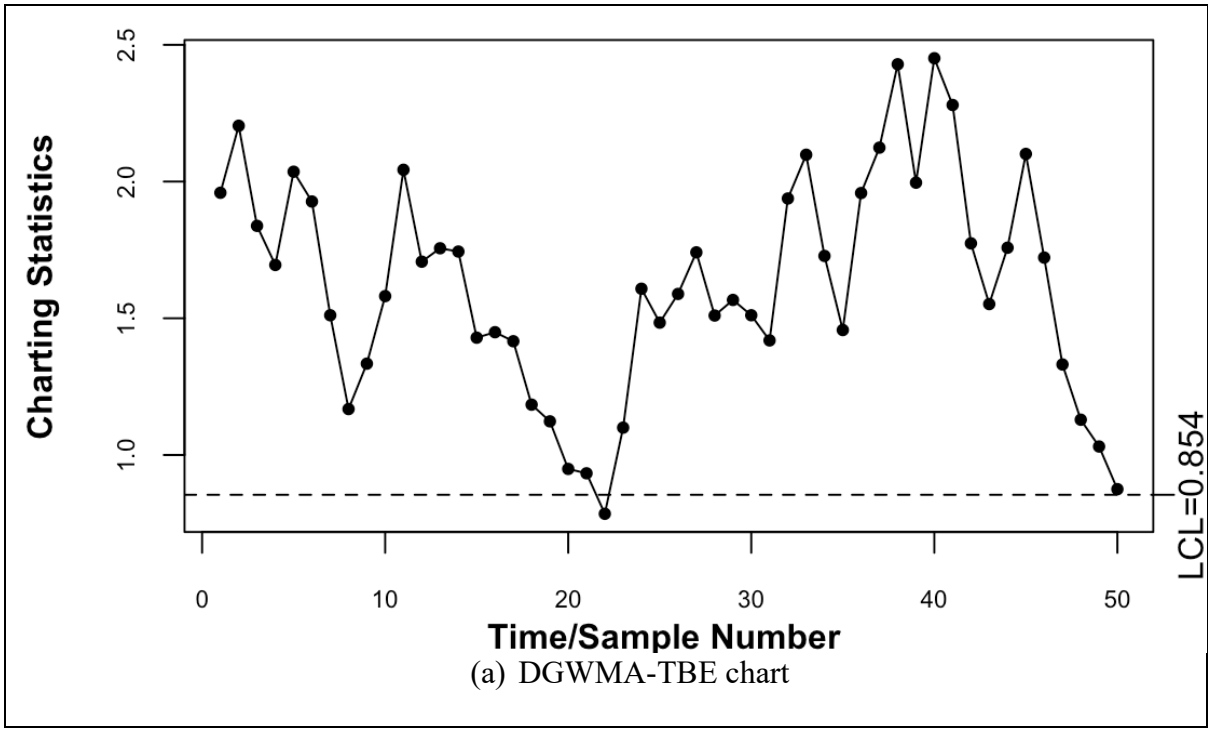

(a) DGWMA-TBE chart

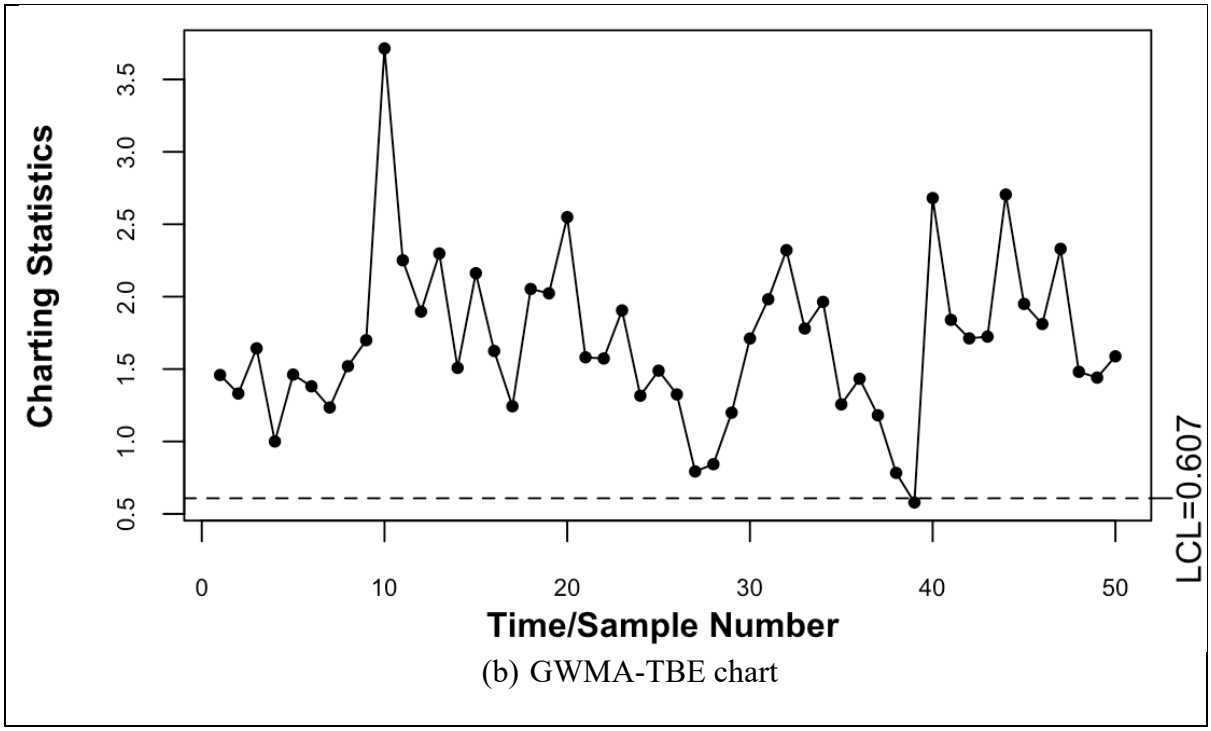

(b) GWMA-TBE chart

Figure 3.35. The DGWMA-TBE (a) and GWMA-TBE (b) charts for the simulated data

3.15.2 Real-life data

To illustrate the application and implementation of the proposed DGWMA-TBE chart in Phase II, a real data set on coal mining accidents is considered. The coal mining accidents data set in Jarrett (1979) is taken to show the construction of the proposed chart. The data set can be obtained from Maguire et al. (1952). The data consist of the time intervals in days between successive coal mining accidents (in days) which involve more than ten men were killed between in Great Britain. Yen et al. (2013) mentioned that the time between accidents has been shown to be exponentially distributed which is the special case of the gamma distribution. The data have been used extensively in the literature for the TBE data, see, for example, Barnard (1953), Cox and Lewis (1966), Jarrett (1979), Gan (1998), and Yang et al. (2016). The mean of the time between accidents is estimated based on the first 50 observations (like Gan (1998)) as 121.64. Thus, the estimated IC mean time between accidents is $\widehat{\theta_0} = 121.64$. The estimated lower control limits for the DGWMA-TBE and GWMA-TBE charts are calculated and are equal to 187.53 and 203.25, respectively. For observation number 51 to observation number 120, the estimated control limits obtained from Phase I sample are used to monitor the process in Phase II. Hence, the figures only include Phase II sample. In Figure 3.36, a process deterioration occurs at the 18^{th} sample number. The proposed DGWMA-TBE chart triggered the OOC shift at sample number 30, whereas for the GWMA-TBE chart the OOC point is detected at sample number 32.

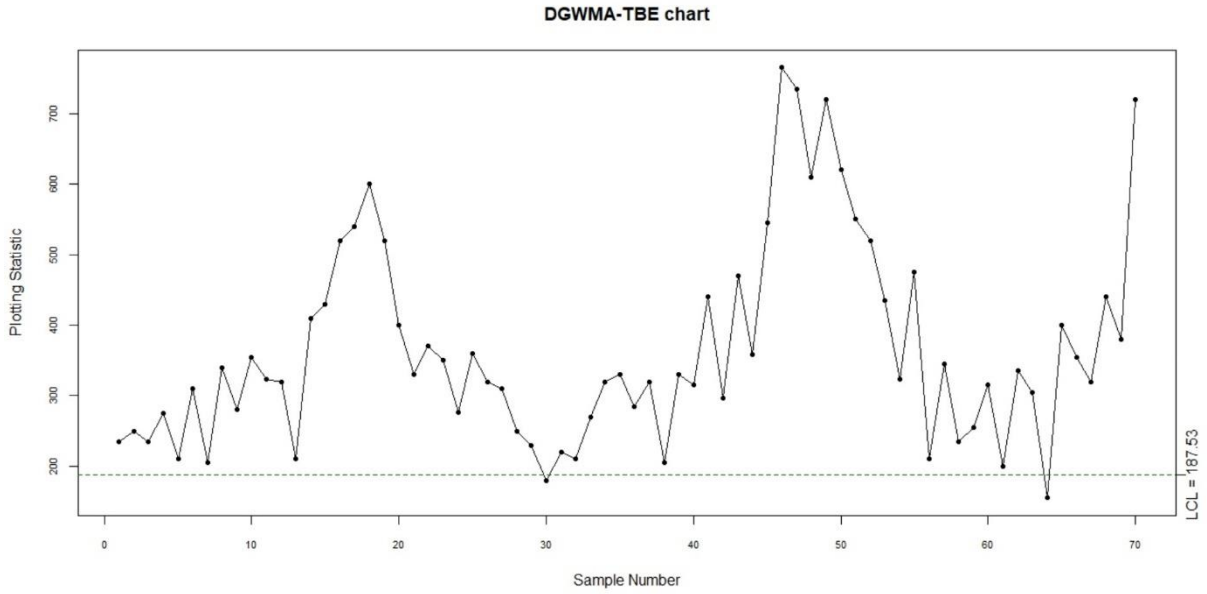

(a) DGWMA-TBE chart

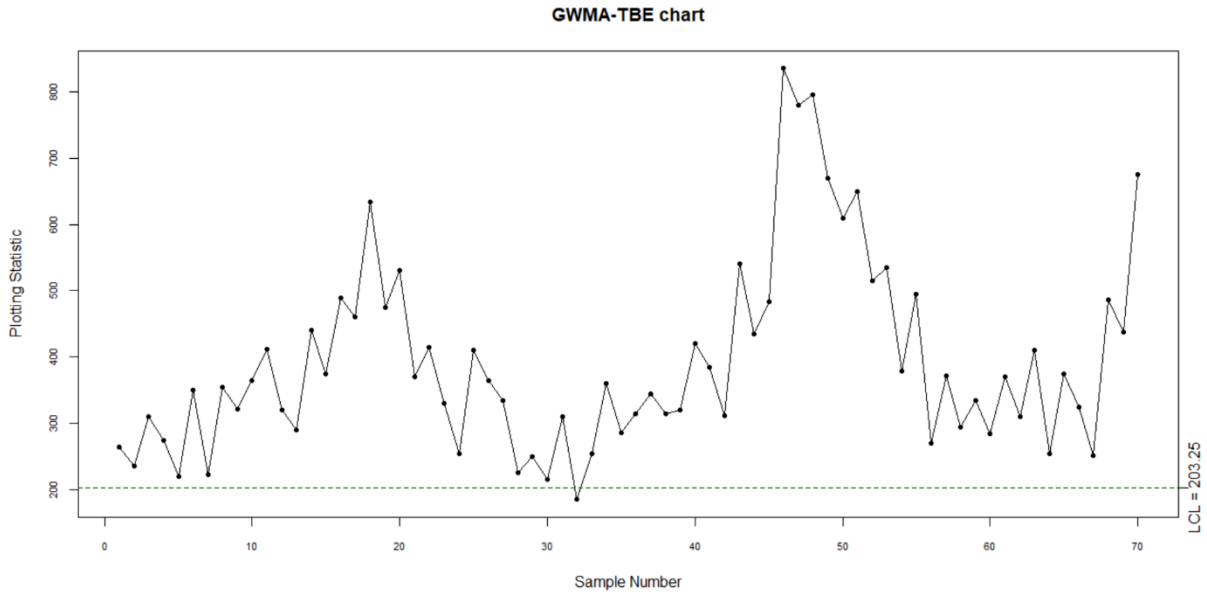

(b) GWMA-TBE chart

Figure 3.36. The DGWMA-TBE (a) and GWMA-TBE (b) charts for the coal mining accidents

3.16 Additional remarks

In this section, some additional remarks that have not been addressed in this chapter are discussed. The contamination for the DGWMA-TBE chart when the shift not occurred at the initial stage is addressed with a simulated example. Also, the performance of one-sided and two-sided DGWMA-TBE charts in terms of the biasdness term is addressed and the shortcomings and obstacles of two-sided DGWMA-TBE chart are outlined.

3.16.1 Contamination for the DGWMA-TBE

The ARL_1 values calculated based on the Monte Carlo simulation are called the zero-state *ARL's* and based on the assumption that the shift occurs at the start-up, i.e., at time $t = 1$. However, it is also of interest to observe whether a DGWMA-TBE chart deigned for optimal performance at start-up performs well for a shift that occurs later in the process, i.e., $t = 50, 100, 300$, etc. This is called the steady-state performance and the *ARL* is referred to as the steady-state *ARL*; the assumption is that a stable process has been operating IC for some time before the shift occurs. The steady-state *ARL* for some (q, α, L) combination when $k = 1,2$ is calculated and compared to the zero-state *ARL*. The results are provided in the following table:

Table 3.13. Zero-state versus steady-state for the DGWMA-TBE chart

					δ								
k	time of a shift	q	α	L	0.975	0.950	0.925	0.9	0.85	0.8	0.7	0.5	0.25
$k = 1$	t =1	0.95	0.9	1.243	263.62	193.61	148.74	116.94	79.12	58.30	37.85	23.49	17.13
	t = 50	0.95	0.9	1.243	266.06	195.72	151.34	120.66	82.75	62.32	41.76	25.73	16.92
	t =100	0.95	0.9	1.243	267.65	194.48	150.65	121.88	80.25	61.10	41.68	24.57	17.45
	t = 150	0.95	0.9	1.243	267.43	193.10	152.65	117.02	81.25	60.52	42.96	23.25	16.82
	t = 300	0.95	0.9	1.243	268.70	196.82	151.96	119.68	82.52	63.98	41.88	22.30	17.30
$k = 2$	t =1	0.95	0.9	1.250	232.53	156.89	113.35	86.60	56.71	41.86	27.87	18.16	13.54
	t = 50	0.95	0.9	1.250	229.88	158.80	116.62	87.65	55.65	43.82	30.80	20.03	14.76
	t =100	0.95	0.9	1.250	230.85	157.60	115.85	88.20	55.45	42.25	28.58	19.84	13.05
	t = 150	0.95	0.9	1.250	231.37	156.30	115.65	87.75	56.32	43.45	29.23	18.50	14.18
	t = 300	0.95	0.9	1.250	230.35	157.25	114.30	86.86	56.45	42.26	28.30	19.96	13.80

The zero-state and steady-state *ARL* are the same for all practical purposes. The minor difference that are observed in the above table are due to the inherent simulation variability. Hence, a DGWMA-TBE chart designed for optimal performance at start-up works well for a shift that occurs later in the process. Note that, the plotting statistics for the Shewhart-TBE chart are mutually independent, irrespective of the time the shift occurs, and hence, the time of shift can always be taken as $t = 1$ when calculating the ARL_1. Human (2009) stated that their proposed chart has a hitch at start-up and most likely give a

"delayed" or a "late" OOC signal instead. Since this glitch is possible, we need to stress an important assumption: the design and implementation of all the charts that are proposed in this chapter are based on an IC process at start-up. In other words, the process is IC at start-up; hence, we want to ensure that the process is IC before we start monitoring the process. To summarize the above discussion, we can state that:

i) The proposed DGWMA-TBE chart has a hitch at start-up but, since the OOC *ARL* values for the zero-state (shift occurs at time $t = 1$) are close to the OOC *ARL* values for the steady-state (shift occurs at the later stage, $t = 50, 100$, etc), the odds of a hitch at start-up are typically small as mentioned by Human (2009); this should be reassuring for the practitioner.

ii) The OOC *ARL* performance of the charts are almost identical and if a shift in the process occurs after start-up i.e., from time $t \geq 1$, both the charts i.e., the zero-state and steady-state can signal a shift/change in the process.

iii) We recommend that practitioners use either zero-state or steady-state charts, but we suggest that they familiarize themselves with the inherent risk associated with the selected chat. Based on the above discussion, it was decided to focus on the proposed DGWMA-TBE chart based on the zero-state *ARL*.

3.16.2 One-sided and two-sided DGWMA-TBE

A well-designed chart should ensure that the *ARL* curves reach their maximum or nominal values at their IC occurrence rates. In other words, the chart is set in such a way that the *ARL* curves attains a maximum in the IC situation, i.e., the chart is *ARL*-unbiased when the IC *ARL* (denoted by ARL_0) or attained *ARL* is equal to or close to a pre-specified or nominal value (denoted by ARL_0^*). The pre-specified value is typically selected as 370 or 500 in practice as recommended by several researchers, for example, Chakraborty et al. (2016) and the references therein.

In SPC, for some charts constructed based on symmetrically placed limits, their *ARL* curves will not reach their maximum values at their pre-specified value which is not desirable for any control chart. Using the parallel between a control chart and a hypothesis test, this corresponds to the case where the power of the corresponding test is smaller than the size of the test, which is undesirable. In the testing literature, such tests are called biased and such charts are called *ARL*-biased charts in the SPC literature.

The following table illustrates that, a two-sided DGWMA-TBE chart, for $\alpha = 1$ vs. $\alpha \neq 1$, encounters bias which puts a concern on their applicability for detecting small shifts in the process. It has been

observed in SPC that for heavy-tailed distribution, a two-sided chart encounters biasdness. Zhang et al. (2006) discussed the proof for a Shewhart-type charts under the exponential and the gamma distribution.

Note that the values inside the parentheses in the following table correspond to the following: q, α (DGWMA-TBE parameters) and $L > 0$ (charting constant), respectively. The values for the shift are selected as 0.2, 0.3, 0.5, 0.6, 0.7, 0.8, 0.9, 0.95, 0.975, 1.0, 1.025, 1.05, 1.1, 1.2, 1.3, 1.4 and 1.5. Note that when $\delta = 1$, the process declares to be IC. The results for the two-sided DGWMA-TBE chart are presented in the following table:

Table 3.14. ARL_1 values for the one-sided and two-sided DGWMA-TBE chart

$\delta = \frac{\theta_1}{\theta_0}$	DGWMA (0.95,0.7,1.397)	DGWMA (0.95,0.8,1.566)	DGWMA (0.95,1.856)
0.2	16.40	16.58	15.33
0.3	26.34	28.77	30.14
0.5	400.60	705.13	800.43
0.6	1563.39	1678.25	1753.80
0.7	1923.80	1940.43	1957.20
0.8	1640.91	1638.98	1652.56
0.9	988.78	987.65	1008.67
0.95	690.39	670.34	675.39
0.975	475.09	480.05	483.35
1.0	370.20	369.80	370.40
1.025	270.75	270.20	274.75
1.05	209.61	208.10	210.33
1.1	128.62	126.54	130.20
1.2	61.20	60.30	62.50
1.3	35.85	36.32	35.32
1.4	23.22	23.80	22.90
1.5	18.53	18.41	18.79

For the shift values in the following interval, $0.5 \leq \delta \leq 0.975$, the two-sided DGWMA-TBE chart is *ARL*-biased. Hence for a one-sided chart DGWMA-TBE chart developed in this chapter, an important characteristic is that unlike the two-sided DGWMA-TBE, the one-sided chart is an is *ARL*-unbiased chart. Note that, Chakraborty et al. (2016) and Chakraborti et al. (2009) concluded similar findings.

3.17 Concluding remarks

Advancements in technological tools available in the present information era led to so-called high-quality or high-yielded processes, where the number of detects are very small – i.e., one in a million or billion. The Shewhart-type attribute charts are effective in detecting large shifts in the process, but inefficient in detecting small shifts in the process. To overcome the drawback of these charts, a generalized time-weighted chart, which sequentially accumulates information from past to present to monitor the TBE data, is proposed. More precisely, a one-sided DGWMA-TBE chart is developed under the gamma distribution and is denoted by DGWMA-TBE. This chart includes a one-sided GWMA-TBE, a one-sided EWMA-TBE, and a one-sided Shewhart-type-TBE charts as limiting cases. Further to this, the special case of the proposed chart that is the DEWMA-TBE chart is also developed and studied. Two cases of the DEWMA-TBE chart depend on the equality and/or inequality of the smoothing parameters, namely as Case 1 (two smoothing parameters) and Case 2 (a single smoothing parameter) are considered in detail. Both cases of the DGWMA-TBE chart, which are based on four parameters (Case 1) and two parameters (Case 2), are investigated and the pros and cons for each are discussed in detail. A relationship graph is provided in Figure 3.1, for the different cases of the DGWMA-TBE and the DEWMA-TBE charts. Alternative discrete distributions are considered for the weights of the GWMA-TBE chart and the performance of the new constructed charts is compared with the DGWMA-TBE chart proposed in this chapter and the GWMA-TBE chart proposed by Chakraborty et al. (2016). The results confirm that one can design a time-weighted chart with different weighting distributions and without the implementation of the double exponential smoothing technique that is effective in detecting small shifts in the process. A detailed comparative study is conducted to measure the OOC performance of the proposed DGWMA-TBE chart (Case 1 and Case 2) and the DEWMA-TBE chart (Case 1 and Case 2) with their counterparts. Two cases exist in the context of the SPC literature dependent on the process parameters (known/unknown): Case K and Case U. In this chapter, both of these cases are developed and studied in detail for the DGWMA-TBE chart and its special case, the DEWMA-TBE chart. An extensive simulation study has been studied and the results reveal that the proposed DGWMA-TBE chart outperforms its counterparts in detecting small or tiny changes in the process.

Chapter 4 A Double Generally Weighted Moving Average Exceedance Control Chart

4.1 Introduction

The monitoring of the location and dispersion measures often presupposes that the underlying process probability distribution is known. Control charts are usually constructed under the assumption of a known (i.e., normal) distribution for the underlying process, which in various applications is unknown or no information available. Hence, the statistical properties of commonly used charts, designed to perform under a distribution assumption, could be highly affected.

Nonparametric control charts provide a robust alternative when there is lack of knowledge regarding the underlying process distribution. A chart is called distribution-free or nonparametric if its in-control (IC) run length distribution remains invariant for all continuous process distributions. However, in some cases, symmetry of the underlying process distribution is required for the chart to be nonparametric.

In numerous practical scenarios, the true process median (location parameter) is unknown (Case U), which limits the applicability of the proposed distribution-free charts based on the well-known nonparametric statistics (e.g., the sign and Wilcoxon signed-rank statistics). Exceedance (EX) or precedence tests, are well-known and the most commonly used nonparametric two-sample tests that do not suffer from these limits. Precedence statistics are defined as the number of observations from one of the samples that exceed a specified (r^{th}) order statistic of the other sample.

Relatively little work has been done on nonparametric schemes in the context of a DGWMA chart, featuring the work of Lu (2018) which is solely focused on Case K and the parameter of interest is the process proportion.

Motivated by these findings, a distribution-free (nonparametric) DGWMA chart based on an EXs for monitoring the unknown median of a process is constructed in this chapter. From the information available, it can be deduced that the proposed chart will be a pioneer work that investigates the performance of the DGWMA chart for Case U in the nonparametric context. This chart is referred to as the DGWMA exceedance (or DGWMA-EX) chart and integrates the virtues of both the GWMA and DEWMA charts, to achieve improved detection ability.

The proposed chart can be viewed as a generalized nonparametric time-weighted chart, such that the GWMA-EX, EWMA-EX, and Shewhart-EX charts are limiting cases. Further to this, the nonparametric DEWMA-EX chart, which is a special case of the DGWMA-EX chart, will be proposed and discussed in detail.

This chapter features a literature review on nonparametric charts for time-weighted charts in Section 4.2. Section 4.3 presents the rationale for constructing the DGWMA-EX chart and the methodologies used in the entire thesis are discussed in detail in Section 4.4. A discussion on precedence or EXs and some fundamental results related to the distribution of the EXs is provided in Section 4.5. Also, Section 4.5 provides the necessary theoretical framework for the DGWMA-EX chart. In Sections 4.6 and 4.7, two types of the DGWMA-EX chart and two types of the DEWMA-EX chart are discussed in detail, respectively. The run length distribution and its methods of calculation are discussed in Section 4.8 for the DGWMA-EX chart and its special case the DEWMA-EX chart. The design and implementation of the proposed chart, including the IC design and the OOC performance are discussed in Sections 4.9 and 4.10, respectively. A discussion with respect to the optimal design and the near optimal design of the DGWMA-EX chart is provided in Section 4.11. Two illustrative examples in the form of simulated data and real-life data are provided in Section 4.12.

4.2 Literature review

There are two major nonparametric statistics adopted in SPC literature. One is the Wilcoxon signed-rank statistic, and the other is the sign statistic. Nonparametric charts are based on either Wilcoxon signed-rank or rank-sum of the observations, such as Bakir (2004), Chakraborti and Eryilmaz (2007), Balakrishnan et al. (2009), Li et al. (2010), Graham et al. (2011) and Abid et al. (2016). Authors concluded that the charts perform well in detecting mean shifts and perform better than parametric counterparts when the underlying process distribution is not normal. The case of nonparametric charts based on the sign statistics include Amin et al. (1995), Amin and Widmaier (1999), Human et al. (2010) and Graham et al. (2010). These authors showed that the proposed sign chart has superior performance when the underlying process distribution is heavy-tailed or highly right skewed. Other recent research on nonparametric charts include, for example, Zhou et al. (2009) and Hawkins and Deng (2010) which developed the nonparametric change-point control charts that are capable of detecting changes in the distribution function that could be a result of changes in the location parameter or scale parameter or both, i.e., location-scale. Yang et al. (2011) established the nonparametric EWMA sign chart. Note that, in this section, only research articles related to nonparametric charts are discussed. For an overview of time-weighted charts and their weighting schemes, the reader is referred to the literature review provided in Section 1.3

Chakraborti et al. (2004) studied a class of nonparametric Phase II Shewhart-type charts based on the exceedance statistics, called the Shewhart-type exceedance charts. This paper is known as the pioneer work for several follow-up papers in this area. Mukherjee et al. (2013) developed a Phase II nonparametric CUSUM charts based on the exceedance statistics, called the exceedance CUSUM chart. Graham et al. (2012) proposed a two-sided nonparametric Phase II EWMA chart based on the exceedance statistics, denoted by EWMA-EX for detecting a shift in the location parameter of a continuous distribution. Recently, Chakraborty et al. (2018) proposed a nonparametric GWMA exceedance chart, referred to as the GWMA-EX chart, which outperforms the EWMA-EX chart in detecting small shifts in process parameters.

The Shewhart-type signed-rank charts were developed by Bakir (2004) as the pioneer work in the context of nonparametric SPC. For more details, refer to Chakraborti et al. (2001) and Bakir (2006). More recently, Lu (2015) and Chakraborty et al. (2016) proposed nonparametric GWMA charts based on the sign statistic (denoted by GWMA-SN) and the Wilcoxon signed-rank (denoted by GWMA-SR), respectively, for the case when the true process median is known (Case K). Lu (2018) developed a nonparametric DGWMA chart (denoted by DGWMA-SN) for when the true process proportion is known (Case K). A class of nonparametric Shewhart-type charts, referred to as Shewhart-type precedence charts, were studied by Graham et al. (2012). Graham et al. (2014) proposed a Phase II nonparametric CUSUM chart (denoted by NPCUSUM) based on exceedance statistic for monitoring the unknown location parameter (Case U). The proposed nonparametric chart is compared with the NPCUSUM-Rank chart proposed by Li et al. (2010) based on the Wilcoxon rank-sum statistic. The advantages of implementing CUSUM charts in practice is documented by Khoo and Teh (2009). Goel (2011) summarized the characteristics and fundamentals of nonparametric CUSUM charts. McDonald (1990) proposed a CUSUM chart for individual observations based on the sequential rank statistics. Jones et al. (2004) investigated the run length distribution of the CUSUM chart with estimated parameters (Case U). Chatterjee and Qiu (2009) developed NPCUSUM chart through control limits obtained from bootstrap method. Lie et al. (2013) proposed a NPCUSUM chart for unknown shifts in the process location parameter. Yang and Cheng (2011) proposed a NPCUSUM chart to monitor the process location parameter. For more information on nonparametric control charts, see the work of Chakraborti et al. (2011)

4.3 Motivation

Nonparametric methods have become a part of the toolkit for practitioners or researchers, it appears that this topic has not been fully embraced in the field of SPC for the DGWMA chart. To this end, Woodall and Montgomery (2014) mentioned that, “Despite their advantages in reducing the distributional assumptions required to design control charts with specified IC performance, it does not seem that nonparametric methods are gaining a foothold with practitioners. This could partially be due to a

lack of available statistical software for implementing the methods, a lack of familiarity, and a lack of textbook coverage. Nevertheless, this research is remaining active."

The exceedance or precedence test is a distribution-free (nonparametric) test based on one the number of observations from one of the samples exceeding or preceding a specified (r^{th}) order statistic of the other sample. Exceedance tests have been found to be useful in numerous applications including reliability analysis, quality control, amongst others. Balakrishnan and Ng (2006) noted that, "Under some positively skewed distributions such as the exponential distribution, gamma distribution, and lognormal distribution, the exceedance tests have higher power values than the Wilcoxon's rank-sum test for small values of r". The majority of research conducted in the SPC literature for nonparametric assumes that the parameters(s) of the underlying process distribution is (are) known (Case K) which is not applicable in numerous real-life applications.

Also, the process mean is assumed frequently in the context of nonparametric SPC as the location parameter of interest. A research question that might be raised is the applicability of the process mean when the parameter of interest is unknown and constructed based on the exceedance statistic. One of the factors that have an impact on the effectiveness of a chart is the type of the reference sample being considered. An optimal design of a control chart is an important concept by itself when it comes to the performance of time-weighted charts. A research question could be raised about the robustness of nonparametric charts under normal and skewed distributions

In the current SPC environment, for the DGWMA chart, the nonparametric chart is only available for Case K based on the sign test and to monitor the process proportion. In numerous practical scenarios, the true process parameter(s) is (are) unknown (Case U), which limits the applicability of the available nonparametric DGWMA chart in the SPC literature. Also, Chakraborti et al. (2011) mentioned that, "The median is a robust estimator of the location and is preferred in situations, where 'large' measurement errors are expected." It would therefore be beneficial and helpful for practitioners and researchers to know what the present state of the art with nonparametric DGWMA charts and what challenges is still remain.

Thus, motivated by such observations, the main objective has been to bring the DGWMA chart constructed under the nonparametric EX (denoted by DGWMA-EX) to the SPC development arena. The proposed nonparametric chart is a generalized time-weighted chart that includes the GWMA-EX and EWMA-EX charts as limiting cases, and the DEWMA-EX chart as a special case for Case U. This chart is useful since it combines the memory-saving (combination of the past and present information) property of the time-weighted charts with the robustness gained from nonparametric statistic to monitor the

process location parameter, i.e., process median. Also, we addressed the question of which reference sample order statistic should be chosen for the design and implementation of the DGWMA-EX chart.

4.4 Methodology

We use a Markov chain approach (see e.g., Fu and Lou, (2003)) to derive the run length distributions, average run lengths, etc. for our proposed DGWMA-EX and DEWMA-EX charts. This approach provides a more unified and compact view of the derivations. Balakrishnan and Koutras (2004) stated that, "The Markov techniques possess a great advantage (over the classical combinatory methods) as they are easily adjustable to many problems; they often simplify the solutions to specific problems they are applied on and remain valid even for cases involving non-identical or dependent trials".

We use a two-step approach to derive the run length distribution which involve the method of conditioning (see e.g., Chakraborti, (2000)). Firstly, the conditional run length distribution is derived and secondly, the unconditional run length distribution by averaging over the joint distribution is derived. The unconditional run length distribution reveals the overall performance of the chart and reflects the bigger picture.

There is a lack of proper guidance to the practitioner on the design and implementation of time-weighted charts and more specifically the DGWMA chart which is the core part of the current research. We consider monitoring the location parameter of a process in the nonparametric setting. The location parameter could be the mean or the median or some percentiles of the distribution. The performance of the proposed DGWMA-EX chart is investigated based on the 25^{th}, 50^{th} and 75^{th} percentiles. The median of the reference sample is chosen as a good representative of the reference data due to its robustness and applicability in practice.

The exact approach utilizes mathematical derivations and combinatorics to obtain a closed-form expression of the run length distribution. This approach is commonly dismissed in the literature since the process of obtaining expressions is cumbersome or difficult to be evaluated numerically.

The popularity of the Monte Carlo simulation stems from the fact that computer simulations can almost always be implemented to calculate the run length distribution fairly accurately, provided the simulation size is big enough. The run length distribution is significantly right skewed (see Barnard (1959)). Hence, the *MDRL* is a better alternative measure for the assessment of chart performance and will be considered as well in this chapter. For more information, the interested reader is referred to Khoo et al. (2011). However, the only practical disadvantage of using the *MDRL* is that finding the exact standard error is cumbersome which is out of scope of for the current thesis and can be considered as a topic for future research.

4.5 The DGWMA-EX chart

4.5.1 Assumptions

The exceedance test first proposed by Epstein (1954) for comparing two distributions based on exceedances. Nelson (1963) proposed the precedence test defined as a distribution-free test which enables a robust and simple comparison of two distribution functions.

A two-sample nonparametric test, known as the precedence or exceedance test, is defined as the number of observations from one of the samples exceeding or preceding a specified (r^{th}) order statistic of the other sample. The precedence probability is defined as the probability that an order statistic from the second sample exceeds an order statistic from the first sample.

Let $X_1, X_2, \dots, X_m \sim$i.i.d $F_X(x)$ denote a Phase I reference sample from an IC process with an unknown continuous c.d.f. $F_X(x)$, where $-\infty < \theta < \infty$ denotes the unknown location parameter. Let $Y_{i1}, Y_{i2}, \dots, Y_{in}$. $i = 1.2. \dots$ denote the i^{th} test sample in Phase II of size $n \geq 1$, with an unknown continuous c.d.f. $G_Y(x) = F_X(x - \theta)$. The main intention is to design a control chart for monitoring the unknown process location. The unknown/true value of the location parameter is denoted by θ_0 and the shifted location parameter is denoted by $\theta_1 = \theta_0 + \delta$, where $-\infty < \delta < \infty$ is the location shift. The process is declared to be IC when the unknown continuous c.d.f.'s F and G are equal (i.e., $G = F$ or $\delta = 0$), and OOC when $G \neq F$ or $\delta \neq 0$.

This chapter's main focus is on Phase II design and implementation of the DGWMA-EX control chart when the process parameter(s) is unknown. However, one can conduct research based on the steps and procedures involved in obtaining an IC Phase I reference sample, which is outside scope of this thesis. Consult the work by Chakraborti et al. (2008) for a detailed discussion on the design and implementation of Phase I charts.

Let U_{ir} denote the number of Y observations in the i^{th} Phase II sample that exceeds the r^{th} order statistic $X_{(r)}$, $r = 1,2\dots, m$ – i.e., from the Phase I sample of size $m \geq 1$. The statistic U_{ir} is called the EX, and the probability $p_r = P\left[Y \geq X_{(r)} \middle| X_{(r)}\right]$ is the exceedance probability. For inference purposes, the exceedance and precedence tests are equivalent in the sense that the two statistics are linearly related and so can be used interchangeably. Hereafter, U_i will be used to denote the EX for the i^{th} sample in Phase II. Fundamental results from Balakrishnan and Ng (2006) related to the distribution of the EXs are discussed next.

Result 4.1. The exceedance statistics U_i, $i = 1,2, \ldots$ are independent and identically distributed binomial random variables with parameters (n, p_r), where n is the sample size of Phase II and the probability is defined as $p_r = 1 - G\left(x_r \middle| X_{(r)} = x_r\right)$, where $G(.)$ is the c.d.f. of the test sample $(Y_{i1}, Y_{i2}, \ldots, Y_{in})$.

Proof:

Since every observation Y, in a test sample has two possible outcomes (smaller or larger than $X_{(r)}$), then the order statistic $X_{(r)}$ follows the properties of a Bernoulli trial. Note that for every Phase II sample, the number of observations – be it smaller or larger than the order statistic – are independent. Hence, the random variable U_i referring to the number of exceedances given by the number of observations in the i^{th} test sample that exceed $X_{(r)}$ follows a binomial distribution with parameters (n, p_r), given $X_{(r)}$, where the probability of success is $p_r = P\left[Y > X_{(r)} \middle| X_{(r)} = x_r\right] = 1 - G\left(x_r \middle| X_{(r)} = x_r\right)$.

Result 4.2. The unconditional IC distribution of exceedance statistics U_i, for all $i = 1, 2, \ldots$ is distribution-free and is given by the p.m.f. $P(U_i = u) = \frac{\binom{u+m-r}{u}\binom{n-u+r-1}{n-u}}{\binom{m+n}{n}}$, $u = 0,1,2, \ldots, n$.

Proof:

From Result 4.1., the probability of EX, U_i conditional on $X_{(r)}$ can be written as:

$$P\left[U_i = u \middle| X_{(r)} = x_r\right] = \binom{n}{u} p_r^u (1 - p_r)^{n-u} = \binom{n}{u} \left(1 - G(x_r)\right)^u G(x_r)^{n-u} \; ; u = 0,1,2, \ldots, n.$$

By implementing the unconditional method, the above probability can be written as:

$$P[U_i = u] = E_{X_{(r)}}\left(P\left[U_i = u \middle| X_{(r)} = x_r\right]\right)$$
$$= \int_{-\infty}^{\infty} \binom{n}{u} \left(1 - G(x_r)\right)^u G(x_r)^{n-u} \frac{m!}{(r-1)!(m-r)!} F(x_r)^{r-1} \left(1 - F(x_r)\right)^{m-r} f(x_r) dx_r \; ;$$

where $f(x_r)$ is the p.d.f. of the order statistic $X_{(r)}$.

When the process is IC, it implies that $G = F$. Therefore, the IC unconditional distribution of U_i is:

$$P[U_i = u] = \binom{n}{u} \frac{m!}{(r-1)!(m-r)!} \int_{-\infty}^{\infty} F(x_r)^{n-u+r-1} \left(1 - F(x_r)\right)^{m+u-r} f(x_r) dx_r$$
$$= \frac{n!}{u!\,(n-u)!} \frac{m!}{(r-1)!\,(m-r)!} \frac{(n-u+r-1)!\,(m+u-r)!}{(m+n)!}$$
$$= \frac{\binom{u+m-r}{u}\binom{n-u+r-1}{n-u}}{\binom{m+n}{n}}.$$

Result 4.3. The unconditional IC expectation of U_i is given by $E(U_i) = n\left(1 - \frac{r}{m+1}\right)$.

Proof:

By implementing unconditional method, the following is true:

$$E(U_i) = E_{X_{(r)}}\left(E\left(U_i|X_{(r)}\right)\right) = E_{X_{(r)}}\left[\sum_{u=0}^{n} P\left[U_i = u|X_{(r)}\right]\right]$$

If the process is IC, then $G = F$ – see Result 5.3. from Chakraborty et al. (2017). Thus:

$$E(U_i) = E_{X_{(r)}}\left(\sum_{u=0}^{n} u\binom{n}{u}\left(1-F(x_r)\right)^u F(x_r)^{n-u}\right) = nE_{X_{(r)}}\left(1-F\left(X_{(r)}\right)\right).$$

Then,

$$E_{X_{(r)}}\left(1-F\left(X_{(r)}\right)\right) = \int_{-\infty}^{\infty}\left(1-F(x_r)\right)\frac{m!}{(r-1)!(m-r)!}F(x_r)^{r-1}\left(1-F(x_r)\right)^{m-r}f(x_r)dx_r$$

$$= \frac{m!}{(r-1)!(m-r)!}\int_{-\infty}^{\infty}F(x_r)^{r-1}\left(1-F(x_r)\right)^{m-r+1}\ f(x_r)dx_r$$

By setting $v = F(x_r)$, and using the probability integral transformation technique:

$$E_{X_{(r)}}\left(1-F\left(X_{(r)}\right)\right) = \frac{m!}{(r-1)!(m-r)!}\int_{-\infty}^{\infty} v^{r-1}(1-v)^{m-r+1}\ dv = \frac{m-r+1}{m+1}.$$

Hence, the unconditional IC expectation is:

$$E(U_i) = nE_{X_{(r)}}\left(1-F\left(X_{(r)}\right)\right) = n\left(1-\frac{r}{m+1}\right).$$

Result 4.4. The unconditional IC variance of the exceedance U_i is given by $var(U_i) = \frac{nr(m-r+1)(m+n+1)}{(m+1)^2(m+2)}$.

Proof:

The unconditional IC variance of U_i is defined as:

$$var(U_i) = var_{X_{(r)}}(E(U_i|\,X_{(r)})) + E_{X_{(r)}}(var(U_i|\,X_{(r)})) \qquad \text{(i)}$$

Since $U_{ir}|X_{(r)} \sim$ Bin $(n.p_r)$, the conditional expectation and variance of U_{ir} are:

$$E(U_i|\,X_{(r)}) = n\left(1-F(x_r)\right) \quad \text{and} \quad var(U_i|\,X_{(r)}) = nF(x_r)\left(1-F(x_r)\right).$$

Hence,

$$var_{X_{(r)}}(E(U_i|\,X_{(r)})) = n^2 Var_{X_{(r)}}\left(1-F(x_r)\right).$$

The next step is to find an expression for $var_{X_{(r)}}\left(1-F(x_r)\right) = E_{X_{(r)}}\left(1-F(x_r)\right)^2 - E^2_{X_{(r)}}\left(1-F(x_r)\right)$.

Firstly,

$$E_{X_{(r)}}\left(1-F(x_r)\right)^2 = \int_{-\infty}^{\infty}\left(1-F(x_r)\right)^2\frac{m!}{(r-1)!(m-r)!}F(x_r)^{r-1}\left(1-F(x_r)\right)^{m-r}f(x_r)\,dx_r$$

$$= \frac{m!}{(r-1)!\,(m-r)!}\int_{-\infty}^{\infty} F(x_r)^{r-1}\big(1-F(x_r)\big)^{m-r+2} f(x_r)\,dx_r.$$

By setting $v = F(x_r)$, and implementing the probability integral transformation technique:

$$E_{X_{(r)}}\big(1-F(x_r)\big)^2 = \frac{m!}{(r-1)!\,(m-r)!}\int_{-\infty}^{\infty} v^{r-1}(1-v)^{m-r+2}\,dv.$$

Therefore,

$E_{X_{(r)}}\big(1-F(x_r)\big)^2 = \frac{(m-r+2)(m-r+1)}{(m+2)(m+1)}$.

The expression for $E_{X_{(r)}}\big(1-F(x_r)\big) = \frac{m-r+1}{m+1}$, (see Result 4.3).

Thus,

$var_{X_{(r)}}\big(1-F(x_r)\big) = \frac{(m-r+2)(m-r+1)}{(m+2)(m+1)} - \left(\frac{m-r+1}{m+1}\right)^2 = \frac{r(m-r+1)}{(m+1)^2(m+2)}$.

Then.

$$var_{X_{(r)}}(E(U_i|\,X_{(r)})) = n^2 var_{X_{(r)}}\big(1-F(x_r)\big) = \frac{n^2 r(m-r+1)}{(m+1)^2(m+2}. \qquad \text{(ii)}$$

The next step is to calculate the second expression in equation (i) as follows:

$$E_{X_{(r)}}(var(U_i|\,X_{(r)})) = n\,E_{X_{(r)}}\Big(F\big(X_{(r)}\big)\big(1-F\big(X_{(r)}\big)\big)\Big).$$

As a result,

$$E_{X_{(r)}}\Big(F\big(X_{(r)}\big)\big(1-F\big(X_{(r)}\big)\big)\Big)$$
$$= \int_{-\infty}^{\infty} F\big(X_{(r)}\big)\big(1-F\big(X_{(r)}\big)\big)\frac{m!}{(r-1)!\,(m-r)!}F(x_r)^{r-1}\big(1-F(x_r)\big)^{m-r} f(x_r)\,dx_r$$
$$= \frac{m!}{(r-1)!\,(m-r)!}\int_{-\infty}^{\infty} F(x_r)^{r-1}\big(1-F(x_r)\big)^{m-r+1} f(x_r)\,dx_r$$
$$= \frac{r(m-r+1)}{(m+2)(m+1)}.$$

Therefore,

$$E_{X_{(r)}}(var(U_i|\,X_{(r)})) = nE_{X_{(r)}}\Big(F\big(X_{(r)}\big)\big(1-F\big(X_{(r)}\big)\big)\Big) = \frac{nr(m-r+1)}{(m+2)(m+1)}. \qquad \text{(iii)}$$

When substituting equations (ii) and (iii) in equation (i), then:

$$var(U_i) = var_{X_{(r)}}(E(U_i|\,X_{(r)})) + E_{X_{(r)}}(var(U_i|\,X_{(r)})) = \frac{n^2 r(m-r+1)}{(m+1)^2(m+2} + \frac{nr(m-r+1)}{(m+2)(m+1)} =$$

$\frac{nr(m-r+1)(m+n+1)}{(m+1)^2(m+2)}$.

Chakraborty et al. (2017) (Results 5.2 and 5.3) concluded that the joint and marginal p.m.f. for the t number of EXs – i.e., $(U_1, U_2, \dots, U_t)$ – are free from the underlying c.d.f. $F(x)$ when the process is IC. These results showed that the control chart based on the EX U_i is distribution-free when the process is IC. An important property of a control chart is its IC robustness, which means that the EX U_i is distribution-free when the process is IC. In the next section, the DGWMA-EX plotting statistic constructed under the EXs and the control limits are defined.

4.5.2 Plotting statistic

The DGWMA-EX plotting statistic is defined as:

$$Z_t^2 = \sum_{i=1}^{t} w_i\, U_{t-i+1} + \left(1 - \sum_{i=1}^{t} w_i\right) Z_0^2 \quad \text{for} \quad t = 1.2.\dots ; \tag{4.1}$$

where $Z_0^2 = E(U_i)$ is the unconditional IC expectation of U_i given by $Z_0^2 = n\left(1 - \frac{r}{m+1}\right)$. To calculate the conditional expectation and variance of the sample statistic U_i, the information regarding the underlying process distribution is required. Therefore, the unconditional IC expectation and variance of the plotting statistic Z_t^2 will be derived first, and thereafter can then be used to determine the control limits of the proposed DGWMA-EX chart.

The unconditional IC expectation of the plotting statistic Z_t^2 can be derived as:

$$E(Z_t^2) = E_{X_{(r)}}\left(E\left(Z_t^2 \middle| X_{(r)}\right)\right) = \sum_{i=1}^{t} w_i\, E_{X_{(r)}}\left(E\left(\left(U_{t-i+1} \middle| X_{(r)}\right)\right)\right) + \left(1 - \sum_{i=1}^{t} w_i\right) n\left(1 - \frac{r}{m+1}\right).$$

Hence.

$$E(Z_t^2) = n\left(1 - \frac{r}{m+1}\right). \tag{4.2}$$

The unconditional IC variance of Z_t^2 is obtained as follows:

$$var(Z_t^2) = var_{X_{(r)}}\left(E\left(Z_t^2 \middle| X_{(r)}\right)\right) + E_{X_{(r)}}\left(var\left(Z_t^2 \middle| X_{(r)}\right)\right).$$

Then,

$$E\left(Z_t^2 \middle| X_{(r)}\right) = \sum_{i=1}^{t} w_i\, E\left(U_{t-i+1} \middle| X_{(r)}\right) + \left(1 - \sum_{i=1}^{t} w_i\right) n\left(1 - \frac{r}{m+1}\right).$$

Hence,

$$var_{X_{(r)}}\left(E\left(Z_t^2 \middle| X_{(r)}\right)\right) = \left(\sum_{i=1}^{t} w_i^2\right) var_{X_{(r)}}\left(E\left(U_{t-i+1} \middle| X_{(r)}\right)\right) = \sum_{i=1}^{t} w_i^2\, \frac{n^2 r(m-r+1)}{(m+1)^2(m+2)}.$$

After this,

$$var\left(Z_t^2 \middle| X_{(r)}\right) = \sum_{i=1}^{t} w_i^2\, var\left(U_{t-i+1} \middle| X_{(r)}\right)$$

and,

$$E_{X_{(r)}}\left(var\left(Z_t^2|X_{(r)}\right)\right) = \sum_{i=1}^{t} w_i^2\, E_{X_{(r)}}\left(var\left(U_{t-i+1}|X_{(r)}\right)\right) = \sum_{i=1}^{t} w_i^2\, \frac{nr(m-r+1)}{(m+2)(m+1)}$$

Therefore, the unconditional IC variance of Z_t^2 is:

$$var(Z_t^2) = \frac{n\left(\frac{r}{m+1}\right)\left(1-\frac{r}{m+1}\right)}{m+2} \sum_{i=1}^{t} w_i^2\,(n+m+1).$$

4.5.3 Control limits

4.5.3.1 Exact control limits

The exact time-varying, symmetrically placed, control limits (denoted by UCL_e and LCL_e) of the two-sided DGWMA-EX chart are given by:

$$LCL_e = n\left(1-\frac{r}{m+1}\right) - L\sqrt{\frac{n\left(\frac{r}{m+1}\right)\left(1-\frac{r}{m+1}\right)}{m+2} \sum_{i=1}^{t} w_i^2\,(n+m+1)}$$

$$UCL_e = n\left(1-\frac{r}{m+1}\right) + L\sqrt{\frac{n\left(\frac{r}{m+1}\right)\left(1-\frac{r}{m+1}\right)}{m+2} \sum_{i=1}^{t} w_i^2\,(n+m+1)}\,; \tag{4.3}$$

where $L > 0$ is the distance of the control limits from the centerline, and the subscript "*e*" denotes the exact control limits.

4.5.3.2 Steady-state control limits

The steady-state control limits, which are based on the asymptotic unconditional variance of the plotting statistic, are given by:

$$LCL_s = n\left(1-\frac{r}{m+1}\right) - L\sqrt{\frac{n\left(\frac{r}{m+1}\right)\left(1-\frac{r}{m+1}\right)}{m+2} Q'(n+m+1)} \tag{4.4}$$

$$UCL_s = n\left(1-\frac{r}{m+1}\right) + L\sqrt{\frac{n\left(\frac{r}{m+1}\right)\left(1-\frac{r}{m+1}\right)}{m+2} Q'(n+m+1)}\,,$$

with centerline $CL = n\left(1-\frac{r}{m+1}\right)$, where the subscript "s" denotes the steady-state control limits, and $Q' = \lim_{t\to\infty} \sum_{i=1}^{t} w_i^2$.

The following points are worth mentioning:

i. The main focus of this chapter is to construct a DGWMA-EX chart with control limits equidistance from the centerline. A one-sided chart can also be designed, depending on the purpose or application.

ii. Steady-state control limits are used to simplify the application and implementation of the DGWMA-EX chart. For a discussion on the preference of control limit use (exact versus steady-state), refer to Chapter 2. Hereafter, *LCL* and *UCL* are used to denote the steady-state control limits defined in equation (4.4).

iii. If any plotting statistic Z_t^2 plots on or outside either of the control limits (steady-state) given in equation (4.4), the process is declared OOC and a search for assignable causes is started. Otherwise, the process is considered to be IC, which implies no location shift has occurred.

4.6 Two types of the DGWMA-EX chart

In Section 2.4, two different types of DGWMA chart have been discussed in detail. For the proposed nonparametric DGWMA-EX chart and based on the number of parameters involved, the chart can be classified as Case 1 (denoted by *DGWMA-EX* $(q_1, q_2, \alpha_1, \alpha_2)$), and Case 2 (*DGWMA-EX* (q, α)). The only nonparametric DGWMA chart currently available in the SPC literature has been introduced and studied by Lu (2018) for the process proportion. This thesis also investigates Case 1 of the proposed DGWMA-EX chart, where all four parameters are involved, and a performance comparison will be conducted to evaluate the aforementioned case with DGWMA-EX (Case 2) and other time-weighted counterparts. More details on the design and implementation as well as the OOC performance are provided in the forthcoming sections.

The relationship between the DGWMA-EX chart and its special case, the DEWMA-EX chart is illustrated in Figure 4.1. Further, the connection between different cases of these charts are also presented.

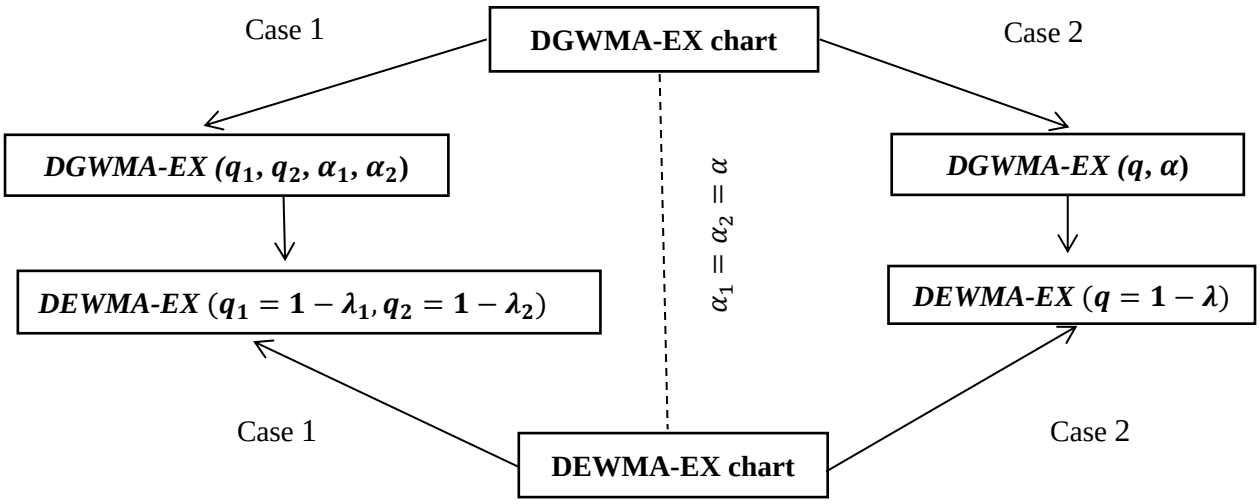

Figure 4.1. Relationship between the DGWMA-EX and the DEWMA-EX charts

The DEWMA-EX chart, a special case of the DGWMA-EX chart, is discussed in the ensuing section in more detail. The main difference between the DGWMA-EX and DEWMA-EX charts is the assumptions made for the chart parameters, i.e., q_1, q_2, α_1, α_2.

4.7 DEWMA-EX chart as special case

In Section 2.4, the special and limiting cases of the DGWMA chart were discussed in detail. The GWMA-EX and EWMA-EX charts are the limiting cases of the proposed DGWMA-EX chart, which are currently available and developed in the SPC literature. The special case of the DGWMA-EX chart – that is, the DEWMA-EX chart (Case 1 and Case 2) – is also introduced in this thesis. These two cases for the nonparametric DEWMA-EX chart are based on the inequality and/or equality of the smoothing parameters and are denoted as *DEWMA-EX* ($\lambda_1 = 1 - q_1$, $\lambda_2 = 1 - q_2$) for Case 1, and *DEWMA-EX* ($\lambda = 1 - q$) for Case 2. For the parametric DEWMA chart (Case K), Zhang and Chen (2005) concluded that the DEWMA chart with equal (or a single) smoothing parameters performs similarly to the DEWMA chart with different (or two) smoothing parameters. However, there is no research currently available in SPC that evaluates the performance of these two cases in the nonparametric paradigm and when the location parameter – i.e., median – is unknown (Case U). Hence, one of the contributions of this chapter and thesis is to study and investigate the behavior of the DEWMA-EX chart and provide the necessary recommendations for practitioners. These results are presented concurrently with the results for the DEWMA-EX chart in the following sections.

4.8 Run length distribution

The design of the DGWMA-EX chart typically involved the calculation of the chart parameters $(q_1, q_2, \alpha_1, \alpha_2, L)$ to obtain a pre-specified *ARL* (denoted by ARL_0^*) – i.e., one wants to solve for the values $q_1, q_2, \alpha_1, \alpha_2$ and L, such that $ARL_0 \approx ARL_0^*$. For the DGWMA-EX chart, since $X_{(r)}$ is a random variable, the computation of the run length distribution is not straightforward in comparison with the DGWMA-TBE chart proposed in Chapter 3. The first step is to calculate the conditional run length distribution, given the order statistic $X_{(r)}$, and after that by unconditioning over the order statistic (i.e., $X_{(r)}$), the run length distribution is obtained. Three standard methods to calculate the run length distribution of the proposed DGWMA-EX chart are discussed next.

4.8.1 Exact approach

The notation for the run length random variable is redefined in this section to distinguish between the test sample size n, and the run length, which were defined as N in the previous chapters. The run length random variable is defined as K for the rest of this chapter. Suppose that the signaling event at the i^{th} sample is denoted by A_i. For $\forall i \geq 1$, the event $A_i^C = [LCL < Z_i^2 < UCL]$ can be rewritten as $A_i^C = [LC_i < U_i < UC_i]$.

$$\begin{cases} UC_i = \dfrac{UCL - \sum_{j=2}^{i} w_j U_{i-j+1} - \left(1 - \sum_{j=1}^{i} w_j\right) n\left(1 - \dfrac{r}{m+1}\right)}{(1-q_1)(1-q_2)} \\ LC_i = \dfrac{LCL - \sum_{j=2}^{i} w_j U_{i-j+1} - \left(1 - \sum_{j=1}^{i} w_j\right) n\left(1 - \dfrac{r}{m+1}\right)}{(1-q_1)(1-q_2)} \end{cases}; \quad (4.5)$$

where $UC_1 = \frac{UCL-(1-w_1)n(1-\frac{r}{m+1})}{(1-q_1)(1-q_2)}$. $LC_1 = \frac{LCL-(1-w_1)n(1-\frac{r}{m+1})}{(1-q_1)(1-q_2)}$, and UCL and LCL are the steady-state control limits defined in equation (4.4).

The advantage of writing A_i^C (i.e., the nonsignaling event) in terms of the nonparametric EX statistic (i.e., $A_i^C = [LC_i < U_i < UC_i]$) is that the joint distribution of a sequence of sample statistics U_i are $U_i \sim i.i.d\ Bin\ (n, p_r)$, given the r^{th} order statistic ($X_{(r)}$), where n is the sample size, and the probability is defined as $p_r = 1 - G\left(x_r \middle| X_{(r)} = x_r\right)$. Hence, in comparison with the joint distribution of a sequence of plotting statistics Z_t^2, which is based on the dependency of the plotting statistic, the joint distribution of the sample statistics is preferred.

The run length is defined as $P[K = k] = E_{X_{(r)}}\left(P\left[K = k \middle| X_{(r)}\right]\right)$, hence the first step is to obtain an expression for $P\left[K = k \middle| X_{(r)}\right]$.

The following expressions are valid from Chapter 2 (see equations (2.22) and (2.24)):

$$P\left[K = 1 \middle| X_{(r)}\right] = P[\,A_1] = 1 - I_1$$

$$P\left[K = k \middle| X_{(r)}\right] = I_{k-1} - I_k \quad \text{for } k = 2,3,\ldots \quad (4.6)$$

Since the sample statistic U_i is $U_i \sim i.i.d\ Bin\ (n, p_r))$ given $X_{(r)}$, then I_k can be written as:

$$I_k = \sum_{LC_1}^{UC_1} \sum_{LC_2}^{UC_2} \ldots \sum_{LC_k}^{UC_k} \left(\prod_{i=1}^{k} P[U_i = u_i \,|\, X_{(r)}]\right); \quad (4.7)$$

where $P\left[U_i = u_i \middle| X_{(r)}\right]$ is given in Result 4.1. Thus, the conditional ARL is $ARL|X_{(r)} = 1 + \sum_{k=1}^{\infty} I_k$. The final step is to obtain an expression for the unconditional ARL as follows:

$$ARL = E_{X_{(r)}}\left(ARL \middle| X_{(r)}\right) = 1 + \sum_{k=1}^{\infty} E_{X_{(r)}}(I_k). \quad (4.8)$$

$E_{X_{(r)}}(I_k)$ is obtained by using equation (4.7) as follows:

$$E_{X_{(r)}}(I_k) = \sum_{LC_1}^{UC_1}\sum_{LC_2}^{UC_2}\dots\sum_{LC_k}^{UC_k}\left(\prod_{i=1}^{k} E_{X_{(r)}}\left(P\left[U_i = u_i \middle| X_{(r)}\right]\right)\right)$$
$$= \sum_{LC_1}^{UC_1}\sum_{LC_2}^{UC_2}\dots\sum_{LC_k}^{UC_k}\left(\prod_{i=1}^{k}\left(P[U_i = u_i]\right)\right). \quad (4.9)$$

By implementing Result 4.2, equation (4.9) can be re-written as:

$$E_{X_{(r)}}(I_k) = \sum_{LC_1}^{UC_1}\sum_{LC_2}^{UC_2}\dots\sum_{LC_k}^{UC_k}\left(\prod_{i=1}^{k}\left(\frac{\binom{u_i+m-k}{u_i}\binom{n-u_i+k-1}{n-u_i}}{\binom{m+n}{n}}\right)\right). \quad (4.10)$$

Finally, the closed-form expression of the unconditional *ARL* is:

$$ARL = 1 + \sum_{k=1}^{\infty}\sum_{LC_1}^{UC_1}\sum_{LC_2}^{UC_2}\dots\sum_{LC_k}^{UC_k}\left(\prod_{i=1}^{k}\left(\frac{\binom{u_i+m-k}{u_i}\binom{n-u_i+k-1}{n-u_i}}{\binom{m+n}{n}}\right)\right). \quad (4.11)$$

The advantage of equation (4.11) is that its evaluation does not require any prior knowledge regarding the distribution of the underlying process when the process is IC. However, the computation of equation (4.11) is cumbersome and complex. Also, the sum does not converge and hence the *ARL* given in equation (4.11) cannot be evaluated numerically.

4.8.2 Markov chain approach

The Markov chain approach is another method that is applied to evaluate the run length distribution and its characteristics through closed-form expressions. A detailed discussion is presented in Chapters 2 and 3 for implementing the Markov chain method for the DGWMA chart and its special case, the DEWMA chart. Closed-form expressions were obtained for the DEWMA-TBE chart (Case 1) in Chapter 3, since this chart can be viewed as a first-order Markov chain. However, there were obstacles and challenges involved in approximating the run length distribution of the DGWMA-TBE chart. The closed-form expressions obtained for the DEWMA-TBE chart– see Chapter 3 – can be obtained for the DEWMA-EX chart by implementing the same methodology. The main differences are highlighted as follows:

(i) Since the DEWMA-EX chart is a nonparametric chart, the X_t for the DEWMA-TBE chart is replaced with the nonparametric EX statistic me U_t. Hence, the transition probability can be written as follows:

$$P\left[S_j - \gamma < Z_t < S_j + \gamma \middle| Z_{t-1} = C_{t-1} = S_i\right]$$
$$= P\left[S_j - \gamma < \lambda_2 C_t + (1-\lambda_2)Z_{t-1} < S_j + \gamma \middle| Z_{t-1} = C_{t-1} = S_i\right]$$
$$= P\left[S_j - \gamma < \lambda_2 C_t + (1-\lambda_2)S_i < S_j + \gamma \middle| Z_{t-1} = C_{t-1} = S_i\right]$$
$$= P\left[S_j - \gamma < \lambda_2(\lambda_1 U_t + (1-\lambda_1)C_{t-1}) + (1-\lambda_2)S_i < S_j + \gamma \middle| Z_{t-1} = C_{t-1} = S_i\right]$$
$$= P\left[S_j - \gamma < \lambda_1\lambda_2 U_t + \lambda_2(1-\lambda_1)S_i + (1-\lambda_2)S_i < S_j + \gamma \middle| Z_{t-1} = C_{t-1} = S_i\right]$$
$$= P\left[\frac{S_j-\gamma-\lambda_2(1-\lambda_1)S_i-(1-\lambda_2)S_i}{\lambda_1\lambda_2} < X_t < \frac{S_j+\gamma-\lambda_2(1-\lambda_1)S_i-(1-\lambda_2)S_i}{\lambda_1\lambda_2}\right]$$

$$= P\left[\frac{S_j-\gamma-S_i(1-\lambda_1\lambda_2)}{\lambda_1\lambda_2} < U_t < \frac{S_j+\gamma-S_i(1-\lambda_1\lambda_2)}{\lambda_1\lambda_2}\right].$$

(ii) The great advantage of the Markov chain for the DEWMA-EX chart compared to the DEWMA-TBE chart is that the evaluation of the expressions does not require any distributional assumption.

4.8.3 Monte Carlo simulation

A numerical Monte Carlo simulation algorithm has been implemented in this chapter to estimate the unconditional run length distribution and its characteristics for the DGWMA-EX chart. Note that the algorithm is discussed in terms of the DGWMA-EX chart (Case 1), where all four parameters are considered. By modifying the algorithm and selecting specific values for the proposed DGWMA-EX chart, the algorithm is also applicable to the limiting cases (i.e., GWMA-EX and EWMA-EX) as well as the special case (i.e., DEWMA-EX – Case 1 and Case 2). The simulation algorithm includes the following steps:

i. Select a combination of the design parameters (i.e., $q_1, q_2, \alpha_1, \alpha_2, L$), the shift to be detected (i.e., δ), the reference and test sample sizes $m \geq 1$ and $n \geq 1$, and the IC distribution parameter θ_0, then identify a process distribution $F_X(x)$. The latter is only used to investigate the OOC run length distribution.

ii. Obtain the r^{th} order statistic $X_{(r)}$ by generating a reference sample of size m from the identified process distribution $F_X(x)$.

iii. A test sample of size $n \geq 1$ is generated to calculate the EX U_i by counting the number of observations Y in the i^{th} sample that met the constraint $Y \geq X_{(r)}$. The test sample is drawn from $F_X(x-\theta_1)$, and it must be noted that when an IC run length distribution is desired, then $\theta_1 = \theta_0$; whereas $\theta_1 = \theta_0 + \delta$ is referred to as an OOC run length.

iv. Calculate the steady-state control limits defined in equation (4.4) by using the design parameters values $(q_1, q_2, \alpha_1, \alpha_2, L)$ obtained from step (i).

v. Calculate the DGWMA-EX plotting statistic Z_t^2 according to equation (4.1) with the starting value taken as $Z_0^2 = n\left(1 - \frac{r}{m+1}\right)$, and compare each plotting statistic with the steady-state control limits obtained from step (iv).

vi. After running 10,000 iterations of steps (i) to (v), the number of samples until the first plotting statistic falls on or outside the steady-state control limits, known as the run length, is calculated

for each of the interactions. These 10,000 empirical run length values are then used to calculate the average run length and other characteristics for the run length.

4.9 The IC design

The IC design of the proposed DGWMA-EX chart consists of obtaining the values for the charting constant – i.e., $L > 0$ for chosen values of m (known as the reference sample size), n (known as the test sample size), and a certain range of values for each (q, α) combination – so that the attained IC *ARL* is close to the desired value ARL^*, which is typically 370 or 500. Chakraborty et al. (2018) considered $m = 49, 99$ and $n = 5,10$ as the values for the reference sample and test sample sizes, respectively; and the following range of values for the GWMA-EX parameters: $q = 0.8, 0.9, 0.95$ and $\alpha = 0.7, 0.8, 0.9, 1.0, 1.3$. To make the comparison fair and reliable, this study also considered the same aforementioned values for m, n and the chart parameters for the DGWMA-EX chart (Case 2). The chart parameters for the DGWMA-EX chart (Case 1) are selected as $q_1 = 0.8, 0.9$, $q_2 = 0.9, 0.95$, $\alpha_1 = 0.7, 0.8, 0.9, 1.0$, and $\alpha_2 = 0.8, 0.9, 1.0, 1.3$. For the DEWMA-EX chart (Case 1), the parameters are chosen as $q_1 = 0.6, 0.7, 0.8, 0.9$, $q_2 = 0.7, 0.8, 0.9, 0.95$, and $\alpha_1 = \alpha_2 = 1$; while for the DEWMA-EX chart (Case 2), the parameters are selected as $q_1 = q_2 = q = 0.6, 0.7, 0.8, 0.9, 0.95$. The grid search procedure is discussed as follows:

- **Input:** The chart parameters are selected as follows, q_1: 0.8(0.1)0.9, q_2: 0.9(0.05)0.95, α_1: 0.7(0.1)1, α_2: 0.7(0.1)0.9, the reference sample is chosen as $m = 49(50)99$ and the test sample is selected as $n = 5(5)10.$, where the values given in the parentheses are representing the step size (grid size). The starting values for the parameters q_1, q_2, α_1, and α_2 are selected as 0.8, 0.9, 0.7, and 0.7, respectively and incremented based on the given step size for other combinations. The starting values for m and n are selected as 49 and 5, respectively.
- **Output:** For the chosen $(q_1, q_2, \alpha_1, \alpha_2, m, n)$ as an input, the algorithm searches for the combination of (L, ARL_0) under the desired $ARL_0^* = 370$. Thereafter, the charting constants $L > 0$ are obtained such that the attained ARL_0 is approximately equal to the desirable value of $ARL_0^* = 370$.

By implementing the simulation algorithm alongside a grid search method, the charting constant $L > 0$ for the chosen $(q_1, q_2, \alpha_1, \alpha_2,)$ combination and specified values of m and n, based on the constraint that $ARL_0^* = 370$, was obtained. The values of $L > 0$ are reported for the DGWMA-EX chart (Case 2) in Tables A.4.1 and A.4.2, the DGWMA-EX chart (Case 1) in Tables A.4.3 to A.4.6, the GWMA-EX and EWMA-EX charts in Tables A.4.7 and A.4.8, and the DEWMA-EX chart (Case 1 and Case 2) in Tables A.4.9 and A.4.10 along with the attained ARL_0 values. All the listed tables are included in the Appendix for Chapter 4. Note that, the results for the CUSUM-EX are embedded within text in this chapter and will be discussed in detail in Section 4.10.

To ensure the simulation yielded reasonable and consistent results and guarantee the validity of the algorithm developed in R, this study's results were compared to those of Chakraborty et al. (2018). For instance, consider the two following scenarios:

i. When $m = 49$ and $n = 10$, then $q_1 = 0.95$, $q_2 = 0$, $\alpha_1 = 0.7$ and $\alpha_2 = 1$, and it can be seen that a value of charting constant $L = 0.737$ gives an attained $ARL_0 = 370.03$. In Chakraborty et al. (2018), the GWMA-EX chart with $q = q_1 = 0.95$ and $\alpha = \alpha_1 = 0.7$, and $L = 0.738$ has an attained $ARL_0 = 370.05$.

ii. When $m = 99$ and $n = 5$, then $q_1 = 0.9$, $q_2 = 0$, $\alpha_1 = 0.7$ and $\alpha_2 = 1$, and it can be observed that a value of charting constant $L = 1.805$ gives an attained $ARL_0 = 370.49$. In Chakraborty et al. (2018), the GWMA-EX chart with $q = q_1 = 0.9$ and $\alpha = \alpha_1 = 0.7$, and $L = 1.807$ has an attained $ARL_0 = 370.58$.

The charting constant values in Tables A.4.1 to A.4.10 (Appendix for Chapter 4) are useful for the design and implementation of the DGWMA-EX chart. This includes the design and implementation of the GWMA-EX, DEWMA-EX, and EWMA-EX charts.

The main objective of this chapter is to focus on the median of the Phase I reference sample – i.e., where $X_{(r)}$ is the median of the Phase I sample. However, a performance analysis is also conducted for the proposed DGWMA-EX and its limiting and special cases using the 25th and 75th percentiles of the Phase I sample and is discussed in more detail in the ensuing section. Based on the results obtained for the selection of other percentiles, the recommendation would be to use the median of the Phase I sample for the DGWMA-EX chart, since the median is a robust measure of the central tendency of distributions, and practitioners are more interested in the median. Therefore, general guidelines are provided for practitioners on the design of the generalized nonparametric DGWMA-EX chart.

Note that, to construct the Phase I charts based on the median obtained from the Phase I sample, first the observations from the m subgroups are combined into one sample size of $N = nm$ observations and arranged from the smallest to largest, where n represents the test sample from Phase II. In this chapter, the values for the r^{th} order statistic are selected as $r = (m + 1)/2$ when m is odd, e.g., 49 and 99. However, Graham and Chakraborti (2019) discussed general case for the pooled median as follows: when N is odd, the median is calculated as $X_{(r)}$, where $r = (m + 1)/2$, whereas when N is even, the median is calculated as $\frac{X_{(r_1)}+X_{(r_2)}}{2}$, where $r_1 = \frac{m}{2}$ and $r_2 = \frac{m+2}{2}$. In this thesis, only odd values for m are considered in order to make a reliable comparison with other charts available in the SPC literature constructed under this assumption. However, note that the index r can be calculated as $r = \left(\frac{P}{100}\right)m$, where P denotes the percentiles of interest. If r is an integer, the percentile of interest is the average of

the values in positions r and $r+1$, whereas when r is not an integer, then round up and the percentile of interest is the value in that position. This scheme is recommended in practice for calculation of percentiles. Calculations provided in this chapter for odd values of m are close to the even values of m that shows the results are fairly close. For example, the ARL_0 for $m = 100$ and $m = 99$ are 369.40 and 370.20, respectively. Note that, from a practical point of view, the practitioner will use the particular values of the reference sample m, in practice, even or odd. For more information, see Graham and Chakraborti (2019).

4.10 The OOC performance

The preliminary step to evaluating the OOC performance is to ensure that the ARL_0 values are close to 370 (when no shift occurs or the process is IC), so that all the charts are at an equal footing. Once different competing charts are designed with an equal ARL_0, a chart with a smaller ARL_1 provides a better performance for practical scenarios.

The results for the OOC performance comparisons are shown in Tables A.4.1 to A.4.10 for multiple combinations of the parameters $(q_1, q_2, \alpha_1, \alpha_2, L)$, as well as for some chosen or specified values of the reference sample m, the test sample n, and the shift sizes δ. Tables A.4.1 and A.4.2 correspond to the DGWMA-EX chart (Case 2), Tables A.4.3 to A.4.6 refer to the DGWMA-EX chart (Case 1), the results in Tables A.4.7 and A.4.8 represent the GWMA-EX and EWMA-EX charts, and Tables A.4.9 and A.4.10 illustrate the results for the DEWMA-EX chart (Case 1 and Case 2). The values for the reference sample are selected as $m = 49, 99$, the test sample is chosen as $n = 5, 10$, and the shift size is equal to $\delta = 0.05, 0.1, 0.25, 0.5, 0.75$, and 1.0. Note that all the tables are available in the Appendix for Chapter 4.

The OOC comparison is divided into different cases dependent on the type of time-weighted chart under consideration and a detailed discussion is provided for each. A quick comparison of the results advocates the below points.

(i) DGWMA-EX (Case 2) versus GWMA-EX and EWMA-EX

The first comparison is conducted between the proposed DGWMA-EX chart (Case 2) and its limiting cases – i.e., the GWMA-EX and EWMA-EX charts – in detecting small or tiny changes in production processes. The OOC results reveal that:

i. The DGWMA-EX chart typically outperforms the GWMA-EX chart when $\alpha < 1$ and for small to moderate shifts, i.e., $\delta \leq 0.25$. For example, to detect a shift of $\delta = 0.1$, a DGWMA-EX chart with $q = 0.9, \alpha = 0.8, L = 0.924$ has an $ARL_1 = 330.57$, whereas the GWMA-EX chart with $q_1 = 0.9$, $q_2 = 0$, $\alpha_1 = 0.8$ and $\alpha_2 = 1$, and $L = 1.596$ has an $ARL_1 = 336.84$ when $m = 49$ and $n = 5$. Note that the values for the IC *ARL* (ARL_0) are equal to 375.32 and 371.98

for the DGWMA-EX and GWMA-EX charts, respectively, so that the charts are at an equal footing. Further to this, the results are obtained from Tables A.4.1 and A.4.7 for the DGWMA-EX and GWMA-EX charts, respectively. Some cases, such as the DGWMA-EX chart with $q = 0.95$ and $\alpha = 0.7, 0.8, 0.9$, are worse than the GWMA-EX chart when $m = 49$ and $n = 5$.

ii. The DGWMA-EX chart generally performs better than the EWMA-EX chart for small shifts $\delta \leq 0.25$. For example, to detect a shift of $\delta = 0.05$, a DGWMA-EX chart with $q = 0.8$, $\alpha = 1.0$, $L = 1.755$ has $ARL_1 = 360.95$ (Table A.4.1 in the Appendix); whereas the EWMA-EX chart with $q_1 = 0.8$, $q_2 = 0$, $\alpha_1 = 1$ and $\alpha_2 = 1$, and $L = 2.249$ has $ARL_1 = 366.63$ (Table A.4.7 in the Appendix) when $m = 49$ and $n = 5$. The IC *ARL* (ARL_0) equals 369.77 and 370.13 for the DGWMA-EX and EWMA-EX charts, respectively.

iii. Overall, for small to moderate shifts, the DGWMA-EX chart works better than the GWMA-EX and EWMA-EX charts. For example, when $q = 0.8$, $\alpha = 0.8$, $m = 49$ and $n = 10$, a comparative plot is illustrated in Figure 4.2 to compare the *ARL* performance and the detection capabilities between the DGWMA-EX, GWMA-EX, and EWMA-EX charts. One can clearly observe that the DGWMA-EX chart outperforms the other counterparts for small shifts, which is one of the main objectives of the proposed DGWMA-EX chart.

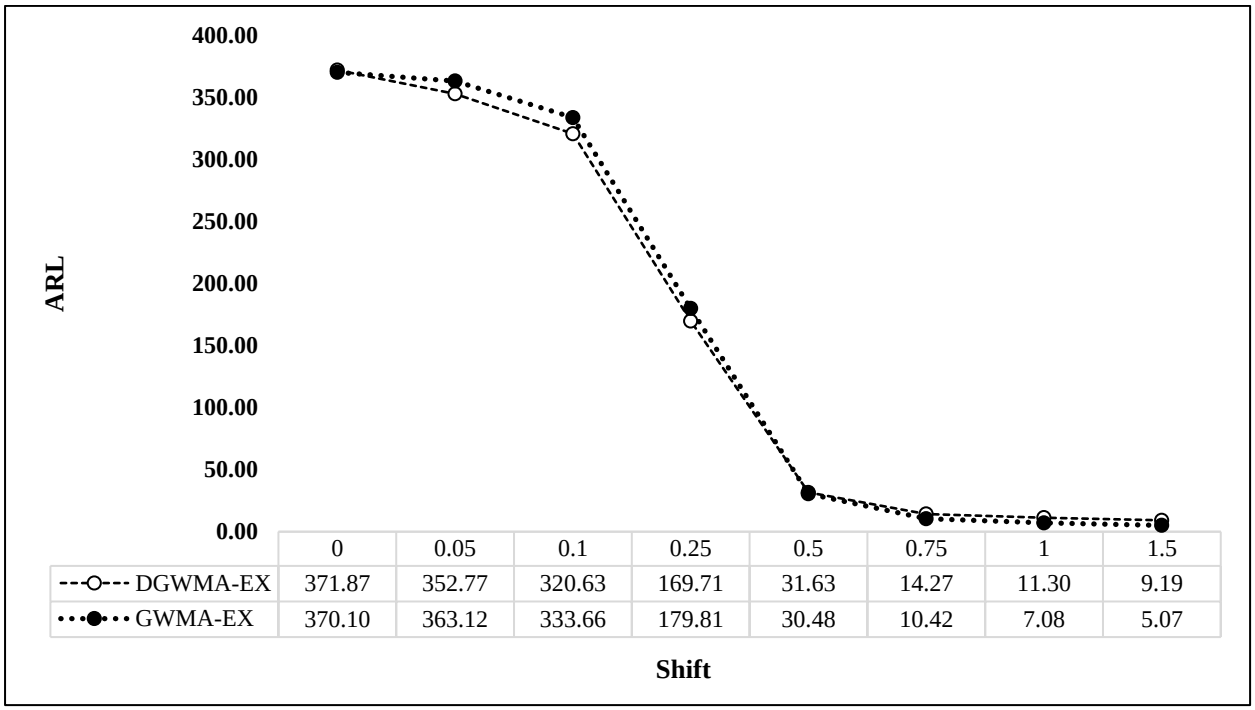

	0	0.05	0.1	0.25	0.5	0.75	1	1.5
DGWMA-EX	371.87	352.77	320.63	169.71	31.63	14.27	11.30	9.19
GWMA-EX	370.10	363.12	333.66	179.81	30.48	10.42	7.08	5.07

Figure 4.2. Comparison between the DGWMA-EX, and GWMA-EX charts when $q = 0.8$, $\alpha = 0.9$, $m = 49$ and $n = 5$

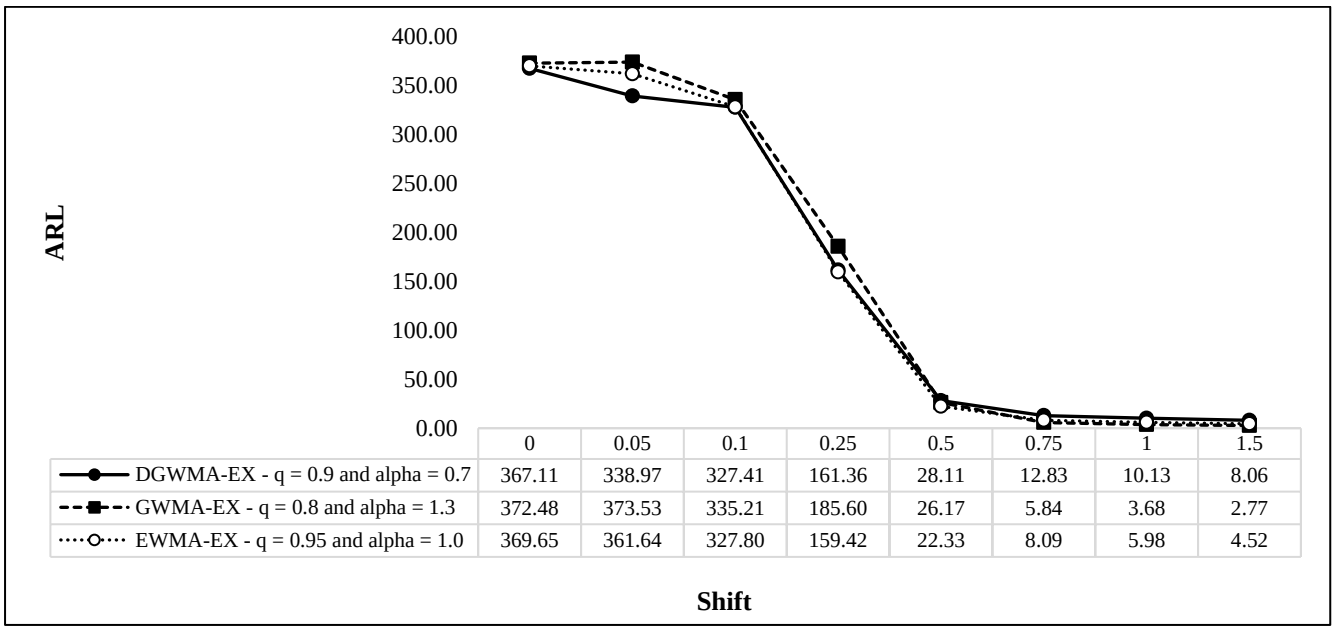

	0	0.05	0.1	0.25	0.5	0.75	1	1.5
DGWMA-EX - q = 0.9 and alpha = 0.7	367.11	338.97	327.41	161.36	28.11	12.83	10.13	8.06
GWMA-EX - q = 0.8 and alpha = 1.3	372.48	373.53	335.21	185.60	26.17	5.84	3.68	2.77
EWMA-EX - q = 0.95 and alpha = 1.0	369.65	361.64	327.80	159.42	22.33	8.09	5.98	4.52

Figure 4.3. Comparison between the DGWMA-EX, GWMA-EX and EWMA-EX charts

In Figure 4.3, the proposed DGWMA-EX chart is compared with the GWMA-EX and EWMA-EX chart. For small shifts, the DGWMA-EX chart outperforms the GWMA-EX and EWMA-EX chart. For medium to large shifts, the EWMA-EX chart outperforms the DGWMA-EX and GWMA-EX charts. Note that, the EWMA-EX chart is the special case of the GWMA-EX chart and is the limiting case of the DGWMA-EX chart.

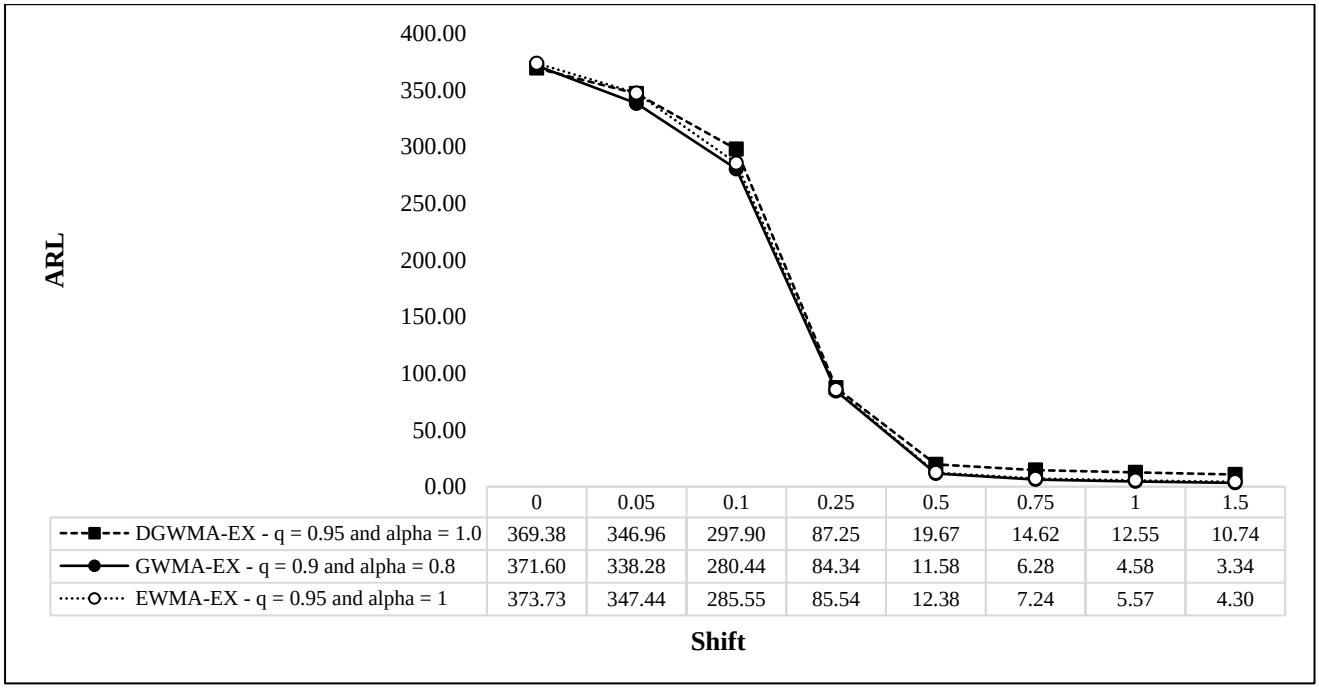

	0	0.05	0.1	0.25	0.5	0.75	1	1.5
DGWMA-EX - q = 0.95 and alpha = 1.0	369.38	346.96	297.90	87.25	19.67	14.62	12.55	10.74
GWMA-EX - q = 0.9 and alpha = 0.8	371.60	338.28	280.44	84.34	11.58	6.28	4.58	3.34
EWMA-EX - q = 0.95 and alpha = 1	373.73	347.44	285.55	85.54	12.38	7.24	5.57	4.30

Figure 4.4. Comparison between the DGWMA-EX, GWMA-EX and EWMA-EX charts

From Figure 4.4, one can conclude that for some parameter combinations, the GWMA-EX outperforms the DGWMA-EX chart in detecting small shifts in the process. However, for the majority of the parameters, the DGWMA-EX still outperforms the GWMA-EX and EWMA-EX charts in detecting small shifts in the process.

(ii) DGWMA-EX (Case 1) versus DGWMA-EX (Case 2)

Sheu and Hsieh (2009) mentioned that the parametric DGWMA chart with four parameters constructed under the assumption of the normal distribution does not perform better than the DGWMA chart with two parameters. As discussed in Chapter 3, it was discovered that there is a DGWMA-TBE chart (Case 1) that outperforms the DGWMA-TBE chart (Case 2). In this section, the performance between two types of DGWMA-EX charts in the nonparametric paradigm is investigated and discussed in detail. Lu (2018) mentioned that the performance of these two charts are identical. However, different conclusions and results are obtained in this chapter. The ARL_0 for these two charts was first computed to ensure both are at an equal footing. The ARL_0 of the DGWMA-EX chart (Case 1) is 370.47, and for the DGWMA-EX chart (Case 2) it is 371.34. The ARL_1 was computed for $q_1 = 0.8, 0.9$, $q_2 = 0.9, 0.95$, $\alpha_1 = 0.7, 0.8, 0.9, 1$, and $\alpha_2 = 0.8, 0.9, 1, 1.3$. To this end, for some combinations of parameters, the DGWMA-EX chart (Case 1) outperforms the DGWMA-EX chart (Case 2). This is due to the flexibility that is gained by using additional parameters. For example, from Table A.4.5, for $q_1 = 0.8$, $q_2 = 0.9$, $\alpha_1 = 0.7$, $\alpha_2 = 0.9$ and $L = 1.456$, the OOC *ARL* is equal to $ARL_1 = 345.42$ and $ARL_1 = 102.39$, for shift sizes (δ) 0.05 and 0.25, respectively. From Table A.4.2, for $q_1 = q_2 = q = 0.8$, $\alpha_1 = \alpha_2 = \alpha = 0.9$ and $L = 1.925$, the OOC *ARL* is equal to $ARL_1 = 364.05$ and $ARL_1 = 111.66$, for shift sizes (δ) 0.05 and 0.25, respectively. The first set of design parameters refers to the DGWMA-EX chart (Case 1), while the latter one alludes to the DGWMA-EX chart (Case 2).

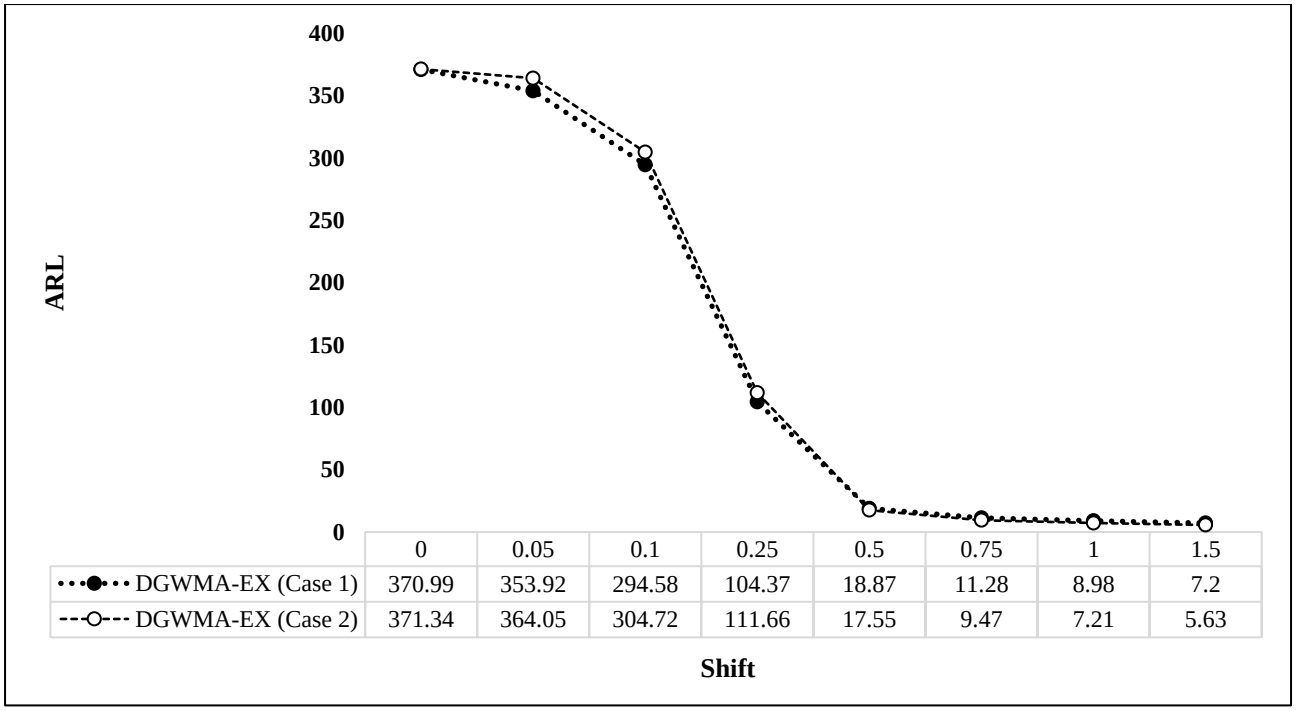

	0	0.05	0.1	0.25	0.5	0.75	1	1.5
DGWMA-EX (Case 1)	370.99	353.92	294.58	104.37	18.87	11.28	8.98	7.2
DGWMA-EX (Case 2)	371.34	364.05	304.72	111.66	17.55	9.47	7.21	5.63

Figure 4.5. Comparison between the DGWMA-EX (Case 1) and the DGWMA-EX (Case 2) charts when $m = 99$ and $n = 5$

The parameter values for the DGWMA-EX chart (Case 1) are selected as $q_1 = 0.8$, $q_2 = 0.9$, $\alpha_1 = 0.8$, $\alpha_2 = 0.9$, and for the DGWMA-EX chart (Case 2) are selected as $q = 0.8$ and $\alpha = 0.9$. The DGWMA-EX chart (Case 1) outperforms the DGWMA-EX chart (Case 2) for tiny to moderate shifts. For large shifts, the DGWMA-EX chart (Case 2) outperforms the DGWMA-EX chart (Case 1).

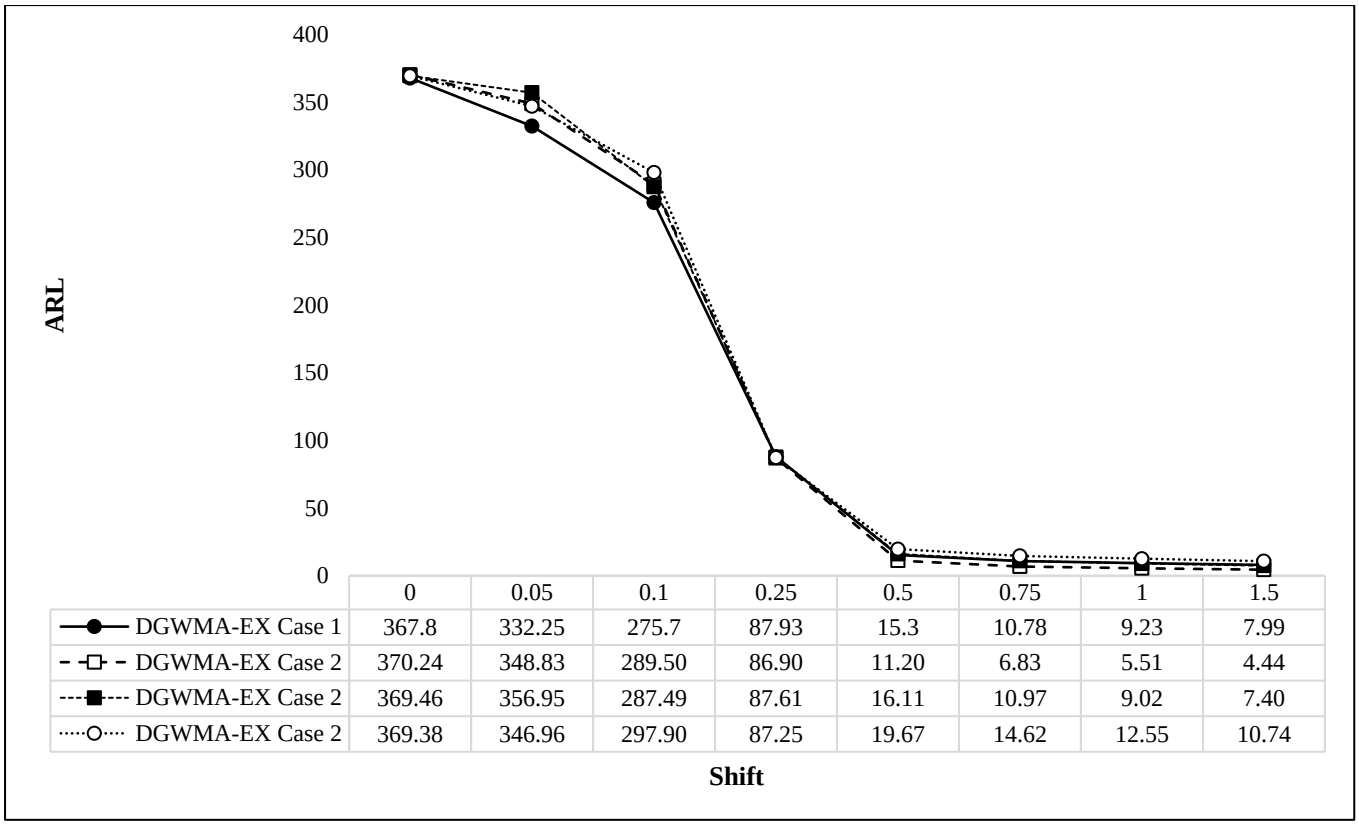

	0	0.05	0.1	0.25	0.5	0.75	1	1.5
DGWMA-EX Case 1	367.8	332.25	275.7	87.93	15.3	10.78	9.23	7.99
DGWMA-EX Case 2	370.24	348.83	289.50	86.90	11.20	6.83	5.51	4.44
DGWMA-EX Case 2	369.46	356.95	287.49	87.61	16.11	10.97	9.02	7.40
DGWMA-EX Case 2	369.38	346.96	297.90	87.25	19.67	14.62	12.55	10.74

Figure 4.6. Comparison between the DGWMA-EX (Case 1) and the DGWMA-EX (Case 2) charts when $m = 99$ and $n = 5$

In Figure 4.6, two different types of the DGWMA-EX chart are compared with each other. For small shifts, the DGWMA-EX chart (Case 1) outperforms other DGWMA-TBE chart (Case 2). However, for medium to large shifts, the performance of the DGWMA-EX chart (Case 2) is better than the DGWMA-EX chart (Case 1). Hence, unlike Lu (2018) which concluded that the performance of both DGWMA cases under nonparametric assumptions are identical, in this section we have shown that some cases exist where the DGWMA-EX chart with four parameters outperform the DGWMA-EX chart with two parameters due to flexibility added to the chart by adding extra parameters.

(iii) DGWMA-EX (Case 1) versus GWMA-EX and EWMA-EX

i. For the DGWMA-EX chart (Case 1), there are some cases where the chart outperforms the GWMA-EX chart. For example, from Table A.4.3, for $q_1 = 0.8$, $q_2 = 0.9$, $\alpha_1 = 0.7$, $\alpha_2 = 0.9$ and L= 1.179, the OOC *ARL* is equal to $ARL_1 = 357.37$ and $ARL_1 = 322.12$, for shift sizes (δ) 0.05 and 0.1, respectively. From Table A.4.7, for $q_1 = 0.8$, q_2 =0, $\alpha_1 = 0.9$, $\alpha_2 = 1.0$ and $L = 2.183$, the OOC *ARL* is

equal to $ARL_1 = 358.99$ and $ARL_1 = 330.36$, for shift sizes (δ) 0.05 and 0.1, respectively. The latter case refers to the GWMA-EX chart, whereas the former is related to the DGWMA-EX chart.

ii. For the DGWMA-EX chart (Case 1), various cases exist, where the chart outperforms the EWMA-EX chart. For example, from Table A.4.6, for $q_1 = 0.8$, $q_2 = 0.95$, $\alpha_1 = 0.9$, $\alpha_2 = 1$ and L = 1.110, the OOC *ARL* is equal to $ARL_1 = 336.33$ and $ARL_1 = 84.99$, for shift sizes (δ) 0.05 and 0.25, respectively. From Table A.4.8, for $q_1 = 0.8$, $q_2 = 0.0$, $\alpha_1 = 1.0$, $\alpha_2 = 1.0$ and L = 2.272, the OOC *ARL* is equal to $ARL_1 = 355.02$ and $ARL_1 = 103.15$, for shift sizes (δ) 0.05 and 0.25, respectively. The former case corresponds to the DGWMA-EX chart, whereas the latter refers to the EWMA-EX chart.

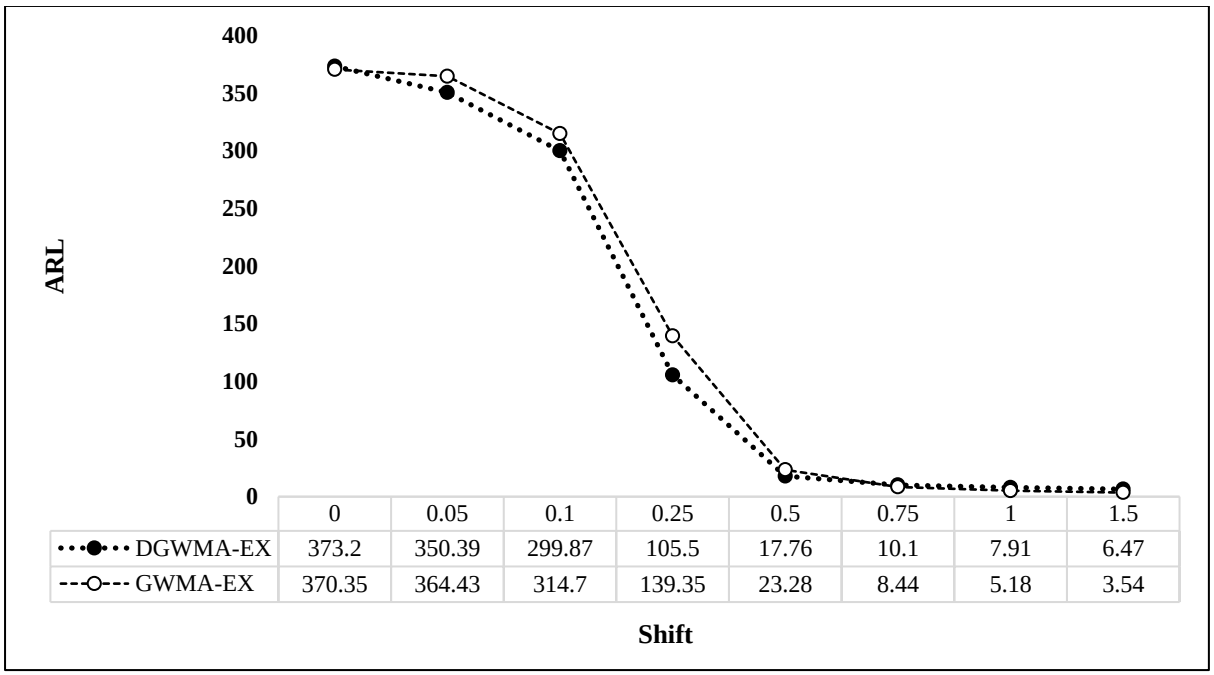

	0	0.05	0.1	0.25	0.5	0.75	1	1.5
DGWMA-EX	373.2	350.39	299.87	105.5	17.76	10.1	7.91	6.47
GWMA-EX	370.35	364.43	314.7	139.35	23.28	8.44	5.18	3.54

Figure 4.7. Comparison between the DGWMA-EX (Case 1) and the GWMA-EX charts when $m = 99$ and $n = 5$

The parameter values for the GWMA-EX chart are selected as $q_1 = 0.8$, $q_2 = 0.0$, $\alpha_1 = 1.0$, $\alpha_2 = 1.3$, and for the DGWMA-EX chart (Case 1) are selected as $q_1 = 0.8$, $q_2 = 0.9$, $\alpha_1 = 0.7$, $\alpha_2 = 1.3$. The DGWMA-EX chart (Case 1) outperforms the GWMA-EX chart (Case 2) for tiny to moderate shifts. For large shifts, the GWMA-EX chart outperforms the DGWMA-EX chart (Case 1).

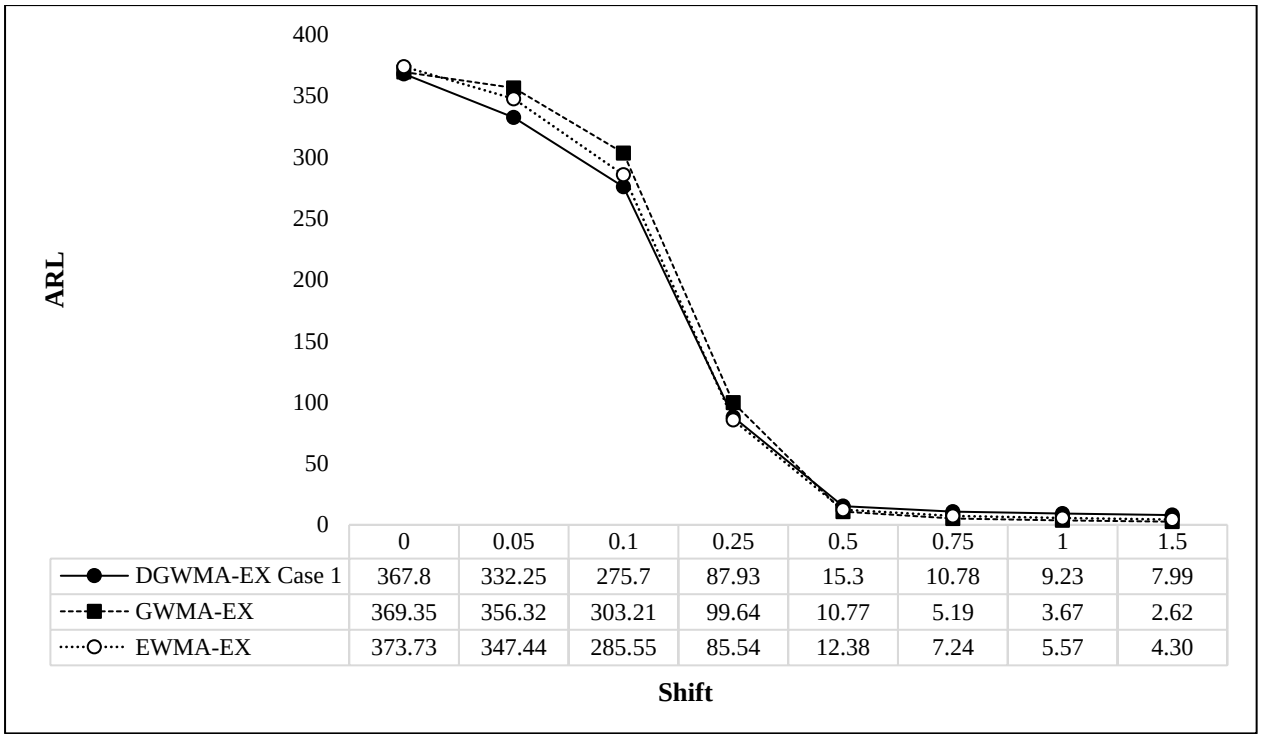

	0	0.05	0.1	0.25	0.5	0.75	1	1.5
DGWMA-EX Case 1	367.8	332.25	275.7	87.93	15.3	10.78	9.23	7.99
GWMA-EX	369.35	356.32	303.21	99.64	10.77	5.19	3.67	2.62
EWMA-EX	373.73	347.44	285.55	85.54	12.38	7.24	5.57	4.30

Figure 4.8. Comparison between the DGWMA-EX (Case 1) and the GWMA-EX charts when $m = 99$ and $n = 5$

The EWMA-EX chart which is the special case of the GWMA-EX chart and the limiting case of the proposed DGWMA-EX is also included in the comparative study and illustrated in Figure 4.6. The DGWMA-EX chart outperforms the GWMA-EX and the EWMA-EX chart in detecting small shifts in the process. However, for medium to large shifts, the GWMA-EX chart outperforms the DGWMA-EX chart. Also, for large shifts, the EWMA-EX chart outperforms the GWMA-EX chart.

(iv) DEWMA-EX (Case 1) versus GWMA-EX and EWMA-EX

i. Zhang and Chen (2005) concluded that the performance of the DEWMA chart for Case 1 and Case 2 is similar for the parametric case. In this research, it was discovered that there are some combinations of the DEWMA-EX chart (Case 1) that outperform the DEWMA-EX chart (Case 2). For example, from Table 4.9, for $q_1 = 0.7$, $q_2 = 0.9$, $\alpha_1 = 1.0$, $\alpha_2 = 1.0$ and $L = 1.562$, the OOC ARL is equal to $ARL_1 = 325.01$ and $ARL_1 = 182.21$, for shift sizes (δ) 0.1 and 0.25, respectively. From Table 4.9 for $q_1 = 0.7$, $q_2 = 0.7$, $\alpha_1 = 1.0$, $\alpha_2 = 1.0$ and $L = 2.072$, the OOC ARL is equal to $ARL_1 = 327.98$ and $ARL_1 = 185.23$, for shift sizes (δ) 0.1 and 0.25, respectively. The first set of design parameters corresponds to the DEWMA (Case 1), whereas the second set refers to the DEWMA (Case 2) chart.

ii. There are some combinations of parameters for the DEWMA-EX chart that outperform the GWMA-EX chart for detecting small shifts. For example, from Table A.4.7, for $q_1 = 0.8$. $q_2 = 0.0$, $\alpha_1 = 0.9$, $\alpha_2 = 1.0$ and L = 2.183, the OOC *ARL* is equal to $ARL_1 = 358.99$ and $ARL_1 = 184.53$, for shift sizes (δ) 0.05 and 0.25, respectively. From Table A.4.9, for $q_1 = 0.8$. $q_2 = 0.95$, $\alpha_1 = 1.0$, $\alpha_2 = 1.0$ and L = 1.148, the OOC *ARL* is equal to $ARL_1 = 357.72$ and $ARL_1 = 175.72$, for shift sizes (δ) 0.05 and 0.25, respectively. The former set refers to the GWMA-EX chart, while the latter case corresponds to the DEWMA-EX chart.

iii. The DEWMA-EX chart outperforms the EWMA-EX chart for the small shifts for each and every combination of the reference sample size and the test sample size, irrespective of the value for the chart parameters, due to the flexibility added by implementing the double smoothing technique.

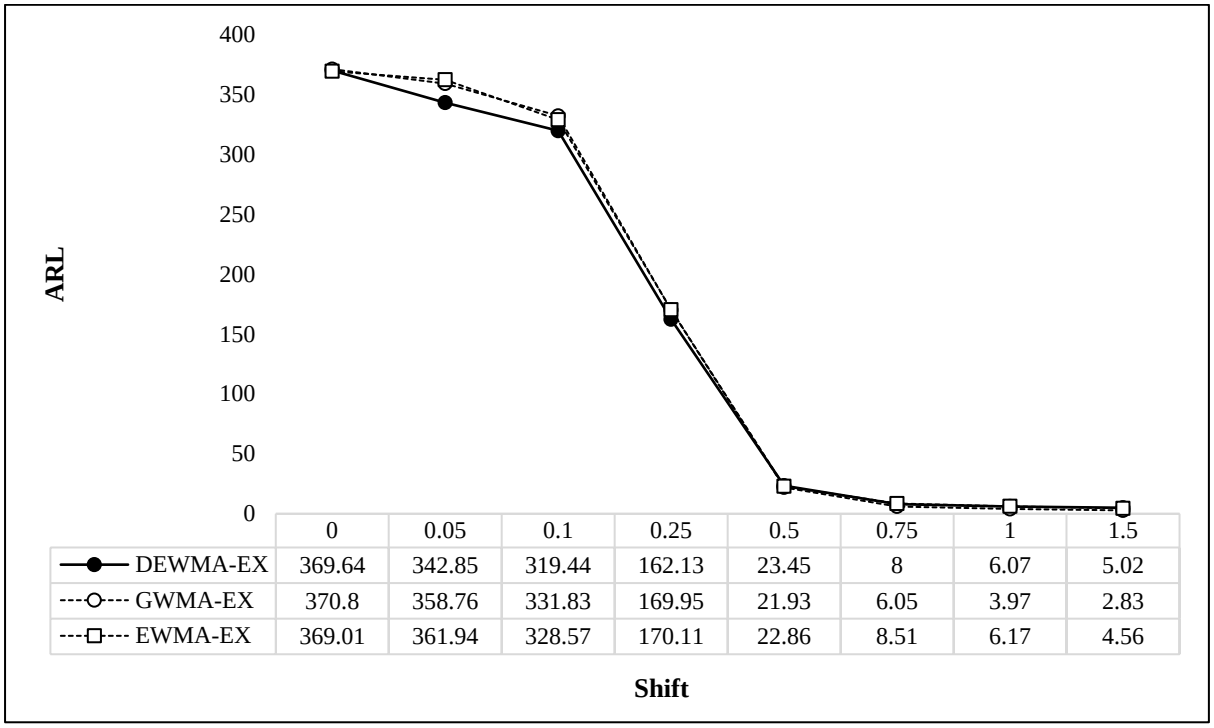

	0	0.05	0.1	0.25	0.5	0.75	1	1.5
DEWMA-EX	369.64	342.85	319.44	162.13	23.45	8	6.07	5.02
GWMA-EX	370.8	358.76	331.83	169.95	21.93	6.05	3.97	2.83
EWMA-EX	369.01	361.94	328.57	170.11	22.86	8.51	6.17	4.56

Figure 4.9. Comparison between the DEWMA-EX, GWMA-EX and EWMA-EX charts

In Figure 4.9, the DEWMA-EX chart is compared with the GWMA-EX and EWMA-EX charts. For small shifts, the DEWMA-EX chart outperforms the GWMA-EX and EWMA-EX charts. For large shifts, the performance of the DEWMA-EX chart is competitive with the GWMA-EX and EWMA-EX chars. Also, the EWMA-EX chart outperforms the GWMA-EX chart in detecting large shifts in the process.

(v) DGWMA-EX (Case 1 and Case 2) versus DEWMA-EX (Case 1 and Case 2)

i. For larger values of the parameter $q \geq 0.9$, the DEWMA-EX chart (Case 2) outperforms the DGWMA-EX chart (Case 2) for all the shift sizes. For example, from Table A.4.1, for $q_1 = 0.95$, $q_2 = 0.95$, $\alpha_1 = 1.0$, $\alpha_2 = 1.0$ and $L = 0.682$, the DEWMA-EX chart (Case 2) outperforms the DGWMA-EX chart (Case 2) for all the values of the parameter α and all the shift sizes (δ).

ii. For larger values of the parameter $q \geq 0.9$, the DEWMA-EX chart (Case 1) outperforms the DGWMA-EX chart (Case 1). For example, from Table A.4.5, for $q_1 = 0.9$, $q_2 = 0.95$, $\alpha_1 = 1.0$, $\alpha_2 = 1.3$ and $L = 1.550$, the OOC ARL is equal to $ARL_1 = 348.48$ and $ARL_1 = 295.12$, for shift sizes (δ) 0.05 and 0.1, respectively. From Table A.4.10, for $q_1 = 0.9$, $q_2 = 0.95$, $\alpha_1 = 1.0$, $\alpha_2 = 1.0$ and $L = 1.018$, the OOC ARL is equal to $ARL_1 = 338.84$ and $ARL_1 = 292.94$, for shift sizes (δ) 0.05 and 0.1, respectively. The second set of design parameters refers to the DEWMA-EX (Case 1), whereas the first is related to the DGWMA-EX (Case 1).

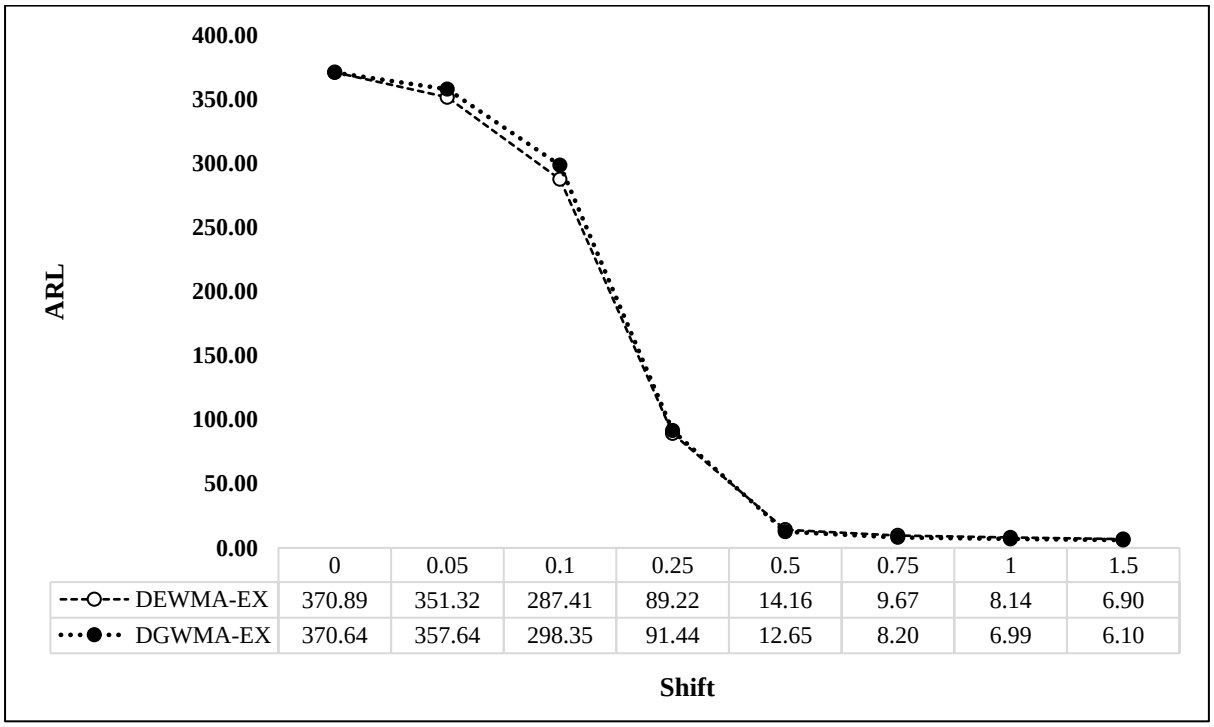

	0	0.05	0.1	0.25	0.5	0.75	1	1.5
DEWMA-EX	370.89	351.32	287.41	89.22	14.16	9.67	8.14	6.90
DGWMA-EX	370.64	357.64	298.35	91.44	12.65	8.20	6.99	6.10

Figure 4.10. Comparison between the DEWMA-EX and the DGWMA-EX charts

The DEWMA-EX chart outperforms the DGWMA-EX chart for tiny or small shifts. For moderate to large shifts, the DGWMA-EX chart outperforms the DEWMA-EX chart. Note that, the parameter

values for the DEWMA-EX chart are selected as $q = 0.9$, $\alpha = 1.0$, and for the DGWMA-EX chart, these values are $q = 0.9$, $\alpha = 1.3$.

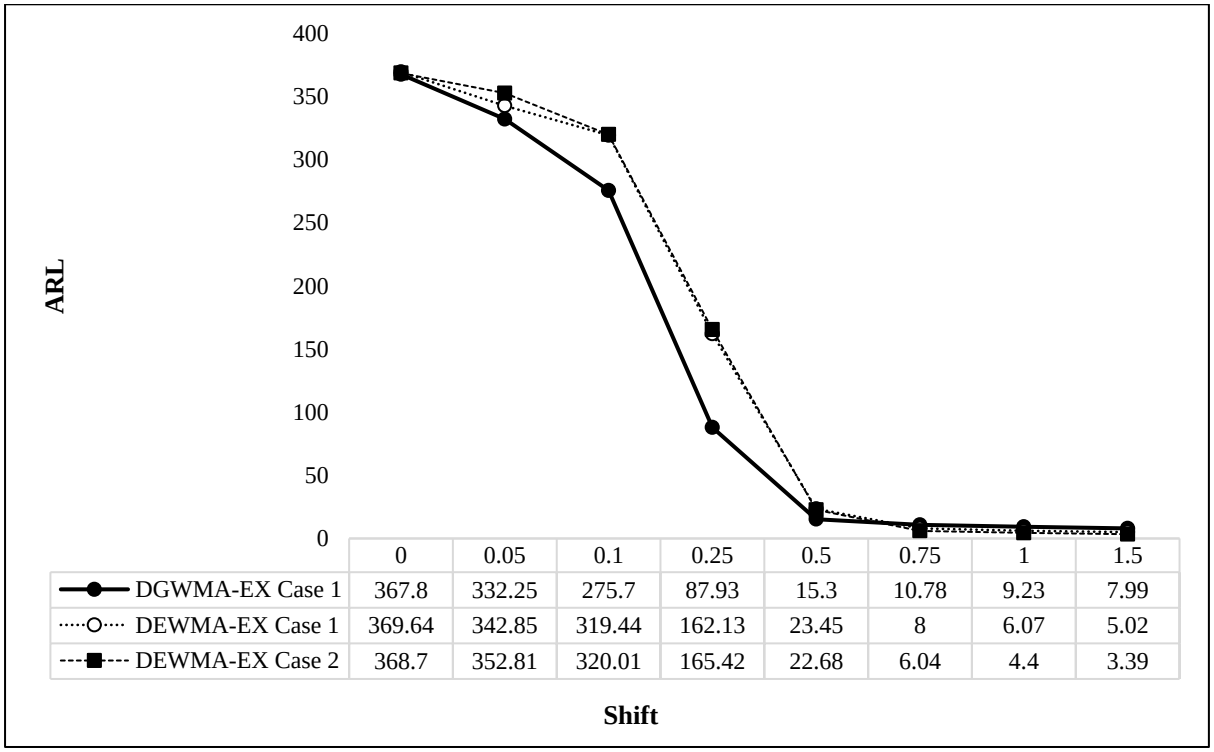

	0	0.05	0.1	0.25	0.5	0.75	1	1.5
DGWMA-EX Case 1	367.8	332.25	275.7	87.93	15.3	10.78	9.23	7.99
DEWMA-EX Case 1	369.64	342.85	319.44	162.13	23.45	8	6.07	5.02
DEWMA-EX Case 2	368.7	352.81	320.01	165.42	22.68	6.04	4.4	3.39

Figure 4.11. Comparison between the DEWMA-EX and the DGWMA-EX charts

In Figure 4.11, the DGWMA-EX chart is compared with two different cases of the DWMA-Ex chart when $m = 49$ and $n = 10$. The DGWMA-EX chart outperforms both cases of the DEWMA-EX charts in detecting small shifts in the process. Also, the performance of the DGWMA-EX chart is competitive with the DEWMA-EX chart in detecting medium to large shifts in the production processes.

The visual presentations of the nonparametric charts discussed so far would provide more insight in terms of the detection capability and superiority of a chart in detecting different shift sizes, specifically the small or tiny shifts, which is the main objective of the current chapter. The design parameters selected for illustration purposes are: $q_1 = 0.8$, $q_2 = 0.8$, $\alpha_1 = 0.8$, $\alpha_2 = 0.8$, L = 1.780 for the DGWMA-EX chart (Case 2) from Table 4.2; $q_1 = 0.8$, $q_2 = 0$, $\alpha_1 = 0.8$, $\alpha_2 = 1.0$, L = 2.397 for the GWMA-EX chart from Table A.4.8.; and $q_1 = 0.8$, $q_2 = 0$, $\alpha_1 = 1.0$, $\alpha_2 = 1.0$, L = 2.503 for the EWMA-EX chart from Table A.4.8. The comparative plot is illustrated in the following figure:

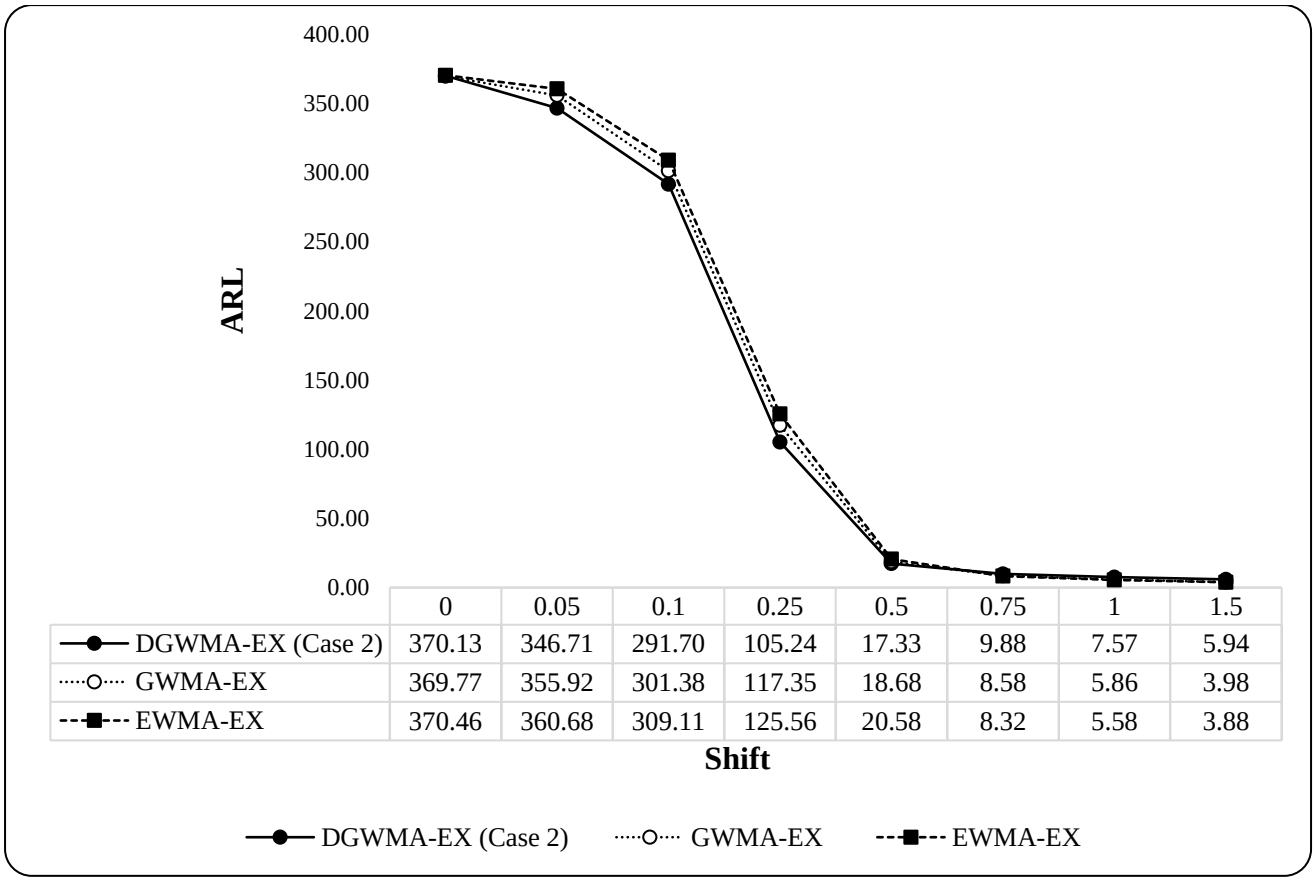

	0	0.05	0.1	0.25	0.5	0.75	1	1.5
DGWMA-EX (Case 2)	370.13	346.71	291.70	105.24	17.33	9.88	7.57	5.94
GWMA-EX	369.77	355.92	301.38	117.35	18.68	8.58	5.86	3.98
EWMA-EX	370.46	360.68	309.11	125.56	20.58	8.32	5.58	3.88

Figure 4.12. Comparative study between the DGWMA-EX (Case 2), the GWMA-EX, and the EWMA-EX charts

From the above plot, one can easily observe that the proposed DGWMA-EX chart (Case 2) outperforms other time-weighted charts (i.e., GWMA-EX and EWMA-EX) in detecting small or tiny shifts. The DGWMA-EX chart (Case 2) is competitive in terms of the moderate shifts compared to its counterparts.

To this end, the effects of the parameters q, α, and test sample size n on the OOC performance of the DGWMA-EX chart are also investigated. The results are presented in Figures 4.13, 4.14 and 4.15.

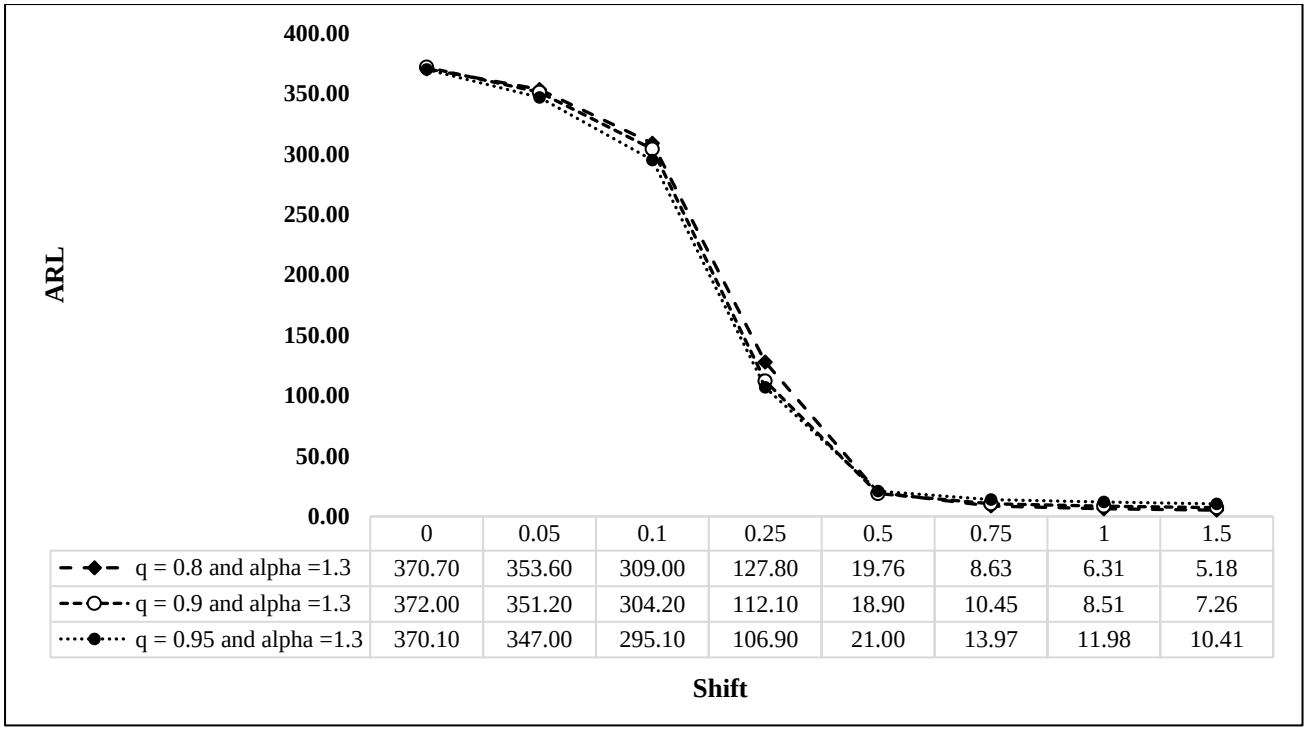

	0	0.05	0.1	0.25	0.5	0.75	1	1.5
q = 0.8 and alpha =1.3	370.70	353.60	309.00	127.80	19.76	8.63	6.31	5.18
q = 0.9 and alpha =1.3	372.00	351.20	304.20	112.10	18.90	10.45	8.51	7.26
q = 0.95 and alpha =1.3	370.10	347.00	295.10	106.90	21.00	13.97	11.98	10.41

Figure 4.13. The effect of the parameter q on the performance of the DGWMA-EX chart (Case 2) when $m = 99$ and $n = 5$

In Figure 4.13, for $\alpha = 1.3$, $m = 99$ and $n = 5$, three different values for q (0.8, 0.9 and 0.95) are selected and, based on the results, larger value of q has better OOC performance for the DGWMA-EX chart.

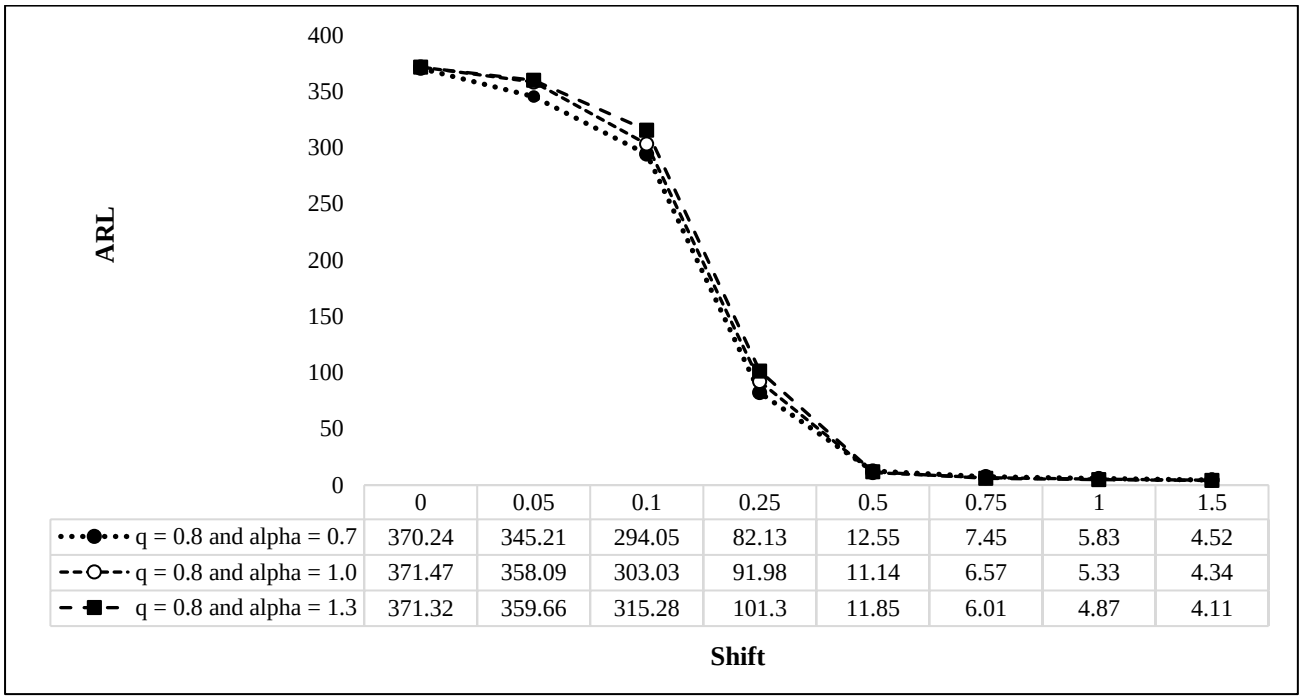

	0	0.05	0.1	0.25	0.5	0.75	1	1.5
q = 0.8 and alpha = 0.7	370.24	345.21	294.05	82.13	12.55	7.45	5.83	4.52
q = 0.8 and alpha = 1.0	371.47	358.09	303.03	91.98	11.14	6.57	5.33	4.34
q = 0.8 and alpha = 1.3	371.32	359.66	315.28	101.3	11.85	6.01	4.87	4.11

Figure 4.14. The effect of the parameter α on the performance of the DGWMA-EX chart (Case 2) when $m = 99$ and $n = 10$

In Figure 4.14, for $q = 0.8$, $m = 99$ and $n = 10$, three different values for α (0.7, 1.0 and 1.3) are considered and, based on the results, smaller values of α, lead to better OOC performance for the DGWMA-EX chart.

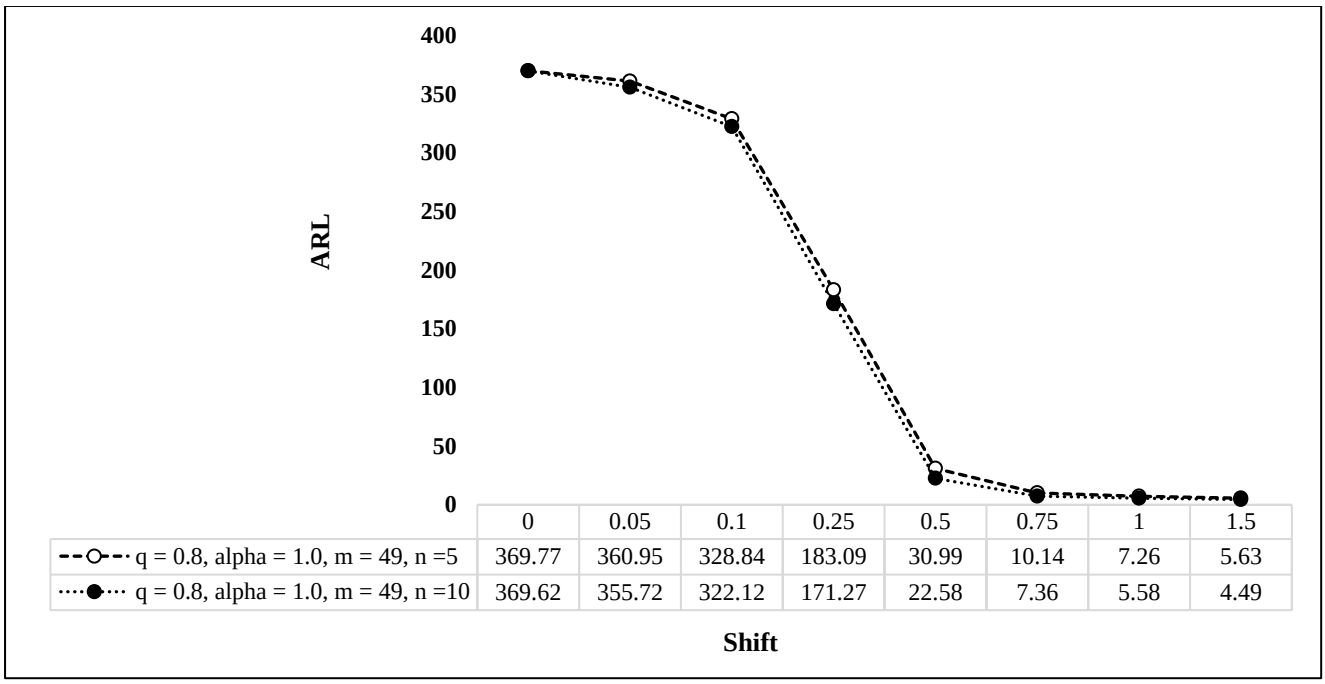

	0	0.05	0.1	0.25	0.5	0.75	1	1.5
q = 0.8, alpha = 1.0, m = 49, n =5	369.77	360.95	328.84	183.09	30.99	10.14	7.26	5.63
q = 0.8, alpha = 1.0, m = 49, n =10	369.62	355.72	322.12	171.27	22.58	7.36	5.58	4.49

Figure 4.15. The effect of the test sample size (n) on the performance of the DGWMA-EX chart (Case 2)

In Figure 4.15, for $q = 0.8$, $\alpha = 1.0$, $m = 49$, two different values are selected for the test sample size n (5 and 10) and based on the results, the larger the test sample size, the better the OOC performance of the DGWMA-EX chart.

(vi) DGWMA-EX versus CUSUM-EX

Janacek and Meikle (1997) proposed a nonparametric Shewhart-type chart where the plotting statistic is the median and the control limits are calculated based on two order statistic obtained from a reference sample in Phase I. Further, Chakraborti et al. (2004) extended the work by considering the r^{th} order statistic of a Phase II test sample as the plotting statistic and referred to as Shewhart-type precedence charts. Chakraborti and Van de Wiel (2008) developed a nonparametric Shewhart-type chart based on the Mann-Whitney statistic for monitoring the process location parameter. McDonald (1990) proposed a CUSUM chart based on the sequential ranks' statistic for individual observations. Bakir (2006) proposed a nonparametric CUSUM chart based on the signed-rank statistic for monitoring the unknown

process median (Case U). Chatterjee and Qiu (2009) developed a nonparametric CUSUM chart by implementing bootstrap methodology to obtain control limits. Li et al. (2010) developed a nonparametric CUSUM chart based on the Mann-Whitney statistic for monitoring the process location parameter.

The proposed DGWMA-EX chart is compared with the nonparametric counterpart of the CUSUM chart proposed by Graham et al. (2014) and denoted by NPCUSUM-EX. Note that, for the sake of brevity we use CUSUM-EX from now on in this thesis. The CUSUM-EX is chosen since this chart is a candidate to monitor small shifts in the process location parameter in the literature. Also, the nonparametric exceedance statistic is considered by Graham et al. (2014) when the location parameter of interest is unknown (Case U). Hence, this nonparametric CUSUM chart constructed based on the exceedance statistics to monitor the unknown location parameter of interest is equivalent to the DGWMA-EX chart proposed in this thesis. This comparison includes the normal distribution and a collection of non-normal distributions that are symmetric, heavy-tailed, and skewed. Specifically, the distribution considered in this part are: (i) the standard normal distribution (ii) the gamma distribution and its special case, the exponential distribution and (iii) the double exponential or Laplace distribution with mean 0 and variance 2. Note that, Graham et al. (2014) mentioned that the double exponential distribution is symmetric and has heavier tails. The reference sample and the test sample are selected as $m = 1000$ and $n = 5, 25$, respectively. The pre-specified value for the A*RL* is selected as 370. Note that, different scenarios are considered in this section to make the comparison sensible and reliable. The IC and OOC characteristics of the run length are as follows:

Table 4.1. The IC and OOC characteristics for the DGWMA-EX and CUSUM-EX charts when $n = 5, 25$, and $m = 1000$ for the $N(0, 1)$ distribution

δ	DGWMA-EX ($n = 5$)	DGWMA-EX ($n = 25$)	CUSUM-EX ($n = 5$)	CUSUM-EX ($n = 25$)
0.00	369.40	368.80	394.68	369.96
0.25	45.36	32.80	70.60	59.22
0.50	20.77	21.45	36.38	25.32
0.75	15.38	11.62	24.72	17.27
1.00	10.34	7.67	19.08	12.08

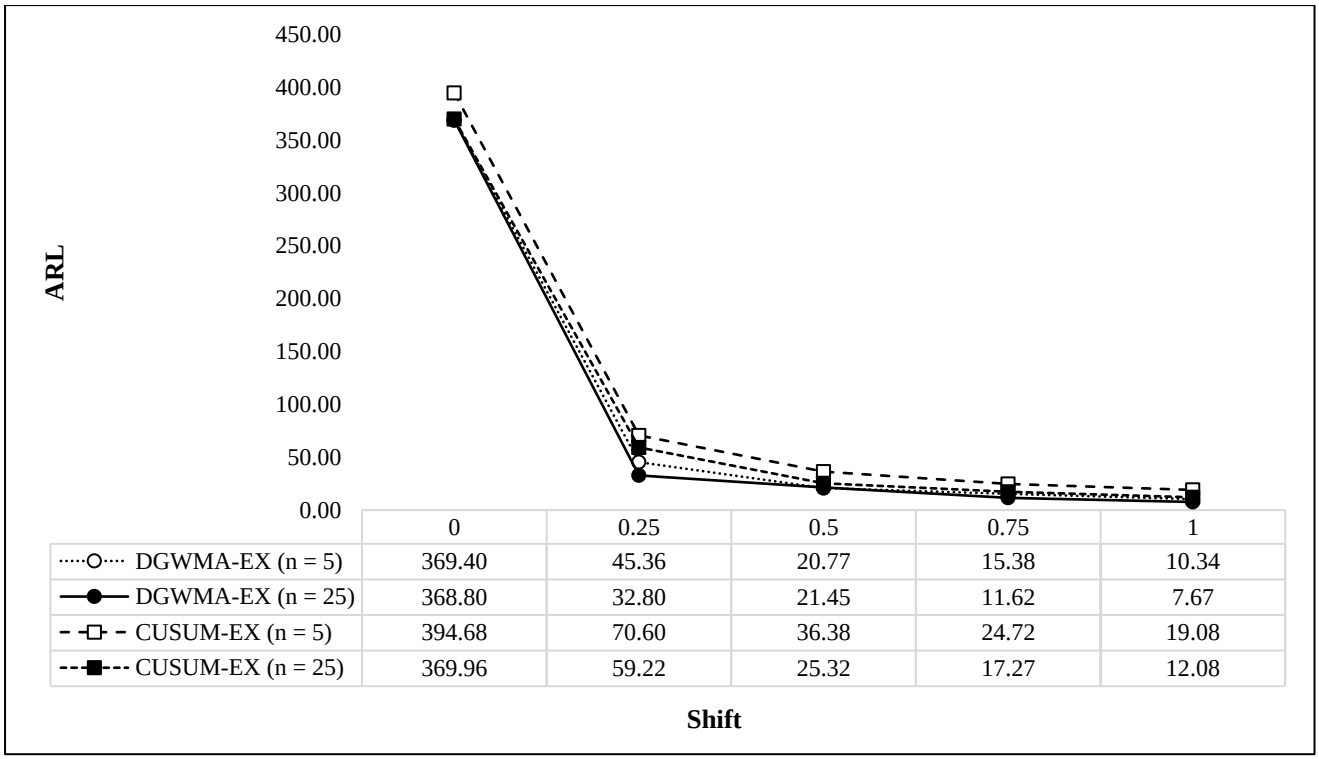

	0	0.25	0.5	0.75	1
DGWMA-EX (n = 5)	369.40	45.36	20.77	15.38	10.34
DGWMA-EX (n = 25)	368.80	32.80	21.45	11.62	7.67
CUSUM-EX (n = 5)	394.68	70.60	36.38	24.72	19.08
CUSUM-EX (n = 25)	369.96	59.22	25.32	17.27	12.08

Figure 4.16. Comparison between the DGWMA-EX chart and the CUSUM-EX chart under the standard normal distribution

From the above plot one can conclude that when the underlying process distribution is standard normal, the proposed DGWMA-EX chart outperforms the CUSUM-EX chart proposed by Graham et al. (2014) in detecting small shifts in the process. Also, in terms of the medium and large shifts, the DGMWA-EX chart is competitive with the CUSUM-EX chart. Further, Figure 4.16 includes different cases of the DGWMA-EX and the CUSUM-EX charts based on the test sample size, i.e., n. For the DGWMA-EX chart, the chart with larger test sample size outperforms the DGWMA-EX chart with smaller test sample. Also, for the CUSUM-EX chart, the larger the test sample size, the better the performance of the chart. Note that, the values for the CUSUM-EX chart are extracted from the results available in Graham et al. (2014) and the results for the DGWMA-EX chart are calculated when $m = 1000$.

Table 4.2. The IC and OOC characteristics when $n = 5, 25$, and $m = 1000$ for the $Exp\ (1)$ distribution

δ	DGWMA-EX ($n = 5$)	DGWMA-EX ($n = 25$)	CUSUM-EX ($n = 5$)	CUSUM-EX ($n = 25$)
0.00	368.65	372.43	384.42	370.80
0.25	42.88	30.79	54.58	44.17
0.50	28.55	16.58	26.24	19.13
0.75	18.98	9.43	16.67	12.01
1.00	12.51	7.61	11.92	8.85

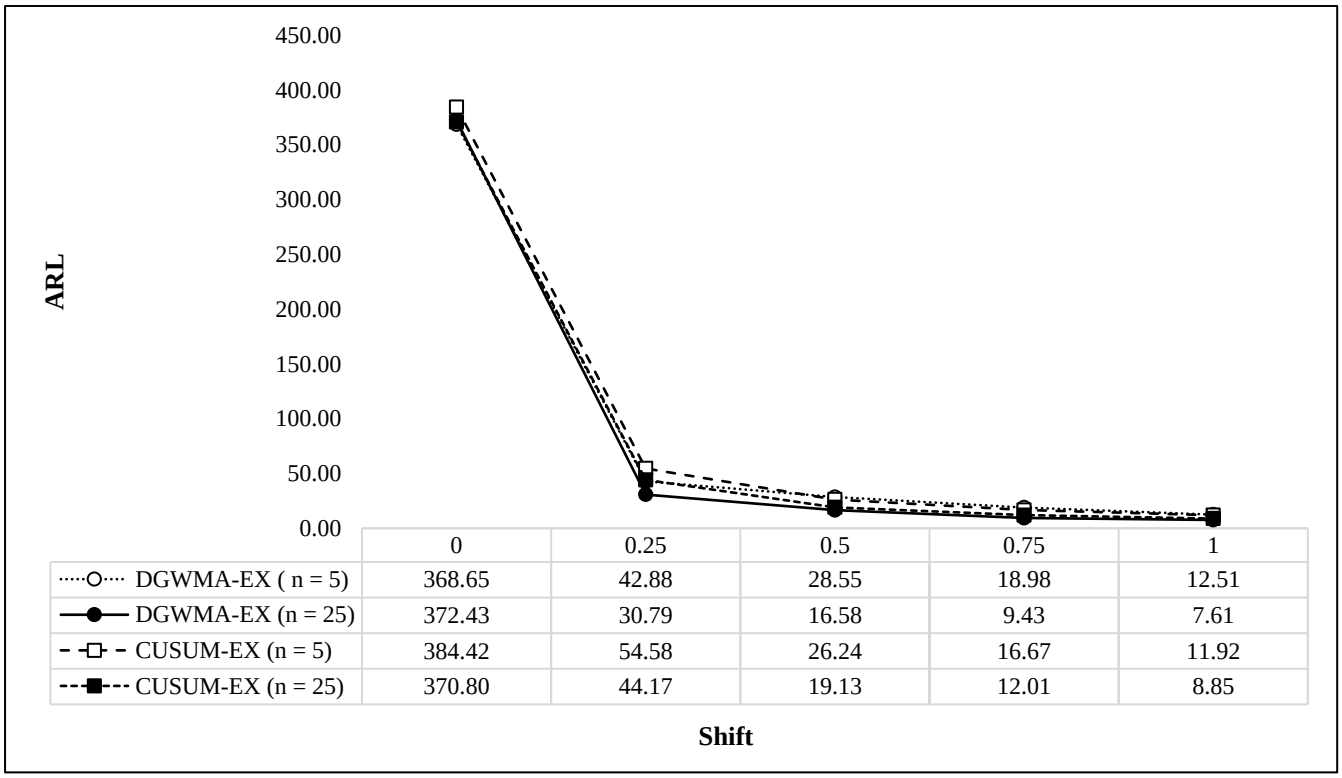

	0	0.25	0.5	0.75	1
DGWMA-EX (n = 5)	368.65	42.88	28.55	18.98	12.51
DGWMA-EX (n = 25)	372.43	30.79	16.58	9.43	7.61
CUSUM-EX (n = 5)	384.42	54.58	26.24	16.67	11.92
CUSUM-EX (n = 25)	370.80	44.17	19.13	12.01	8.85

Figure 4.17. Comparison between the DGWMA-EX chart and the CUSUM-EX chart under the exponential distribution

The performance of the proposed DGWMA-EX for test sample size $n = 5$ and $n = 25$ is compared with CUSUM-EX chart for the same set of test sample. The DGWMA-EX chart outperformed the CUSUM-EX chart in detecting small shifts in the process, when the underlying process distribution is exponential. Note that, the definition of the small shift size is all the shifts in the following interval $0.25 \leq \delta \leq 0.5$. Also, charts with large test sample size, i.e., $n = 25$, performs better than small test sample size, i.e., $n = 5$.

Table 4.3. The IC and OOC characteristics when $n = 5, 25$, and $m = 1000$ for the $Gamma(3, 1)$ distribution

δ	DGWMA-EX ($n = 5$)	DGWMA-EX ($n = 25$)	CUSUM-EX ($n = 5$)	CUSUM-EX ($n = 25$)
0.00	369.26	367.80	383.33	416.70
0.25	61.67	38.85	72.56	54.68
0.50	26.60	16.55	32.53	23.00
0.75	16.13	9.70	21.68	14.87
1.00	12.70	5.88	16.28	10.90

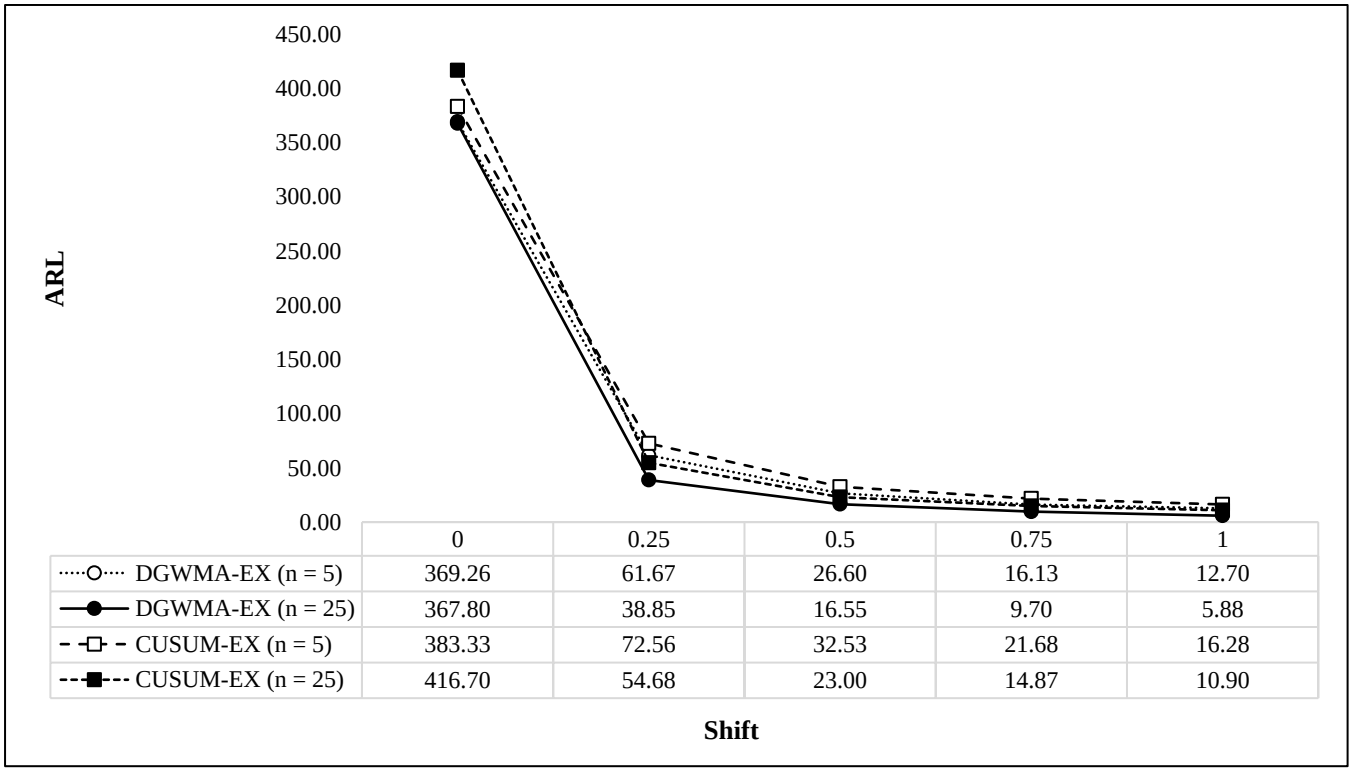

Figure 4.18. Comparison between the DGWMA-EX chart and the CUSUM-EX chart under the gamma distribution

For the gamma distribution as the underlying process distribution, the DGWMA-EX chart with $n = 25$, outperforms the CUSUM-EX chart for both test sample sizes $n = 5$ and $n = 25$ in detecting small shifts in the process. However, the CUSUM-EX chart when $n = 25$ outperforms the DGWMA-EX chart when $n = 5$. Hence, unlike the standard normal and the exponential distribution, there is a case where the CUSUM-EX chart outperforms the DGWMA-EX chart in detecting small shifts in the process.

Table 4.4. The IC and OOC characteristics when $n = 5, 25$, and $m = 1000$ for the $DE(0, 1)$ distribution

Shift	DGWMA-EX (n = 5)	DGWMA-EX (n = 25)	CUSUM-EX (n = 5)	CUSUM-EX (n = 25)
0.00	370.27	366.54	385.70	370.72
0.25	58.35	42.87	43.10	30.07
0.50	32.68	28.23	23.99	14.37
0.75	24.45	19.58	17.45	10.09
1.00	18.76	13.56	14.07	7.83

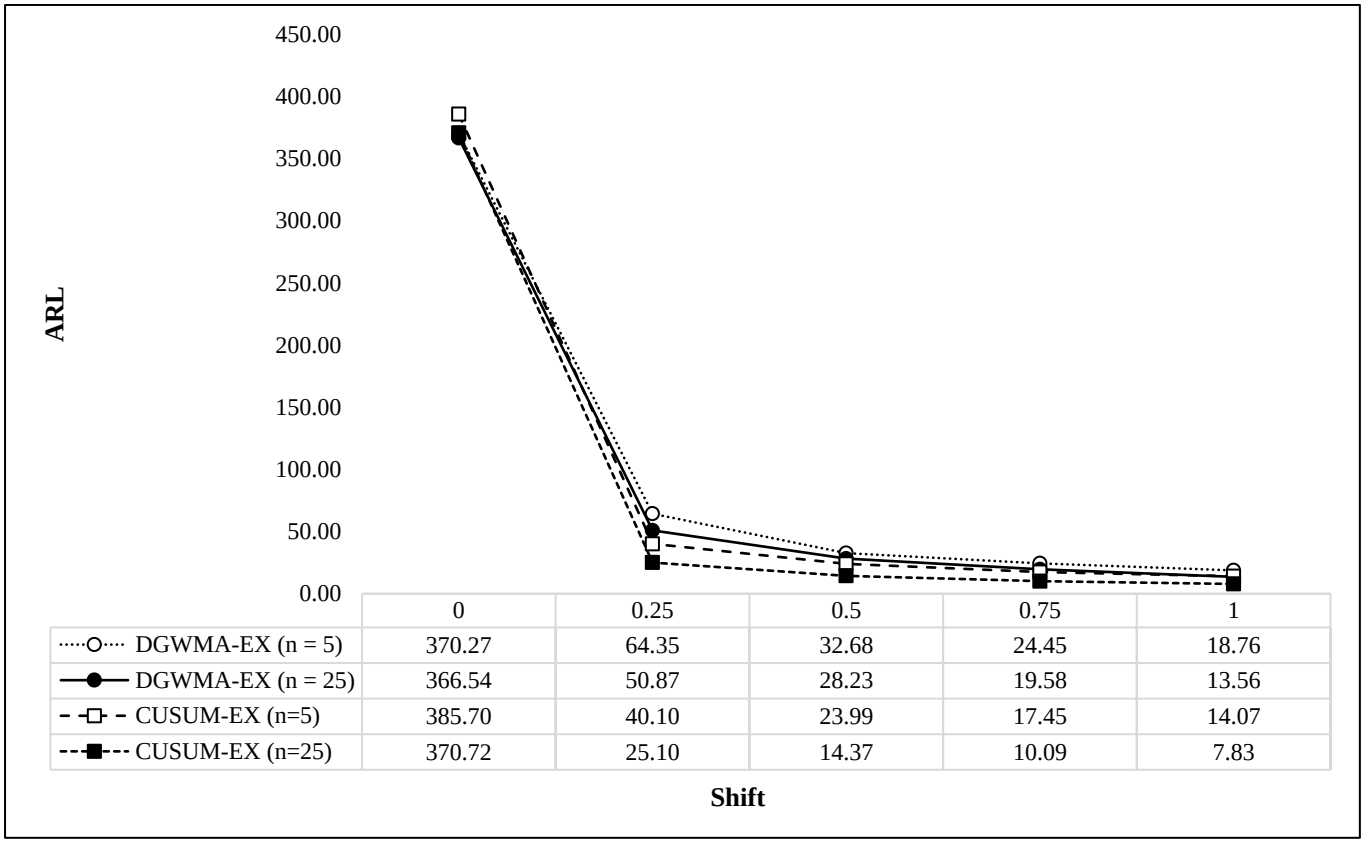

Figure 4.19. Comparison between the DGWMA-EX chart and the CUSUM-EX chart under the double exponential distribution

From the above plot one can conclude that when the underlying process distribution is double exponential, the CUSUM-EX chart proposed by Graham et al. (2014) outperformed the DGWMA-EX chart in detecting small, medium, and large shifts in the process. Note that, the CUSUM-EX outperformed the DGWMA-EX chart for both test sample size $n = 5$ and $n = 25$.

Also, since the run length distribution is significantly right skewed, researchers have advocated using other measures for the assessment of a chart's performance, more specifically, the *MDRL*, which provides more insightful information in comparison to the *ARL*. In SPC, the idea of considering other

percentiles of the run length distribution, is discussed by Barnard (1959), Gan (1994), Chakraborti et al. (2007) and Khoo et al. (2011). The comparison is conducted between the DGWMA-EX chart (Case 1 and Case 2) and the CUSUM-EX chart. The reference sample and the test sample are selected as $m = 100$ and $n = 5$, respectively. Also, the CUSUM-EX charts included in the comparative study are based on three different values for the reference value, i.e., d. The pre-specified value for the *MDRL* is selected as 350. The IC and OOC characteristics of the run length are as follows:

Table 4.5. The IC and OOC characteristics when $n = 5$, and $m = 100$ for the $N(0, 1)$ distribution

δ	DGWMA-EX (C1)	DGWMA-EX (C2)	CUSUM-EX ($d = 6.550$)	CUSUM-EX ($d = 14$)	CUSUM-EX ($d = 18$)
0	351.00	352.00	349.80	351.25	350.10
0.25	197.10	184.65	236.00	203.00	218.00
0.5	67.52	52.96	129.00	79.00	64.00
0.75	44.45	35.31	73.00	41.00	30.00
1	18.75	15.25	41.00	27.00	18.00

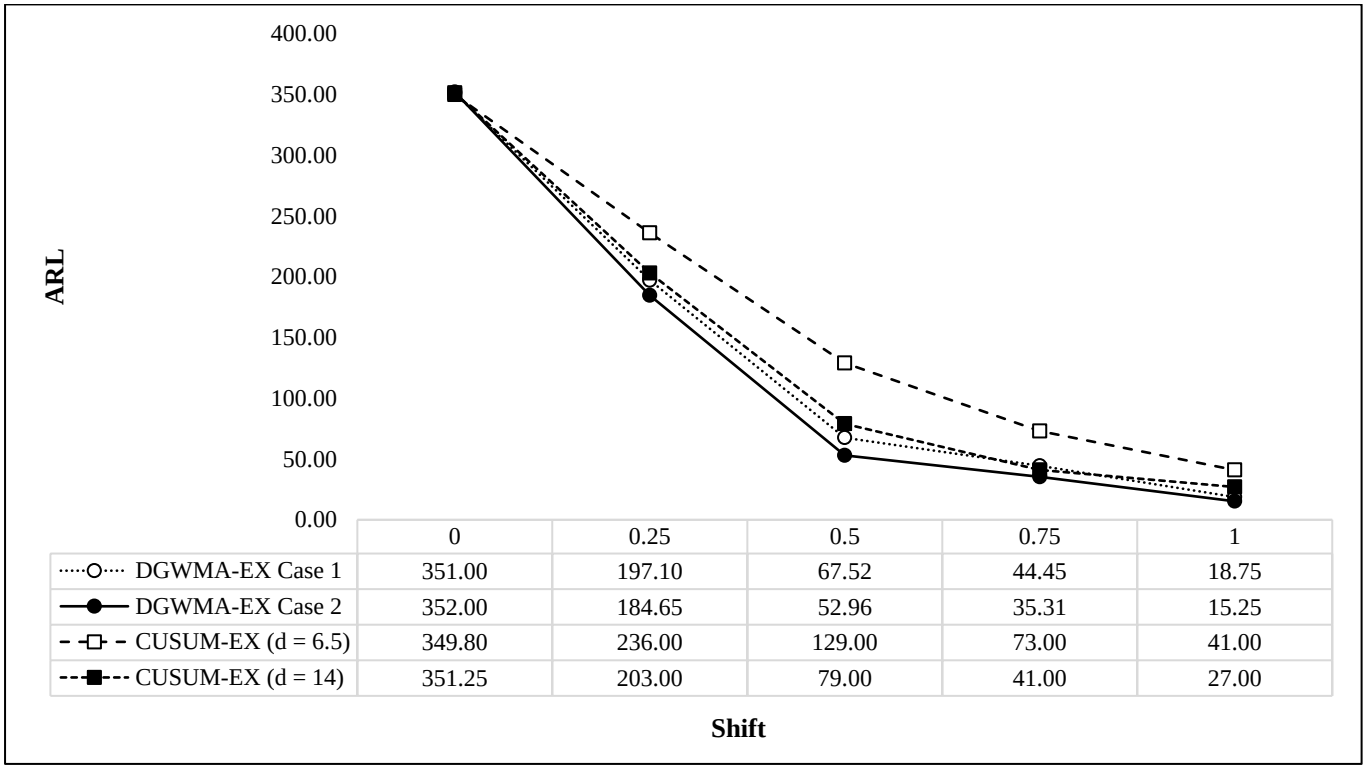

Figure 4.20. Comparison between the DGWMA-EX chart and the CUSUM-EX chart under the standard normal distribution

From Figure 4.20, one can conclude that both cases of the DGWMA-EX chart outperform the CUSUM-EX chart in detecting small shifts in the process. For the CUSUM-EX chart, for large reference value, i.e., d, the chart performs better in comparison with the small reference value. Note that, in this comparison, the *MRL* is used as the performance metric.

Table 4.6. The IC and OOC characteristics when $n = 5$, and $m = 100$ for the $Exp(1)$ distribution

δ	DGWMA-EX (C1)	DGWMA-EX (C2)	CUSUM-EX ($d = 6.550$)	CUSUM-EX ($d = 14$)	CUSUM-EX ($d = 18$)
0	353.00	350.00	353.50	355.20	351.22
0.25	135.00	115.00	161.00	129.00	148.00
0.5	32.00	24.00	65.00	34.00	36.00
0.75	13.00	12.00	27.00	14.00	15.00
1	7.82	7.00	10.00	7.00	8.00

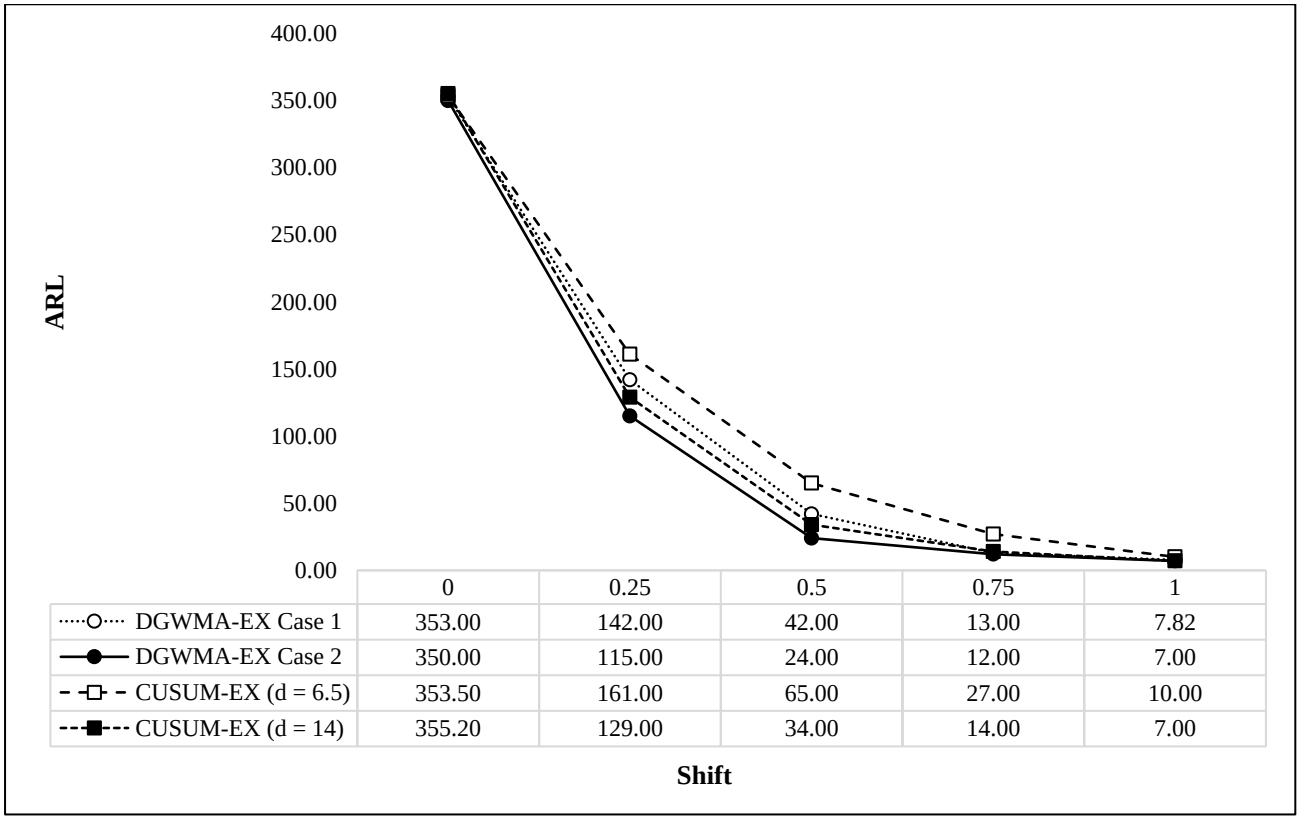

Figure 4.21. Comparison between the DGWMA-EX chart and the CUSUM-EX chart under the exponential distribution

The DGWMA-EX chart (Case 2) outperforms the CUSUM-EX chart with reference values $d = 6.5$ and $d = 14$, in detecting small shifts in the process when the underlying process distribution is exponential. However, the CUSUM-EX chart outperforms the DGWMA-EX chart (Case 1) in detecting

small shifts in the process. Also, by increasing the value for the reference parameter for the CUSUM-EX chart, the performance of the chart improves.

Table 4.7. The IC and OOC characteristics when $n = 5$, and $m = 100$ for the $Gamma(3, 1)$ distribution

δ	DGWMA-EX (C1)	DGWMA-EX (C2)	CUSUM-EX ($d = 6.550$)	CUSUM-EX ($d = 14$)	CUSUM-EX ($d = 18$)
0	349.00	352.00	358.35	351.29	350.00
0.25	145.00	135.00	203.00	180.00	190.00
0.5	37.50	40.00	104.00	60.00	52.00
0.75	20.00	16.00	53.00	29.00	23.00
1	13.00	14.00	27.00	17.00	13.00

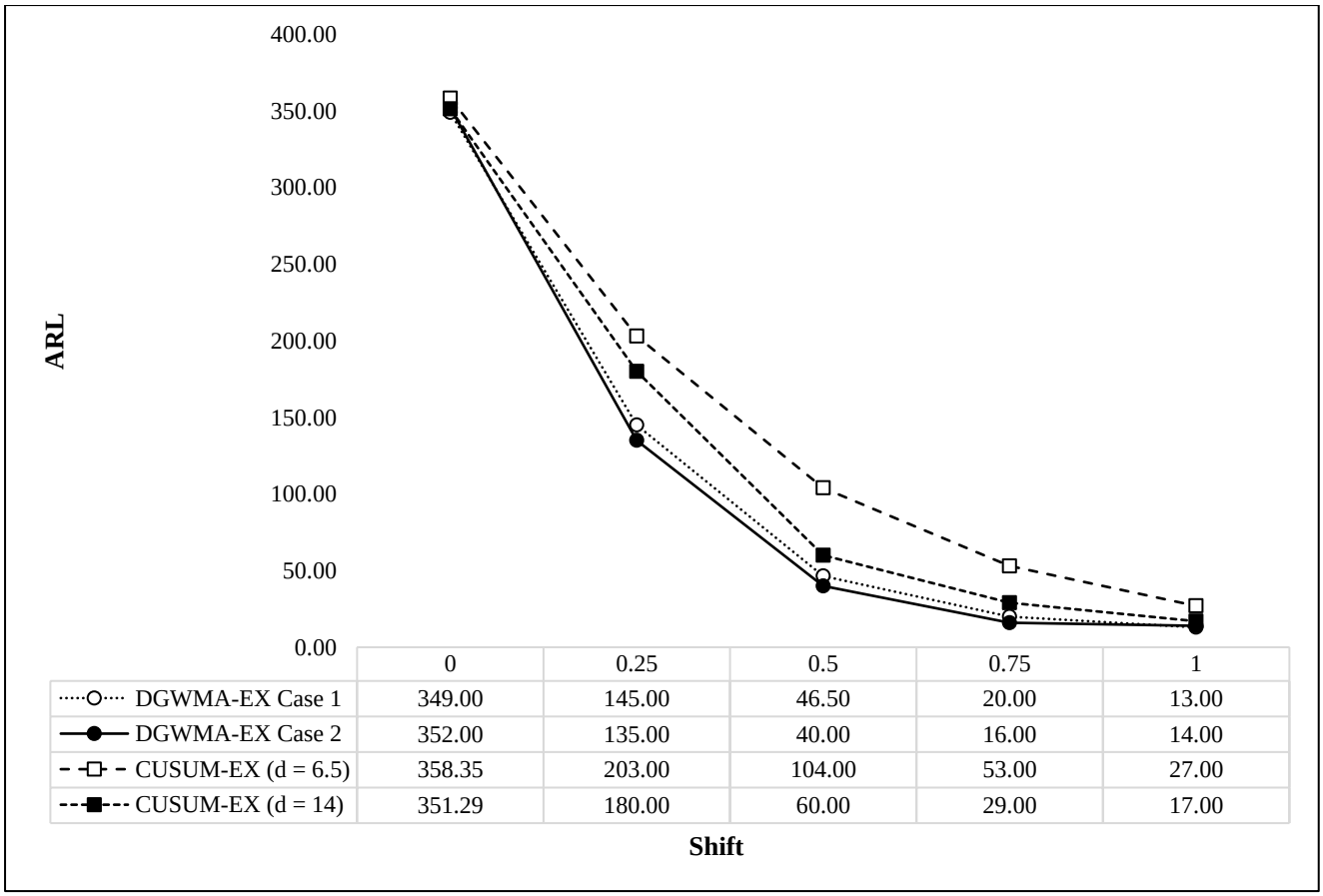

Figure 4.22. Comparison between the DGWMA-EX chart and the CUSUM-EX chart under the gamma distribution

In Figure 4.22, the performance of the DGWMA-EX chart (Case 1 and Case 2) is compared with the CUSUM-EX chart when the underlying process distribution is gamma. From the graph, one can conclude that, both cases of the proposed DGWMA-EX chart outperform the CUSUM-EX chart in detecting small to medium shifts in the production processes. Further, the DGWMA-EX chart (Case 2) outperforms the DGWMA-EX chart (Case 1) in detecting small shifts in the process.

Table 4.8. The IC and OOC characteristics when $n = 5$, and $m = 100$ for the $DE(0, 1)$ distribution

δ	DGWMA-EX (C1)	DGWMA-EX (C2)	CUSUM-EX ($d = 6.550$)	CUSUM-EX ($d = 14$)	CUSUM-EX ($d = 18$)
0	350.00	350.10	352.55	350.00	351.90
0.25	38.00	40.00	120.00	98.00	126.00
0.5	16.00	20.50	54.00	29.00	32.00
0.75	12.00	12.65	32.00	17.00	17.00
1	12.00	10.00	18.00	12.00	11.00

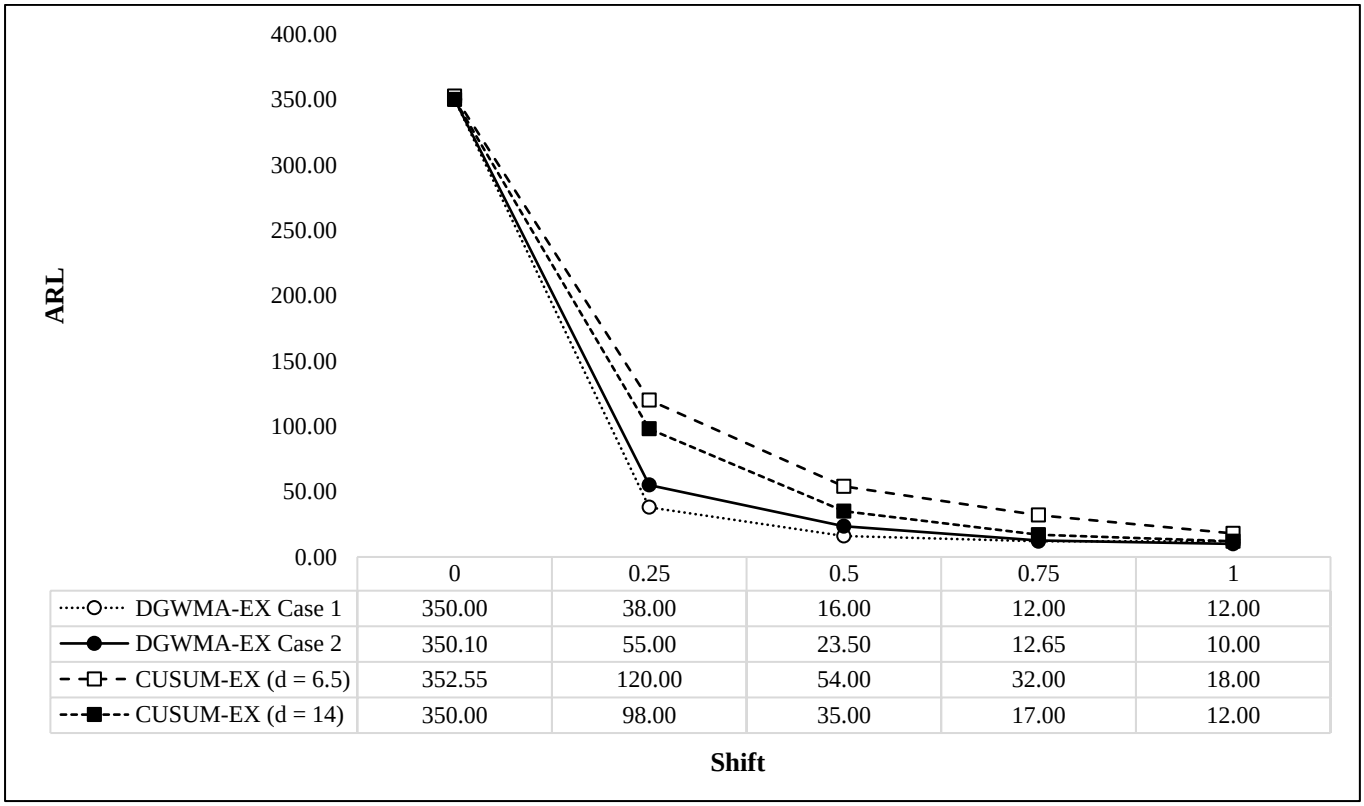

	0	0.25	0.5	0.75	1
DGWMA-EX Case 1	350.00	38.00	16.00	12.00	12.00
DGWMA-EX Case 2	350.10	55.00	23.50	12.65	10.00
CUSUM-EX (d = 6.5)	352.55	120.00	54.00	32.00	18.00
CUSUM-EX (d = 14)	350.00	98.00	35.00	17.00	12.00

Figure 4.23. Comparison between the DGWMA-EX chart and the CUSUM-EX chart under the double exponential distribution

The DGWMA-EX chart (Case 1 and Case 2) are compared with the CUSUM-EX chart when the underlying process distribution is double exponential. From Figure 4.23, one can conclude that, the

proposed DGWMA-EX chart (Case 1) outperforms the CUSUM-EX chart in detecting small shifts in the process. Also, the DGWMA-EX chart (Case 2) outperforms the CUSUM-EX chart in detecting small shifts.

As a conclusion and based on the results provided in this section, the proposed DGWMA-EX chart outperforms the CUSUM-EX chart in detecting small shifts in the process. Also, Lu (2018) whom developed the nonparametric DGWMA chart under sign statistic, concluded that the DGWMA chart not only perform quite favourably but provides a good alternative to the CUSUM mean chart when the underlying process distribution is unknown and in detecting small process shifts. Hence, our findings in the comparative study between the DGWMA-EX chart and the CUSUM-EX chart corresponds to the conclusions obtained by Lu (2018).

Other characteristics of the run length distribution, including the standard deviation (denoted by *SDRL*) and percentile points (denoted by P_i), where i = 5, 25, 50, 75, 95 might be of interest for the practitioners, are also calculated and available in the Appendix.

In practice, one could select an r^{th} order statistic from the Phase I sample, other than considering the median. Hence, a comparative study was conducted for the DGWMA-EX chart (Case 1 and Case 2) and its limiting and special cases using the 75th and 25th percentiles. For $X_{(r)} = 25^{th}$ percentile, the run length distribution encounters bias, that is ARL_1 is greater than ARL_0, which makes the performance of the control chart worse than in the median case. For $X_{(r)} = 75^{th}$ percentile, there is a considerable improvement in terms of the run length distribution for each choice of design parameters $(q_1, q_2, \alpha_1, \alpha_2, L)$ and shift size δ. The relative results are presented for the DGWMA-EX chart (Case 2) in Table A.4.11, the DGWMA-EX chart (Case 1) in Table A.4.12, the GWMA-EX and EWMA-EX charts in Table A.4.13, the DEWMA-EX chart (Case 1) in Table A.4.14, and the DEWMA-EX chart (Case 2) in Table A.4.15 when $m = 49$ and $n = 5$. All of tables listed here are presented in the Appendix for Chapter 4.

A performance study for the DGWMA-EX chart based on the median run length (*MDRL*) is also performed by taking $X_{(r)}$ as the 75th, 50th and 25th percentiles. The reference sample size is taken as $m = 100$, the test sample size is taken as $n = 5$, and a typical value for the *MDRL* is taken as $MRL_0^* = 350$. For m, n and (q, α). L values are obtained so that the attained $MRL_0^* = 350$, when $X_{(r)}$ is selected as the 75th, 50th and 25th percentiles. These results are reported in Table A.4.16 for the DGWMA-EX chart (Case 2), Table A.4.17 for the DGWMA-EX chart (Case 1), Table A.4.18 for the GWMA-EX and EWMA-EX charts, Table A.4.19 for the DEWMA-EX chart (Case 1), and Table 4.20 for the DEWMA-EX chart (Case 2), and show similar results as the *ARL* study. When $X_{(r)}$ is selected as the 25th percentile, it has a poorer performance than $X_{(r)} = 50^{th}$ percentile, and the problem of bias in the run length

distribution remains a major issue. Hence, there is no significant improvement observed in the performance of these nonparametric charts when the study is based on the *MDRL*.

In conclusion, the median is known to be a better percentile whenever the direction of the shift to be detected is not specified and is thus recommended to practitioners.

The DGWMA charts are more sensitive and detect a shift quicker than its main time-weighted counterpart, the GWMA chart, in the case of a small or tiny shift – for examples, see Huang et al. (2014), Lu (2018), Sheu and Hsieh (2009), and the references therein. Therefore, it is logical to compare the OOC performance of the proposed DGWMA-EX chart with the DGWMA-$\bar{X}$, GWMA-$\bar{X}$, DGWMA-EX (Case 2), DEWMA-EX (Case 1), DEWMA-EX (Case 2), GWMA-EX and EWMA-EX charts under the normal and various non-normal distributions when the parameter of interest is unknown (Case U). To this end, three non-normal symmetric (around zero) process distributions are considered. which have heavier or lighter tails than the normal distribution. The logistic (0, $\sqrt{3}/\pi$) distribution, the uniform (-$\sqrt{3}$, $\sqrt{3}$) distribution, and the Laplace (0, 1/$\sqrt{2}$) distribution were considered. The parameters of these distribution are selected in such a manner that the variance is 1, which makes the results comparable across different distributions. For skewed distributions, the gamma distribution was considered with shape parameters 1, 2 and 3 and scale parameters set equal to 1 in each case.

The OOC performance results are summarized in the following sections.

(a) DGWMA-EX (Case 1 and Case 2) versus GWMA-EX, EWMA-EX, DEWMA-EX (Case 1 and Case 2), DGWMA-$\bar{X}$ and GWMA-$\bar{X}$ under symmetric distributions

From the results in Tables A.4.1 to A.4.10 (see Appendix for Chapter 4), it is advocated that the DGWMA-EX chart generally outperforms the GWMA-EX and EWMA-EX under the standard normal distribution. However, the rigid assumption of normality might not hold in all cases, hence it is vital to evaluate the performance of the DGWMA-EX chart under non-normal distributions. For comparison purposes, the reference sample size is taken as $m = 49$, the test sample size is $n = 5$, and the design parameters are selected as $q_1 = q_2 = q = 0.8$, $\alpha_1 = \alpha_2 = \alpha = 0.7$ and $L = 1.304$ for the DGWMA-EX chart (Case 2). Table A.4.19 illustrates that for the aforementioned combination, the DGWMA-EX chart (Case 1) performs better than the DGWMA-EX (Case 2), GWMA-EX, EWMA-EX and DEWMA-EX (Case 1 and Case 2) charts under the logistic distribution for the shift size $\delta = 0.1$. For instance, when the process follows a logistic (0, $\sqrt{3}/\pi$) distribution and shift size $\delta = 0.1$, the DGWMA-EX chart (Case 2) with parameters $q = 0.8$, $\alpha = 0.7$ and $L = 1.304$ has $ARL_1 = 306.82$; while the DGWMA-EX chart (Case 1) with parameters $q_1 = 0.8$, $q_2 = 0.9$, $\alpha_1 = 0.8$, $\alpha_1 = 1.0$ and $L = 1.342$ has $ARL_1 = 299.78$; the GWMA-EX chart with parameters $q_1 = 0.8$, $q_2 = 0.0$, $\alpha_1 = 0.7$, $\alpha_2 = 1.0$ and $L = 2.032$ has $ARL_1 = 314.89$; the EWMA-EX chart with parameters $q_1 = 0.8$, $q_2 = 0.0$, $\alpha_1 = 1.0$, $\alpha_2 = 1.0$ and $L = 2.249$ has $ARL_1 = 316.07$; the DEWMA-EX chart (Case 1) with

parameters $q_1 = 0.8$, $q_2 = 0.9$, $\alpha_1 = 1.0$, $\alpha_2 = 1.0$ and $L = 1.460$ has $ARL_1 = 310.28$; and the DEWMA-EX chart (Case 2) with parameters $q_1 = 0.8$, $q_2 = 0.8$, $\alpha_1 = 1.0$, $\alpha_2 = 1.0$ and $L = 1.755$ has $ARL_1 = 324.90$. When the process follows a uniform (-$\sqrt{3}$, $\sqrt{3}$) distribution assuming a shift size of $\delta = 0.25$, the DGWMA-EX chart (Case 2) with parameters $q = 0.8$, α =0.7 and $L = 1.304$ has $ARL_1 = 235.28$; the DGWMA-EX chart (Case 1) with parameters $q_1 = 0.8$, $q_2 = 0.9$, $\alpha_1 = 0.8$, $\alpha_2 = 1.0$ and $L = 1.342$ has $ARL_1 = 245.75$; the GWMA-EX chart with parameters $q_1 = 0.8$, $q_2 = 0.0$, $\alpha_1 = 0.7$, $\alpha_2 = 1.0$ and $L = 2.032$ has $ARL_1 = 251.50$; the EWMA-EX chart with parameters $q_1 = 0.8$, $q_2 = 0.0$, $\alpha_1 = 1.0$, $\alpha_2 = 1.0$ and $L = 2.249$ has $ARL_1 = 255.67$; the DEWMA-EX chart (Case 1) with parameters $q_1 = 0.8$, $q_2 = 0.9$, $\alpha_1 = 1.0$, $\alpha_2 = 1.0$ and $L = 1.460$ has $ARL_1 = 245.56$; and the DEWMA-EX chart (Case 2) with parameters $q_1 = 0.8$, $q_2 = 0.8$, $\alpha_1 = 1.0$, $\alpha_2 = 1.0$ and $L = 1.755$ has $ARL_1 = 258.60$. For the Laplace (0, 1/$\sqrt{2}$) distribution and same set of parameters considered for the logistic and uniform distributions and shift size $\delta = 0.05$, the OOC ARL (ARL_1) is 319.88, 321.56, 327.60, 333.09, 328.95 and 327.45 for the DGWMA-EX (Case 2), DGWMA-EX (Case 1), GWMA-EX, EWMA-EX, DEWMA-EX (Case 1) and DEWMA-EX (Case 2) charts, respectively.

Similarly, to Sheu and Lin (2003), a comparative study was conducted to compare the performance of the DGWMA-EX chart with the DGWMA-$\bar{X}$ and GWMA-$\bar{X}$ charts under the assumption of an underlying normal distribution specifically for Case U.

The parameters for all of the time-weighted control charts included in the comparative analysis are taken to be the same, since the main intention is to see whether the same parameter combination provides similar robust performance under different non-normal symmetric distributions, when $\bar{X}$ is replaced by the EX in the DGWMA chart. The mechanism for designing parametric control charts for Case U is to use an IC Phase I sample and obtaining the estimates for the unknown process parameters. Thereafter, these estimates will be used to calculate the control limits and studying the performance of the run length characteristics. Table 4.21 reveals that, under the normality assumption, the DGWMA-$\bar{X}$ chart outperforms the DGWMA-EX, GWMA-EX, EWMA-EX and DEWMA-EX charts. This is an expected outcome since the DGWMA-$\bar{X}$ chart is designed under the normality assumption. However, when the process distribution departs from normality, the behavior of the DGWMA-$\bar{X}$ chart is influenced and its attained ARL_0 starts moving further from the standard value of 370. This does not hold for the logistic distribution since the IC *ARL* does not depart that further from 370 when the underlying process distribution is not normal. For this specific distribution, the attained ARL_0 for DGWMA-$\bar{X}$ chart is 367.04; whereas for the uniform and the Laplace distributions, the attained ARL_0 is 396.90 and 391.43, respectively. On the contrary, the nonparametric counterpart proposed in this chapter, the DGWMA-EX chart is IC robust under non-normality. Hence, when the underlying process distribution

is either unknown or cannot be identified, the DGWMA-EX chart is a better alternative since it is IC robust under non-normality, whereas the DGWMA-$\bar{X}$ chart is non-robust.

Furthermore, the robust IC and OOC performances for the DGWMA-EX chart under the symmetric non-normal distributions, i.e., the logistic distribution, the uniform distribution, and the Laplace distribution, as well as the standard normal distribution are presented in Figure 4.24.

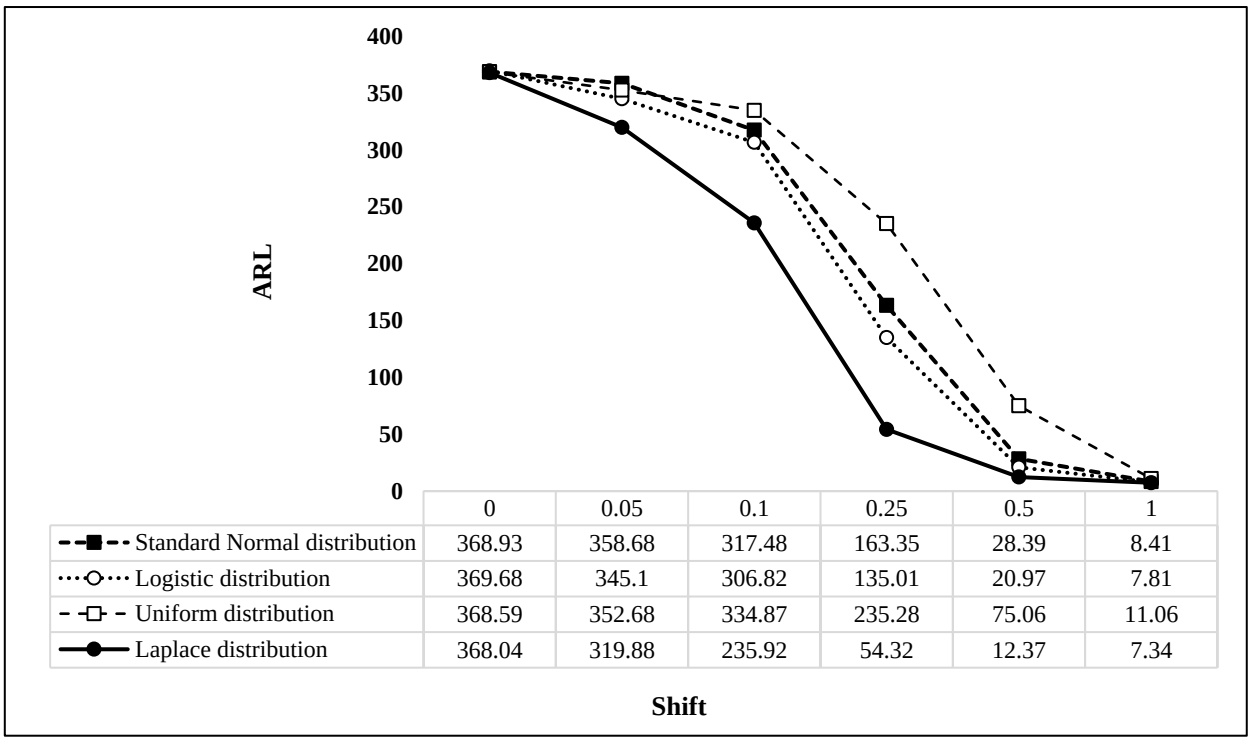

	0	0.05	0.1	0.25	0.5	1
Standard Normal distribution	368.93	358.68	317.48	163.35	28.39	8.41
Logistic distribution	369.68	345.1	306.82	135.01	20.97	7.81
Uniform distribution	368.59	352.68	334.87	235.28	75.06	11.06
Laplace distribution	368.04	319.88	235.92	54.32	12.37	7.34

Figure 4.24. The DGWMA-EX chart under different symmetric distributions

The parameter values for the DGWMA-EX chart are selected as $q = 0.8$ and $\alpha = 0.7$. Note that the main logic behind the above plot is to illustrate the IC and OOC robustness for the DGWMA-EX chart under the standard normal and non-normal distributions.

(b) DGWMA-EX (Case 1 and Case 2) versus GWMA-EX, EWMA-EX, DEWMA-EX (Case 1 and Case 2), DGWMA-$\bar{X}$ and GWMA-$\bar{X}$ under skewed distributions

In this section, the performance of the DGWMA-EX, GWMA-EX, EWMA-EX, DEWMA-EX, DGWMA-$\bar{X}$ and GWMA-$\bar{X}$ charts are studied for the underlying skewed distributions. For this purpose, the Gamma (k, θ) distribution is considered as the underlying model and the p.d.f. is given in equation (3.1).

For a given value of the shape parameter k, the scale parameter θ would change in mean and variance. Hence, for the gamma distribution, it is not possible to assume mean 0 and variance 1 as in the comparative study pertaining to symmetric distributions.

The IC and OOC scale parameters are denoted as θ_0 and θ_1, respectively. Note that, the shift for the gamma distribution is defined as $\delta = \theta_1/\theta_0$, which is different from the symmetric distributions considered in the previous section. The reason is as follows: if X ~ Gamma (k, θ), then Y = X/(θ) ~ Gamma $(k, 1)$. In other words, the IC scale parameter can be taken as 1, hence the shift, which is defined as the ratio between θ_1 and θ_0 (i.e., $\delta = \theta_1/\theta_0$), is equal to the OOC scale parameter ($\delta = \theta_1$). As a result, X/θ_1 and Y/(δ) ~ Gamma$(k, 1/(\delta))$ have the same distribution as long as the ratio δ stays the same. However, for the absolute difference between the IC and OOC scale parameters, which is defined as $|\theta_1 - \theta_0|$, the effect of the shift depends on the magnitude of θ_0. Therefore, considering $\theta_0 = 1$ would make the chart applicable for any IC θ_0, whereas the OOC performance differs based on different values for θ_0 and θ_1. For the IC process, the shift value is considered as 1 ($\delta = 1$); and for the OOC, the values are chosen as $\delta = 0.975, 0.95, 0.9, 0.8, 0.7$. Note that, as mentioned by Chakraborty et al. (2018) for the GWMA-$\bar{X}$ chart, the control limits used for the normal distribution in the case of the DGWMA-$\bar{X}$ chart (Case U) are inapplicable for the gamma distribution since the mean and the variance are no longer 0 and 1, respectively.

To calculate the control limits for the DGWMA-$\bar{X}$ chart, the estimation of the process mean (μ) and the standard deviation (σ) from the IC Phase I sample is required. Thereafter, these estimates – denoted by $\hat{\mu}$ and $\hat{\sigma}$ – can be used to calculate the estimated control limits. Results for the gamma distribution are presented in Table A.4.20, which reveals that the DGWMA-$\bar{X}$ is not IC robust and the issue related to the bias of the run length distribution exists. For example, for the DGWMA-$\bar{X}$ chart with $q = 0.8$, $\alpha = 0.7$, $L = 2.992$, $m = 49$ and $n = 5$ has $ARL_0 = 436.02$ for Gamma (1,1) distribution, $ARL_0 = 441.70$ for Gamma (2,1) distribution, and $ARL_0 = 432.24$ for Gamma (3,1) distribution. Furthermore, when the shape parameters $k = 1, 2, 3$, the DGWMA-EX chart (Case 2) outperforms the DGWMA-EX chart (Case 1), GWMA-EX, EWMA-EX and DEWMA-EX (Case 1 and Case 2) charts for all shift $\delta \geq 0.7$. The only exception is for case of $k = 3$ and $\delta = 0.7$, where the DEWMA-EX chart (Case 1), which is the special case of the proposed DGWMA-EX chart and also introduced in this chapter, outperforms the DGWMA-EX (Case 1 and Case 2), GWMA-EX, EWMA-EX and DEWMA-EX (Case 1) charts. The IC and OOC *ARL* performance for the DGWMA-EX chart (Case 2) under the gamma distribution with different shape parameters is presented in Figure 4.25. Based on the illustration, the DGWMA-EX chart with a larger shape parameter performs better than others.

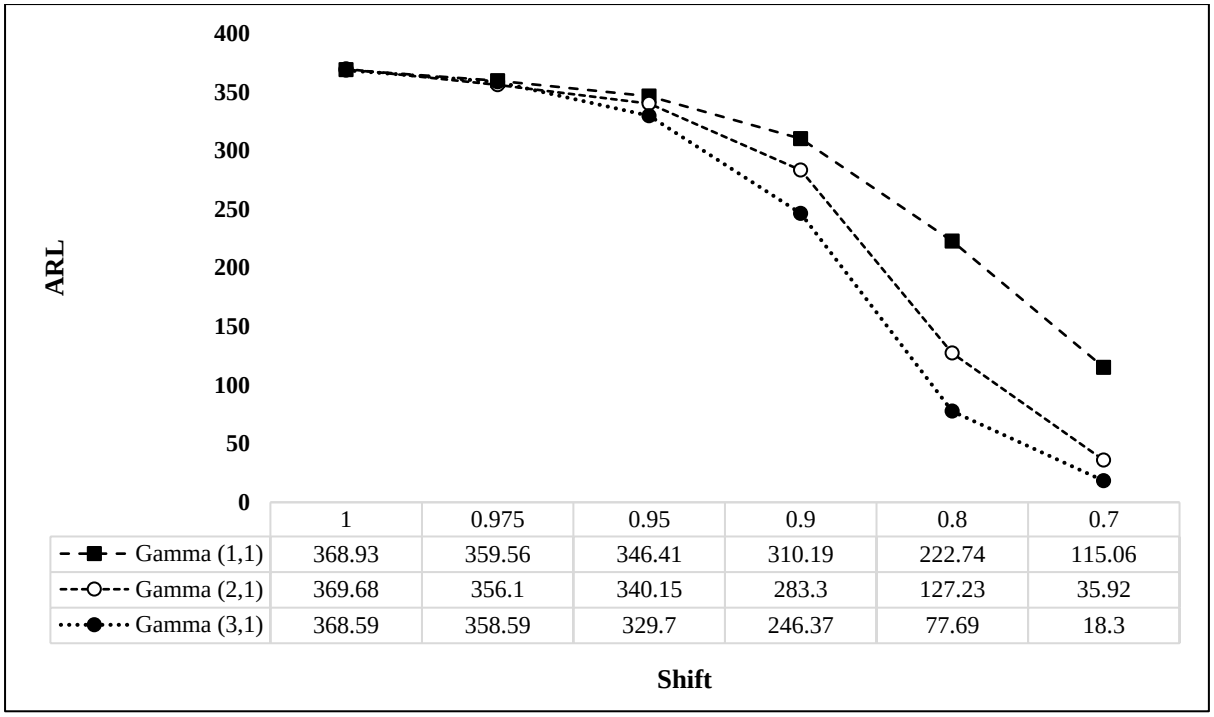

	1	0.975	0.95	0.9	0.8	0.7
Gamma (1,1)	368.93	359.56	346.41	310.19	222.74	115.06
Gamma (2,1)	369.68	356.1	340.15	283.3	127.23	35.92
Gamma (3,1)	368.59	358.59	329.7	246.37	77.69	18.3

Figure 4.25. The DGWMA-EX chart under different skewed distributions

4.11 The optimal design

The optimal design for the proposed DGWMA-EX chart would consist of specifying the desired ARL_0 and ARL_1 values, as well as the magnitude of the process shift and then selecting the combination of design parameters that provides the desired ARL_0 with the minimum ARL_1. For instance, in Table 4.1 the combination ($q = 0.8$, $\alpha = 0.7$, $L = 1.304$) has the minimum $ARL_1 = 317.48$ among the chosen range of parameters for shift size $\delta = 0.1$ when $m = 49$ and $n = 5$. Since the IC distribution of the EX is symmetric when $X_{(r)}$ is selected as the median, only the positive shifts $\delta = 0.05, 0.1, 0.25, 0.5, 0.75, 1.0, 1.5$ are considered for the OOC performance (ARL_1). The "near optimal" design consists of a combination of the design parameters (q, α, L) that yield the smallest ARL_1 for a specified shift size (δ) given the $ARL_0 = 370$. The near optimal combinations of the parameters (q, α, L) as well as the ARL_1 values for different δ, and m = 49, 99 and n = 5, 10 for the DGWMA-EX chart (Case 2) are provided in Table 4.3. For other nonparametric charts – i.e., the DGWMA-EX (Case 1), GWMA-EX, EWMA-EX and DEWMA-EX charts– the near optimal values are provided in Tables 4.9, 4.10, 4.11, 4.12 and 4.13.

Table 4.9. Near optimal (q, α, L) combinations with corresponding ARL values for the DGWMA-EX chart (Case 2)

	$m = 49$ $n = 5$				$m = 49$ $n = 10$				$m = 99$ $n = 5$				$m = 99$ $n = 10$			
δ	ARL_1	q	α	L	ARL_1	q	α	L	ARL_1	q	α	L	ARL_1	q	α	L
0.05	352.77	0.9	0.9	1.092	338.97	0.9	0.7	0.579	344.78	0.8	0.7	1.611	344.40	0.8	0.8	1.472
0.1	317.48	0.8	0.7	1.304	310.97	0.8	0.8	1.177	285.50	0.9	0.7	0.939	285.89	0.8	0.8	1.472
0.25	163.35	0.8	0.7	1.304	149.35	0.8	0.7	1.031	101.78	0.9	0.8	1.152	82.13	0.8	0.7	1.313
0.5	28.39	0.8	0.7	1.304	22.06	0.8	0.7	1.031	17.20	0.8	1.0	2.040	11.14	0.8	1.0	1.757
0.75	10.14	0.8	1.0	1.755	6.95	0.8	1.3	1.750	8.63	0.8	1.3	2.300	6.01	0.8	1.3	2.069
1.0	6.69	0.8	1.3	2.056	5.06	0.8	1.3	1.750	6.31	0.8	1.3	2.300	4.87	0.8	1.3	2.069
1.5	5.27	0.8	1.3	2.056	4.17	0.8	1.3	1.750	5.18	0.8	1.3	2.300	4.11	0.8	1.3	2.069

A quick summary of Table 4.9 reveals the following points:

- For small and tiny shifts ($\delta = 0.05, 0.1$), the combination of ($q = 0.9$, $\alpha = 0.9$ and $L = 1.092$) and ($q = 0.8$, $\alpha = 0.7$ and $L = 1.304$) provides the near optimal design for the DGWMA-EX chart when $m = 49$ and $n = 5$. A similar interpretation can be made for other combinations of the reference sample size (i.e., $m = 49, 99$) and the test sample size (i.e., $n = 5, 10$).
- The combination of ($q = 0.8$, $\alpha = 0.7$ and $L = 1.304$) provides the near optimal design when the shift size (δ) is 0.25 and 0.5, respectively, when $m = 49$ and $n = 5, 10$. For the shift size $\delta = 0.75$, the ($q = 0.8$, $\alpha = 1.0$ and $L = 1.755$) combination provides the near optimal design when $m = 49$ and $n = 5$.
- For large shifts ($\delta = 1.0, 1.5$), the combination of ($q = 0.8$, $\alpha = 1.3$ and $L = 2.056$) provides the near optimal design for all combinations of the reference sample and the test sample.
- Different combinations of the following parameter values $q = 0.8, 0.9$, and $\alpha = 0.7, 0.8, 0.9, 1.0, 1.3$, provide the near optimal design for the DGWMA-EX chart dependent on the size for the reference sample and the test sample.

Table 4.10. Near optimal $(q_1, q_2, \alpha_1, \alpha_2, L)$ combinations with corresponding ARL values for the DGWMA-EX chart (Case 1)

	$m = 49$ $n = 5$				$m = 49$ $n = 10$				m = 99 n = 5				$m = 99$ $n = 10$			
	ARL_1	q_1, q_2	α_1, α_2	L	ARL_1	q_1, q_2	α_1, α_2	L	ARL_1	q_1, q_2	α_1, α_2	L	ARL_1	q_1, q_2	α_1, α_2	L
0.05	344.88	0.9, 0.95	0.7, 0.8	0.627	333.94	0.8, 0.95	0.7, 1.0	0.790	339.95	0.9, 0.95	0.7, 1.3	1.198	332.25	0.9, 0.95	0.9, 1.3	1.180
0.1	311.95	0.8, 0.95	0.8, 1.0	1.069	313.08	0.8, 0.9	0.7, 1.3	1.157	283.49	0.9, 0.95	0.7, 0.8	0.786	275.7	0.9, 0.95	0.9, 1.3	1.472
0.25	165.13	0.8, 0.9	0.9, 1.0	1.118	155.14	0.8, 0.95	0.7, 0.1	0.790	98.04	0.8, 0.95	0.7, 0.9	1.133	82.58	0.8, 0.9	0.7, 0.8	1.313
0.5	28.96	0.8, 0.9	0.7, 1.3	1.451	22.47	0.8, 0.9	0.9, 1.0	1.127	17.58	0.8, 0.9	0.9, 1.3	1.915	11.67	0.8, 0.9	1.0, 1.3	1.704
0.75	10.77	0.8, 0.9	1.0, 1.3	1.701	8.13	0.8, 0.9	1.0, 1.3	1.394	9.7	0.8, 0.9	1.0, 1.3	1.979	7.36	0.8, 0.9	1.0, 1.3	1.704
1.0	8.05	0.8, 0.9	1.0, 1.3	1.701	6.41	0.8, 0.9	1.0, 1.3	1.394	7.67	0.8, 0.9	1.0, 1.3	1.979	6.16	0.8, 0.9	1.0, 1.3	1.704
1.5	6.51	0.8, 0.9	1.0, 1.3	1.701	5.32	0.8, 0.95	0.7, 0.8	0.628	6.36	0.8, 0.9	1.0, 1.3	1.979	5.18	0.8, 0.9	1.0, 1.3	1.704

A quick summary of Table 4.10 reveals the following points:

- For small and tiny shifts ($\delta = 0.05, 0.1$), the combination of ($q_1 = 0.9$, $q_2 = 0.95$, $\alpha_1 = 0.7$, $\alpha_2 = 0.8$ and $L = 0.627$) and ($q_1 = 0.8$, $q_2 = 0.95$, $\alpha_1 = 0.8$, $\alpha_2 = 1.0$ and $L = 1.069$) provides the near optimal design for the DGWMA-EX chart (Case 1) when $m = 49$ and $n = 5$. A similar interpretation can be made for other combinations of the reference sample size (i.e., $m = 49$, 99) and the test sample size (i.e., $n = 5$, 10).
- The combination of ($q_1 = 0.8$, $q_2 = 0.9$, $\alpha_1 = 1.0$, $\alpha_2 = 1.3$ and $L = 1.701$) provides the near optimal design when the shift size (δ) is 0.75, 1.0, and 1.5, respectively, when $m = 49$ and $n = 5$.

Table 4.11. Near optimal $(q_1, q_2, \alpha_1, \alpha_2, L)$ combinations with corresponding ARL values for the GWMA-EX chart

	$m = 49$ $n = 5$				$m = 49$ $n = 10$				m = 99 n = 5				$m = 99$ $n = 10$			
	ARL_1	q_1, q_2	α_1, α_2	L	ARL_1	q_1, q_2	$\alpha_1., \alpha_2$	L	ARL_1	q_1, q_2	α_1, α_2	L	ARL_1	q_1, q_2	α_1, α_2	L
0.05	347.62	0.95, 0.0	0.8, 1.0	1.089	343.67	0.95, 0.0	0.8, 1.0	0.852	339.03	0.9, 0.0	0.7, 1.0	1.805	338.28	0.9, 0.0	0.8, 1.0	1.602
0.1	310.26	0.95, 0.0	0.8, 1.0	1.089	317.31	0.95, 0.0	0.8, 1.0	0.852	287.91	0.9, 0.0	0.9, 1.0	2.038	276.48	0.9, 0.0	0.9, 1.0	1.715
0.25	165.64	0.95, 0.0	0.9, 1.0	1.228	153.10	0.95, 0.0	0.7, 1.0	0.737	99.19	0.9, 0.0	0.8, 1.0	1.380	78.6	0.9, 0.0	0.9, 1.0	1.715
0.5	29.67	0.9, 0.0	1.0, 1.0	1.820	19.23	0.9, 0.0	1.0, 1.0	1.478	17.14	0.9, 0.0	1.0, 1.0	2.132	10.77	0.8, 0.0	0.9, 1.0	2.213
0.75	9.5	0.9, 0.0	1.3, 1.0	2.067	5.84	0.8, 0.0	1.3, 1.0	2.119	8.25	0.9, 0.0	1.3, 1.0	2.335	4.92	0.8, 0.0	1.3, 1.0	2.409
1.0	5.81	0.8, 0.0	1.3, 1.0	2.381	3.68	0.8, 0.0	1.3, 1.0	2.119	5.18	0.8, 0.0	1.3, 1.0	2.589	3.49	0.8, 0.0	1.3, 1.0	2.409
1.5	3.84	0.8, 0.0	1.3, 1.0	2.381	2.71	0.8, 0.0	0.7, 1.0	1.715	3.54	0.8, 0.0	1.3, 1.0	2.589	2.62	0.8, 0.0	1.3, 1.0	2.409

A quick summary of Table 4.11 reveals the following points:

- For small and tiny shifts ($\delta = 0.05, 0.1$), the combination of ($q_1 = 0.95$, $q_2 = 0.0$, $\alpha_1 = 0.8$, $\alpha_2 = 1.0$ and $L = 1.089$) provides the near optimal design for the GWMA-EX chart when $m = 49$ and $n = 5$. A similar interpretation can be made for other combinations of the reference sample size (i.e., $m = 49$, 99) and the test sample size (i.e., $n = 5$, 10).
- The combination of ($q_1 = 0.9$, $q_2 = 0.0$, $\alpha_1 = 1.3$, $\alpha_2 = 1.0$ and $L = 2.067$) provides the near optimal design when the shift size (δ) is 0.75 when $m = 49$ and $n = 5$. For shift sizes 1.0 and 1.5, ($q_1 = 0.8$, $q_2 = 0.0$, $\alpha_1 = 1.3$, $\alpha_2 = 1.0$ and $L = 2.381$) provides the near optimal design.

Table 4.12. Near optimal $(q_1, q_2, \alpha_1, \alpha_2, L)$ combinations with corresponding ARL values for the EWMA-EX chart

	$m = 49$ $n = 5$				$m = 49$ $n = 10$				m = 99 n = 5				$m = 99$ $n = 10$			
	ARL_1	q_1, q_2	α_1, α_2	L	ARL_1	q_1, q_2	α_1, α_2	L	ARL_1	q_1, q_2	α_1, α_2	L	ARL_1	q_1, q_2	α_1, α_2	L
0.05	357.90	0.9, 0.0	1.0, 1.0	1.820	353.45	0.8, 1.0	1.0, 1.0	1.943	350.08	0.95, 0.0	1.0, 1.0	1.667	339.07	0.9, 0.0	1.0, 1.0	1.817
0.1	330.96	0.95, 0.0	1.0, 1.0	1.365	324.07	0.9, 0.0	1.0, 1.0	1.478	295.54	0.95, 0.0	1.0, 1.0	1.667	284.37	0.9, 0.0	1.0, 1.0	1.817
0.25	177.20	0.95, 0.0	1.0, 1.0	1.365	159.42	0.95, 0.0	1.0, 1.0	0.737	101.53	0.95, 0.0	1.0, 1.0	1.667	85.54	0.95, 0.0	1.0, 1.0	1.362
0.5	29.67	0.9, 0.0	1.0, 1.0	1.820	19.23	0.9, 0.0	1.0, 1.0	1.478	17.14	0.9, 0.0	1.0, 1.0	2.132	10.96	0.9, 0.0	1.0, 1.0	1.817
0.75	9.76	0.8, 0.0	1.0, 1.0	2.249	6.07	0.8, 0.0	1.0, 1.0	1.943	8.32	0.8, 0.0	1.0, 1.0	2.503	5.11	0.8, 0.0	1.0, 1.0	2.272
1.0	5.95	0.8, 0.0	1.0, 1.0	2.249	3.89	0.8, 0.0	1.0, 1.0	1.943	5.58	0.8, 0.0	1.0, 1.0	2.503	3.67	0.8, 0.0	1.0, 1.0	2.272
1.5	6.21	0.95, 0.0	1.0, 1.0	1.365	2.71	0.8, 0.0	1.0, 1.0	1.943	3.88	0.8, 0.0	1.0, 1.0	2.503	2.79	0.8, 0.0	1.0, 1.0	2.272

A quick summary of Table 4.12 reveals the following points:

- For small and tiny shifts ($\delta = 0.05, 0.1$), the combination of ($q_1 = 0.9$, $q_2 = 0.0$, $\alpha_1 = 1.0$, $\alpha_2 = 1.0$ and $L = 1.820$) and ($q_1 = 0.95$, $q_2 = 0.0$, $\alpha_1 = 1.0$, $\alpha_2 = 1.0$ and $L = 1.365$) provide the near optimal design for the EWMA-EX chart when $m = 49$ and $n = 5$. A similar interpretation can be made for other combinations of the reference sample size (i.e., $m = 49, 99$) and the test sample size (i.e., $n = 5, 10$).
- The combination of ($q_1 = 0.8$, $q_2 = 0.0$, $\alpha_1 = 1.0$, $\alpha_2 = 1.0$ and $L = 1.943$) provides the near optimal design when the shift size (δ) is 0.75, 1.0, and 1.5 when $m = 49$ and $n = 10$.

Table 4.13. Near optimal $(q_1, q_2, \alpha_1, \alpha_2, L)$ combinations with corresponding ARL values for the DEWMA-EX chart (Case 1)

	$m = 49$ $n = 5$				$m = 49$ $n = 10$				m = 99 n = 5				$m = 99$ $n = 10$			
	ARL_1	q_1, q_2	α_1, α_2	L	ARL_1	q_1, q_2	α_1, α_2	L	ARL_1	q_1, q_2	α_1, α_2	L	ARL_1	q_1, q_2	α_1, α_2	L
0.05	354.34	0.7, 0.9	1.0, 1.0	1.562	342.85	0.7, 0.9	1.0, 1.0	1.257	342.37	0.6, 0.95	1.0, 1.0	1.536	335.76	0.6, 0.8	1.0, 1.0	1.245
0.1	319.09	0.7, 0.95	1.0, 1.0	1.211	318.07	0.9, 0.95	1.0, 1.0	0.806	291.61	0.6, 0.95	1.0, 1.0	1.536	284.05	0.7, 0.9	1.0, 1.0	1.563
0.25	172.53	0.6, 0.95	1.0, 1.0	1.250	154.75	0.7, 0.95	1.0, 1.0	0.956	103.77	0.6, 0.95	1.0, 1.0	1.536	84.51	0.8, 0.95	1.0, 1.0	1.145
0.5	28.97	0.7, 0.95	1.0, 1.0	1.211	20.02	0.7, 0.8	1.0, 1.0	1.577	17.27	0.7, 0.9	1.0, 1.0	1.859	10.92	0.6, 0.8	1.0, 1.0	1.998
0.75	9.74	0.6, 0.7	1.0, 1.0	2.186	5.97	0.6, 0.7	1.0, 1.0	1.879	8.21	0.6, 0.7	1.0, 1.0	2.427	5.15	0.6, 0.7	1.0, 1.0	2.187
1.0	5.90	0.6, 0.7	1.0, 1.0	2.186	4.1	0.6, 0.7	1.0, 1.0	1.879	5.52	0.6, 0.7	1.0, 1.0	2.427	3.89	0.6, 0.7	1.0, 1.0	2.187
1.5	4.29	0.6, 0.7	1.0, 1.0	2.186	3.18	0.6, 0.7	1.0, 1.0	1.879	4.2	0.8, 0.7	1.0, 1.0	2.427	3.12	0.6, 0.7	1.0, 1.0	2.187

A quick summary of Table 4.13 reveals the following points:

- For small and tiny shifts ($\delta = 0.05, 0.1$), the combination of ($q_1 = 0.7$, $q_2 = 0.9$, $\alpha_1 = 1.0$, $\alpha_2 = 1.0$ and $L = 1.562$) and ($q_1 = 0.7$, $q_2 = 0.95$, $\alpha_1 = 1.0$, $\alpha_2 = 1.0$ and $L = 1.211$) provide the near optimal design when $m = 49$ and $n = 5$.
- The combination of ($q_1 = 0.6$, $q_2 = 0.7$, $\alpha_1 = 1.0$, $\alpha_2 = 1.0$ and $L = 2.427$) provides the near optimal design when the shift size (δ) is 0.75, 1.0, and 1.5 when $m = 99$ and $n = 5$.

Table 4.14. Near optimal $(q_1, q_2, \alpha_1, \alpha_2, L)$ combinations with corresponding ARL values for the DEWMA-EX chart (Case 2)

	$m = 49$ $n = 5$				$m = 49$ $n = 10$				m = 99 n = 5				$m = 99$ $n = 10$			
	ARL_1	q_1, q_2	α_1, α_2	L	ARL_1	q_1, q_2	α_1, α_2	L	ARL_1	q_1, q_2	α_1, α_2	L	ARL_1	q_1, q_2	α_1, α_2	L
0.05	355.64	0.9, 0.9	1.0, 1.0	1.255	352.81	0.7, 0.7	1.0, 1.0	1.750	346.03	0.95, 0.95	1.0, 1.0	1.075	346.96	0.95, 0.95	1.0, 1.0	0.862
0.1	318.89	0.9, 0.9	1.0, 1.0	1.255	320.01	0.7, 0.7	1.0, 1.0	1.750	291.16	0.95, 0.95	1.0, 1.0	1.075	287.41	0.9, 0.9	1.0, 1.0	1.256
0.25	170.47	0.95, 0.95	1.0, 1.0	0.866	164.02	0.9, 0.9	1.0, 1.0	1.002	102.01	0.9, 0.9	1.0, 1.0	1.529	87.25	0.95, 0.95	1.0, 1.0	1.145
0.5	30.99	0.8, 0.8	1.0, 1.0	1.755	22.66	0.6, 0.6	1.0, 1.0	2.010	17.20	0.8, 0.8	1.0, 1.0	2.040	10.91	0.7, 0.7	1.0, 1.0	2.080
0.75	9.54	0.7, 0.7	1.0, 1.0	2.072	5.81	0.6, 0.6	1.0, 1.0	2.010	8.26	0.7, 0.7	1.0, 1.0	2.332	5.45	0.7, 0.7	1.0, 1.0	2.080
1.0	5.84	0.6, 0.6	1.0, 1.0	2.299	3.88	0.6, 0.6	1.0, 1.0	2.010	5.39	0.6, 0.6	1.0, 1.0	2.520	4.21	0.7, 0.7	1.0, 1.0	2.080
1.5	3.87	0.6, 0.6	1.0, 1.0	2.299	3.08	0.6, 0.6	1.0, 1.0	2.010	3.81	0.6, 0.6	1.0, 1.0	2.520	3.32	0.7, 0.7	1.0, 1.0	2.080

A quick summary of Table 4.14 reveals the following points:

- For small and tiny shifts ($\delta = 0.05, 0.1$), the combination of ($q_1 = 0.9$, $q_2 = 0.9$, $\alpha_1 = 1.0$, $\alpha_2 = 1.0$ and $L = 1.255$) provides the near optimal design when $m = 49$ and $n = 5$. ($q_1 = 0.7$, $q_2 = 0.7$, $\alpha_1 = 1.0$, $\alpha_2 = 1.0$ and $L = 1.750$) provides the near optimal when $m = 49$ and $n = 10$.
- The combination of ($q_1 = 0.6$, $q_2 = 0.6$, $\alpha_1 = 1.0$, $\alpha_2 = 1.0$ and $L = 2.299$) provides the near optimal design when the shift size (δ) is 1.0, and 1.5 when $m = 49$ and $n = 5$.

4.12 Illustrative example

4.12.1 Simulated data

In this section, a simulated example is presented to demonstrate the applicability of the proposed DGWMA-EX chart. A reference sample of size $m = 49$ is drawn from a standard normal (N (0,1)) distribution as a Phase I dataset to estimate the process median. Thereafter, 200 Phase II random samples of size $n = 5$ are drawn, from a N (0.25,1) distribution, which can be viewed as an OOC observation following a location shift of $\delta = 0.25$. Two sets of design parameters are used: ($q = 0.8$, $\alpha = 0.7$, $L = 1.304$) and ($q_1 = 0.8$, $q_2 = 0, \alpha_1 = 0.7$, $\alpha_2 = 1$, $L = 2.032$), as in Tables 4.1 and 4.7. The first set results in a DGWMA-EX chart, whereas the second one leads to a GWMA-EX chart. Any other combination can be chosen, although these values are chosen only for illustrative purposes. The IC ARL (ARL_0) for both charts are close to 370, which put them at an equal footing to perform a valid comparison. From Table A.4.1, the DGWMA-EX chart has an OOC ARL of 163.35; while from Table A.4.7, the GWMA-EX chart has an OOC ARL of 182.06 when $\delta = 0.25$. Control limits for the DGWMA-EX chart are obtained as UCL = 3.008 and LCL = 1.991, whereas for the GWMA-EX chart these limits are obtained as UCL = 3.437 and LCL = 1.562. The two control charts are displayed in Figure 4.26. As a conclusion, the DGWMA-EX chart detects the shift $\delta = 0.25$ (small shift) earlier than the GWMA-EX chart, which provides similar results to those presented based on the comparative study.

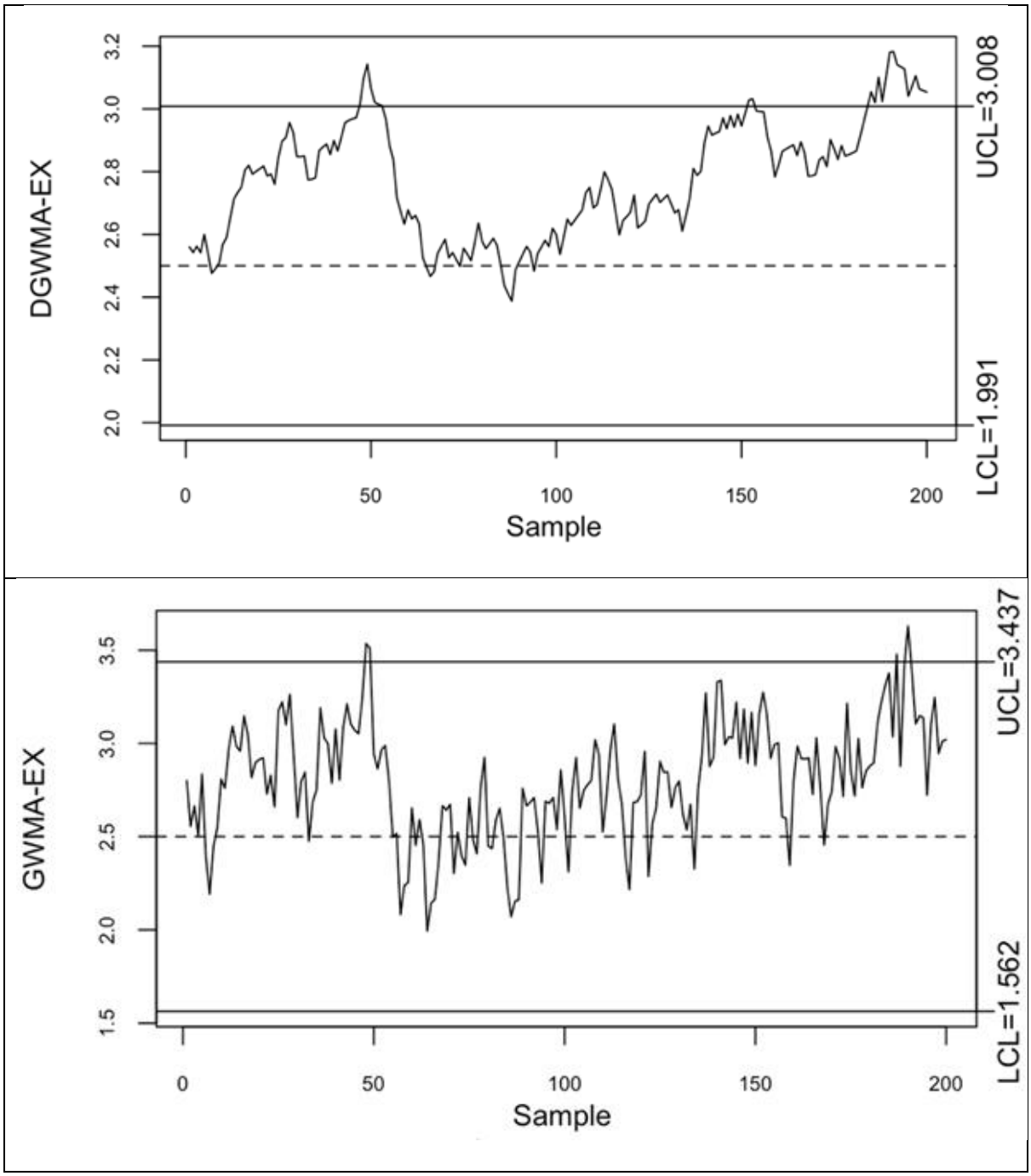

Figure 4.26. The DGWMA-EX and the GWMA-EX charts for the simulated dataset

4.12.2 Real-life data

A well-known dataset from Montgomery (2013, Table 6.3 and Table 6E.7) is considered to illustrate the application of the proposed DGWMA-EX chart. The same dataset is considered by Graham et al. (2012) and Mukherjee et al. (2013) for the nonparametric Phase II EWMA-EX and CUSUM-EX charts, respectively. This dataset is based on the inside diameters of piston rings for an automotive engine and are manufactured by a forging process. This data is also available in R software under "qcc" package (version 2.7). Twenty-five retrospective Phase I samples, each of size five, that were collected when the process was in IC is given in Table 6.3. Montgomery (2013) concluded that these data are from an IC process and hence can be assumed as Phase I reference sample. We assume that the underlying process distribution is symmetric (since a goodness of fit test for normality assumption is not rejected for this dataset). The reference sample has a median equal to 74.001.

Table 6E.7 is used to calculate the Phase II exceedance charts. This table contains fifteen prospective or Phase II samples each of five observations ($n = 5$). The desired shift to be detected was taken to be small (δ =0.25). For comparison purposes, the GWMA-EX and CUSUM-EX charts are included. For the CUSUM-EX chart we use $d = 0$ and set $h = 7.5$ for an $ARL_0 \approx 370$. The values for the parameters d and h are given by Graham et al. (2012). The lower and upper control limits for the CUSUM-EX chart are given by Graham et al. (2012) as 4.25 (-4.25,4.25). For the GWMA-EX chart and the DGWMA-EX chart, the parameters are selected as $q = 0.95$ and $\alpha = 0.7$. The control limits for the GWMA-EX chart is calculated as $LCL = 1.375$ and $UCL = 3.715$. The upper control limit and the lower control limit for the DGWMA-EX chart is calculated as $LCL = 1.105$ and $UCL = 3.835$. These charts for the Montgomery piston ring data are illustrated in the following figures:

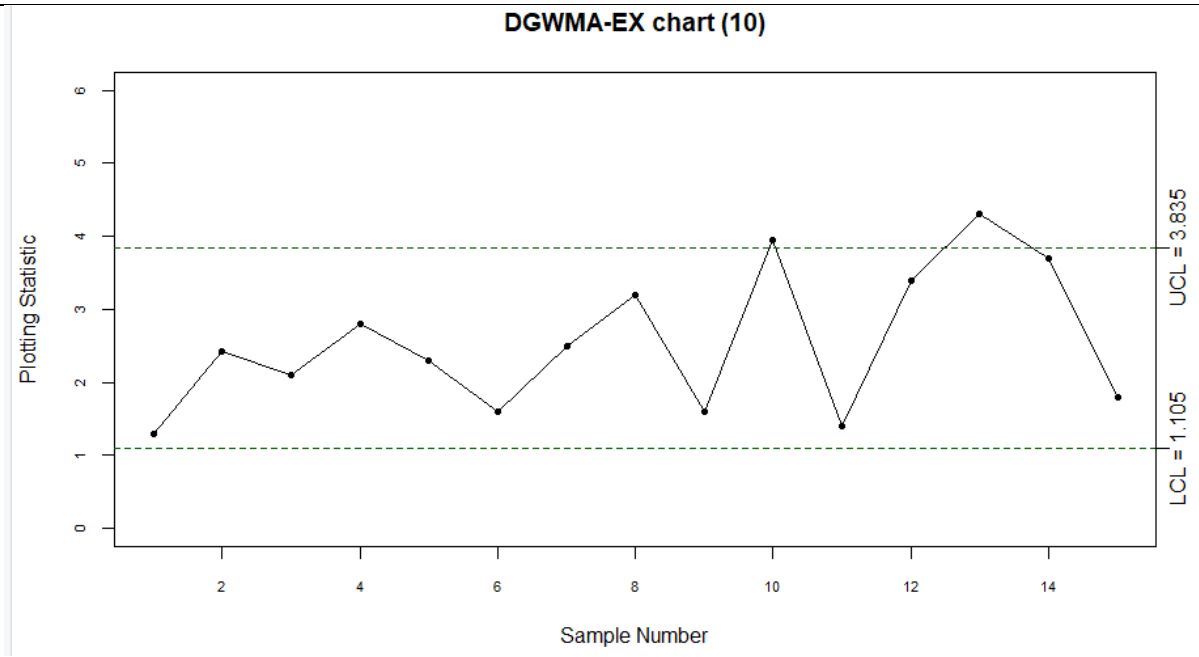

(a) DGWMA-EX chart

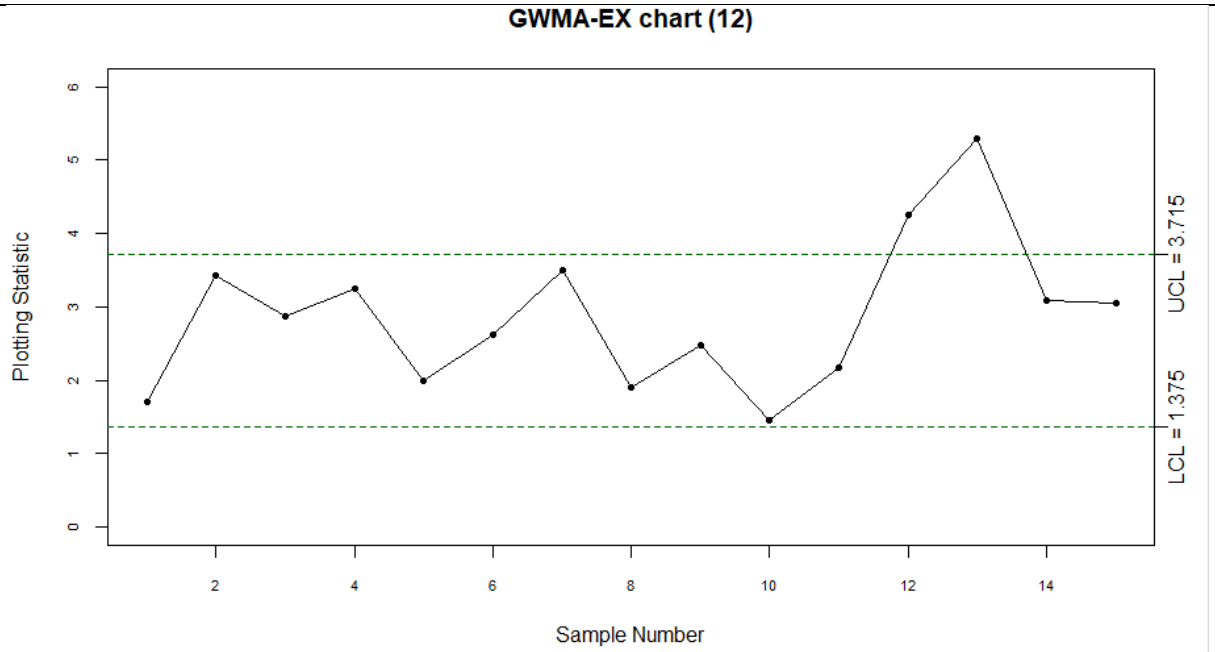

(b) GWMA-EX chart

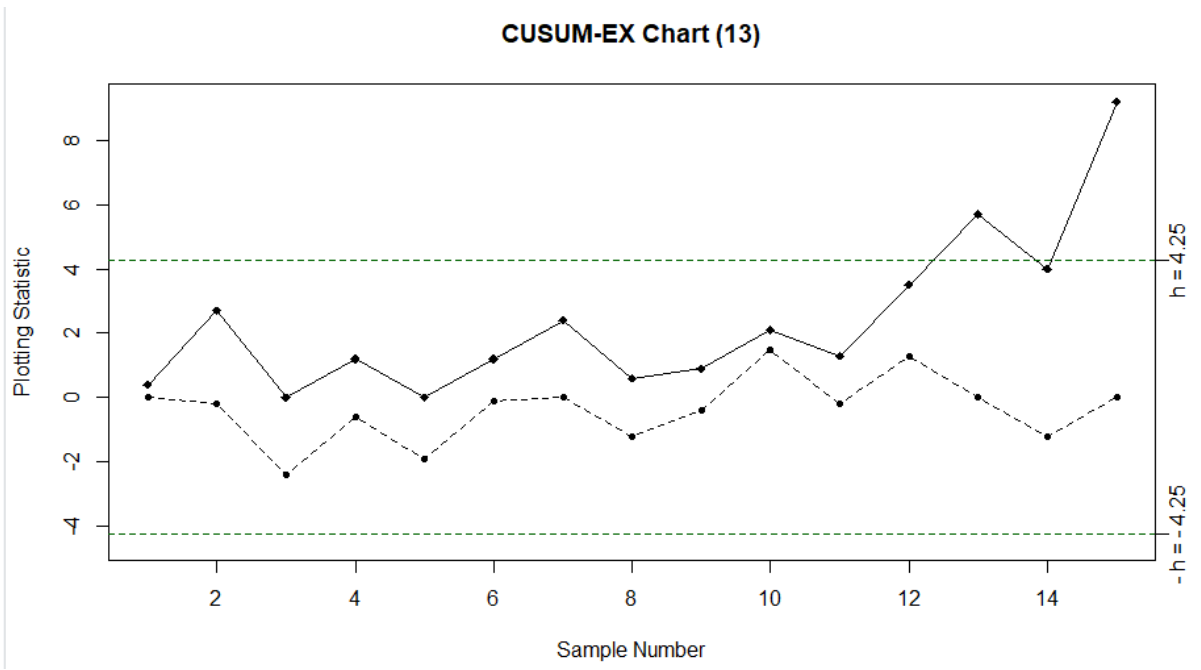

(c) CUSUM-EX chart

Figure 4.27. The DGWMA-EX (a), the GWMA-EX (b), and the CUSUM-EX (c) charts for the piston rings dataset

From the above figures, it can be observed that the DGWMA-EX chart signals first at sample number 10, whereas the CUSUM-EX chart and the GWMA-EX chart signals later at sample number 13 and sample number 12, respectively. Thus, the DGWMA-EX chart outperformed the GWMA-EX and the CUSUM-EX charts in detecting small shifts in the process.

Note that due to access restrictions and a necessity for granting special permissions, we could not use a data set from other resources.

4.13 Concluding remarks

Nonparametric control charts offer an efficient technique to monitor a process, especially if the form of the underlying distribution is unknown or not exactly specified. A new distribution-free (nonparametric) control chart based on an EX (denoted as the DGWMA-EX chart) is introduced. This chart provides a method for monitoring when no information is available in connection with the process distribution to monitor an unknown (Case U) process location parameter (median). The main advantage of the proposed nonparametric chart is that the DGWMA chart takes the sequential (time ordered) accumulation of all the information from the start until the most recent observation, and is known to be more efficient at detecting smaller shifts, as shown in this chapter. Both cases of the proposed DGWMA-EX chart (Case 1 and Case 2) are discussed and further investigated. The proposed chart can be viewed as a

generalized nonparametric time-weighted chart, which includes the GWMA-EX and EWMA-EX charts as limiting cases that already exist in the SPC literature. Further to this, the DEWMA-EX chart (Case 1 and Case 2) which is known as a special case of the proposed DGWMA-EX chart is also introduced and studied in this chapter for Case U. The closed-form expressions for the run length distribution and its characteristics are obtained for the DGWMA-EX chart through the exact approach. Also, the closed-form expressions for the run length distribution are obtained through the Markov chain method for the DEWMA-EX chart. A Monte Carlo simulation algorithm has been developed for the design and calculation of the run length distribution of the proposed DGWMA-EX chart, which can be modified for the special and limiting cases of the aforementioned chart. A comparative OOC performance analysis is performed for the proposed DGWMA-EX chart under some symmetric distributions, i.e., the logistic distribution, the Laplace distribution, the uniform distribution, and skewed distribution, i.e., the gamma distribution, and the necessary recommendations are provided for practitioners. The 25^{th} and 75^{th} percentiles have also been considered, instead of the 50^{th} percentile, to further study and investigate the behavior of the *ARL* in terms of the biasness of a control chart. Moreover, the *MDRL* has been considered as an alternative to the *ARL*, which provides similar results. The DGWMA-EX chart outperforms the GWMA-EX and the EWMA-EX charts in detecting tiny shifts in the process and provides a robust performance when the underlying process distribution is not normal.

Chapter 5 Concluding remarks and future research

High-yield or high-quality processes are in more demand nowadays since the accessibility to new technology for manufacturing purposes is increasing. Thus, to maintain the quality of a process, efficient detection of small or tiny process shifts is becoming a top priority and a mission for the quality engineers and practitioners. Control charts are the most well-known and commonly used advanced tools to maintain and monitor the quality in a manufacturing process. The Shewhart-type (memory-less) charts are frequently used in practice due to their global performance and ease of implementation, and they have a vital standing amongst practitioners. However, these types of charts are inefficient and ineffective in detecting small or tiny sustained step shifts originating from the high-yield processes. To circumvent this drawback, time-weighted (memory-type or memory-based) charts have been proposed in the context of the SPC literature. These charts sequentially accumulate information from past to present to monitor and detect a shift in the process. Sheu and Hsieh (2009) developed a generalized type of time-weighted control chart under the normal distribution, often denoted as DGWMA chart, by implementing the double or dual exponential smoothing technique proposed by Brown (1962) to enhance the performance of the GWMA chart proposed by Sheu and Lin (2003). Sheu and Hsieh (2009) conducted a comparative performance analysis and concluded that DGWMA charts have a better detection capability than the GWMA and the DEWMA charts for small or tiny shifts when the underlying process distribution is normal.

An increasing number of papers have been published in the past decade with the main focus on time-weighted charts. A bibliometric analysis has been performed in Chapter 1 (Section 1.3). Results revealed that out of the 366 articles published in this period (2009 to 2018), only 1.64% consider the DGWMA chart, which indicates the research opportunities and research gaps that exist within this domain. For recent developments of DGWMA charts, consult the work by Chiu and Lu (2015), Huang et al. (2014), Lu (2018), and Teh et al. (2011). Also, relatively very little work has been done on DGWMA control charts for Case U and when the underlying process distribution is unknown or little information is available.

In this thesis, the DGWMA chart has been viewed as a generalized type of time-weighted chart that includes the GWMA, EWMA, and Shewhart-type charts as the limiting cases, and the DEWMA chart as a special case. The DGWMA chart introduced and developed in this work considers both parametric and nonparametric scenarios. A list of some of the main contributions of the research conducted in this thesis are provided, and possible research opportunities that could be persuade in future are discussed.

- **Chapter 1** provides a brief literature review on the different types of weighting techniques available in the SPC literature, highlighting the scope and objectives of the thesis. A bibliometric metric analysis is also performed to illustrate the necessity of further research in the domain of the DGWMA chart. General guidelines and recommendations are provided for the practitioners in terms of how to use the developed charts in practice, and the chapter concludes by addressing some fundamental concepts and terminology in the SPC environment.
- **Chapter 2** consists of the preliminaries and statistical framework on the theory of the DGWMA chart as well as a detailed literature review on DGWMA charts. In general, the DGWMA chart can be classified as Case 1 and Case 2, depending on the number of parameters used in the design stage. If all four parameters of the DGWMA chart (i.e., q_1, q_2, α_1, α_2) are involved, then Case 1 is of interest; whereas when the parameters are assumed to be equal (i.e., $q_1 = q_2 = q$ and $\alpha_1 = \alpha_2 = \alpha$), Case 2 is looked at. In the SPC literature, Case 1 is neglected and dismissed frequently by researchers due to the computational time and other complexities. However, in this chapter, both of these cases have been studied and discussed in detail. The weighting mechanism of time-weighted charts plays a vital role in allocating the weights to the past and present information. The weighting structure of the DGWMA chart and its limiting and special cases have been studied in detail. The shape of the weights for these charts has a direct impact in increasing the detection capability of time-weighted charts. The literature review witnesses the obstacles and challenges involved in calculating the run length distribution for the DGWMA charts, as mentioned by various researchers. However, a comparative and detailed study in terms of the run length distribution is lacking from current SPC literature. This research has studied three approaches to calculate the run length distribution: (i) the exact approach, (ii) the Markov chain approach, and (iii) the Monte Carlo simulation. The closed-form expressions based are obtained for the DGWMA and the DEWMA chart. The major issue with the first two approaches is the lack of available software packages that can numerically evaluate these expressions.
- In **Chapter 3**, a parametric DGWMA control chart is proposed to monitor the TBE in high-yield processes. Shewhart attributes charts are inefficient in detecting nonconformities in the high-yield processes, where the number of failures is often very small (i.e., one in a million or billion). To overcome this shortcoming, more efficient types of time-weighted control charts based on the gamma distribution are suggested and referred to as TBE charts, denoted as the DGWMA-TBE chart. Furthermore, symmetrically placed control limits (i.e., two-sided chart) are only applicable if the plotting statistic has a symmetric distribution. However, in the case of the DGWMA-TBE, since the underlying process distribution is gamma (a skewed

distribution), then a linear combination of gamma random variables is used and, in such a case, a one-sided chart is constructed, as the two-sided chart is ARL-biased (i.e., ARL_0 is less than ARL_1). A one-sided generalized parametric control chart (namely DGWMA-TBE) proposed in this chapter includes a one-sided GWMA-TBE chart, a one-sided EWMA-TBE chart, and a one-sided Shewhart-TBE chart as the limiting cases. Further to this, a one-sided DEWMA-TBE chart, which is the special case of the proposed DGWMA-TBE chart, is also proposed and studied in detail. Case 1 (one smoothing parameter) and Case 2 (two smoothing parameters) have been considered for the DEWMA-TBE chart. For a one-sided DEWMA chart, the Markov chain method is devised to find the closed-form expressions for the run length distribution and its other characteristics. The exact approach is devised to calculate the run length distribution of a one-sided DGWMA-TBE chart. A comparative performance analysis is conducted to compare the above mentioned three methods for the run length distribution as well the CPU time. The design and implementation of the DGWMA-TBE and DEWMA-TBE charts for Phase II (Case U) are also detailed. The DGWMA-TBE chart proposed in this chapter, outperforms the GWMA-TBE, the EWMA-TBE, and the Shewhart-TBE charts in detecting tiny shifts in the process. Further to this, new GWMA-TBE charts are developed by considering alternative discrete distributions for the weights. As a result, one can design an optimal GWMA-TBE chart that outperforms the DGWMA-TBE chart without the implementation of the double exponential smoothing technique.

- In various applications, the assumption of a known (normal) distribution for the underlying process is not valid. Therefore, the statistical properties of commonly used charts designed to perform under the normal distribution could be highly affected. In Chapter 4, a nonparametric version of the DGWMA control chart (Case 1 and Case 2) based on the EXs, namely the DGWMA-EX control chart is proposed for Case U to monitor the location parameter. The proposed chart can be viewed as a generalized nonparametric time-weighted chart that includes the GWMA-EX and EWMA-EX charts as limiting cases, which already exist in the context of the SPC literature. Moreover, the DEWMA-EX chart (Case 1 and Case 2) – that is, the special case of the DGWMA-EX chart – is also proposed in this chapter and the necessary results are provided. The closed-form expressions for the run length distribution and its characteristics are derived for the DGWMA-EX chart through the exact approach. The Monte Carlo simulation algorithm is developed to design and calculate the run length distribution and other characteristics. The performance of the proposed DGWMA-EX chart has been evaluated under different symmetric and skewed distributions in comparison with its main counterparts, and the necessary results and recommendations are provided for practitioners.

In the next sections, a list of possible future research opportunities and limitations pertaining to the current work are discussed.

5.1 Future research

i) From a theoretical perspective, more research needs to be conducted for the DGWMA chart in terms of monitoring the location and scale parameters simultaneously for the parametric and nonparametric cases. Currently, Teh et al. (2010) are the only researchers to have addressed this issue in their work.

ii) One of the assumptions for the DGWMA-TBE chart proposed in Chapter 3 is that the variable of interest is the time of the k^{th} failures in which k is an integer and specified. One possible extension is to consider non-exponential inter-arrival process (e.g., gamma inter-arrival process and Weibull inter-arrival process). For example, if a gamma inter-arrival process is considered, then the shape parameter of the gamma distribution is not necessarily an integer and it may be unknown.

iii) From the information available, there are no multivariate TBE control charts in the context of the SPC literature, which can be considered in future research by extending the univariate DGWMA-TBE and DEWMA-TBE charts proposed in Chapter 3.

iv) There are several articles available in the literature for monitoring the TBE and the magnitude of an event separately. Thus, one can design a control chart for simultaneously monitoring the time interval and magnitude.

v) Relatively little work has been done on Phase I monitoring regarding the DGWMA chart for parametric and nonparametric cases. From the studies available, the only paper that considered Case U is that of Lu (2018), but the topic of Phase I monitoring has not been mentioned or studied by this author.

vi) A detailed literature review on the developments of the DGWMA charts would be of interest and great benefit for new researchers interested in conducting research within this domain.

vii) The economical design of the proposed DGWMA charts in this chart would be of great interest and advantage to determine various design parameters that minimize total economic costs.

viii) The performance of the proposed nonparametric control chart in Chapter 4 (i.e., DGWMA-EX) under Lehman alternatives would be of great interest for future research.

ix) Further research is required for another special case of the DGWMA chart, known as the EGWMA chart.

x) The performance of the control chart methodologies proposed in this thesis depends on the choice of the weight function (a discrete probability distribution) and the parameters involved in the weight function (i.e., $\alpha_1, \alpha_2, q_1, q_2$). Choosing a suitable weight function and specifying appropriate values of the parameters can be challenging in practical situations. Hence, one possible research direction is to consider a weight function with interpretable parameters so that the practitioners can easily specify the values of the parameters with a particular purpose.

xi) One of the limitations of the newly developed control charts is their accessibility to the quality engineers and practitioners. Software developers would provide great assistance by including the developed charts in the statistical packages, which are popular amongst practitioners (e.g., SAS, R, etc.), and bridging the gap between the academics and researchers.

xii) The closed-form expressions obtained in this thesis for the DGWMA charts through the exact approach are often time-consuming and numerically cumbersome to evaluate. There is a necessity to develop efficient algorithms that can evaluate and calculate the run length distribution through these expressions.

5.2 R programming scripts

For the sake of brevity, a selection of R scripts that has been used in the current research are available at:
https://drive.google.com/open?id=1H8Zee8VY45kHJ4naV266if2Q_LKdCocl

5.3 Appendix

The results provided in this thesis in terms of supplementary tables can be found in the following link:

https://drive.google.com/open?id=18RNg2woAbFJ49PkyPYeWS2kuskpUCvEJ

References

Abbas, N., Riaz, M., & Does, R. J. (2013). Mixed exponentially weighted moving average-cumulative sum charts for process monitoring. *Quality and Reliability Engineering International, 29(3)*: 345-356.

Abbas, N., Riaz, M., & Does R. J. (2013). Memory-Type Control Charts for Monitoring the Process Dispersion. *Quality and Reliability Engineering International,* 30: 623-632. https://doi.org/10.1002/qre.1514

Abbas, N., Riaz, M., & Does, R. J. M. (2014). An EWMA-type control chart for monitoring the process mean using auxiliary information. *Communications in Statistics – Theory and Methods, 43(16),* 3485 – 3498.

Abbasi, S. A., & Miller, A. (2012). On proper choice of variability control chart for normal and non-normal processes. *Quality and Reliability Engineering International*, *28*(3), 279–296. https://doi.org/10.1002/qre.1244

Abbasi, S. A., & Miller, A. (2013). MDEWMA chart: an efficient and robust alternative to monitor process dispersion. *Journal of Statistical Computation and Simulation,* 83(2): 247-268. https://doi.org/10.1080/00949655.2011.601416

Abbasi, S. A. (2010). On sensitivity of EWMA control charts for monitoring process dispersion. In *Proceedings of the World Congress on Engineering*, 3: 2027-2032.

Abid, M., Nazir, H. Z., Riaz, M., & Lin, Z. (2016). An efficient nonparametric EWMA Wilcoxon signed-rank chart for monitoring location. *Quality and Reliability Engineering International, 33:* 669-685. https://doi.org/10.1002/qre.2048

Acosta-Mejia, C. A., Pignatiello, J. J., & Rao, B. V. (1999). A comparison of control charting procedures for monitoring process dispersion. *IIE Transactions, 31(6):* 569-579.

Alemi, F., & Neuhauser, D. (2004). Time-between control charts for monitoring asthma attacks. *Joint Commission Journal on Quality and Patient Safety, 30:* 95-102.

Alevizakos, V., Koukouvinos, C., & Lappa, A. (2018). Monitoring of time between events with a double generally weighted moving average control chart. *Quality and Reliability Engineering International, 35(2),* 685-710.

Al-Huniti, A. A., & Al-Diyan, G. R. (2012). Discrete Burr Type III distribution. *American Journal of Mathematics and Statistics, 2(5),* 145-152.

Ali, S., Pievatolo, A., & Gob, R. (2016). An Overview of Control Charts for High-quality Processes. *Quality and Reliability Engineering International, 32,* 2171-2189.

Alkahtani, S. S. (2013). Robustness of DEWMA versus EWMA control charts to non-normal processes. *Journal of Modern Applied Statistical Methods, 12(1),* 148-163.

Alwan, L.C., & Roberts, H. V. (1988). Time-series modelling for statistical process control. *Journal of Business & Economic Statistics, 6,* 87-95.

Amin, R. W., & Searcy, A. J. (1991). A nonparametric exponentially weighted moving average control scheme. *Communication in Statistics – Simulation and Computation, 20,* 1049-1072.

Amin, R. W., Reynolds, M. R., & Bakir, S. T. (1995). Nonparametric quality control charts based on the sign statistic. *Communications in Statistics – Theory and Methods, 24*: 1579-1623.

Amin, R. W., & Widmaier, O. (1999). Sign control charts with variable sampling intervals. *Communications in Statistics – Theory and Methods, 28*: 1961-1985.

Apley, D. W., & Lee, H. C. (2003). Design of exponentially weighted moving average control charts for autocorrelated processes with model uncertainty. *Technometrics, 45(3):* 187-198.

Areepong, Y. (2015). Generally weighted moving average control chart for zero-inflated Poisson. *Far East Journal of Mathematical Sciences, 98*(1), 103–118. https://doi.org/10.17654/FJMSSep2015_103_118

Aslam, M., Al-marshadi, A. H., & Jun, C. H. (2015). Monitoring process mean using generally weighted moving average chart for exponentially distributed characteristics. *Communications in Statistics-Simulation and Computation.*

Aslam, M., Azam, M., & Jun, C. H. (2014). A new exponentially weighted moving average sign chart using repetitive sampling . *Journal of Process Control, 24:* 1149-1153.

Atienza, O. O., Tang, L. C., & Ang, B. W. (1998). A SPC procedure for detecting level shifts of autocorrelated processes. *Journal of Quality Technology, 30*: 340-351.

Bakir, S. T. (2004). A distribution-free Shewhart quality control chart based on signed-ranks. *Quality Engineering*, *16*(4), 613–623. https://doi.org/10.1081/QEN-120038022

Bakir, S. T. (2006). Distribution-free quality control charts based on signed-rank-like statistics. *Communications in Statistics - Theory and Methods*, *35*(4), 743–757. https://doi.org/10.1080/03610920500498907

Bakir, S. T., & Reynolds, M. R. (1979). A Nonparametric Procedure for Process Control Based on Within-Group Ranking. *Technometrics, 21(2),* 175-183.

Balakrishnan, N., & Ng, H. K. T. (2006). *Precedence-Type Tests and Applications*. Wiley, Hoboken https://doi.org/10.1002/0470037849

Balakrishnan, N., Triantafyllou, I. S., & Koutras, M. V. (2009). Nonparametric control charts based on runs and Wilcoxon-type rank-sum statistics. *Journal of Statistical Planning and Inference, 139*: 3177-3192.

Barbiero, A. (2013). Parameter Estimation for Type III Discrete Weibull Distribution: A Comparative Study. *Journal of Probability and Statistics,* http://dx.doi.org/10.1155/2013/946562

Barnard, G. A. (1953). Time intervals between accidents – a note on Maguire, Pearson, and Wynn's paper. *Biometrika, 40:* 212-213.

Barnard, G. A. (1959). Control charts and stochastic processes. *Journal of the Royal Statistical Society, 21(2),* 239-271.

Benneyan, J. C. (2001). Number between g-type statistical quality control charts for monitoring adverse events. *Health Care Management Science, 4:* 305-318.

Bhattacharya, P. K., & Frierson, D. (1981). A nonparametric control chart for detecting small shifts disorders. *Annals of Statistics, 9:* 544-554.

Borror, C. M., Keats, J. B., & Montgomery, D. C. (2003). Robustness of the time between events CUSUM. *International Journal of Production Research, 41(15)*: 3435-3444.

Borror, C. M., Keats, J. B., & Montgomery, D. C. (2010). Robustness of the time between events control charts. *Inf Sci, 180:* 1051-1059.

Bourke, P. D. (2001). The geometric CUSUM chart with sampling inspection for monitoring fraction defective. *Journal of Applied Statistics, 28:* 951-972.

Brook, D., & Evans, D. A. (1972). An approach to the probability distribution of CUSUM run length. *Biometrika*, *59*(3), 539–549. https://doi.org/10.1093/biomet/59.3.539

Brown, R. G. (1962). Smoothing, Forecasting and Prediction of Discrete Time Series. Dover Phoenix Editions.

Burr, I. W. (1942). Cumulative frequency functions. *Annals of Mathematical Statistics, 13:* 215-232.

Butler, R. W. (2007). Saddlepoint Approximations with Applications, Cambridge University Press.

Calvin, T. W. (1983). Quality control techniques for zero-defects. *IEEE Transactions on Components, Hybrid, and Manufacturing Technology, 6:* 323-328.

Capizzi, G., & Masarotto, G. (2003). An adaptive exponentially weighted moving average control chart. *Technometrics, 45(3)*: 199-207.

Castagliola, P., Celano, G., & Fichera, S. (2009). A new CUSUM-S^2 control chart for monitoring the process variance. *Journal of Quality and Maintenance Engineering, 15(4)*: 344-357.

Chakraborti, S., & Eryilmaz, S. (2007). A nonparametric Shewhart type signed rank control chart based on runs. *Communications in Statistics – Simulation and Computation, 36*: 335-356.

Chakraborti, S. (2007). Run Length Distribution and Percentiles: The Shewhart Chart with Unknown Parameters. *Journal of Quality Engineering, 19(2),* 119-127.

Chakraborti, S., Van Der Laan, P., & Bakir, S. T. (2001). Nonparametric control charts: An overview and some results. *Journal of Quality Technology*, *33*(3), 304–315. https://doi.org/10.1080/00224065.2001.11980081

Chakraborti, S., Human, S. W., & Graham, M. A. (2011). Nonparametric (Distribution-Free) Quality Control Charts. *Handbook of Methods and Applications of Statistics: Engineering, Quality Control, and Physical Sciences.* N. Balakrishnan, Ed. 298-329, John Wiley & Sons, New York.

Chakraborti, S., Human, S. W., & Graham, M. A. (2009). Phase I statistical process control charts: An overview and some results. *Quality Engineering*, *21*(1), 52–62. https://doi.org/10.1080/08982110802445561

Chakraborti, S., Human, S. W., & Graham, M. A. (2008). Phase I Statistical Process Control Charts: An Overview and Some Results, *Quality Engineering, 21(1):* 52-62.

Chakraborti, S., & Van de Wiel, M. (2008). A nonparametric control chart based on the Mann-Whitney statistic. *Institute of Mathematical Statistics Collections, 1:* 156-172.

Chakraborty, N., Chakraborti, S., Human, S. W., & Balakrishnan, N. (2016). A generally weighted moving average signed-rank control chart. *Quality and Reliability Engineering International*, *32*(8), 2835–2845. https://doi.org/10.1002/qre.1968

Chakraborty, N., Human, S. W., & Balakrishnan, N. (2017). A generally weighted moving average chart for time between events. *Communications in Statistics – Simulation and Computation*, *46*(10), 7790–7817. https://doi.org/10.1080/03610918.2016.1252397

Chakraborty, N., Human, S. W., & Balakrishnan, N. (2018). A generally weighted moving average exceedance chart. *Journal of Statistical Computation and Simulation*, *88*(9), 1759–1781. https://doi.org/10.1080/00949655.2018.1447573

Chakraborty, N. (2017). Generally Weighted Moving Average control charts for small shifts (Doctoral thesis).

Champ, C. W., & Jones, L. A. (2004) Designing phase I $\bar{X}$ charts with small sample sizes. *Quality and Reliability Engineering International, 20:* 497-510.

Chan, L. K., & Zhang, J. (2000). Some issues in the design of EWMA chart. *Communications in Statistics-Simulation and Computation, 29(1), 201-217*.

Chatterjee, S., & Qiu, P. (2009). Distribution-free cumulative sum control charts using bootstrap-based control limits. *Annals of Applied Statistics, 3(1)*: 349-369.

Chen, G., & Cheng, S. W. (1998). MAX chart: Combining X-bar chart and S chart. *Statistica Sinica, 8:* 263-271.

Chen, G. M., Cheng, S. W., & Xie, H. S. (2001). Monitoring Process Mean and Variability with one EWMA Chart. *Journal of Quality Technology, 33*, 223-233.

Chen, G.M., Cheng, S. W., & Xie, H. S. (2001). Monitoring process mean and variability with one EWMA chart. *Journal of Quality Technology*, *33(2):* 223-233.

Cox, D. R., & Lewis, P. A. W. (1966). The statistical analysis of series of events. London: Methuen.

Dogu, E. (2012). Monitoring time between medical errors to improve health-care quality. *International Journal for Quality Research, 6:* 151-157.

Domangue, R., & Patch, S. C. (1991). Some omnibus exponentially weighted moving average statistical process monitoring schemes. *Technometrics, 33:* 299-313.

Lowry, C. A., Woodall, W. H.; Champ, C. W., & Rigdon, S. E. (1992). A multivariate Exponentially Weighted Moving Average Control Chart. *Technometrics, 34:* 46-53.

Li, C., Mukherjee, A., Su, Q., & Xie, M. (2016). Design and Implementation of Two CUSUM Schemes for Simultaneously Monitoring the Process Mean and Variance with Unknown Parameters. *Quality and Reliability Engineering International*, *32*, 2961– 2975. 10.1002/qre.1980.

Chang, T. C., & Gan, F. F. (1995). Cumulative sum control chart for monitoring process variance. *Journal of Quality Technology*, *27*: 109-119.

Chiu, W. K. (1973). The Economic Design of Cusum Charts for Controlling Normal means. *Journal of the Royal Statistical Society, 23(3),* 420-433.

Chiu, W.-C., & Lu, S.-L. (2015). On the steady-state performance of the Poisson double GWMA control chart. *Quality Technology & Quantitative Management*, *12*(2), 195–208. https://doi.org/10.1080/16843703.2015.11673376

Chou, Y.M., Mason, R.L., & Young, J.C. (2006). The sprt control chart for standard deviation based on individual observations. *Quality Technology Management, 3(3):* 335-345.

Crowder, S. V. (1989). Design of exponentially weighted moving average schemes. *Journal of Quality Technology*, *21*(3), 155–162.

Crowder, S. V. (1987). A simple method for studying run-length distributions of exponentially weighted moving average charts. *Technometrics*, *29*(4), 401-407. https://doi.org/10.2307/1269450

Crowder, S. V., & Hamilton, M. (1992). Average Run Lengths of EWMA Controls for Monitoring a Process Standard Deviation. *Journal of Quality Technology*, 24, 44-50.

Deming, W. E. (1993). The New Economics for Industry, Government, and Education. Cambridge, MA: Massachusetts Institute of Technology Centre for Advanced Engineering Study.

Epstein, B. (1954). Tables for the Distribution of the Number of Exceedances. *The Annals of Mathematical Statistics, 25(4):* 762-768.

Ewan, W. D., & Kemp, K. W. (1960). Sampling Inspection of Continuous Processes with No Autocorrelation Between Successive Results. *Biometrika, 47(3),* 363-380.

Ewan, W. D. (1963). When and How to Use Cu-Sum Charts. *Technometrics, 5(1),* 1-22.

Frisen, M. (2007). Financial surveillance. New York: Wiley.

Fu, J. C., & Lou, W. Y. W. (2003). *Distribution Theory of Runs and Patterns and Its Applications: A Finite Markov Chain Imbedding Approach. World Scientific*. WORLD SCIENTIFIC. https://doi.org/doi:10.1142/4669

Gan, F. F. (1992). Exact run length distributions for one-sided exponential CUSUM schemes. *Statistica Sinica, 2(1)*: 297-312.

Gan, F. F. (1994). Design of optimal exponential CUSUM control charts. *Journal of Quality Technology, 26:* 109-124.

Gan, F. F. (1998). Designs of one- and two-sided exponential EWMA charts. *Journal of Quality Technology, 30*(1), 55-69. https://doi.org/10.1080/00224065.1998.11979819

Gibra, I. N. (1975). Recent developments in control chart techniques. *Journal of Quality Technology, 7(4):* 183-192.

Goel, A. L., & Wu, S. M. (1971). Determination of A.R.L. and a Contour Nomogram for Cusum Charts to Control Normal Mean. *Technometrics, 13(2),* 221-230.

Goh, T. N. (1987). A control chart for very high yield processes, *Quality Assurance, 13:* 18-22.

Gibbons, J. D., & Chakraborti, S. (2010). Nonparametric Statistical Inference. 5th edition, CRC press.

Goel, A. L., & Wu, S. M. (1971). Determination of A.R.L. and a contour nomogram for CUSUM charts to control normal mean. *Technometrics, 13:* 221-230.

Goldsmith, P. L. & Whitfield, H. (1961). Average Run Lengths in Cumulative Chart Quality Control Schemes. *Technometrics, 3(1),* 11-20.

Graham, M. A., Chakraborti, S., & Human, S. W. (2011a). A nonparametric exponentially weighted moving average signed-rank chart for monitoring location. *Computational Statistics & Data Analysis*, *55*(8), 2490–2503. https://doi.org/10.1016/j.csda.2011.02.013

Graham, M. A., Chakraborti, S., & Human, S. W. (2011b). A nonparametric EWMA sign chart for location based on individual measurements. *Quality Engineering*, *23*(3), 227–241. https://doi.org/10.1080/08982112.2011.575745

Graham, M. A., Mukherjee, A., & Chakraborti, S. (2012). Distribution-free exponentially weighted moving average control charts for monitoring unknown location. *Computational Statistics & Data Analysis*, *56*(8), 2539–2561. https://doi.org/10.1016/j.csda.2012.02.010

Graham, M. A., Chakraborti, S., & Mukherjee, A. (2014). Design and implementation of CUSUM Exceedance Control Charts for Unknown Location. *International Journal of Production Research, 52(18):* 5546-5564.

Graham, M. A., & Chakraborti, S. (2019). *Nonparametric Statistical Process Control*, John Wiley & Sons, New York.

Haas, M., & Pigorsch, C. (2011). Financial Economics, fast-tailed distributions. *Complex Systems in Finance and Econometrics.* Meyers, R. A. (ed). Ed. Springer New York, 308-339.

Haq, A. (2013). A new hybrid exponentially weighted moving average control chart for monitoring process mean. *Quality and Reliability Engineering International, 29(7):* 1015-1025.

Haq, A., & Ul Abidin, Z. (2018). An enhanced GWMA chart for process mean. *Communications in Statistics – Simulation and Computation*, https://doi.org/10.1080/03610918.2018.1484479

Haq, A. (2017a). A new nonparametric EWMA control chart for monitoring process variability. *Quality and Reliability Engineering International*, *33*(7), 1499–1512. https://doi.org/10.1002/qre.2121

Haq, A. (2017b). A New EWMA control charts for monitoring process dispersion using auxiliary information. *Quality and Reliability Engineering International*, 33(8), 2597-2614.

Hawkins, D. M. (1992). Evaluation of the average run length of cumulative sum charts for an arbitrary data distribution. *Communication in Statistics – Simulation and Computation, 21*: 1001-1020.

Hawkins, D. M. (1981). A CUSUM for a scale parameter. *Journal of Quality Technology, 13(4):* 228-231.

Hawkins, D. M., & Olwell, D. H. (1997). Inverse Gaussian cumulative sum control charts for location and shape. *The Statistician, 46(3):* 323-335.

Hawkins, D. M., & Olwell, D. H. (1998). Cumulative Sum Charts and Charting for Quality Improvements. Springer, New York.

Hawkins, D. M. (1991). Multivariate quality control based on regression-adjusted variables. *Technometrics, 33*: 61-75. https://doi.org/10.2307/1269008

Hawkins, D. M. (1992). Cumulative sum control charting: An underutilized SPC tool. *Quality Engineering, 5(3):* 463-477.

Hawkins, D. M., & Wu, Q. (2014). The CUSUM and the EWMA Head-to-Head. *Quality Engineering,* 26(2): 215-222.

Hawkins, D. M., & Deng, Q. (2010). A nonparametric change-point control chart. *Journal of Quality Technology, 42:* 165-173.

Hawkins, D. M., & Zamba, K. D. (2003). On Small Shifts in Quality Control. *Quality Engineering, 16(1)*: 143-149.

Hawkins, D. M., & Zamba, K. D. (2005). Statistical Process Control for shifts in Mean or Variance using a Change point formulation. *Technometrics , 47*: 164-173.

Hawkins, D. M., & Zamba, K. D. (2005). A change point model for shift in variance. *Journal of Quality Technology, 37(1):* 21-31.

Hawkins, D. M. (1987). Self-starting CUSUM charts for Location and Scale. *The Statistician, 36:* 299-315.

Hawkins, D. M., Qiu, P., & Kang, C. W. (2003). The changepoint model for statistical process control. *Journal of Quality Technology, 35(4):* 355-366.

Hawkins, D. M., & Zamba, K. D. (2018). A Change-Point Model for a Shift in Variance. *Journal of Quality Technology, 37(1):* 21-31.

Hoaglin, D.C., Mosteller, F., & Tuckey, J. W. (1983). Understanding robust and exploratory data analysis. Ed. John Wiley and Sons, Inc.

Hoerl, R. W. (2000). Discussion of "Controversies and contradictions in statistical process control". *Journal of Quality Technology, 32(4),* 351-355.

Hotelling, H. (1947). Multivariate quality control – illustrated by the air testing of sample bomb sights. *Techniques of Statistical Analysis,* McGraw Hill, New York.

Huang, C. J. (2014). A sum of squares generally weighted moving average control chart. *Communications in Statistics- Theory and Methods, 43(23),* 5052-5071.

Huang, C. J., Tai, S. H., & Lu, S. L. (2014). Measuring the performance improvement of a double generally weighted moving average control chart. *Expert Systems with Applications An International Journal*, *41*(7), 3313–3322. https://doi.org/10.1016/j.eswa.2013.11.023

Human, S. W., Chakraborti, S., & Smit, C. F. (2010). Nonparametric Shewhart-type sign control charts based on runs. *Communications in Statistics – Theory and Methods, 39:* 2046-2062.

Huang, W., Shu, L., Jiang, W., & Tsui, K. L. (2013). Evaluation of run-length distribution for CUSUM charts under gamma distributions. *IIE Transactions, 45(9):* 981-994.

Hunter, J. S. (1986). The exponentially weighted moving average. *Journal of Quality Technology*, *18*(4), 203–210. https://doi.org/10.1080/00224065.1986.11979014

Janacek, G. J., & Meikle, S. E. (1997). Control charts based on medians. *Journal of Royal Statistical Society Series D – The Statistician, 46*: 19-31.

Jarrett, R. G. (1979). A note on the intervals between coal mining disasters. *Biometrika, 66:* 191-193.

Jensen, J. L. (1995). Saddlepoint Approximations. Oxford University Press, New York.

Johnson, R. A., & Bagshaw, M. (1974). The effect of serial autocorrelation on the performance of CUSUM tests. *Technometrics, 16,* 103-112. 10.1080/00401706.1975.10489274

Johnson, N. L. (1961). A Simple Theoretical Approach to Cumulative Sum Control Charts. *Journal of the American Statistical Association, 56(296),* 835-840.

Johnson, N. L., & Leone, F. C. (1962a). Cumulative Sum Control Charts Mathematical Principles Applied to their construction and use, Part I. *Industrial Quality Control, 18*: 15-21.

Johnson, N. L. (1966). Cumulative sum control charts and the Weibull distribution. *Technometrics, 8(3),* 481-491.

Johnson, N. L. (1962). Cumulative sum control charts: Mathematical principles applied to their construction and use. *Industrial Quality Control, 19,* 22-28.

Jones, L. A., Champ, C. W., and Rigdon, S. E. (2001). The performance of exponentially weighted moving average charts with estimated parameters. *Technometrics, 43(2):* 156-167.

Jones, L. A. (2002). The statistical design of EWMA control charts with estimated parameters. *Journal of Quality Technology, 34(3)*: 277-288.

Jones-Farmer, L. A., Ezell, J. D., & Hazen, B. T. (2014). Applying control chart methods to enhance data quality. *Technometrics*, *56*(1), 29–41. https://doi.org/10.1080/00401706.2013.804437

Khoo, M. B. C., Teh, S. Y., & Wu, Z. (2010). Monitoring process mean and variability with one double EWMA chart. *Communications in Statistics - Theory and Methods*, *39*(20), 3678–3694. https://doi.org/10.1080/03610920903324866

Kim, S. B., Jitpitaklert, W., Park, S. K., & Hwang, S. J. (2012). Data mining model-based control charts for multivariate and autocorrelated processes. *Expert Systems with Applications, 39:* 2073-2081.

King, E. P. (1954). Probability limits for the average chart when process standards are unspecified. *Industrial Quality Control, 10:* 62-64.

Knoth, S. (2006). Comparison of the ARL for CUSUM-S^2 schemes. *Computational Statistics & Data Analysis, 51(2):* 499-512.

Knoth, S., & Morais, M. C. (2015). On ARL-Unbiased Control Charts. *Frontiers in Statistical Quality Control*, Springer, Cham.

Koning, A. J. (2006). Model-based control charts in Phase I statistical process control. *Statistica Neerlandica, 60:* 327-338.

Krishna, H., & Pundir, P. S. (2009). Discrete Burr and discrete Pareto distributions. *Elsevier-Statistical Methodology, 6,* 177-188.

Lehman, E. L. (1953). The power of rank tests. *Annals of Mathematical Statistics*, 28-43.

Li, S., Tang, L., & Ng, S. (2010). Nonparametric CUSUM and EWMA control charts for detecting mean shifts. *Journal of Quality Technology, 42:* 209-226.

Li, S.-Y., Tang, L.-C., & Ng, S.-H. (2010). Nonparametric CUSUM and EWMA control charts for detecting mean shifts. *Journal of Quality Technology*, *42*(2), 209–226. https://doi.org/10.1080/00224065.2010.11917817

Li, Z., Zou, C., Gong, Z., & Wang, Z. (2014). The computation of average run length and average time to signal: An overview. *Journal of Statistical Computation and Simulation*, *84*(8), 1779–1802. https://doi.org/10.1080/00949655.2013.766737

Lizarelli, F.L., Bessi, N.C., Oprime, P.C., Do Amaral, R.M., & Chakraborti, S. (2016). A bibliometric analysis of 50 years of worldwide research on statistical process control. *Gestão & Produção*, *23*(4), 853–870. https://dx.doi.org/10.1590/0104-530x1649-15

Lowry, C. A., Woodall, W. H., Champ, C. W., & Rigdon, S. (1992). A Multivariate Exponentially Weighted Moving Average Control Chart. *Technometrics, 34(1):* 46-53.

Luo, P., DeVol, T. A., & Sharp, J. L. (2012). CUSUM analyses of time-interval data for online radiation monitoring. *Health Physics, 102:* 637-64

Lu, C. W., & Reynolds, M. R. (1999a). EWMA control charts for monitoring the mean of autocorrelated processes. *Journal of Quality Technology, 31(2):* 166-188.

Lu, C. W., & Reynolds, M. R. (1999b). Control charts for monitoring the mean and variance of autocorrelated processes, *Journal of Quality Technology, 31(2): 259-274.*

Lu, S. L. (2015). An extended nonparametric exponentially weighted moving average sign control chart. *Quality and Reliability Engineering International*, *31*(1), 3–13. https://doi.org/10.1002/qre.1673

Lu, S. L. (2018). Non-parametric double generally weighted moving average sign charts based on process proportion. *Communications in Statistics - Theory and Methods*, *47*(11), 2684–2700. https://doi.org/10.1080/03610926.2017.1342832

Lucas, J. M. (1982). Combined Shewhart-CUSUM quality control schemes. *Journal of Quality Technology, 14(2)*: 51-59.

Lucas, J. M. (1985). Counted data CUSUM's. *Technometrics, 27(2)*: 529-539.

Lucas, J. M., & Saccucci, M. S. (1990). Exponentially weighted moving average control schemes: Properties and enhancements. *Technometrics*, *32*(1), 1–12. https://doi.org/10.1080/00401706.1990.10484583

Lucas, J. M., & Crosier, R. B. (1982). Fast initial response for CUSUM quality-control schemes: give your CUSUM a head start. *Technometrics, 24:* 199-205.

Lugananni, R., & Rice, S. (1980). Saddle Point Approximation for the Distribution of the Sum of Independent Random Variables. *Advances in Applied Probability, 12(2),* 475-490.

Macgregor, J. F., & Harris, T. J. (1993). The exponentially weighted moving variance. *Journal of Quality Technology*, *25*(2), 106–118. https://doi.org/10.1080/00224065.1993.11979433

Maguire, B. A., Pearson, E. S., & Wynn, A. H. A. (1952). The time intervals between industrial accidents. *Biometrika, 39:* 168-180.

Mahmoud, M. A., & Woodall, W. H. (2010). An evaluation of the double exponentially weighted moving average control chart. *Communications in Statistics: Simulation and Computation*, *39*(5), 933-949. https://doi.org/10.1080/03610911003663907

Masoumi Karakani, H., Human, S. W., & van Niekerk, J. (2019). A double generally weighted moving average exceedance control chart. *Quality and Reliability Engineering International*.

McDonald, D. (1990). A cusum procedure based on sequential ranks. *Naval Research Logistic, 37:* 627-646.

McGilchrist, C. A., & Woodyer, K. D. (1975). Note on a Distribution-free CUSUM Technique. *Technometrics, 17(3),* 321-325.

Mohsin, M., Aslam, M., & Jun, C. H. (2016). A new generally weighted moving average control chart based on Taguchi's loss function to monitor process mean and dispersion. *Journal of Engineering Manufacture, 230(8):* 1537-1547.

Montgomery, D. C. (2013). *Introduction to Statistical Quality Control*. Hoboken, NJ: Wiley.

Montgomery, D. C., & Mastrangelo, C. M. (1991). Some statistical process control methods for autocorrelated data. *Journal of Quality Technology, 23*: 179-204.

Mukherjee, A., Graham, M. A., & Chakraborti, S. (2013). Distribution-Free Exceedance CUSUM control charts for location. *Communication in Statistics – Simulation and Computation, 42(5):* 1153-1187.

Nakagawa, T., & Osaki, S. (1975). The discrete Weibull distribution. *IEEE Transactions on Reliability*, *R-24*(5), 300–301. https://doi.org/10.1109/TR.1975.5214915

Nelson, L. S. (1963). Tables for a Precedence Life Test. *Technometrics, 5(4):* 491-499.

Ng, C. H., & Case, K. E. (1989). Development and evaluation of control charts using exponentially weighted moving averages. *Journal of Quality Technology, 21*(4), 242–250. https://doi.org/10.1080/00224065.1989.11979182

Nikolaidis, Y., & Tagaras, G. (2017). New indices for the evaluation of the statistical properties of Bayesian $\bar{x}$ control charts for short runs. *European Journal of Operational Research*, *259*(1), 280–292. https://doi.org/10.1016/j.ejor.2016.09.039

Ou, Y., Khoo, M.B, & Chen, N. (2015). A rational sequential probability ratio test control chart for monitoring process shifts in mean and variance. *Journal of Computational Statistics, 85(9):* 1765-1781.

Ozsan, G., Testik, M. C., & Weib, H. C. (2010). Properties of the exponential EWMA chart with parameter estimation. *Quality and Reliability Engineering International*, *26*: 555-569.

Padgett, W. J., & Spurrier, J. D. (1985). Discrete Failure Models. *IEEE Transactions on Reliability, 34(3)*: 253.256.

Page, E. S. (1954). Continuous Inspection Scheme. *Biometrika, 41*, 100-115. https://doi.org/10.1093%2Fbiomet%2F41.1-2.100

Pehlivan, C., & Testik, M. C. (2010). Impact of model misspecification on the exponential EWMA charts: A robustness study when the time-between-events are not exponential. *Quality and Reliability Engineering International, 26:* 177-190.

Pignatiello, J. J., Acosta-Mejia, C. A., & Rao, B. V. (1995). The performance of control charts for monitoring process dispersion. In *4th Industrial Engineering Research Conference,* 320-328.

Psarakis, S., & Papaleonida, G.E.A (2007). SPC procedures for monitoring autocorrelated processes. *Quality Technology and Quantitative Management, 4*, 501-540.

Qiu, P., & Hawkins, D. M. (2003). A nonparametric multivariate cumulative sum procedure for detecting shifts in all directions. *The Statistician, 52(2)*: 151-164.

Qu, L., Wu, Z., & Liu, T. I. (2011). A control scheme integrating the T chart and TCUSUM chart. *Quality and Reliability Engineering International, 27(4):* 529-539.

Radaelli, G. (1998). Planning time-between events Shewhart control charts. *Total Quality Management, 9:* 133-140.

Raza, S. M. M., Riaz, M., & Ali, S. (2015). On the performance of EWMA and DEWMA control charts for censored data. *Journal of the Chinese Institute of Engineers, 38(6),* 714-722.

Riaz, M. (2008). Monitoring process mean level using auxiliary information. *Statistica Neerlandica 62(4),* 458 – 481.

Riaz, M., & Akber Abbasi, S. A. (2016). Nonparametric double EWMA control chart for process monitoring. *Revista Colombiana de Estadística*, *39*(2), 167–184. https://doi.org/10.15446/rce.v39n2.58914

Roberts, S. W. (1959). Control chart tests based on geometric moving averages. *Technometrics*, *1*(3), 239–250. https://doi.org/10.1080/00401706.1959.10489860

Roberts, S. W. (1966). A comparison of some control chart procedures. *Technometrics*, *8*(3), 411–430. https://doi.org/10.1080/00401706.1966.10490374

Robinson, P. B., & Ho, T. Y. (1978). Average run lengths of geometric moving average charts by numerical methods. *Technometrics, 20(1),* 85-93.

Roy, D. (2003). The discrete normal distribution. *Communications in Statistics- Theory and Methods, 32(10):* 1871-1883.

Roy, D. (2004). Discrete Rayleigh distribution. *IIIE Transactions on Reliability, 53(2)*: 255-260.

Ruggeri, F., Kenett, R. S., & Faltin, F. W. (2007). Exponentially weighted moving average (EWMA) control chart. *Encyclopedia of Statistics in Quality and Reliability*, 2, 633-639, John Wiley & Sons, New York.

Scariano, S. M., & Calzada, M. E. (2003). A note on the lower-sided synthetic chart for exponentials. *Quality Engineering, 15:* 677-680.

Schmid, W. (1997). On EWMA charts for time series. *Frontiers in Statistical Quality Control, 5*, 115-137.

Schuster, E. F. (1984). Classification of probability laws by tail behavior. *Journal of the American Statistical Association, 79*: 936-939.

Shafae, M. S., Dickinson, R. M., Woodall, W. H., & Camelio, J. A. (2014). Cumulative Sum Control Charts for Monitoring Weibull-distributed Time Between Events. *Quality and Reliability Engineering International, 31(5):* 839-849.

Shamma, S. E., & Shamma, A. K. (1992). Development and evaluation of control charts using double exponentially weighted moving averages. *The International Journal of Quality & Reliability Management*, *9*(6), 18-25.

Sheu, S. H. (1998). A generalized age and block replacement of a system subject to shocks. *European Journal of Operational Research, 108*: 345-362.

Sheu, S. H. (1999). Extended optimal replacement model for deteriorating systems. *European Journal of Operational Research, 112:* 503-516.

Sheu, S. H., & Griffith, W. S. (1996). Optimal number of minimal repairs before replacement of a system subject to shocks. *Naval Research Logistics, 43*: 319-333.

Sheu, S. H., & Chiu, W. C. (2007). Poisson GWMA control chart. *Communications in Statistics– Simulation and Computation*, *36*(5), 1099–1114. https://doi.org/10.1080/03610910701540037

Sheu, S. H., & Hsieh, Y. T. (2009). The extended GWMA control chart. *Journal of Applied Statistics*, *36*(2), 135–147. https://doi.org/10.1080/02664760802443913

Sheu, S. H., & Lin, T. C. (2003). The generally weighted moving average control chart for detecting small shifts in the process mean. *Quality Engineering*, *16*(2), 209–231. https://doi.org/10.1081/QEN-120024009

Sheu, S. H., & Lu, S. (2013). The generally weighted moving average variance chart. *Communications in Statistics - Theory and Methods*, *42*(17), 3204–3214. https://doi.org/10.1080/03610926.2011.622845

Sheu, S. H., Tai, S. H., Hsieh, Y. T., & Lin, T. C. (2009). Monitoring process mean and variability with generally weighted moving average control charts. *Computers & Industrial Engineering*, *57*(1), 401–407. https://doi.org/10.1016/j.cie.2008.12.010

Sheu, S. H., & Yang, L. (2006). The generally weighted moving average control chart for monitoring the process median. *Quality Engineering*, *18*(3), 333–344. https://doi.org/10.1080/08982110600719431

Sheu, S.-H., & Hsieh, Y.-T. (2009). The extended GWMA control chart. *Journal of Applied Statistics*, *36*(2), 135–147. https://doi.org/10.1080/02664760802443913

Shewhart, W. A. (1931). Economic Control of Quality Manufactured Product. *Bell Telephone Laboratories*, The University of Wisconsin.

Shewhart, W. A. (1939). Statistical method from the viewpoint of quality control. *Department of Agriculture*. https://doi.org/10.1038/146150e0

Shu, L., & Jiang, W. (2008). A New EWMA Chart for Monitoring Process Dispersion. *Journal of Quality Technology*, 40(3): 319-331. https://doi.org/10.1080/00224065.2008.11917737

Simoes, B. F. T., Epprecht, E. K., & Costa, A. F. B. (2010). Performance comparisons of EWMA control chart schemes. *Quality Technology and Quantitative Management, 7(3)*: 249-261.

Sparks, R. S. (2000). CUSUM charts for singling varying location shifts. *Journal of Quality Technology, 32:* 157-171.

Stein, W. E., & Dattero, R. (1984). A new discrete Weibull distribution. *IIIE Transactions on Reliability, 33(2)*: 196-197.

Steiner, S. H. (1999). Exponentially weighted moving average control charts with time-varying control limits and fast initial response. *Journal of Quality Technology, 31(1)*: 75-86.

Stoumbos, Z.G., & Reynolds, M. R. (1996). Control charts applying a general sequential test at each sampling point. *Sequential Analysis, 15(2-3):* 159-183.

Sullivan, J. H., & Woodall, W. H. (1996). A control chart for preliminary analysis of individual observations. *Journal of Quality Technology, 28(3):* 265-278.

Sun, J., & Zhang, G. X. (2000). Control charts based on the number of consecutive conforming items for the near zero-nonconformity processes. *Total Quality Management, 11:* 235-250.

Tadikamalla, P. R. (1980). A look at the Burr and Related Distributions. *International Statistical Review, 48(3):* 337-344.

Tai, S., Hsieh, Y., & Huang, C. (2010). The combined double generally weighted moving average control chart for individual observations. *International Conference on Management and Service Science*, Wuhan, 1-4.

Teh, S. Y., Khoo, M. B. C., & Wu, Z. (2011). A sum of squares double exponentially weighted moving average chart. *Computers & Industrial Engineering*, *61*(4), 1173–1188. https://doi.org/10.1016/j.cie.2011.07.007

Teh, S. Y., Khoo, M. B. C., & Wu, Z. (2012). Monitoring process mean and variance with a single generally weighted moving average chart. *Communications in Statistics - Theory and Methods*, *41*(12), 2221–2241. https://doi.org/10.1080/03610926.2011.558659

Triantafyllopoulos, K., & Bersimis, S. (2016). Phase II control charts for autocorrelated processes. *Quality Technology & Quantitative Management, 13(1),* 88-108.

Tsai, C. F., Lu, S. L., & Huang, C. J. (2016). Design of an extended nonparametric EWMA sign chart. *International Journal of Industrial Engineering: Theory, Applications and Practice.*

Tsiamyrtzis, P., & Hawkins. D. M. (2008). A Bayesian EWMA method to detect jumps at the start-up phase of a process. *Quality and Reliability Engineering International, 24:* 721-735.

Tuprah, K., & Ncube, M. (1987). A comparison of dispersion quality control charts. *Sequential Analysis, 6(2):* 155-163.

Van Dobben de Bruyn, C. S. (1968). Cumulative sum tests: Theory and practice, Griffin, London.

Vardeman, S., & Ray, D. (1985). Average Run Lengths for CUSUM Schemes When Observations are Exponentially Distributed. *Technometrics, 27(2),* 145-150.

Wetherill, G. B. (1969). Sampling inspection and quality control, Methuen, London.

Woodall, W. H., & Montgomery, D. C. (2014). Some current directions in the theory and application of statistical process monitoring. *Journal of Quality Technology*, 46(1), 78-94.

Woodall, W. H., Zhao, M. J., Paynabar, K., Sparks, R., & Wilson, J. D. (2017). An overview and perspective on social network monitoring. *IISE Transactions*, *49*(3), 354–365. https://doi.org/10.1080/0740817X.2016.1213468

Woodall, W. H. (2017). Bridging the gap between theory and practice in basic statistical process monitoring. *Quality Engineering, 29(1),* 2-15.

Woodall, A. H. (1983). The distribution of the run length of one-sided CUSUM procedures for continuous random variables. *Technometrics, 25:* 295-301.

Woodall, W. H. (2006). The use of control charts in healthcare and public health surveillance (with distinction). *Journal of Quality Technology, 38,* 89-104.

Wortham, A. W., & Ringer, L. J. (1971). Control via exponential smoothing. *Transportation and Logistic Review, 7, 33-39.*

Wortham, A. W., & Heinrich, G. F. (1972). Control charts using exponential smoothing techniques. *Annual Technical Conference Transactions.* American Society for Quality Control, Milwaukee, WI, 451-458.

Wu, Z., Yang, M., & Khoo, M.B.C. (2010). Optimization designs and performance comparison of two CUSUM Schemes for monitoring process shifts in mean and variance. *European Journal of Operational Research, 205(1):* 136-150.

Wu, Z., Wang, P. H., & Wang, Q. N. (2009). A loss function-based adaptive control chart for monitoring the process mean and variance. *International Journal of Advanced Manufacturing Technology, 40:* 948-959.

Xie, M., Goh, T. N., & Lu, X. S. (1998). A comparative study of CCC and CUSUM charts. *Quality and Reliability Engineering International, 14:* 339-345.

Yang, S. F., Lin, J. S., & Cheng, S. W. (2011). A new nonparametric EWMA sign control chart. *Expert Systems with Applications An International Journal*, *38*(5), 6239–6243. https://doi.org/10.1016/j.eswa.2010.11.044

Yang, S. F., & Arnold, B. C. (2015). A new approach for monitoring process variance. *Journal of Statistical Computation and Simulation, 86(14),* 2749-2765. https://doi.org/10.1080/00949655.2015.1125901

Ye, N., & Chen, Q. (2001). An anomaly detection technique based on a chi-squared statistic for detecting intrusions into information systems. *Quality and Reliability Engineering International, 17,* 105-112.

Yu, Y. (2007). Some contributions to Statistical Process Control. Master's dissertation. McMaster University, Hamilton, Ontario.

Wald, A. (1947). Sequential Analysis. New York: Wiley.

Zacks, S., & Kenett, R. S. (1994). Process Tracking of Time Series with Change Points. *Recent advances in Statistics and Probability,* 155-171.

Zamba, K. D., & Hawkins, D. M. (2006). A Multivariate Change-Point Model for Statistical Process Control, *Technometrics, 48(4):* 539-549.

Zamba, K. D., Tsiamyrtzis, P., & Hawkins, D. M. (2008). A Sequential Bayesian Control Model for Influenza-Like Illnesses and Early Detection of Intentional Outbreaks. *Quality Engineering, 20(4):* 495-507.

Zamba, K. D., & Hawkins, D. M. (2009). A Multivariate Change-Point Model for Change in Mean Vector and/or Covariance Structure. *Journal of Quality Technology, 41(3):* 285-303.

Zamba, K. D., & Hawkins, D. M. (2013). A multivariate change point mode for statistical process control. *Technometrics, 48(4)*: 539-549.

Zhang, N. F. (1998). A statistical control char for stationary process data. *Technometrics, 40(1):* 24-38.

Zhang, L., & Chen, G. (2005). An Extended EWMA Mean Chart. *Quality Technology & Quantitative Management*, *2*(1), 39–52. https://doi.org/10.1080/16843703.2005.11673088

Zhang, L., Govindaraju, K., Lai, C. D., & Bebbington, M. S. (2003). Poisson DEWMA Control Chart. *Communications in Statistics Part B: Simulation and Computation*, *32*(4), 1265–1283. https://doi.org/10.1081/SAC-120023889

Zhang, C. W., Xie, M., Liu, J. Y., & Goh, T. N. (2007). A control chart for the Gamma distribution as a model of time between events. *International Journal of Production Research, 45*(23), 5649–5666. https://doi.org/10.1080/00207540701325082

Zhang, C., Peng, Y., Schuh, A., Megahed, F., & Woodall, W. H. (2013). Geometric charts with estimated control limits. *Quality and Reliability Engineering International, 29,* 209-223.

Zhang, P., Su, Q., Li, C., & Wang, T. (2014). An economically designed sequential probability ratio test control chart for short-run production. *Computational Industrial Engineering, 78:* 74-83.

Zhang, J., Zou, C., & Wang, Z. (2011). A new chart for detecting the process mean and variability. *Communications in Statistics – Simulation and Computation, 40(5):* 728-743.

Zou, C., Zou, C., Zhang, Y., & Wang, Z. (2009). Nonparametric control chart based on change-point model. *Statistical Papers, 50:* 13-28.

Zwetsloot, I. M., & Woodall, W. H. (2017). A head-to-head comparative study of the conditional performance of control charts based on estimated parameters. *Quality Engineering, 29(2):* 244-253.